

2019

The Role of Mesenchymal Cells in the Regeneration of Salivary Gland Tissue

Davies, Jonathan Paul

<http://hdl.handle.net/10026.1/14299>

<http://dx.doi.org/10.24382/1153>

University of Plymouth

All content in PEARL is protected by copyright law. Author manuscripts are made available in accordance with publisher policies. Please cite only the published version using the details provided on the item record or document. In the absence of an open licence (e.g. Creative Commons), permissions for further reuse of content should be sought from the publisher or author.

Statement of Copyright

This copy of the thesis has been supplied on condition that anyone who consults it is understood to recognise that its copyright rests with its author and that no quotation from the thesis and no information derived from it may be published without the author's prior consent.



**UNIVERSITY OF
PLYMOUTH**

**The Role of Mesenchymal Cells in the
Regeneration of Salivary Gland Tissue**

By

Jonathan Paul Davies

A thesis submitted to the University of Plymouth,
in partial fulfilment for the degree of

Doctor of Philosophy

University of Plymouth, Faculty of Medicine and Dentistry
Peninsula Dental School

September 2018

Acknowledgements

The author would like to thank the members of their supervisory team:

Dr Bing Hu (University of Plymouth),

Professor Wan-Fai Ng (Newcastle University, Sjogren's Registry)

Professor Stephen Creanor (University of Plymouth)

Professor Christopher Tredwin (University of Plymouth)

This work is supported by PUPSMD PhD studentship

The research group:

Dr Louise Bellfield, Dr Zoe Brookes, Dr Wai-Ling Kok, Dr Tulay Gulsen, Dr Heng Zhaung,

Donald Singer, Jemma Walker, Portia Grayson, Chloe Walker, Charlotte Illsley

Tracy Edwards, Yan Gao, Yuying Liu, Dr Quinguo Lai

Other Academic Support:

Dr Rebecca Smith, Szi-Kay Leung (University of Exeter)

Further Acknowledgements:

Everybody tells you that a PhD is hard, and it is very true, but harder in ways you would not have anticipated. It's emotionally draining and challenges your health, your fitness, and your outlook on a scientific career. You have to learn to balance yourself, your colleagues, your family and your supervisor, and it is not always an easy challenge.

Firstly, thanks go to Dr Bing Hu for his management and leadership throughout this project. We may have approached ideas from different directions on a few occasions but ultimately we both wanted to produce high quality scientific work and develop a worthy project to submit as my thesis and to publish impactful journal articles. Thank you also to Professor Christopher Tredwin, Dr Zoe Brookes, and Professor Stephen Creanor for their continued academic support during the writing of this thesis.

My research group have been exceptional. It was lovely to be working with colleagues who all cared and helped each other whenever needed. Jemma, Donald, Tracy, Portia, Charlotte and Chloe, thank you all so much. We had such a laugh in the lab and office, and I would not have retained any sanity if I didn't know other people were struggling through the same torment as myself.

Above all others, I would like to thank my closest friend Jemma Dunn, who lived with me, laughed with me and celebrated with me like nobody else has before, and I know I am now stuck with her for the rest of my life. We ate far too much food but loved life and those moments of singing and dancing in the kitchen.

Other colleagues who worked alongside me, to whom I am massively indebted for their love, and hugs, and laughter include: Tracey Evans, Sarah Ellwood, Jade Lyons-Rimmer,

Kayleigh Bassiri, Karolina Jaworek, Robert Button, Chris Bulman, Jackie Kinvig, and the post-graduate student support staff who were there when I needed help.

I want to thank my expanding family who have all been so encouraging for the past ten years. Thank you to my parents; Frances and Ian, my siblings; Andrew, Matthew and Rebecca, their respective partners; Bertie, Robyn and Josh, and their growing brood of children; Alice, George, and baby on the way. They have all coped with me being a hermit and not visiting very often for a few years and always being busy and stressed, but I promise I will make up for it.

Finally, and most importantly, my partner Mark has always been there at home, waiting for me to finish writing, giving me space, hugging me and feeding me, making me laugh and smile, and reminding me that I need to find the motivation within myself. Ultimately, as always, he is right; a PhD is nothing but a lot of difficult work that you just have to get on with; there's no point complaining or moaning, you just have to do it, just as everyone else just gets on with their work. Thank you Mark for being relentlessly yourself, as I wouldn't love you any other way.

Ultimately, if you endeavour to pursue a PhD: make sure you sing and dance for twenty minutes as crazily as you can when you get home from work every day; your stresses will vanish and your heart will lift. Learn to swear like a sailor, so that you learn to laugh at yourself for being so silly about the small things in life. Be bold and learn to say no; you are your own number one priority, don't play their game, and...

"Nolite te bastardest carborundorum."

Author's Declaration

At no time during the registration for the degree of Doctor of Philosophy has the author been registered for any other University award without prior agreement of the Graduate Sub-Committee. Work submitted for this research degree at the Plymouth University has not formed part of any other degree either at the University of Plymouth or at another establishment.

This study was financed with the aid of a studentship from Marie Curie Action and carried out in collaboration with The Sjogren's Registry, Newcastle University.

A programme of advanced study was undertaken, which included supervision and training of students, attendance of relevant scientific seminars and conferences, at which work was often presented; external institutions were visited for consultation purposes and several papers prepared for publication.

Publications: In Preparation

Presentation of Work and Conferences Attended:

BSODR Cardiff 2015 – Poster Presentation

BSODR Plymouth 2017 – Junior Colgate Prize 2017 – Best Early Career Researcher Poster Presentation

External Contacts: Professor Wan-Fai Ng, University of Newcastle.

Word count of main body of thesis: 52,835

Signed: 

Date: 2018.09.19

Jonathan Paul Davies

Table of Abbreviations

Abbreviation	Unabbreviated form
SG	Salivary Gland
SMG	Submandibular Gland
SLG	Sublingual Gland
PG	Parotid Gland
LN	Lymph Node
PSS	Primary Sjogren's Syndrome
MCs	Mesenchymal Cells
MSCs	Mesenchymal Stem Cells
SCs	Stem Cells
CDH1	E-Cadherin/Cadherin 1
Vim	Vimentin
Ptch	Patched
Smo	Smoothened
SHH	Sonic Hedgehog

Contents

STATEMENT OF COPYRIGHT	1
<u>THE ROLE OF MESENCHYMAL CELLS IN THE REGENERATION OF SALIVARY GLAND TISSUE</u>	3
ACKNOWLEDGEMENTS	5
FURTHER ACKNOWLEDGEMENTS:	7
AUTHOR'S DECLARATION	9
PRESENTATION OF WORK AND CONFERENCES ATTENDED:	9
WORD COUNT OF MAIN BODY OF THESIS: 52,835	11
TABLE OF ABBREVIATIONS	13
CONTENTS	15
LIST OF FIGURES	18
LIST OF TABLES	21
ABSTRACT: THE ROLE OF MESENCHYMAL CELLS IN THE REGENERATION OF SALIVARY GLAND TISSUE.	22
<u>1. INTRODUCTION</u>	25
1.1. THE IMPORTANCE AND ROLE OF SALIVA	25
1.2. SALIVARY GLANDS, STRUCTURE AND FUNCTION	28
1.3. SALIVARY GLAND DEVELOPMENT	35
1.4. STEM CELLS IN THE SALIVARY GLAND	42
1.5. DISEASES AFFECTING SALIVARY GLAND TISSUE	50
1.5.1. SJOGREN'S SYNDROME	52
1.5.2. RADIOTHERAPY	60
1.5.3. CURRENT THERAPIES FOR XEROSTOMIA	70
1.6. HYPOTHESIS	73
1.7. AIMS	75

2. MATERIALS AND METHODS	77
2.1. HUMAN TISSUE SAMPLES	77
2.2. MOUSE TISSUE SAMPLES	80
2.3. IMMUNOFLUORESCENCE STAINING	82
2.4. HISTOLOGICAL STAINING	84
2.5. IMAGING	87
2.6. ANTIBODY LISTS	88
2.7. LASER CAPTURE MICRODISSECTION	93
2.8. GENERAL CELL CULTURE	95
2.8.1. COLLAGEN COATING ONE	98
2.8.2. COLLAGEN COATING TWO	98
2.8.3. POLY-D-LYSINE COATING	99
2.8.4. PASSAGING CELLS	99
2.8.5. FREEZING CELLS	100
2.8.6. THAWING CELLS	100
2.8.7. SEMI-SOLID ORGAN CULTURE	101
2.9. PRIMARY AND SECONDARY MOUSE ORGANOID CULTURES	102
2.10. HUMAN ORGANOID CULTURES	104
2.11. FLOW CYTOMETRY	105
2.12. RNA EXTRACTION & cDNA PRODUCTION	106
2.13. Q-PCR	107
2.14. STATISTICS	111

3. RESULTS	113
3.1. CHARACTERISATION OF PSS AND NON-PSS PATIENT LABIAL SALIVARY GLAND TISSUE	113
3.1.1. IMMUNOFLUORESCENCE OF PSS VERSUS NON-PSS SALIVARY GLAND TISSUE	116
3.1.2. REGIONAL ANALYSIS OF NON-PSS VERSUS PSS TISSUE BY LCM	136
3.1.3. DISCUSSION	144
3.1.4. CONCLUSION	153
3.2. DEVELOPMENT OF MURINE ORGANOID MODELS	155
3.2.1. MOUSE CELL CULTURE AND ORGANOID MODEL METHODS	162
3.2.2. IMMUNOFLUORESCENT CHARACTERISATION OF MURINE SMG	165
3.2.3. DEVELOPING MURINE CELL CULTURE AND ORGANOID MODELS	176
3.2.4. DISCUSSION	194
3.2.5. CONCLUSION	203
3.3. ESTABLISHING 3D ORGANOGENESIS ASSAYS DERIVED FROM HUMAN PATIENT BIOPSIES	205
3.3.1. HUMAN CELL CULTURE AND ORGANOID METHODS	207
3.3.2. OPTIMISING CELL CULTURES OF HUMAN DERIVED CELLS	210
3.3.3. CASE/CONTROL COHORTS PRESENT WITH DIFFERENT REGENERATIVE POTENTIALS IN HUMAN-MOUSE ORGANIDS.	220
3.3.4. DISCUSSION	224
3.3.5. CONCLUSION	229
4. OVERALL DISCUSSION	231
4.1. REVIEW OF PROJECT AIMS	231
4.2. CHARACTERISING AND INVESTIGATING MOLECULAR CHANGES OF PSS TISSUE	231
4.3. GENERATING ORGANOID MODELS USING MOUSE AND HUMAN TISSUE	235
4.4. IDENTIFYING THE RADIOTHERAPY IMPACT ON MESENCHYMAL CELLS.	237
4.5. LIMITATIONS OF THIS INVESTIGATION	238
4.6. FUTURE WORK	241
4.7. CONCLUDING REMARKS	243
5. REFERENCES	245
6. APPENDIX	265
6.1. IMPACT OF X-RAY IRRADIATION ON THE REGENERATIVE POTENTIAL OF SALIVARY GLAND MESENCHYMAL CELLS	265
6.2. PRIMER VALIDATION AND FURTHER QPCR ANALYSIS.	283

List of Figures

Figure 1.2-1	30
Figure 1.2-2	32
Figure 1.3-1	39
Figure 1.3-2	41
Figure 1.4-1	43
Figure 1.4-2	45
Figure 1.5-1	55
Figure 3.1-1	118
Figure 3.1-2	119
Figure 3.1-3	122
Figure 3.1-4	123
Figure 3.1-5	124
Figure 3.1-6	126
Figure 3.1-7	129
Figure 3.1-8	131
Figure 3.1-9	133
Figure 3.1-10	136
Figure 3.1-11	137
Figure 3.1-12	138
Figure 3.1-13	141
Figure 3.1-14	142
Figure 3.1-15	143

Figure 3.2-1.	166
Figure 3.2-2.	167
Figure 3.2-3	168
Figure 3.2-4.	169
Figure 3.2-5..	170
Figure 3.2-6.	171
Figure 3.2-7.	172
Figure 3.2-8	177
Figure 3.2-9.	178
Figure 3.2-10.	179
Figure 3.2-11. s.....	181
Figure 3.2-12	182
Figure 3.2-13	183
Figure 3.2-14	184
Figure 3.2-15.	185
Figure 3.2-16.	187
Figure 3.2-17..	188
Figure 3.2-18	189
Figure 3.2-19.	190
Figure 3.2-20	192
Figure 3.3-1	211
Figure 3.3-2..	213
Figure 3.3-3	215
Figure 3.3-4..	218

Figure 3.3-5..	221
Figure 3.3-6..	223
Figure 4.2-1..	233
Figure 6.1-1..	268
Figure 6.1-2 ..	270
Figure 6.1-3..	271
Figure 6.1-4..	272
Figure 6.1-5..	274
Figure 6.2-1..	289
Figure 6.2-2..	289
Figure 6.2-3..	290
Figure 6.2-4 ..	292
Figure 6.2-5..	292
Figure 6.2-6..	293
Figure 6.2-7 .	294
Figure 6.2-8 ..	295
Figure 6.2-9..	296

List of Tables

Table 1.1-1 Components of saliva and the impact of their loss.	26
Table 1.3-1 A demonstration of the physical similarities and functionality of salivary glands across humans and mice	35
Table 2.6-1 Listings of all Primary Antibody used in all Immunofluorescence and Flow Cytometry on Mouse and Human Tissue.....	88
Table 2.6-2 Catalogue of Human and Mouse Mesenchymal Stem Cell Marker Identification Kit Contents from R&D Systems.....	91
Table 2.8-1 Cell culture media contents with additional supplements and antibiotics.	96
Table 2.8-2 Contents of B27 Supplement,	97
Table 2.13-1 Primer Sequences Targeting Mouse RNA Sequences.....	109
Table 2.13-2 Primer Sequences Targeting Human RNA Sequences.	109
Table 2.13-3 Program of the PCR cycles used for QPCR on the Roche LightCycler.	110
Table 3.1-1. An overview of immunofluorescent staining presented in human labial salivary gland biopsies.	135
Table 3.2-1 Overview of staining patterns in mouse salivary gland tissue.....	174
Table 6.2-1 Primers designed against mouse tissue derived RNA sequences.....	285
Table 6.2-2 Primers designed for analysis of human tissue derived RNA.	287

Abstract: The Role of Mesenchymal Cells in the Regeneration of Salivary Gland Tissue.

Primary Sjogren's Syndrome (PSS) patients will suffer a variable degree of damage to their salivary glands, caused by lesions of immune infiltrates into the tissue surrounding duct structures. Some patients present with extensive lesions that destroy any residual secretory acinar tissue, leading to hyposalivation. This damage, and reduced salivation, can lead to deleterious effects on the oral health, such as increased risk of caries and periodontitis, and will impact the general quality of life of the patients and can increase their risk of developing other, more serious conditions.

Previously, there has been limited knowledge and characterisation of how different cell populations are impacted by PSS. Therefore, this project developed clear characterisation of labial salivary gland tissue from patients presenting with PSS compared to non-PSS patient samples. It was shown that regions that were not directly associated to lesions present with the same phenotypical profile as observed in non-PSS patients, indicating a very limited focal impact of the disorder. These regions stained positively for E-cadherin and Vimentin in patterns that were comparable to non-PSS patient samples. Simultaneously, the directly affected lesion regions presented with complete absence of any healthy salivary gland cell markers. Peri-lesion tissue presented with subtle changes to marker expression; here we could identify changes to mesenchymal cell markers such as PDGFRb and CD29 between the PSS and non-PSS tissue. The established immunofluorescent markers could further be used in later experimentations to identify each cell population, particularly when developing cell cultures and organoid models.

In order to investigate the impact of PSS on the ability of cells to proliferate and perform a rudimentary regenerative function, the group developed cell cultures that were representative of epithelial and mesenchymal cell types and recombined them to form organoid models. These models were first developed using mouse derived cell cultures before being adapted for use with human derived cells. Using these organoid models, it was possible to demonstrate that mesenchymal cells isolated from PSS positive patients had a reduced ability to direct the regenerative capacity of the epithelial spheroid structures, resulting in smaller, less complex, and less functionally advanced organoids than those developed using non-PSS derived cells.

During this study, standard techniques were used such as quantitative real-time PCR of relative mRNA expression levels, immunofluorescent staining, and laser capture microdissection (LCM), whilst a novel organoid culture technique was optimised.

Since these models have been established, it is thought that they could be adapted to investigate other disease or environmental impact on the salivary gland tissue, with some preliminary studies attempting to investigate the impact of x-ray irradiation exposure on the tissue. Furthermore, the technique could possibly be extrapolated to other tissue types to aid the understanding of the effect of other autoimmune conditions on their target tissues.

In conclusion, this project shows mesenchymal cells appear to play an important and necessary role within tissue regeneration models. There is a significant change to cell fate determination pathways in PSS positive patient biopsies, and these mechanistic changes now need to be studied further within the constraints of the organoid model that has been developed.

1.Introduction

1.1. The Importance and Role of Saliva

The secretion of saliva is imperative for a variety of reasons; primarily saliva contains a raft of important components, as detailed in Table 1.1-1, including digestive enzymes, which starts the digestive processes, whilst offering a protective barrier against bacterial infections. Saliva also helps to remove residual food waste between teeth and aids in the formation of the acquired enamel pellicle that prevents tartar build up and caries forming (Cassolato and Turnbull, 2003; Siqueira *et al.*, 2007).

The lubricative elements of saliva are vital for the formation and swallowing of a food bolus, also for aiding speech and maintaining mucosa integrity. Lipid content of saliva can range from 3-23ug/ml (Brasser *et al.*, 2011) and when separated chromatographically, saliva has been shown to contain squalene, cholesterol esters, wax esters, triglycerides, fatty acids and cholesterol (Brasser *et al.*, 2011). Squalene and wax esters are specific biomarkers for the sebaceous gland, squalene being a by-product of cholesterol production, the presence of these two elements specifically have been linked to maintaining moisture levels within the mouth, preventing dehydration of the labial region. Alternatively, they have been suggested to be an evolutionary inheritance from more aquatic based lifeforms as they would maintain any differences between the outside and the inside of the mouth (Lindholm *et al.*, 1981; Do *et al.*, 2009). Other lipids and fatty acids in sebum on the skin have also been indicated to have anti-microbial

properties, so it could therefore be suggested that these elements could be involved in the innate immune system in oral homeostasis (Slomiany *et al.*, 1996).

Salivary Component	Role in Oral Cavity	Effect if Lost
Water	Digestion, lubrication	No formation of food bolus and restricted movement into oesophagus
Bicarbonate	Buffers pH, neutralises acidic food	Minimised control of pH, damage to tooth enamel, lack of remineralisation
Amylase	Digestive enzyme of carbohydrates into sugars	Reduced digestive efficiency, reduced protective capacity.
Mucins	Lubrication, hydrophilic, prevents dehydration, anti-microbial barrier, digestion	Higher risk of microbial infection, damage to oral mucosa,
Salts	Maintains tonicity of saliva and pH buffer	Reduced water secretion, thick sticky saliva, reduced buffering capacity
Lipids	Lubrication, hydrophobic, prevents dehydration	Reduced swallowing and phonation, reduced protective barrier.
Growth factors	Wound healing, tissue homeostasis	Reduced repair of damaged tissue,

Table 1.1-1 Components of saliva and the impact of their loss (Tabak *et al.*, 1982; Tabak, 2006; Holsinger D. T., Holsinger and Bui, 2007; Brassler *et al.*, 2011).

Saliva is essential for maintaining the integrity of the oral mucosa, as keeping the mucosa hydrated and well lubricated can prevent the formation of small fissures, which can lead to an increased risk of infection (Cassolato and Turnbull, 2003). It is the loss of mucin

production that is one of the key elements in the initiation of a xerostomia condition (Cassolato and Turnbull, 2003; Guggenheimer and Moore, 2003).

The presence of saliva also facilitates taste sensation, lubricating vocal cords for phonation and prevents excessive demineralisation of the teeth, with experiments indicating that dental crowns have a reduced enamel erosion when previously washed with saliva (Featherstone, Behrman and Bell, 1993). The saliva also aids the formation of the acquired enamel pellicle, which is a protein film, binding salivary glycoproteins which protect against acids secreted by bacteria that would otherwise destroy tooth surface enamel (Peters *et al.*, 2010; Siqueira *et al.*, 2010). Table 1.1-1 also demonstrates that without saliva present, patients present with an increase in tooth erosion and cavity formation, they also suffer great discomfort, struggle to swallow food and have to increase drinking in order to maintain moisture levels in their mouth (Tabak *et al.*, 1982; Tabak, 2006; Thelin *et al.*, 2008).

1.2. Salivary Glands, Structure and Function

There are three pairs of major salivary glands in the human body; the parotid, the submandibular, and the sublingual glands. These are all shown in Figure 1.2-1 in a sketch depicting the location of the salivary glands within the human face. There are also between 800-1000 minor salivary glands distributed across the oral mucosa, with a considerable number in the labial region (Denny, Ball and Redman, 1997; Holsinger D. T., Holsinger and Bui, 2007). The three major glands have significant differences in their histology and their defining roles within the oral homeostasis. The parotid gland, situated in the pre-auricular region, produces enzymes used in primary digestion stages, and water-based secretions; this gland is responsible for approximately 20% of the unstimulated salivary flow in the mouth. The submandibular gland is a mixed gland, containing both serous and mucous cell types, and produces 60-70% of the unstimulated salivary flow in the oral cavity, despite being smaller in size than the parotid gland. It is situated within the confines of the mandible, below the sublingual glands. The sublingual gland is the smallest gland and sits beneath the tongue in the floor of the mouth, just below the oral mucosa. It is formed of mostly mucous secretory cells, producing mucins, lipids and other lubrication to aid swallowing and promote homeostasis of the oral mucosa. The sublingual gland is responsible for secreting only 5% of the total unstimulated salivary flow and, along with the main Bartholin's Duct, it also possesses many other smaller excretory ducts that excrete saliva into the oral cavity. In contrast, the other salivary glands follow an hierarchical duct system, with the only ducts excreting saliva being the Stenson's Duct in the parotid gland and Wharton's

Duct in the submandibular gland (Denny, Ball and Redman, 1997; Holsinger D. T., Holsinger and Bui, 2007).

Salivary gland tissue is mostly comprised of epithelial cells, with supporting stromal cells which facilitate cell-cell signalling and provide the connective tissue that separates acinar structures from one another: forming lobes and defining the arboreal appearance. Besides mesenchymal cells, there are myoepithelial cells which surround the acinar structures, enabling secretion of saliva. Sometimes referred to as basket cells, they provide passive constriction around the salivary gland lobules, enabling the unstimulated secretion of saliva by preventing further expansion of cells, but when stimulated by peripheral nerves, the α -Smooth Muscle Actin (α SMA) filaments allow for a more contractile behaviour that facilitates large amounts of saliva to be expressed by the acinar tissue.

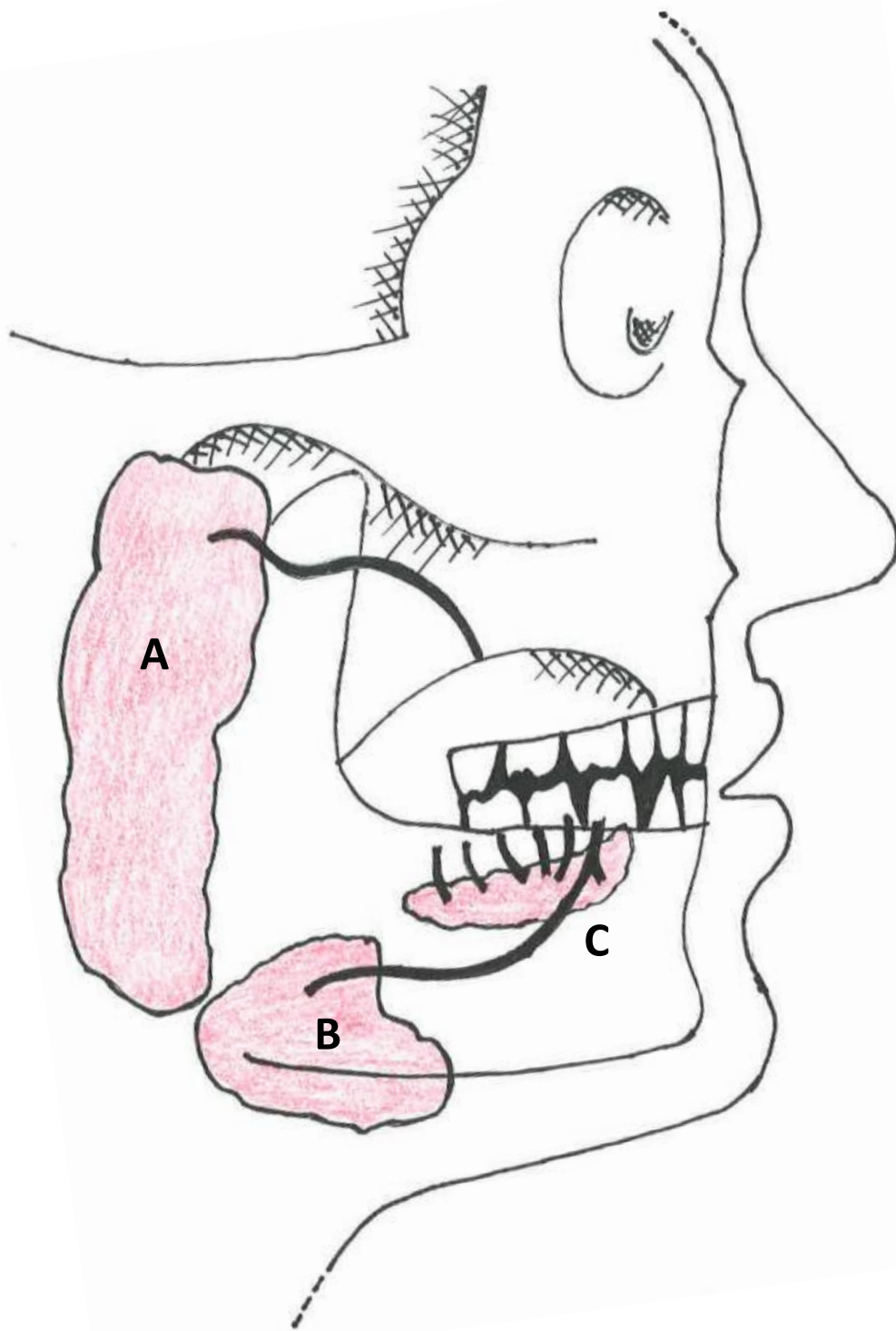


Figure 1.2-1 The sagittal view of a human head, indicating three locations for the major salivary glands; A) the parotid gland, B) the submandibular gland, C) the sublingual gland. Drawn and edited by Jonathan Davies.

The secretory units of the tissue excrete saliva into a tiered duct structure, first through small canaliculi into the intercalated duct (ID). These ducts are made of cuboidal epithelial cells, and surrounded by myoepithelial cells. It has been shown that this region of ductal tissue is rich in stem cell markers, and experiments incorporating BrdU labelling have indicated a potential for these cells to replenish cells, in a conveyor belt fashion, in either an acinar or ductal direction (Denny, Ball and Redman, 1997; Okumura *et al.*, 2003; Amano *et al.*, 2012). The ID empties saliva into the striated duct (SD) and finally into the excretory duct (ED). The SD performs a similar function to the nephron of the kidney, by moderating and selectively reabsorbing salivary contents such as sodium and potassium salts, bicarbonates, and water. It is able to perform this function due to the capillary beds providing the tissue with a counter-flow of blood (Korff and Augustin, 1999; Holsinger D. T., Holsinger and Bui, 2007; Amano *et al.*, 2012). The elevated levels of mitochondria in these cells and the basal infolding cell membranes increases the cell surface area, and results in their 'striated' appearance in electron microscopy (Amano *et al.*, 2012). Finally, the excretory duct leads saliva to the surface of the oral mucosa where it is able to perform its role in oral health and homeostasis.

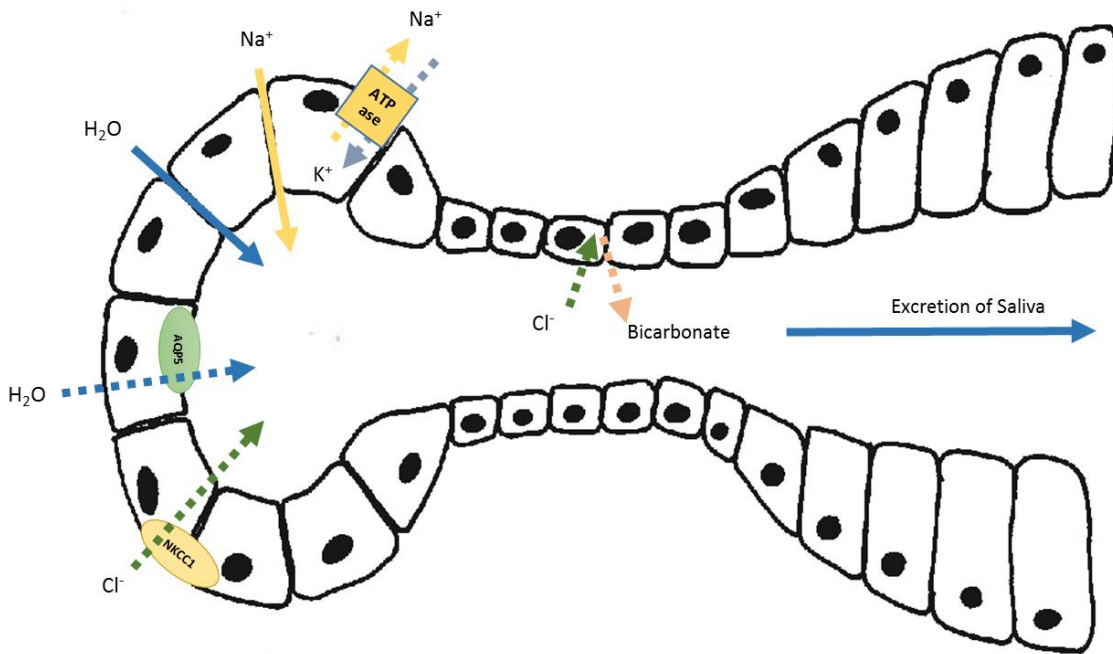


Figure 1.2-2 A diagram indicating the process of saliva secretion adapted from (Proctor, 2016). Drawn and edited by Jonathan Davies.

Figure 1.2-2 demonstrates the transport pathways that generate ionic potential across acinar cells from the basement membrane to lumen. Na⁺/K⁺ pumps maintain intracellular sodium concentration, enabling transport of Cl⁻ ions. This allows rapid movement of water by osmosis across the acinar epithelial structures to generate an isotonic saliva solution that is moderated by ductal epithelial cells as it passes along the striated ducts. Selective reabsorption of ionic salts and additional secretion of bicarbonate generates a hypotonic, buffered saliva containing a variety of essential proteins which are released from vesicles or granular exocytosis.

Cells within acinar tissue are highly polarised, with the nucleus towards the basal membrane of the cells whilst the apical membrane is dense with ion transport proteins and water channels (Proctor and Carpenter, 2014; Proctor, 2016). Tight junctions, transmembrane adhesion junctions, maintain acinar structure integrity, whilst being

'leaky' enough to allow minor passive movement of water, ions, and small proteins through from the basal membrane, between cells (paracellular) through to the lumen. In the ductal epithelium, particularly the SD, the tight junctions are more numerous, allowing no movement between cells (Baker, 2010).

As depicted in Figure 1.2-2, the movement of water from the basolateral membranes of acinar cells to the lumen is facilitated through salt secretion and active transport mechanisms. Sodium is pumped out of cells via the ATPase sodium/potassium pump, which maintains the decreasing transcellular ionic gradient (Evans and Turner, 1998). By blocking these sodium/potassium pumps, secretion of saliva can be completely inhibited (Bundgaard, Møller and Poulsen, 1977). When salivary acinar structures are stimulated by the peripheral nervous system (Proctor and Carpenter, 2014), generating an increase in intracellular calcium, a chloride influx will be observed via the chloride channel TMEM16A (Romanenko *et al.*, 2010). The movement of chloride coincides with the paracellular movement of Na⁺ ions between cells to the lumen. This hypertonic environment in the lumen facilitates osmosis of water through and around cells from the capillary beds on the basal side of the acinar structures, into the lumen. When water is being transported out of the acinar cells, the water transport membrane protein known as Aquaporin 5 becomes active. This protein is present on the apical membrane surface of acinar cells and is an established marker for fully differentiated and functional epithelial acinar cells in the salivary gland (Gresz *et al.*, 2001, 2004; Aure, Ruus and Galtung, 2014). The movement of water into the lumen turns the saliva into an isotonic solution, which is moderated as it moves along the duct structures, becoming hypotonic through the selective reabsorption of sodium and chloride ions, and potassium/proton

exchange pumps (Roussa, 2011). To maintain the movement of ions through ductal cells through to the interstitial space, ductal cell basement membranes have a microvillus structure with many mitochondria facilitating active transport of sodium and chloride (Roussa, 2011). Meanwhile, bicarbonate will be secreted by acinar and ductal cells in order to buffer the saliva to a near neutral pH, this will also aid in preventing excessive demineralisation of tooth enamel (Bardow *et al.*, 2000).

Another key component of saliva are proteins, which are secreted through exocytosis of granular structures from within the acinar cells and are known to be linked to autonomic nerve stimulation (Ambort *et al.*, 2012). This dense packaging of proteins into granules also incorporates calcium ions, which are used to “buffer” the high density positive charge of the proteins (Ambort *et al.*, 2012). The types of proteins packed and released through granular transport tend to be larger more complex charged proteins such as mucins. Smaller proteins such as digestive enzymes can be released through vesicle transport. Vesicle secretion methods are also more prevalent during non-stimulated salivary flow as the granular secretion facilitates a larger deposition of material from within a cell when required and is only stimulated when necessary (Gorr, Venkatesh and Darling, 2005; Proctor, 2016).

1.3. Salivary Gland Development

It is important for us to consider the manner in which salivary glands develop during early embryonic and foetal stages, as this will aid our understanding of the regenerative pathways that the body would attempt to mimic during recovery of damaged tissue. However, our understanding of human salivary gland development has been extrapolated from rodent and porcine animal models, although similarities between the salivary glands between the two origins are detailed in Table 1.3-1.

	Human		Mouse	
	Physiology	Secretes	Physiology	Secretes
Parotid Gland	Secretes 50% stimulated saliva, prominent adipose cells. Located at rear of mandible in front of ear.	Purely serous acinar cells, high water and enzyme secretion.	Second largest major gland.	Purely serous, high water and enzyme secretion.
Submandibular	60-70% of unstimulated salivary secretion. Located within the mandibular arch and beneath the tongue.	Mixed gland of mucous and serous cells.	Well defined duct structures. 70% of total unstimulated salivary secretion.	Only serous cells. Produces majority of saliva in mice. Highly enzymatic and non-viscous.
Sublingual	Smallest major gland. Only secretes 3-5% of unstimulated saliva. Has many small ducts that secretes into oral cavity. Located beneath and either side of the tongue.	Mixed gland of mucous and serous cells. But mostly mucous.	Has single main excretory duct that secretes behind incisors.	Mixed gland of mucous and serous cells. Mostly secretes mucous. Discrete delineation between submandibular and sublingual glands
Minor Glands	800-1000 minor glands sub oral mucosa.	Mixed glands, near-constant secretion for homeostasis and protection.	Shown to be present. Infrequently studied. (Barbeau and Deslauriers, 1995)	Assumed to be similar to humans. Lubricative elements for homeostasis.

Table 1.3-1 A demonstration of the physical similarities and functionality of salivary glands across humans and mice (Holsinger D. T., Holsinger and Bui, 2007; Amano *et al.*, 2012; Maruyama *et al.*, 2018).

The primary developmental pattern of the salivary gland tissue is similar, not only across mammalian species, but also across most epithelial based tissues within the body, such as teeth, hair follicles, nails and is highly conserved across a variety of species. Resulting in tissues that have similar functional and histological presentation, as detailed in Table 1.3-1. For example; feathers, scales and beaks all develop in very similar ways to hairs and teeth and salivary glands (Pispa and Thesleff, 2003; Li *et al.*, 2016). The later, more specific stages of development observed in salivary glands are highly conserved in other secretory organs, such as tear glands, and mammary glands (Pispa and Thesleff, 2003; Wells *et al.*, 2014).

In humans, development of the salivary glands starts with a thickening of the oral mucosa at embryonic week 6 to week 7 (Larsen, Yamada and Musselmann, 2010). As mentioned previously, the development is highly conserved in mammals and it is therefore important to note that mice salivary glands start to develop at embryonic day 11.5 (Tucker, 2007). In both mice and humans, this thickening placode forms an epithelial bud and invaginates down into the underlying mesenchyme, with the mesenchyme providing important signalling stimulation that directions the epithelial cell replication and maturation, whilst physically providing a supportive structure in which the epithelial structures can form (Pispa and Thesleff, 2003). Increased cell proliferation is observed during placode formation, but is not imperatively necessary during the stratification of the placode, with changes to cell polarity enabling invagination of the epithelial structure into the mesenchymal tissue below.

This primary bud structure undergoes dichotomisation, the formation of a cleft in the apical tip of the bud, which leads to the development of two buds. The dichotomisation

division is stimulated through molecular signalling pathways, and will lead to further budding and branching of the developing organ. This stage is known as the pseudoglandular stage, during which, the salivary gland rudiment will express 4-5 buds. Cleft formation is highly dependent on Epidermal Growth Factor (EGF) and Fibroblast Growth Factor (FGF) signalling back forth between the epithelial and mesenchymal cell populations, specifically FGFR2b and FGF10 (Pispa and Thesleff, 2003; Veltmaat *et al.*, 2003). To demonstrate the importance of these two signalling molecules, work has been done to establish phenotypes of the salivary gland in the absence of EGF and FGF signalling; EGFR1 null mice have reduced branching morphogenesis (Jaskoll and Melnick, 1999), and removing FGFRs can completely inhibit salivary gland formation (De Moerlooze *et al.*, 2000). Furthermore, Mizukoshi *et al.* demonstrated the significance of Sonic Hedgehog (SHH) signalling by activating the EGF-FGF, ERK-1/2 pathways that instigate branching in their model of ex-vivo embryonic salivary gland rudiments (Mizukoshi *et al.*, 2016).

Sonic Hedgehog (SHH) is known to be highly involved in the spatial organisation and development of many organ types, canonically it was described in embryogenesis of drosophila larvae and is key for cell polarisation and stimulating cell proliferation (Nüsslein-Volhard and Wieschaus, 1980). However, there is only a small selection of papers published on SHH in the salivary gland, whilst there is a complete absence of any studies investigating the impact of Primary Sjogren's Syndrome on SHH signalling. Although, when the SHH pathways are transiently activated in radiation exposure experiments, there is clear evidence to suggest a reduced hyposalivation phenotype in mice, either by over expression of SHH itself, or by using an agonist of Smoothed to

stimulate the downstream effectors (Hai *et al.*, 2014). This could suggest an important role in tissue recovery, post-disease or environmental impact, for elements of the SHH pathway. Evidently, without effective SHH pathways, there would be dysregulation in cell proliferation, lack of polarisation and cellular organisation, characterised by impaired or stunted salivary gland development. For example, Jaskoll *et al.*, 2004 demonstrated the importance of SHH during submandibular gland organogenesis. By culturing *ex-vivo* E18.5 salivary gland tissue samples of SHH-null mice, the team were able to treat the tissues with excess SHH peptide and they recovered the developmental phenotype of the previously underdeveloped salivary gland structures. This stimulation by SHH will stimulate the release of Gli family members from their repressive binding with SUFU, as demonstrated in Figure 1.3-1, which then go on to promote proliferation, and anti-apoptotic cues driving organ development as transcription factors (Kasper *et al.*, 2006). SHH as a well conserved pathway of activation in which the ligand SHH binds to the receptor Patched causing a conformational change, preventing the inhibition of Smoothed by Patched. The transmembrane protein Smoothed will then translocate to the cilia structures, which are protrusions of the phospholipid cell membrane known to be associated with cell signalling processes. Smoothed can activate GLI and GLIS proteins through the inhibition of the inhibitor SUFU. The GLI and GLIS proteins may be moderated further facilitating the translocation to the nucleus of the cells and fulfil their role as transcription factors.

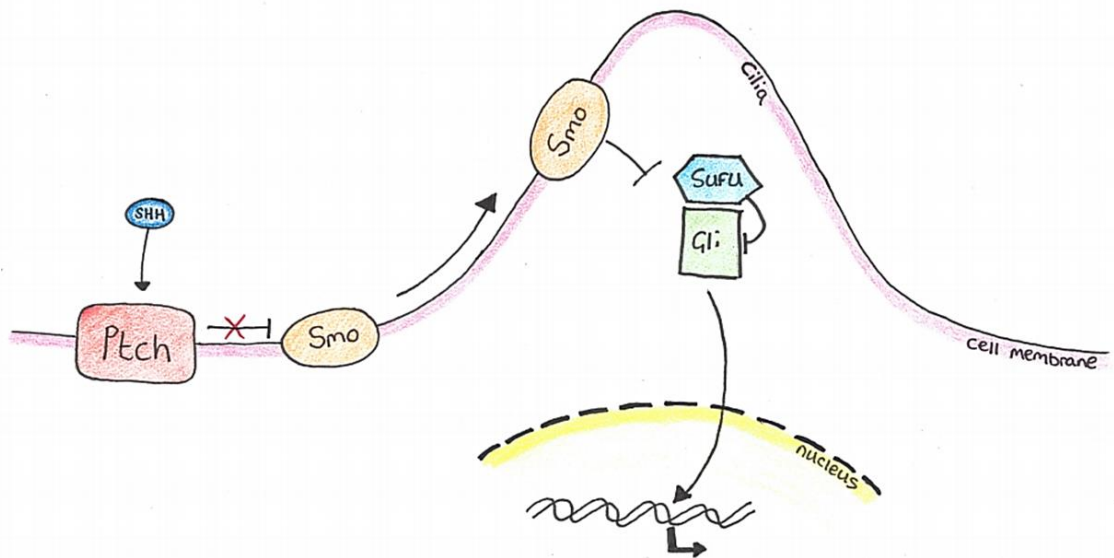


Figure 1.3-1 A diagrammatic representation of the Sonic Hedgehog (SHH) signalling pathway. The SHH signalling pathway is vital for SG organogenesis. Associated to cilia structures, when Patched 1 is deactivated by SHH, Smoothened translocates to the cilia and promotes Gli protein activation, which work as transcription factors and promote cell growth and prevents apoptosis. Figure adapted from (Huangfu and Anderson, 2006), drawn by Jonathan Davies.

However, the cleft formation is not only directed by growth factor signalling, but also by the physical presence of extra cellular matrix proteins such as various laminin isoforms and perlecan (Patel *et al.*, 2007; Rebutini *et al.*, 2007), some of which are secreted by fibroblast-like cells, dictating the structure of the supporting scaffold around the secretory tissue. This has been demonstrated in culture models of angiogenesis by using fibroblasts to secrete a dense and rich extracellular matrix that, when combined with the secretion of essential growth factors, could successfully stimulate endothelial cells to form capillary-like tubes that mimic angiogenesis *in vivo* (Berthod *et al.*, 2006).

Fibronectin is another, specific extra-cellular-matrix protein considered imperative for the branching morphogenesis pathway in salivary glands, as fibronectin accumulation around the leading bud will lead to the reduction of E-cadherin expression levels in the

epithelial cells; reducing E-cadherin stimulates a highly conserved pathway in the migration of cells, which is involved in wound healing and cancer progression. It initiates a loss of polarity and cell organisation, whilst in the developing salivary gland it allows for cleft formation to proceed (Patel, Rebutini and Hoffman, 2006; Patel and Hoffman, 2014).

At the pseudoglandular stage of development, it is possible to dissect out the developing embryonic salivary gland for use in organ culture experiments, and is frequently done to study developmental biology of the glands. The excretory duct's opening into the oral mucosa is already visible, as the lumen formation has already been initiated and starts from the oral mucosa, driving further up into the branching structures of the salivary gland. It will only appear as a small dot on the oral mucosa, but for organ culture work it is essential to preserve this structure as it is the focal orientation point from which the tissue will develop (Tucker, 2007; Wells *et al.*, 2014).

After the pseudoglandular stage follows the canilicular stage, where the epithelial structures start to form extended ducts, with lumen formation progressing as duct elongation occurs, with ductal and acinar cell differentiation. During this stage, programmed cell death and lumen formation can be observed, with apoptotic cells known to be more frequent and changes to cell polarity presenting as early as embryonic day 12.5 (Tucker, 2007; Teshima *et al.*, 2016). Finally, we have the terminally differentiated bud, in which the epithelial cells have reached their mature differentiated state, expressing markers such as AQP5, a water channel protein, and the digestive enzyme, amylase. As observed in Figure 1.3-2, we can observe a three-tiered duct structure that allows collection and deposition of saliva into the oral cavity.

Stages of Development

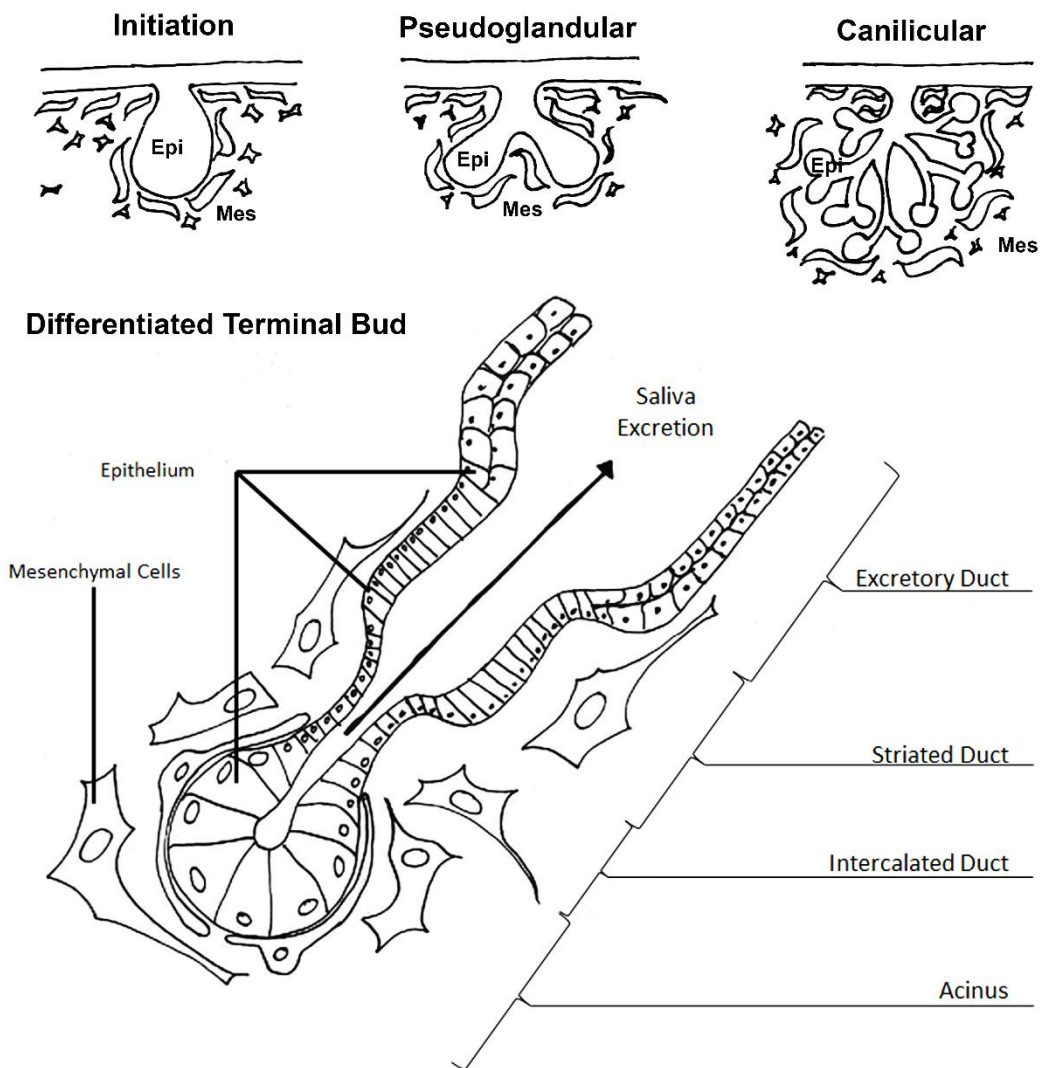


Figure 1.3-2 The stages of development of the salivary gland acinus and associated duct structures. Initiation of the epithelial membrane forms a placode and initial bud. The bud undergoes dichotomisation, which divides further and has lumen formation occur. The final image demonstrates the three-tiered duct structures and associated stromal cells. Drawn and edited by Jonathan Davies.

Damage to this complex arboreal structure could result in reduced production and transportation of saliva through the ducts into the oral cavity, resulting in xerostomia symptoms. Although not a malignant or acutely dangerous condition, it will lead to a reduction in the quality of life of patients and increase the risk of developing other infections, decrease in dental and oral health and other systemic long-term health complications (Antoniuzzi *et al.*, 2009).

1.4. Stem Cells in the Salivary Gland

The role of epithelial structures within the salivary gland is well studied and defined. Within the epithelial structures, a stem cell niche has been identified between the striated and intercalated ducts that replenishes diminished cells in the duct and acinar structures by proliferating away from the intercalated duct structures in either direction (Takahashi and Yamanaka, 2006; Sánchez Alvarado and Yamanaka, 2014; Shi *et al.*, 2017). In general, stem cells proliferate and develop into transit amplifying cells before reaching terminal differentiation; this is the classical description of stem cell life cycle. As demonstrated in Figure 1.4-1, quiescent stem cells in normal healthy tissue are self-perpetuating, proliferating in a manner that will maintain a stem cell pool. A proportion of these cells, when stimulated by the correct signalling pathways, can differentiate along a defined lineage to become transit-amplifying stem cells. The daughter cells in this cell division will maintain the population of transit amplifying cells at a stable number, but also will provide cells that are able to follow the differentiation pathway to a specific cell phenotype. Once cells have transitioned from one state to another, it was previously thought that they were unable to return to a previous state. However, with the rise of induced pluripotent stem cell research we know this is not actually the case; cells in culture can be induced into pluripotency, which has led to the investigation of the role that cells perform *in vivo* and their ability to revert naturally from fully differentiated cells into pluripotent precursors.

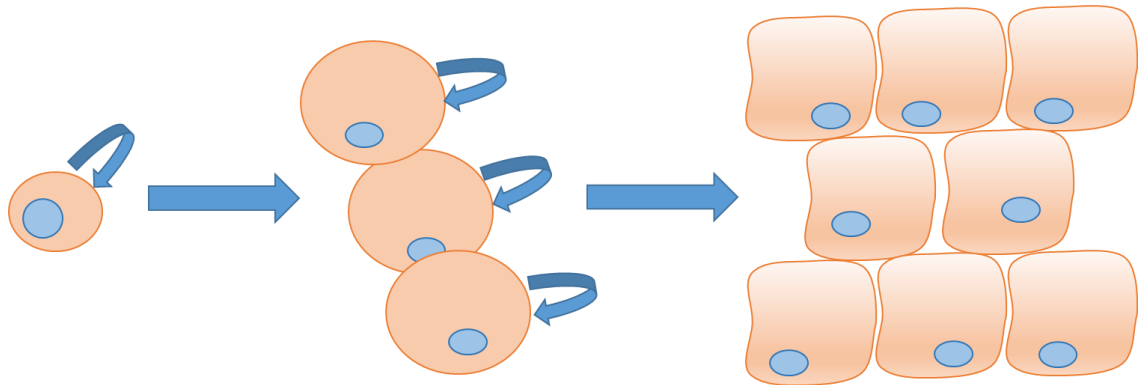


Figure 1.4-1 Pluripotent stem cell fate is a conserved mechanism across tissues. A pluripotent stem cell is capable of self-replication, and differentiating into transit amplifying or precursor cells, which can also self-replicate or transition into fully-differentiated, mature, functional cells. Drawn and edited by Jonathan Davies.

In the fully differentiated cells, the potential for post-mitotic proliferation has been demonstrated using ^3H -thymidine incorporation lineage tracing assays, where the ^3H -thymidine is only incorporated into the DNA of proliferating cells. Exposure to ^3H -thymidine is then stopped and a “chase-period” allowed to pass before detection of the levels of ^3H -thymidine in, not only the original cells that were exposed, but also the subsequent daughter cells (Denny *et al.*, 1993; Aure, Arany and Ovitt, 2015). These experiments indicate how additional daughter cells can be produced in the epithelial terminal bud, where previously it was thought to only possess fully mature and differentiated acinar cells. By creating an index of the percentage of positively marked nuclei from the total number of cells, it is then possible to identify the most proliferative regions of tissue, and then to chase the level of marked cells and their progeny to identify which regions replenish the tissue. The intercalated duct was shown to have the highest number of positive nuclei immediately after exposure. However, when the samples were left for 24 and 48 hours and incubated with a non-labelled thymidine, it was then possible to trace the progeny of exposed cells. Denny *et al* could demonstrate that over time, the striated granular duct and the acinar tissue would increase in the

number of cells positive for the ^3H -thymidine marker, suggesting that the original cells are proliferating away from the ID in a conveyor belt fashion as demonstrated in Figure 1.4-2, adapted from (Aure, Arany and Ovitt, 2015; Aure, Konieczny and Ovitt, 2015).

However, the ID was not the only duct region to take up the ^3H -thymidine: with the acinar region and other ductal sections also having a small population of positive cells. Through further label retaining cell studies and genetic lineage tracing, it was possible for Aure *et al* to demonstrate how fully differentiated salivary acinar cells could self-renew and proliferate, despite being characterised as post-mitotic. Initially, the group used a thymidine analogue, EdU to label proliferating cells. EdU becomes incorporated into the DNA of dividing cells during the S phase of the cell cycle and then the tissue is probed for antibodies raised against EdU and also other proliferative cell markers. They could identify a very small percentage of cells (0.9-1.4%) within the acinar structures, which had stained positive for EdU, a slightly larger percentage of cells also stained positive for Ki67 and NKCC1, identifying a very small population of cells that were proliferating at the time of exposure.

Developing their hypothesis further, Aure *et al* turned to R26 Brainbow2.1 reporter gene technology that enabled the identification of clonal proliferation activity in the acinar structures of the salivary gland. After a period of 6 months, whole acini were populated with fluorescently labelled clones derived from the activated cells, signifying that there was no significant contribution of ID stem cells into the secretory cell niche, as shown in Figure 1.4-2. These findings stand in stark contrast to previously established theories surrounding tissue homeostasis, which stresses the role of stem cell niches in replenishing acinar cell populations (Pringle, Van Os and Coppes, 2013). However, it was

interesting to note that the research group identified differences in clonal expansion patterns between the PG, SMG and SGs, with the SGs presenting with fewer regions of clonal expansion, more frequently presenting with preserved singularly labelled cells (Aure, Konieczny and Ovitt, 2015).

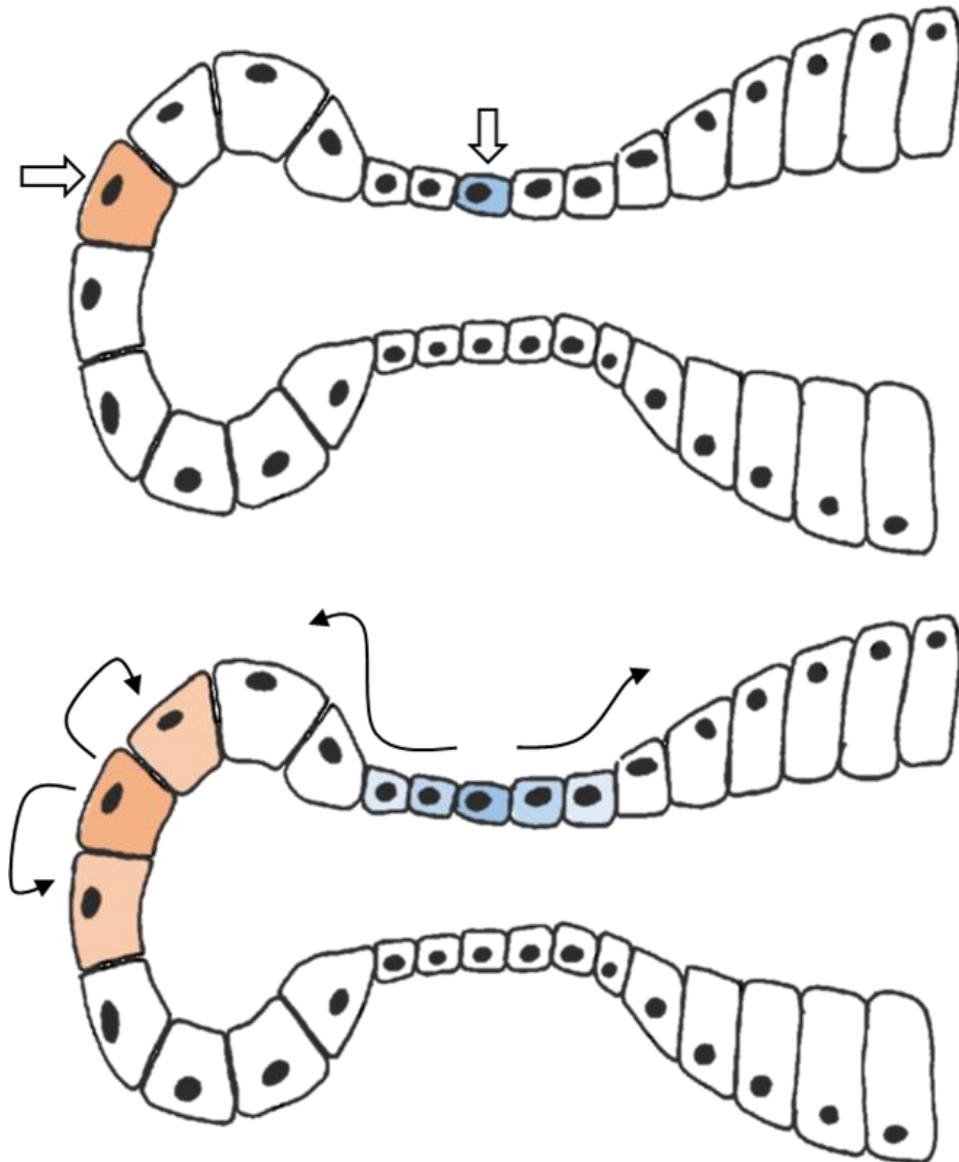


Figure 1.4-2 Processes of stem cell expansion in the salivary gland duct and acinus. Stem cells are shown to proliferate away from the intercalated duct to supply differentiated cells to the acinar and striated duct epithelial cells. However, acinar epithelial cells are post-mitotic and can replenish via clonal expansion (Aure, Arany and Ovitt, 2015; Aure, Konieczny and Ovitt, 2015). Blue coloured cells represent H3-thymidine incorporation assays, whilst orange is the Brainbow assay indicating clonal mitotic expansion. Drawn and edited by Jonathan Davies.

This suggests that, even though there is a population of stem-like cells within the salivary gland epithelial tissue, the organ is not reliant on this population for survival or to repair damage through wound healing or tissue regeneration pathways, whilst other pathways can be initiated to trigger the post-mitotic proliferation of fully differentiated cells.

Through previous knowledge of salivary gland development, it is already known that c-kit positive epithelial cells within ductal structures self-replicate to replace dying cells at the acinar blub tips of the secretory structures (Aure, Arany and Ovitt, 2015; Aure, Konieczny and Ovitt, 2015). As yet, a mesenchymal stem cell niche or population distributed throughout the salivary glands has yet to be identified and characterised. Although the range of markers to identify potential MSCs is growing, thanks to translational work from other research fields, and could be indicative of a global but infrequent distribution of MSCs throughout the tissue as opposed to a dense nucleus of cells in specific loci.

In preliminary stages of development, the mesenchyme is proportionally the larger part of the salivary gland tissue, but it diminishes throughout development to a very small percentage of the overall tissue (Holmberg and Hoffman, 2014). It is understood that the supporting tissue is not an homogenous population of mesenchymal cells, but also contains blood vessels, nerves, fibroblasts, lymphoid tissue, myoepithelial cells, and circulating immune cells (Holmberg and Hoffman, 2014). Work to understand the regenerative capacity of the mesenchymal cells, and possibly mesenchymal stem cells, and how they are affected by environmental impact, would help elaborate the complex relationship between the many populations of cells, defining which tissues are responsible for allowing recovery and tissue regeneration.

Stem cells have frequently been considered for use in therapies to reduce tissue damage and studies have been undertaken to investigate epithelial stem cells, or embryonic salivary gland stem cell populations. There is some suggestion that in Sjogren's Syndrome, or in radiation therapy exposure, stem cells of epithelial and mesenchymal origin are able to persist. But, identifying populations of stem cell or progenitor cells in human clinical samples can be difficult; as cKit has previously been suggested to be a specific stem cell marker in cultured cells derived from salivary gland tissue, but has subsequently been shown to be in very low abundance when looking at *in vivo* molecular profiles (Chibly *et al.*, 2014). By using label-retaining technology, Chibley *et al* were able to demonstrate which cells were salivary gland progenitor cells and persisted in stem cell niches in the mature gland, and therefore, which other markers were expressed by these cells. By injecting postnatal day 10 mice with EdU and harvesting organs to characterise the uptake and lineage tracing 8 weeks later. The EdU labelling was found to correspond with cells that expressed a range of other progenitor cell markers such as Keratin 5 and Kit. Furthermore, this population of cells were shown to be resistant to Ionising Radiation (IR), which offers serious clinical significance in the translation of this work to clinical conditions (Chibly *et al.*, 2014).

Alternatively, Lin Lu *et al* have successfully demonstrated the isolation, expansion and self-renewing ability of mesenchymal cell populations taken from human minor salivary glands (Lu *et al.*, 2015). By performing FACS on cells derived from human labial biopsies, and keeping these cells in culture for 5, 10, 15 and 20 passages, they could demonstrate the capacity of the cells to maintain a stem cell phenotype with the increased expression level of markers such as CD29, CD90 and Sox2, generating a 'purified' cultured stem cell

population. As is a key hallmark of Mesenchymal Stem Cells (MSCs), these cells were also induced to differentiate into; an osteogenic lineage, expressing high levels of RUNX2; adipogenic lineage, with an increase in FABP4 and PPAR γ ; a chondrogenic lineage with elevated COL2A1; and a neurogenic lineage with elevated Nestin (Lu *et al.*, 2015). These types of induced differentiation experiments are frequently observed in studies demonstrating that their isolated cell types are purified mesenchymal stem cell populations. However, due to the strength of the induction, our understanding of required growth factors etc, and the frequency that this is able to happen, it may be suggested that this test is becoming more redundant over time.

For many types of assays, cells are isolated from mouse or human salivary gland tissue. However, it is also possible to induce a desired cell phenotype from isolated stem cells. For example; it has been shown that stem cells isolated from adipose tissue can be induced into an epithelial acinar phenotype and were shown to display the typical markers of these cells (Lee, Park and Roh, 2015). This was achieved by co-culturing cells together in trans-well insert culture conditions, or by using conditioned media from acinar derived cells to induce a change of phenotype. The conclusion of this work was that this method could be used to generate suitable cells to transplant into a patient suffering from hyposalivation or tissue destruction from radiotherapy by taking cells from any fat pads in the body instead of relying on sourcing cells from heavily depleted acinar structures or from allogenic grafts.

MSCs within salivary gland tissue are having markers attributed to them more frequently as more research focuses on this cell niche. Through selection of mesenchymal cells from bone marrow and fat tissue using FACS or MACS, it is possible to procure a

mesenchymal stem cell population from the stromal tissue surrounding the acinar structures. Using a panel of mesenchymal stem cell markers, raised against bone marrow derived mesenchymal stem cells, it is possible to generate a panel which positively marks the salivary gland MSC niche. Some of the markers identified include CD90, CD105, CD106, CD29, PDGFR β and CD44 (Jones *et al.*, 2002; Dominici *et al.*, 2006; Bühring *et al.*, 2007; Schwarz and Rotter, 2012; Schwarz *et al.*, 2014). However, CD106 is also known as VCAM1 and can be highly present on endothelial cells, whilst CD44 is present on migrating white blood cells, so therefore could suggest an impure cell population in the works above. The expression of the above markers, and absence of markers such as CD45 and CD34, is defined as one of the key characteristics that proscribe MSCs. These cells also should be observed to be plastic in nature with the potential to be induced into different lineages, as well as being adherent in cell culture conditions (Dominici *et al.*, 2006).

MSCs are driven through maturation by the structure of basement membrane proteins, and various transcription factors, dictating which cell lineage is desired. A key marker of mesenchymal stem cell identity is that any cell from any origin can be stimulated down a chondrogenic, adipogenic or osteogenic lineage (Pittenger *et al.*, 1999a). Culture conditions containing a raft of chemicals that drive differentiation down these different lineages have been used as proof of multipotency in MSCs. Therefore, this has facilitated research such as injecting MSCs, identified by their multipotency potential, into irradiated salivary gland structures and demonstrating an ability of these to differentiate and restore functionality to the affected tissue (Lv *et al.*, 2014; Schwarz *et al.*, 2014; Chen *et al.*, 2016; Han *et al.*, 2017)

1.5. Diseases Affecting Salivary Gland Tissue

This research will specifically focus on salivary gland tissue affected by Primary Sjogren's Syndrome (PSS), as currently there is little understanding of how the disease is initiated, and how it impacts the individual cell niches within the salivary gland tissue. We will also look at radiotherapy exposure and the damage that this can cause to the tissue. Other conditions that are known to damage the tissue and reduce salivary flow rates are sialadenitis (inflammation of salivary gland due to bacteria or viral infection), sialolithiasis (salivary gland stones), and blunt force trauma.

The epidemiology of PSS is contested because of the late presentation in clinics and the prevalence in certain populations, such as the elderly, giving large biases within PSS studies (Mavragani and Moutsopoulos, 2010; Bolstad and Skarstein, 2016). In generic population studies such as one from China (Zhang *et al.*, 1995) and one from Slovenia (Tomsic *et al.*, 1999), they found that 0.7% or 0.6% of the population present with PSS respectively. This is compared to a study from Norway (Roesink *et al.*, 2001) in which participants were at least 80 years of age; this study identified a 3.39% prevalence of PSS in their population, and demonstrated that the incidence of PSS increases with age.

Of patients that present with PSS in clinical situations, 90% will present with oral dryness, 50% will have parotid gland enlargement and 95% will suffer from ocular dryness (Skopouli *et al.*, 2000). We are focussing on PSS, rather than secondary Sjogren's syndrome, as the second is normally acquired by patients who already present with an autoimmune condition; frequently presenting with rheumatoid arthritis or lupus erythematosus. Working with patient samples that have confounding disease conditions

could impact our understanding of the disease condition, whilst working with PSS patient samples enables us to control more variables within our scientific experimental design.

Meanwhile, in patients who have received radiation therapy for head and neck cancers, more than 90% of patients will experience hyposalivation (Epstein *et al.*, 1999), with other conditions such as pain, dysphagia, and increased tooth decay being recorded (Dirix, Nuyts and Van Den Bogaert, 2006).

As the condition of hyposalivation or xerostomia is subjective, it may be difficult to directly compare results from different studies. It may also be the case that patients go un-detected because of their lack of awareness of the condition or their elevated perception of oral or ocular dryness. Alternatively, there may be cultural beliefs that older people will suffer from dry mouth symptoms and medical assistance may not be sought. With 30% of people over 65 years of age suffering from some form of dry mouth, it is easy to see how these misconceptions may have arisen (Baer and Walitt, 2017).

1.5.1.Sjogren's Syndrome

Sjogren's Syndrome is a systemic autoimmune disease that destroys secretory tissue, such as salivary glands, lacrimal glands, and vaginal lubricative glands. It is a debilitating condition that has no unanimously agreed upon cause and the mechanisms of disease are subject to investigation. Without the ability to secrete saliva, the PSS (Primary Sjogren's Syndrome) patient suffers a decrease in quality of life through a reduced ability to digest food, phonation, swallowing, impaired oral health due to reduced innate immune responses, increased risk of dental caries and periodontitis (Jorkjend *et al.*, 2003; Antoniazzi *et al.*, 2009; Mavragani and Moutsopoulos, 2014a). The majority of patients diagnosed with this condition are post-menopausal women, with less than 10% of the patients being male (Mavragani, Fragoulis and Moutsopoulos, 2012), suggesting some implications for the hormonal moderations of menopause for the initiation of the disease.

Diagnosis of the condition must be confirmed with minor salivary gland biopsies, with haematoxylin and eosin staining that demonstrates immune infiltrate focal lesions (Pijpe *et al.*, 2007; Carubbi *et al.*, 2014). Patient tissue is assigned a focus score and will also be tested for auto-antibody positivity against Ro/SSA and La/SSB. This invasive biopsy will most frequently be taken from the labial region of the oral mucosa, and only from patients who have presented with PSS symptoms, such as xerostomia, poor oral health, difficulty swallowing, dry eyes, cutaneous dryness and irritation, dry vagina, and other sicca symptoms (Mavragani and Moutsopoulos, 2014a). There is also an indication that taking small punch biopsies from the skin could also be used as an effective diagnostic method, or even a secondary method to catch patients who may not test positive

through the normal salivary gland biopsies (Roguedas *et al.*, 2010; Tobón *et al.*, 2011). It is newly established that some healthy control patients can also present with very small focal lesions despite not presenting with any other symptoms or displaying other pathogenic phenotypes (Radfar *et al.*, 2002).

Patients will frequently present when the disease has already inflicted damage on the tissue (Mavragani and Moutsopoulos, 2014b), so understanding the very first stages of the disease is particularly difficult. However, in large cohort studies there is the chance of identifying individuals with early stages of PSS and occasionally individuals in their mid-twenties are known to present with the disease, which may be acute forms of the disease or could provide insight into the earlier stages of disease initiation (Sandhya *et al.*, 2015; Khalele, 2016). Histologically, early presentations of the disease would commonly include small focal infiltrates of CD4 positive T cells surrounding ductal structures in the salivary gland (Voulgarelis and Tzioufas, 2010; Kramer, 2014; Mavragani and Moutsopoulos, 2014a; Evans *et al.*, 2016). This progresses to larger lesions, with destruction of neighbouring secretory acinar tissue, auto-antibodies start to be produced, giving rise to the specific destruction of the acinar secretory tissue. The destruction of this tissue mainly happens through apoptosis (Herrera-Esparza *et al.*, 2008) which could also be the main pathway in which auto-antigens are generated against Ro/SSA and La/SSB, as apoptotic keratinocytes have been found to present these markers on their cell surface (Casciola-Rosen, Anhalt and Rosen, 1994; Katsiogiannis *et al.*, 2006; Katsiogiannis, Tenta and Skopouli, 2015). Although there is the suggestion that autophagy could aid in the presentation of antigens and increased tissue loss, demonstrated by a study linking elevated autophagy of T cells with the focus score and

disease progression in patients (Katsiogiannis, Tenta and Skopouli, 2015; Alessandri *et al.*, 2017). Regardless, any tissue that is damaged through these cell death pathways is not repaired or replaced; instead fibrotic lesions are deposited and cannot be removed by the body (Skopouli *et al.*, 1998) (Carubbi *et al.*, 2014; Kramer, 2014).

The lesions will increase in size as the CD4 positive T cells start to recruit dendritic cells and CD19 positive B cells, replacing the epithelial secretory tissue with immune infiltrates and fibrous scar tissue, reducing the ability of the salivary glands to produce sufficient saliva. These B cells can then form dense foci which have the potential to develop germinal centres with heightened lymphoproliferation; a precursor and risk factor for developing Non-Hodgkin's Lymphoma (Voulgarelis and Tzioufas, 2010; Nocturne and Mariette, 2013). Alongside acinar destruction, it has been shown that ductal epithelial tissue hyperproliferates to generate epi-myoeptithelial islands (Morgan and Castleman, 1953; Anderson and Talal, 1972). It is important to note this phenomenon, as the primary focal lesions appear in the peri-ductal regions of the tissue, and the auto-antibodies present in PSS are raised against Ro/SSA and La/SSB, two markers which are present in healthy ductal epithelial cells. Lymphoproliferative lesions are not just restrained to the glandular tissue; with extreme cases of advanced PSS, there are recorded cases of extra-glandular malignant lymphoproliferation affecting neighbouring lymph nodes and peripheral tissue, leading to a much more significant prognosis for the patient (Anderson and Talal, 1972).

Although no initiation pathways have been conclusively proven, the process of immune cell recruitment is well established and is described in Figure 1.5-1. Whether the initiation event is a change in hormones, exposure to pathogens or a combination of

environmental influences, this recruitment of immune cells and antigen presentation is highly conserved. Furthermore, it has been noted that epithelial cells have the potential to perform the role of antigen presenting cells and they do secrete chemokines that would result in the immune recruitment seen in PSS (Tsunawaki *et al.*, 2002). The epithelial structures become dysregulated in patients with PSS, stimulated by inflammatory cytokines TNF- α and IFN- γ , with reduced tight junction formation and therefore redistribution or down regulation of claudin-3 and -4, and ZO-1 (Ewert *et al.*, 2010).

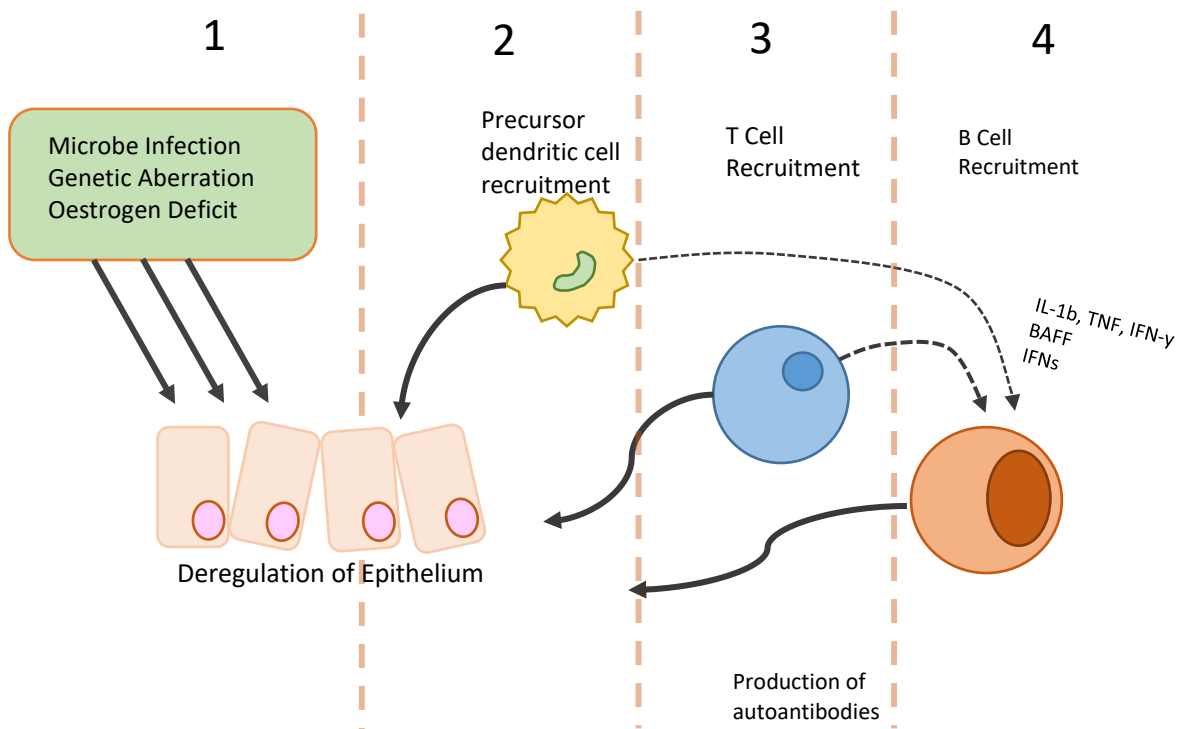


Figure 1.5-1 The stages of Primary Sjogren's Syndrome (PSS) progression, from an unknown initiation event that stimulates an autoimmune response through the activation of T Cells, the presentation of auto-antigens that generates auto-antibodies, and the recruitment of B Cells into the target tissue.

The mortality rates of patients with PSS is only mildly elevated, mostly since the disease may be chronic but is not often life threatening. Any increased risk of attrition is closely correlated to the development of a more advanced lymphoproliferative disease, leading to non-Hodgkin's lymphoma, or the associated elevated risk of developing cardiac diseases and other complex rheumatic diseases, when already diagnosed with one autoimmune disease (Mavragani and Moutsopoulos, 2010; Valim *et al.*, 2016).

The morbidity of the condition is varied yet significant, potentially having significant effects systemically on the deterioration of other organs. PSS has proven links to atherosclerosis, rheumatoid arthritis, periodontitis, nephritis, and interstitial lung disease (Parambil *et al.*, 2006; Valim *et al.*, 2016). PSS patients are more likely to develop heart related conditions such as hypertension and dyslipidaemia, which can lead to an elevated risk of atherosclerosis (Valim *et al.*, 2016). Whilst also being at a significant risk of developing non-Hodgkin's Lymphoma (Antoniazzi *et al.*, 2009; Voulgarelis and Tzioufas, 2010; Voulgarelis *et al.*, 2012; Kramer, 2014). One key finding was that patients with PSS who were positive for autoantibodies, would have a significantly low ankle-brachial blood pressure ratio, an associated symptom for increased risk of peripheral arterial disease and atherosclerosis (Garcia *et al.*, 2016). Furthermore, patients with interstitial lung diseases, such as pneumonia, may develop exacerbated progression of the disease if they also have PSS. There appears to be an increased morbidity and mortality rate due to the complications associated with additional presence of PSS, which may only be curtailed with treatment by prednisone and other immunosuppressant therapies (Parambil *et al.*, 2006).

Treatment with Rituximab, which is an anti-CD20 antibody, and previously used to treat some cancers and Rheumatoid Arthritis and Lupus Erythematosus, has been shown to have a significant impact on improving salivary flow rate reducing lesion sizes and diminishing germinal centres in patients with PSS (Pijpe *et al.*, 2009). However, the study itself recognises that more trials would need to be carried out to confirm their results and to assess the potential off-target effects and other dangerous side effects. They have further shown that acinar tissue does proliferate and striated duct tissue has re-differentiated, indicating a novel therapeutic approach to treat PSS patients (Delli *et al.*, 2016).

In the majority of the research concerning PSS, the main focus is on regenerating epithelial tissue, sometimes with the aid of other tissue types, and investigating the initiation and progression of the disease and effect on the epithelial tissue (Knox *et al.*, 2013; Nelson *et al.*, 2013). However, as discussed previously, there are many cell types within the salivary gland tissue and we believe that the mesenchymal cells are a particular cellular niche that is understudied and work should be done to investigate how these cells are impacted by PSS; specifically, if these cells are involved in the initiation pathways of the disease, how these cells change during PSS and if this could be contributing to the inability of the tissue to recover functionality.

Attempts to produce Sjogren's syndrome animal models have had limitations but are invaluable for studying preliminary stages of disease initiation, potentially identifying early stage clinical markers. In theory, PSS models would enable scientists to develop potential therapies and characterise the negative impact of the disease on distinct aspects of the tissue. One of these models, using generic NOD/ShiLtJ mice (Non-Obese

Diabetic Mice) promises a systemic autoimmune exocrinopathy which would mimic PSS. The tissue does present with significant immune infiltrations, however, the phenotypical changes to cell marker expression, and tissue apoptosis is not observed as it is in human clinical cases (Gervais *et al.*, 2015). Some NOD mice strains have spontaneously generated xerostomia symptoms and autoimmune pathologies, the development of these spontaneous autoimmune models has produced; NZB/W F1, MRL/lpr, and NFS/sld mice. NFS/sld mice suffer from excessive mucous producing acinar cells due to a premature disturbance in the cell differentiation pathway, but also present with CD4+ T cell focal infiltrates that greatly mimic human PSS (Haneji *et al.*, 1994).

Due to the variety of mouse lines produced, some NOD models do not express any decrease in salivary function. For example, the NOD. IFN- γ -/- mice, lacked the presence of immune infiltrates. IFN- γ is a T-helper cell cytokine and appears to be essential for initiating autoimmune exocrinopathies such as PSS (Meng *et al.*, 2017). In the IFN- γ knock out models, these pro-inflammatory cytokines aren't produced, therefore T cells aren't recruited and the key stages of the immune infiltrations are not initiated (Cha *et al.*, 2004). The mice do not present with an autoimmune condition, and do not develop focal lesions of immune cells; therefore, it cannot be considered a model for PSS. Knocking out IFN- γ would prevent the normal immune processes in patients, limiting the translational application of this knowledge.

The more successful Sjogren's Syndrome models are genetically engineered mice lines as they allow the manipulation of specific genes of interest on the outcome of disease in the tissue. For example, the ID3 knockout mice, which suffer interference of B cell development and immune cell survival, will develop lymphocyte infiltrations (Pan *et al.*,

1999). These infiltrations will affect lacrimal and salivary glands, with the effects apparently increasing with the age of the mouse, a phenomenon that correlates strongly with PSS. ID3 regulates proliferation of cells through the control of transcription factor binding mechanisms, particularly having influence over T-cell receptor expression, an effect that could be linked to an increase in tumour formation in these mice (Li *et al.*, 2010). ID3 KO mice appear to suffer from general immune reactivity as well as developing this PSS phenotype, with immune lesions identified in both salivary and lacrimal glands.

To the best of our knowledge there has not been any correlation demonstrated between PSS and the SHH signalling pathway and we feel that this is a key area for investigation within the field of PSS research, as any impact on SHH could be a potential cause of a reduced regenerative environment. During PSS, we observe a reduction in the secretory epithelial structure, an increase in apoptotic markers within the ductal tissue, but fail to observe an increase in proliferation markers in PSS positive labial biopsies (Herrera-Esparza *et al.*, 2008). SHH should promote cell proliferation and prevent apoptosis, so it would be of interest to investigate if these pathways are diminished within PSS as a mechanistic reason for impaired tissue regeneration.

1.5.2. Radiotherapy

Radiotherapy is used as a keystone therapy for patients diagnosed with head and neck tumours, however, there is significant impact on salivary flow rates of these patients. The irradiation of salivary gland tissue causes direct tissue damage, resulting in hyposalivation, which can lead to more serious complications and a reduced quality of life for patients. However, the self-renewal ability of the tissue is also affected, meaning that the tissue is unable to return to pre-exposure levels of salivary production (Braam *et al.*, 2005).

As an example of a routine treatment, patients who have been diagnosed with head or neck cancers would be given high intensity doses of 20Gy followed by adjuvant therapies of 2Gy, possibly up to a total dosage of 70Gy, this may or may not be used in conjunction with surgery and chemotherapy (Dirix, Nuyts and Van Den Bogaert, 2006; Grundmann, Mitchell and Limesand, 2009; Vissink *et al.*, 2015).

Immediately after treatment, the salivary flow rate is greatly reduced, often from 50-60% decrease in functionality (Franzén *et al.*, 1992; Dirix, Nuyts and Van Den Bogaert, 2006), and will slowly return over a period of 24 months, but it will never reach the same level of production as before IR treatment (Roesink *et al.*, 2001; Braam *et al.*, 2005).

Cell death will follow one of three established pathways: apoptosis, necrosis and autophagy. Apoptosis is a method of programmed cell death which breaks cells down into small fragments which can be phagocytosed and removed with no further damage to surrounding tissue. It is a highly regulated pathway and can be stimulated by the cell detecting stress or by neighbouring cells detecting stress and stimulating the target cell

to undergo apoptosis. The process can be detected in tissue by demonstrating activation of caspase-3, which are proteases responsible for initiating the cell destruction, the externalisation of phosphatidylserine, or identifying physiological changes to cell morphology such as nuclear condensation, or apoptotic blebbing (Krysko *et al.*, 2008).

Alternatively, necrosis is characterised by a degradation of organelle structures, a cytoplasmic swelling, and a terminal rupturing of the cell membrane (Krysko *et al.*, 2008). Necrosis is normally associated with unwanted cell death and damage to tissue, frequently linked to environmental impact and increased stress impacting cell function and survival. The stress induced death can be rapid and instantaneous, however, it is also known that certain signalling pathways are also capable of inducing necrosis in a more controlled and regulated manner (Festjens, Vanden Berghe and Vandenabeele, 2006).

Through both of these pathways, immune cells are recruited in order to clear dead cells and instigate an immune response in the neighbouring tissue. Both apoptotic and necrotic cells will be phagocytosed by macrophages, but this happens through different pathways, and can be used to aid the identification of the different type of cell death occurring. Apoptotic cells will produce blebs, which are sections of cell membrane engulfing small portions of the cytoplasm and recycled organelles. These blebs will be phagocytosed through the 'zipper' method, where the cell membrane of the macrophage will fuse with that of the bleb and will internalise the whole structure before recycling the contents internally in an endosome. Necrotic cells will rupture quickly, therefore, the cell debris is cleared by pinocytosis, the internalisation and active

transport of cellular debris into endosomes. These differences can be observed through transmission electron microscopy (Krysko *et al.*, 2008).

Finally, autophagy is characterised by the digestion and recycling of cytoplasmic components that can be utilised in either a protective or pro-death manner (Martinet *et al.*, 2006). It is a key pathway that balances resources at critical moments within tissue homeostasis. The process is used in a 'last-ditch- attempt to protect tissue homeostasis during external stresses (Morgan-Bathke *et al.*, 2015). It is a highly conserved pathway from bacteria that promotes survival by the removal of waste or under used cellular components. The process starts with the formation of a phagophore, which collects cellular components into a double membrane structure. This 'cargo' and phagophore structure fuses with the lysosome to form an autophagosome, in which acids and proteases can digest the contents through proteolytic degradation (Glick, Barth and Macleod, 2010). Within autophagy, elements that are still poorly understood are the process in which the cell decides which cellular components to target for degradation, and how the initial phagosome forms, and which cellular signalling pathways are triggering this self-degradation pathway (Glick, Barth and Macleod, 2010).

Although we know that apoptosis has a significant role to play within the degradation of tissue exposed to IR, the inclusion of necrosis and autophagy cannot be discounted and currently there is not enough knowledge of these pathways to conclusively agree on their involvement. Particularly as the exposure to IR generates an incredibly stressful environment for the salivary gland tissue, it could be naïve to not consider the potential role necrosis has to play in the initial disease state, and how autophagy may be being

used in an attempt to preserve as much of the tissue as possible whilst also contributing to major cell loss.

In clinical samples, it is difficult to judge the immediate causes of tissue attrition, as biopsies are not often taken immediately after radiotherapy, or before as controls. However, by using animal models, we can extrapolate findings to estimate the impact of IR on the salivary glands. In rat IR experiments, it was concluded that only 2-3% of cells had undergone apoptosis 6 hours after exposure to doses ranging from 2.5 to 25Gy (Paardekooper *et al.*, 1998). However, mice had a much more significant correlation between dose and level of apoptosis, this time detected by caspase-3 staining, with approximately 30% of the salivary gland cells testing positive for apoptosis after a single dose of 5Gy, 24 hours after exposure (Humphries *et al.*, 2006).

From whichever process of cell death, it is evident that the salivary gland tissue is considerably impaired due to exposure of IR and therefore, it must be suggested that immune recruitment and cell signalling pathways are also involved in preventing tissue recovery and impacting salivary flow. There is also the suggestion that even small incidence of cell death could result in cell signalling cascades that could inhibit saliva production of neighbouring cells by disrupting the muscarinic receptor pathway that involved in stimulating secreting of saliva. Further damage to the tissue results from the death of stem cell populations and a lack of ability to replace the functional acinar cells (Konings, Coppes and Vissink, 2005).

Multiple other pathways could also be responsible for the dysregulation and damage to salivary gland tissue, including the activation of p53 pathway. Exposure to IR was shown to increase p53 expression and increase apoptosis within mice salivary gland tissue, this

phenomenon was inverted in transgenic mice that overexpressed the anti-apoptotic Akt protein, with less apoptosis occurring and preservation of the tissue (Limesand, Schwertfeger and Anderson, 2006). Alternatively, p53 null mice did not express markers of apoptosis and had a preserved salivary flow rate after being exposed to 2-5Gy of IR (Grundmann, Mitchell and Limesand, 2009).

In IR exposed tissue, here has been observed a decrease in expression of salivary excretory proteins such as AQP5, which is an essential water channel protein involved in the secretion of saliva. However, when tissue was treated with cevimeline (an agonist for parasympathetic salivary gland stimulation) pre-IR exposure, the mice being used did not present with such a decrease in salivary flow as untreated animals, and AQP5 expression was not depleted to the same degree (Takakura *et al.*, 2007).

There are other pathways that are instigated by exposure to IR that could contribute to salivary gland dysfunction; the creation of free radicals disrupts plasma membranes and cause DNA damage, the direct impact on tissue vasculature has the potential to generate an ischemic environment that results in hypoxia and later, will cause cell death long after the primary initiation stages of IR impact. Duct obstruction would also initiate inflammatory pathways with the release of histamines and inflammatory cytokines.

The initial cell death is compounded by the deposition of radiation-induced fibrotic lesions, as described by Delanian *et al* (Delanian and Lefaix, 2004). They suggest that the residual fibroblast cells are dysregulated and overexpress extra cellular matrix component (Delanian and Lefaix, 2004; Stramandinoli-Zanicotti *et al.*, 2013). These lesions were previously thought to be an irreversible and permanent damage inflicted on the salivary gland tissue, however, there has been significant strides in treating

patients with pentoxifylline and vitamin-E during RT with significant reduction in fibrotic lesions being observed (Delanian *et al.*, 2005). Salivary glands are some of the most radio-sensitive organs in the body and suffer severely when exposed in comparison to other tissues (Rubin and Casarett, 1968). The susceptibility of the salivary glands to the effects of IR are surprising as the tissue is mostly post-mitotic, with few established stem cell populations or differentiating cells, and it is classically agreed upon that post-mitotic tissue is reasonably resistant to ionising radiation exposure, but this is not the case with salivary gland tissue (Nagler, 2002).

Exposure to IR will not only damage the acinar secretory cells but will also impact the salivary vasculature. Alongside interstitial fibrosis, dilation of blood vessels can be observed in tissue exposed to IR, with an increase in capillary permeability (Okumura, Shinohara and Endo, 2012). This direct impact on the vasculature can have long term secondary impacts on the tissue by impeding regeneration, or causing a secondary loss of tissue (Grundmann, Mitchell and Limesand, 2009). Treatment with G-CSF (granulocyte colony stimulating factor) can mitigate some of the vascular damage, by stimulating the recruitment of bone marrow cells to the site of injury where they differentiate into vascular endothelial cells in an established, wound healing, repair mechanism. Furthermore, treatment with pilocarpine before IR can stimulate cellular proliferation in an attempt to mitigate the amount of damage caused during exposure (Lombaert, Brunsting, Wierenga, *et al.*, 2008; Burlage *et al.*, 2009; Okumura, Shinohara and Endo, 2012).

The most common lesions during exposure to ionizing radiation, x-rays and some anti-tumour drugs, are DNA double stranded breaks, single stranded breaks, and intra- and

inter-strand crosslinking. DNA breaks can be detected by the proteins KU70/80 and DNA-PK, which initiate phosphorylation pathways to initiate repair mechanisms (Elmore, 2007). Furthermore, there are complex signalling cascades, involving Brca1 and Brca2, P53, and ATM, all known to have established roles in cancer progression and metastasis, which all facilitate DNA repair (Lee *et al.*, 2010; Maréchal and Zou, 2013; Toufektchan and Toledo, 2018). These pathways determine cell fate into one of four directions; 1) DNA is successfully repaired, 2) the cell cycle is arrested, 3) cells undergo apoptosis, and 4) cells enter a senescent state (Blanpain *et al.*, 2011; Mandal, Blanpain and Rossi, 2011). All of these fates will occur in salivary gland tissue exposed to x-ray irradiation to varying degrees and will result in tissue loss and atrophy, and a reduced capacity for tissue regeneration. Coppes *et al* demonstrated that cells taken from the salivary gland of mice exposed to x-ray irradiation have a reduced proliferative capacity compared to unexposed controls, but this potential was on a similar proliferative level to cells taken from aged mice, indicating that IR exposure could prematurely age salivary gland tissue (Coppes and Stokman, 2011; Maimets *et al.*, 2015).

Van Luijk *et al* have investigated the effects of “shower-and-bath” exposures at lethal and sub-lethal doses of radiation, and how these lower dose levels and more distributed exposures can further damage the tissue. Their outcome was that using higher doses in very targeted therapy would be more appropriate to conserve as much tissue as possible, and minimise any offsite damage (van Luijk *et al.*, 2009; Vissink *et al.*, 2015). This research group also demonstrated the effect of preserving very specific regions of tissue before radiation therapy. They demonstrated that within the parotid salivary gland of rats, there is a highly c-kit positive region in the epithelial structures of the

intercalated ducts that contained a larger proportion of stem cells than any other region of the epithelial tissue. It was shown that, if IR therapy could be applied to the tissue whilst minimising the exposure to these specific regions, the tissue would have a greater propensity to regenerate (van Luijk *et al.*, 2015). These findings would be enough to help improve patient outcome during treatment, but it still doesn't help to explain how specific cell niches are affected in the salivary gland tissue when exposed to IR.

Exposure to RT causes MSCs to undergo some form of cell death but can also lead to stochastic changes within the cell. We observe an increase in gene expression relating to toxicity and stress response, and a decrease in cell number when working with cultured cells (Guo *et al.*, 2015). Furthermore, when mice who have been exposed to acute radiation are left untreated, we observe animal death, tissue damage through apoptosis and necrosis and a reduced immune response. However, this can be mitigated through treatment with haematopoietic MSCs, suggesting that the residual MSC populations within the tissue are negatively impacted by the radiation exposure, and only with the replacement of these damaged cells through a transplant of BMCs will the tissue survive and recover functionality (Hu *et al.*, 2010).

In order to translate previous experimental knowledge to a large mammal model, that would closely mimic patient experience of IR exposure, researchers have turned to Brazilian mini-pigs. The pigs were exposed to IR treatments, which would be relative to patient therapeutic doses, over a three-week treatment course, before having parotid salivary glands removed and studied histologically. The research group were able to demonstrate acinar atrophy, reduced volume of the whole gland, hyperchromatic aberrant nuclei, ductal dilation and significant fibrosis associated with cellular debris

(Stramandinoli-Zanicotti *et al.*, 2013). The group is hoping that this model could be used and developed to model treatments to prevent or mitigate tissue damage during radiation therapy.

One mechanism to be investigated is incubating cells with basic FGF for four hours before IR exposure and immediately post exposure. This treatment of cell cultures appears to send cells into a longer G2 cell cycle phase, allowing a greater chance for recovery before mitosis, and increasing clonogenic survival (Cohen-Jonathan *et al.*, 1997; Ree *et al.*, 2006; Blanpain *et al.*, 2011). At the end of the G2 phase, there is a cell cycle checkpoint during which the cell is able to detect DNA damage and will attempt to repair. When cell cycle arrest at G2 is inhibited, this checkpoint does not take place and cell death is demonstrated to increase (Ree *et al.*, 2006). The authors suggest that the stem cells are likely to be impacted by IR and, by pushing the cells into the cell cycle but not yet at mitosis, cells have a better chance of survival and are able to repair any DNA damaging effects as they occur. Because of this mechanism, cells that have entered a quiescent state will accumulate genetic mutations without being able to repair them, until the cells re-enter the cell cycle and have the potential to form tumours or result in increased cell death (Kim *et al.*, 2015; Minakawa *et al.*, 2016). This compounds the initial loss of tissue from radiation exposure, with a secondary loss of cells as the quiescent cell population start to proliferate in an attempt to replenish lost tissue, resulting in more cell death and reduction in the resident quiescent stem cell population.

The risks of tissue damage will always be associated with radiotherapy but these studies have suggested ways to reduce the impact by minimising exposure or to promote innate repair and response mechanisms. What is yet to be answered is: how have each of the

cell niches specifically changed in the residual tissue post-exposure, particularly the mesenchymal cells, and how is this change preventing the ability of the tissue to repair itself?

1.5.3. Current Therapies for Xerostomia

Current therapy for xerostomia is purely symptomatic relief, with some ability to promote saliva production in the damaged tissue. Artificial lubricants, such as muco-adhesives, saliva replacement gels and solutions, can be used to aid digestion and improve swallowing and phonation (Kang *et al.*, 2017), whilst increased oral hygiene must occur to protect against infection, such as increased teeth brushing, use of mouthwashes and dental floss and more frequent trips to oral hygienists (Fox, 2005; Mavragani and Moutsopoulos, 2014a). Furthermore, drugs such as pilocarpine or cevimeline can be used to stimulate salivary flow (Valdez *et al.*, 1993; Berk, 2008; Barbe, 2017), but does put extra strain on tissue, reduces the difference between stimulated and unstimulated flow and ultimately does not cure the patient from the underlying pathology (Barbe, 2017). They are also known to have significant off-target effects through their very generic mechanism of action, potentially causing side effects that would negate the use of the drug in the first place, creating a worse quality of life for the patient, such as constant diarrhoea, runny nose and nausea (Mavragani, Moutsopoulos and Moutsopoulos, 2006).

The more long-term solutions for treating xerostomia would be to consider regenerating the tissue. There are two alternatives to consider, in that, the tissue could be stimulated to repair itself, with drugs or the addition of stem cells, or a bioengineered salivary gland tissue could be generated and implanted into the patient in the hope that it can replace the functionality of the original tissue without suffering the same fate of auto-immune attack, in the case of PSS patients.

The other limitation is that, in xerostomia from whichever disease origin, it is most likely to occur in adults and therefore the stem cell niches will be completely different when studied in younger or embryological models. There is a need to focus investigations on the role that each cell type plays in attempting to recover the tissue during the wound healing process, how the regeneration of the tissue is impeded, and what stem cell niches are there currently in the tissue to be taken advantage of. We need to ask ourselves: what happens to these cells during the disease process and can they be recovered, or can we perform allograft transplants from pre-exposure to post-irradiation treatment, or from elsewhere in a patients' own salivary gland tissue if the whole gland is not affected? Alternatively, is it possible to take biopsies from a patient with PSS and extract and purify a stem cell population in order to re-introduce them back to the patient to promote tissue regeneration. Furthermore, if we identify key molecular changes in cells effected in the tissue, it could be possible to reverse these alterations and promote regeneration through non-surgical processes, such as targeting mechanistic changes within the cell populations or using targeted gene therapy.

Being able to isolate or purify mesenchymal stem cell populations based on the cell surface marker profile is already being exploited as therapeutic approaches to conditions such as radiation exposure (Lombaert, Knox and Hoffman, 2011), and CD29, CD105, PDGFR β markers are frequently demonstrated as being used to identify mesenchymal stem cell populations (Khalili *et al.*, 2012). If we could identify this mesenchymal stem cell population within our research project, we could investigate how this population is directly impacted by PSS or IR exposure. We want to know if these cells have undergone mechanistic changes that prevent the normal homeostatic

behaviour in regards to tissue development, wound healing, differentiation and epithelial-mesenchymal cell signalling. Before starting this research, we had no concept of which pathways would be altered within our cell populations and had to approach the conundrum with a very broad scope.

1.6. Hypothesis

We hypothesise that we will generate cell cultures representative of variable cell populations and combine them to generate an organoid assay that can be used to study functionality of isolated patient cells. These three-dimensional organoid models will be reliant on mesenchymal cells to generate reliable structures that represent salivary gland development *in vivo*. Furthermore, the PSS positive patient derived mesenchymal cells, and mesenchymal cells exposed to ionising radiation, will have a reduced regenerative potential as a result of a pathological impact on ability of the cells to continue the cell cycle, to undergo fate determination and express differentiation markers.

1.7. Aims

Salivary gland tissue affected by Primary Sjogren's Syndrome presents with immune infiltrates, fibrotic lesions and an inability of the tissue to repair and regenerate over time. Currently, there is a lack of knowledge of how the mesenchymal cell niche is affected and how this could result in impaired epithelial-mesenchymal cell interactions and reduced differentiation of stem cells to mature differentiated mesenchymal tissue resulting in impaired regeneration.

The aim of this thesis, therefore, was to optimise the development of organoid models of salivary glands, incorporating PSS affected mesenchymal cells; with the intention that this would demonstrate the degree to which tissue regeneration has been affected within this cell population. A further aim was to then use these organoid structures to demonstrate the effect of ionising radiation on salivary gland mesenchymal cells, and to characterise which mechanisms of action were damaged via analysis of the molecular expression profiles in the cells of interest.

As part of the aims, it was also intended to demonstrate that the inclusion of PSS or IR exposed mesenchymal cells present lead to altered development of organoid structures. Simultaneously, essential signalling pathways involved in cell proliferation and differentiation were investigated, establishing a mechanistic reason for the impaired functionality of the cells.

To achieve this, four experimental questions were proposed:

1. Is there a significant phenotypic change between PSS and non-PSS tissue?
Immunofluorescent staining, and QPCR analysis of patient samples were undertaken to understand the difference in molecular expression profiles between the cellular compartments in patients with and without PSS.
2. Can an organoid culture model be developed using human patient derived cells?
Existing protocols for organoid culture models were adapted to grow salivary gland rudiments in culture from mouse derived primary cell cultures and human patient derived cell cultures. Techniques were optimised until the formation of consistent and reliable organoid structures was demonstrated.
3. What is the impact of PSS exposure on the development potential of mesenchymal cells incorporated into the spheroid assays? It was demonstrated that non-diseased mesenchymal cells have a significant role within salivary gland regeneration, and that mesenchymal cells derived from human PSS-positive patients are impacted by the disease with a reduced ability to form rudimentary organoid structures
4. Can the impact of ionising radiation on the behaviour of mesenchymal cells be modelled? It was intended to develop IR exposure models and recombine cells into an established three-dimensional assay.

2. Materials and Methods

2.1. Human Tissue Samples

Patient samples were collected in accordance with the Human Tissue Act 2004. Current Primary Sjogren's Syndrome patients registered with the Newcastle University NHS Foundation Trust were invited to contribute to the research project. Each patient consented to the removal of excess diagnostic material and were requested to invite friends and family as 'healthy control' patients for the project. Alternatively, patients who presented with symptoms and were referred to the PSS clinic as outpatients for further diagnostic processes were also offered the chance to contribute tissue to the biobank. Consent was taken for all contributing volunteers, and labial biopsies, sputum and some blood samples were taken. The collection of samples by the Sjogren's Registry was approved by the University of Newcastle NHS Foundation Trust, Framework of Research Ethics Committee. FREC: 09/H1010/19+5, IRAS Application Number: 149333. Whilst the University of Plymouth FREC: 15/16-514 approved work on the human tissue, acting under the ethics approved for Newcastle. Furthermore, a Materials Transfer Agreement was set up between the two institutions with the lead of research groups being Dr Bing Hu and Professor Wan-Fai Ng.

Therefore, we have two cohorts of samples; the Primary Sjogren's Syndrome positive patients, with a confirmed diagnosis of the disorder, whilst the other cohort is non-Primary Sjogren's Syndrome patients. These non-PSS patients may have presented with symptoms that could be attributed to PSS, however they had labial biopsies removed

and were demonstrated to be absent of immune lesions and auto-antibodies. In these cases, it would be wrong to call them healthy controls or disease free, as they may be suffering from another disorder which could have contributed to PSS-like symptoms. This division of the cohorts must then be taken into consideration as one of the limitations of the study.

Samples were stored in liquid nitrogen for long term storage at the Sjogren's Registry biobank and were transferred to -80°C at our facility, as samples were only stored short term. All the PSS positive patient samples selected were low grade, with less developed lesions, to enable our analysis of the effect of the disease on residual tissue and potentially on earlier stages of the disease. However, it is impossible to ascertain the duration of time a patient has presented with the disease purely from the lesion size, as the disease is subjective and can be accelerated and chronic in patients, causing a range of potential damage.

In total, we were sent 11 non-PSS patient frozen samples and 11 PSS-positive frozen samples, for use in immunofluorescence and histological staining. We were also sent 12 freshly excised tissues directly from the biopsy removal surgery, sent on ice, so that we could generate cell cultures with the maximum potential yield. The diagnosis of these patients was sent to us a few days after the tissue had arrived and been converted to primary cell lines. This meant that we produced two cell lineages that were non-PSS, six cell lineages that were PSS-positive, of different grades, and four additional samples which did not survive cell culture and were discarded. Finally, we were sent seven pairs of slides mounted with FFPE processed biopsy sections, four non-PSS and three PSS-

positive, which were additional diagnostic material and were used for preliminary experiments to identify the diseased tissues using histological staining techniques.

The access to these tissues was the major limitation to this research field as we could only access very small amounts of tissue. Fresh tissue was even more precious, as we had to wait for the surgery to be performed, and frequently patients wouldn't consent to their tissue being used for research purposes.

Standard immunofluorescence and Haematoxylin and Eosin staining protocols were followed as described below. When performing immunofluorescent and histological staining, matched pairs of patient slides were taken, one being non-PSS and the other from a PSS-positive patient. Diagnosis was performed by pathology staff at the Sjogren's Registry at Newcastle University and Newcastle Hospitals NHS Foundation Trust as part of standard diagnostic procedures. Frozen tissue was processed onto slides as described below, blinding was not necessary as each patient tissue presented with obvious pathological lesions, which needed to be considered when imaging the tissue. Slides were allowed to thaw briefly, until the frost had disappeared, before fixing the tissue in pre-cooled 4% PFA or formalin.

2.2. Mouse Tissue Samples

Approval for the use of animals within the remit of the research project was approved by the Local Ethical Review Committee at the University of Plymouth. Students and members of staff working on this project completed an animal handling qualification in line with the Animal (Scientific Handling) Act 1986, in order to monitor and sacrifice animals in accordance with the law and in-house standards of practice. ICR (CD-1[®]) mice, bred in house, were sacrificed at postnatal days; 2, 7 and 30, with some older mice at one year and two years old. The salivary glands were immediately excised and used for cell culture, immunofluorescence, histology or Flow Cytometry. To remove the tissue, an incision was made into the skin of the ventral side of the neck, and extended in a “V” shape up towards the ear on each side of the animal’s head. The skin was separated from the underlying membrane, and lifted up to expose the salivary glands attached to the underside of the mandible. The glands were very carefully separated from the membranes, and cut away at the excretory ducts and neurovascular connection. To cryo-preserve tissue, glands were placed in pre-cooled 2-methylbutane (M32631-500ML, Sigma) for 5 minutes, or immersed in liquid nitrogen. Frozen tissue was then stored at -20°C. Alternatively, fresh tissue was embedded in O.C.T. Compound (Polyvinyl alcohol and polyethylene glycol, 4583, 118mL, Tissue-Plus, SciGen) and frozen at -80C or snap frozen in liquid nitrogen. Fresh tissue was also fixed in 4% Paraformaldehyde (P6148 Sigma) diluted in phosphate buffered saline (PBS, P4417-100TAB, Sigma) over night and then stored in PBS at 4°C. Fixed tissue was then processed through to paraffin embedded blocks using a tissue processor (Histocore Pearl, Leica), and embedded using

embedding apparatus (EG1150H, Leica); these samples could then be stored at room temperature.

C57B/L6 (Black 6) mice, an inbred mouse strain, were also occasionally used but no difference was observed in salivary gland phenotype, IF staining patterns or molecular expression profiling. Black 6 mice were used when CD1 mice were unavailable, but were only used to optimise and test experimental protocol. All results produced during the project were generated using CD1 mice to maintain consistency and accuracy.

2.3. Immunofluorescence Staining

Tissue, whether biopsies, whole mouse submandibular glands or organoid structures, were embedded in OCT and sectioned using a Leica CM1850 cryostat. The tissue was sectioned using a Leica CM1850 cryostat. 5µm or 10µm sections were collected and mounted onto Polysine™ Microscope Adhesion Slides (J2800AMNZ, Thermo Scientific) and allowed to air dry for 30 minutes before being fixed in ice cold Acetone (34850, Sigma Aldrich) or freshly made ice cooled 4% Paraformaldehyde (PFA) (158127, Sigma Aldrich) solution in 10mM Phosphate Buffered Saline (PBS) (P4417, Sigma) for 30 minutes and then washed three times in PBS(T) (PBS containing 0.1% Triton-X100, Sigma) for 5 minutes per wash. Inclusion of Triton(T) was dependent on the target molecule and optimisation was performed for each antibody, relating to whether antigens were known to be cell surface antigens and risked being cleaved through incubation with a detergent, or alternatively were known to be nuclear markers and disruption of the cell membrane would enhance any staining.

We also collected 30µm thick sections of the human labial biopsies onto LCM PEN Membrane slides for use in Laser Capture microdissection at a later date. These slides were stored in slide boxes at -80°C until needed.

For the whole-mount staining of spheres, the spheres were fixed in PFA overnight at 4°C and washed carefully with PBS. Spheres were either kept suspended in PBS and stained using a whole mount staining protocol, or they were isolated gently and spread onto microscope slides, where they were allowed to dry out completely to allow strong

adhesion to the slides. These spheres could then be washed and stained in the same manner as a tissue section.

Non-specific binding was blocked by incubating for 60 minutes with PBS(T) containing 5% Donkey Serum (D9663, Sigma), 0.25% cold-water fish gelatine (G7765, Sigma) and 0.25% Albumin from Bovine Serum (A2153, Sigma).

Primary antibodies were incubated overnight, after which, the samples were washed three times in PBS(T) at room temperature before incubation with secondary antibodies for 2hrs at room temperature. Nuclei were counterstained with 2 μ g/ml 4',6-diamidino-2-phenylindole (DAPI) (D9542, Sigma-Aldrich) for 10 minutes. An overview of the antibodies used is compiled in Table 2.6-1.

2.4. Histological Staining

Histological staining was performed on both FFPE and fresh frozen tissue. The fresh frozen tissue was sectioned on a cryostat and the FFPE tissue was sectioned on a standard microtome onto warm water before being collected onto microscope slides.

Fresh frozen tissue was embedded in OCT and sectioned using a Leica CM1850 cryostat. With whole labial biopsies, the whole biopsy was sectioned, with 10µm sections being collected across 20 Polysine microscope slides. We also collected 30µm thick sections onto LCM PEN Membrane slides for use in Laser Capture microdissection at a later date. These slides were stored in slide boxes at -80°C until needed. For mouse submandibular glands, sections were taken from the centre of the submandibular gland only, at 10 µm, collected across Polysine slides, spreading consecutive sections across slides.

Sections were mounted onto Polysine™ Microscope Adhesion Slides (J2800AMNZ, Thermo Scientific) and allowed to air dry for 30 minutes before fixing in ice cold Acetone (34850, Sigma Aldrich) or freshly made, ice cold 4% Paraformaldehyde (PFA) (158127, Sigma Aldrich) solution in 10mM Phosphate Buffered Saline (PBS) (P4417, Sigma) for 30 minutes and then washed three times in PBS(T) (PBS containing 0.1% Triton-X100, Sigma) for 5 minutes per wash. Inclusion of Triton(T) was dependent on the target molecule and optimisation was performed for each antibody.

Before staining, the FFPE samples were left to dry completely for 24 hours, at room temperature. They were then heated to 60°C for 20 minutes, to allow excess wax to run clear of the slide. The slides were incubated in xylene for 10 minutes to remove residual paraffin wax, changing the xylene after 5 minutes. The slides were then passed through

100% alcohol for five minutes, 95% alcohol for five minutes, 75% alcohol for five minutes and then distilled water for five minutes; this process allows for rehydration of the tissue. Rehydration of the tissue is imperative, as xylene and paraffin are hydrophobic and would prevent the antibody staining solution from penetrating the tissue.

From this point in the protocol, both tissue types are treated the same, with slight variations in timings made, depending on tissue sample origin. This is because histological dyes have a variance in their staining capacity based on tissue thickness, density, age of sample, fixation method and other variables.

First, the slides were incubated in 2ml Harris Haematoxylin (HSS16-500ML, Sigma Aldrich) for five minutes, until nuclei of cells appear purple but not black. Slides were washed gently in running tap water to agitate the dye, removing excess particles. The slides were then washed with acid alcohol (56694-100ML-F, Sigma Aldrich) for 30 seconds, this regresses the haematoxylin and fixes the stain. The slides were gently washed in tap water as the alkalinity will allow 'blueing' of the stain, which contrasts better with the pink and orange shades gained by Eosin staining. If the tap water is neutral to acidic, a wash with 'blueing solution' is necessary, often containing diluted NaOH. Constant flow from tap water allows better agitation of the tissue, dislodging any particulates from the stain, improving visualisation. The slides were incubated in 75% alcohol for two minutes and 95% alcohol for two minutes. This is because Eosin is hydrophobic and needs to be dissolved in a solution that is at least 60% alcohol. The slides are covered with Eosin Y (230251-25G, Sigma Aldrich) working solution (stock solution 1:4 with 80% alcohol) until the tissue is stained sufficiently, approximately one to three minutes. The slides were then washed in fresh 95% alcohol solutions three

times to remove excess dye. If the stain intensity is too strong, the slides can be washed in 60% alcohol to remove some Eosin staining before continuing. When desired staining intensity is present, the slides are washed in 100% alcohol and xylene for two minutes each. The slides could then be mounted using Eukitt quick-hardening mounting medium (0389-100ML, Sigma Aldrich) and 0.13-0.17mm thick coverslips.

Histological staining was imaged using a Leica DM1000 microscope, a Leica MC170HD camera and analysis via LAS V4.4 software.

2.5. Imaging

Immunofluorescence images were captured using a Leica DMI6000 confocal microscope with a Leica TCS SP8 attachment at a scanning thickness of 1µm per section, this microscope ran LAS AF software from Leica, or a Zeiss (5-10 LSM). Post imaging processing was conducted using Adobe Photoshop CC maintaining image in a TIFF format. Low quality imaging was also performed using a Nikon fluorescent microscope and image capture and analysis performed in NIS Elements software and Fiji/Image J.

When imaging tissue, it was preferable to image specific regions of the tissue and to remain purely objective during acquisition. For each staining profile, four images were taken that had a majority focus of acinar tissue, with some intercalated and striated duct structures, four images of excretory duct structures with surrounding tissue, and four images that attempted to cover both regions. These areas of interest were acquired randomly. In the PSS-positive tissue, the same regions were kept, but focused on taking images of regions that presented with immune lesions.

Formatting of fluorescence intensity and distribution could be done using LAS software, Adobe Photoshop CC or in Fiji/Image J using in-built tools in each software. Whilst using Photoshop, only brightness and contrast were modified, and batch processing tools were used to ensure consistency across samples. Alternatively, in small groups of images, the degree to which any modifications were performed was recorded and maintained throughout each image. Images taken of each antibody duplex for control and diseased tissues were processed concurrently.

2.6. Antibody Lists

Table 2.6-1 Listings of all Primary Antibody used in all Immunofluorescence and Flow Cytometry on Mouse and Human Tissue.

<i>Name</i>	Clone	Reactivity	Host	Supplier	Cat. Number	Dilution
<i>Aquaporin 5 (C-19)</i>	Polyclonal	Human, Mouse, Rat	Goat	Santa Cruz	sc-9891	1:50
<i>αSMA</i>	Polyclonal	Mouse	Rabbit	Abcam	Ab5694	1:50
<i>Caspase3</i>	Asp175	Human, Monkey, Mouse, Rat	Rabbit	Cell Signalling	9661S	1:100
<i>CD105</i>	166707	Human	Mouse	R&D	MAB10971	1:50
<i>CD105</i>	209701	Mouse	Rat	R&D	MAB1320	1:50
<i>CD106</i>	BBIG-V1(4B2)	Human	Mouse	R&D	BBA5	1:50
<i>CD106</i>	112734	Mouse	Rat	R&D	MAB6432	1:50
<i>CD106/VCAM1</i>	429	Mouse	Rat	eBioscience	14-1061-82	1:50
<i>CD117/c-kit</i>	ACK2	Mouse	Rat	eBioscience	14-1172-85	1:50
<i>CD11b</i>	M1/70	Mouse	Rat	R&D	MAB1124	1:50
<i>CD133 ae2</i>	80-b2-5-8	Human, Mouse	Mouse	Denis Corbeil	n/a	1:50
<i>CD140a (PDGFRα)</i>	APA5	Mouse	Rat	eBioscience	16-1401	1:50
<i>CD140b (PDGFRβ)</i>	182106	Mouse	Rat	R&D	MAB1042	1:50
<i>CD146</i>	128018	Human	Mouse	R&D	MAB932	1:50
<i>CD166</i>	105902	Human	Mouse	R&D	MAB6561	1:50

<i>CD19</i>	4G7-2C5	Human	Mouse	R&D	MAB4867	1:100
<i>CD19</i> (APC Conjugated)	HIB (RUO)	Human	Mouse	BD Biosciences	555415	1:50
<i>CD29</i>	265917	Mouse	Rat	R&D	MAB2405	1:100
<i>CD29</i> (Integrin b-1)	TS2/16	Human	Mouse	eBioscience	14-0299-82	1:100
<i>CD4</i> (FITC Conjugated)	SK4, SK3	Human	Mouse	BD Biosciences	347413	1:50
<i>CD45/LCA/Ly5</i>	30-F11	Mouse	Rat	eBioscience	14-0451-85	1:50
<i>CD49f</i> (Integrin a-6)	GoH3	Human, Mouse	Rat	eBioscience	14-0495-82	1:50
<i>CD90</i>	Thy-1A1	Human	Mouse	R&D	MAB2067	1:50
<i>c-Kit</i> (C-19)	Polyclonal	Human, Mouse, Rat	Rabbit	Santa Cruz	sc-168	1:50
<i>E-Cadherin</i>	5H9	Human, Mouse, Rat	Mouse	Abcam	8995-1	1:200
<i>E-Cadherin</i>	Polyclonal	Human, Mouse	Goat	R&D	BAF748	1:200
<i>K14</i> (MK14)	Polyclonal	Human, Mouse, Primate, Rat	Rabbit	Covance	PRB-155P- 100	1:250
<i>Keratin 5</i>	Poly19055	Human, Mouse, Rat	Rabbit	Biologend	905504	1:100
<i>Ki67</i>	Polyclonal	Mouse	Sheep	R&D	AF7649	1:1000
<i>La/SSB</i> (D20)	Polyclonal	Human, Mouse, Rat	Goat	Santa Cruz	sc-21393	1:50
<i>Neurofilament</i>	Polyclonal	Chicken, Human, Mouse, Rat	Chicken	Abcam	Ab4680	1:10000

<i>NSUN2</i>	Ag14791	Human, Mouse	Rabbit	Proteintech	20854-1-AP	1:50
<i>PDGFRβ</i> (958)	Polyclonal	Human	Rabbit	Santa Cruz	sc-432	1:50
<i>Ro/SSA</i> (M-20)	Polyclonal	Mouse, Rat	Goat	Santa Cruz	sc-21367	1:50
<i>Sca-1</i>	177228	Mouse	Rat	R&D	MAB1226	1:50
<i>SOX2</i>	Polyclonal	Human, Mouse, Rat	Goat	R&D	AF2018	1:50
<i>Stro-1</i>	STRO-1	Human	Mouse	R&D	MAB1038	1:50
<i>TenascinC</i>	578	Human, Mouse	Rat	R&D	MAB2138	1:200
<i>Thy1/CD90</i>	G7	Mouse	Rat	eBioscience	14-0901	1:50
<i>Vimentin</i>	280618	Human, Mouse, Rat	Rat	R&D	MAB2105	1:200
<i>Vimentin</i>	EPR3776	Human, Mouse, Rat	Rabbit	Abcam	Ab92547	1:200

Table 2.6-2 Catalogue of Human and Mouse Mesenchymal Stem Cell Marker Identification Kit Contents from R&D Systems. All antibodies in these kits were used at a dilution of 1:50, for immunofluorescence and flow cytometry. Kits were designed to identify mesenchymal stem cell populations from any single cell suspension in flow cytometry, but antibodies could also work in immunofluorescence.

<i>SC017 Human MSC Kit R&D Systems</i>						
<i>Primary</i>	<i>Clone</i>	<i>Part #</i>	<i>Catalog #</i>	<i>IgG</i>	<i>Catalog #</i>	<i>Secondary</i>
<i>Stro-1</i>	STRO-1	965608	MAB1038	IgM	MAB1038	Alexa 488 donkey-anti mouse IgG Life Technologies A21202
<i>CD44</i>	2C5	965614	BBA10	IgG2A	MAB003	Alexa 488 donkey-anti mouse IgG Life Technologies A21202
<i>CD90</i>	Thy-1A1	965609	MAB2067	IgG2A	MAB003	Alexa 488 donkey-anti mouse IgG Life Technologies A21202
<i>CD105</i>	166707	965611	MAB10971	IgG1	MAB002	Alexa 488 donkey-anti mouse IgG Life Technologies A21202
<i>CD106</i>	BBIG-V1	965610	BBA5	IgG1	MAB002	Alexa 488 donkey-anti mouse IgG Life Technologies A21202
<i>CD146</i>	128018	965612	MAB932	IgG1	MAB002	Alexa 488 donkey-anti mouse IgG Life Technologies A21202
<i>CD166</i>	105902	965613	MAB6561	IgG1	MAB002	Alexa 488 donkey-anti mouse IgG Life Technologies A21202
<i>CD19</i>	4G7-2C5	965615	MAB4867	IgG1	MAB002	Alexa 488 donkey-anti mouse IgG Life Technologies A21202
<i>CD45</i>	2D1	965616	MAB1430	IgG1	MAB002	Alexa 488 donkey-anti mouse IgG Life Technologies A21202

SC018 Mouse R&D
 MSC Kit Systems

Primary	Clone	Part #	Catalog #	Rat IgG	Catalog #	Secondary
<i>Sca-1</i>	177228	965955	MAB1226	IgG2A	MAB006	Alexa 488 donkey-anti rat IgG Life Technologies A21208
<i>CD29</i>	265917	965959	MAB2405	IgG2A	MAB006	Alexa 488 donkey-anti rat IgG Life Technologies A21208
<i>CD44</i>	polyclonal	967443	AF6127	IgG2B	MAB0061	Alexa 488 donkey-anti rat IgG Life Technologies A21208
<i>CD73</i>	496406	965958	MAB4488	IgG2A	MAB006	Alexa 488 donkey-anti rat IgG Life Technologies A21208
<i>CD105</i>	209701	965957	MAB1320	IgG2A	MAB006	Alexa 488 donkey-anti rat IgG Life Technologies A21208
<i>CD106</i>	112734	965956	MAB6432	IgG2A	MAB006	Alexa 488 donkey-anti rat IgG Life Technologies A21208
<i>CD11b</i>	M1/70	965961	MAB1124	IgG2B	MAB0061	Alexa 488 donkey-anti rat IgG Life Technologies A21208
<i>CD45</i>	30-F11	965962	MAB114	IgG2B	MAB0061	Alexa 488 donkey-anti rat IgG Life Technologies A21208

2.7. Laser Capture Microdissection

Frozen tissue was sectioned at 50-200µM thickness using a cryostat onto PEN membrane slides for LCM. The slides were washed in PBS and incubated in a blocking buffer as in IF staining. Primary antibodies were added to the slides at twice the concentration previously required for IF, and incubated for 30 minutes at room temperature. Slides were washed in PBS before the addition of secondary antibodies, also at twice the concentration previously required for IF, and incubated at room temperature for another 30 minutes. The slides were then washed in PBS, and then in sterilised pure water several times to remove any residual salts from the PBS, which may interfere with the laser cutting.

Slides were then left to dry completely, for approximately 30 minutes. The tissue had to be completely dried to allow successful cutting of the membranes and detachment from the slides. The slides were mounted into the Arcturus LCM Microscope system, with Macro LCM caps. The key regions for selection were: 1) ductal epithelial tissue, 2) peri-ductal/peri-lesion region, 3) control epithelial acinar region far from the lesion, 4) the immune lesion.

These regions were drawn around and collected, immediately being placed into Tri-reagent for RNA collection, as described later. Each slide, which represented one patient, produced three or four tubes of tissue lysate, one for each type of region selected. The protocol had to be carried out as quickly as possible to maximise the RNA yield, and avoid degradation of tissue before staining. It was necessary to change the protocol from performing immunofluorescence to using histological staining techniques

with haematoxylin and eosin staining. This was due to the tissue degrading very quickly: fixation could not be used as RNA quality would be been impacted, and therefore immunofluorescent staining was ineffective for the purpose.

The histological protocol used was adapted from the haematoxylin and eosin protocol described in the materials and methods. Timings were reduced considerably as fresh tissue was being used, and intense staining profiles were not required. LCM Macro slides were briefly thawed from the -80°C freezer until the frost had disappeared from the slides, and then dipped into methanol for 10 seconds to slightly dehydrate the tissue. Slides were then washed in DEPC treated water, dipped for 60 seconds in haematoxylin, and washed in DEPC water again. Blueing was achieved by creating a blueing solution with DEPC water and NaOH solution, in which the slide was incubated for 1 minute. The slide was then washed in in Eoisin Y solution for 1 minute, and washed again in DEPC water and then pure water and finally another wash with methanol, in order to allow faster drying of the slide for use on the Arcturus LCM. For these LCM experiments, there was an n number of 4 samples for the non-PSS and PSS positive cohorts

Analysis of the RNA expression levels was performed by QPCR on a Roche Lightcycler 480 II, as described later in section 2.12 and 2.13. Statistical analysis is described later in section 2.16 Statistics.

2.8. General Cell Culture

Cells were extracted from excised submandibular glands from post-natal day 30 (P30) CD1 mice, from P5 CD1 mice, or from excised biopsies of human clinical patients for diagnostic purposes, or the HGEPP (Human Gingival Epithelial Cells, Pooled) cell line bought commercially. HGEPP cells were used in some of the experiments for irradiation exposure as a control cell line. For mice tissue, excessive tissue including the lymph nodes were dissected off, as were the parotid and sublingual glands, leaving the submandibular gland to be incubated in 1% Collagenase I (C0130-1G, Sigma) in Hank's Balanced Salt Solution (14175-053, Gibco) with 1% penicillin-streptomycin (SV30079.01, Hyclone) and 1% Fungizone® (15290-018, Gibco) for 60 minutes.

For human tissue, the biopsies were received within 24 hours of surgery suspended in a media cocktail, kept cool on ice. Tissue was incubated directly with the same collagenase cocktail as for mouse tissue. Both tissue types were inverted as a method of agitation every ten minutes, which dissociates the tissue for better cell yield. The collagenase enzyme was deactivated with Dulbecco modified Eagle's medium/F12 (31331-028, Gibco) containing 10% Foetal Bovine Serum (F7524, Sigma) and 1% penicillin-streptomycin or 1% Antibiotic-Antimycotic. The cell suspension was centrifuged at 1000rcf for 5 min to form a pellet, before supernatant was removed and the pellet was suspended in the appropriate media cocktail and added to 6cm dishes where cell outgrowths could be observed over the next couple of days. Media was selected to promote the survival of epithelial and mesenchymal cell phenotypes.

More specific culture methods are detailed in results sections where appropriate.

Table 2.8-1 Cell culture media contents with additional supplements and antibiotics.

<i>Media</i>	<i>Supplements</i>	<i>Antibiotics</i>
<i>Dulbecco modified Eagle's medium/F12 (31331-028, Gibco-Mouse)</i>	B-27® Supplement (50X), minus Vitamin A (12587-010, Gibco), Recombinant Mouse EGF CF (20ng/ml) (2028-EG-200, R&D Systems) Recombinant Mouse FGF basic CF (3139-FB-025/CF, R&D Systems),	1% penicillin-streptomycin (SV30079.01, Hyclone) or 1% Antibiotic-Antimycotic (15240062, Gibco)
<i>Dulbecco modified Eagle's medium/F12 (31331-028, Gibco-Human)</i>	B-27® Supplement (50X), minus vitamin A (12587-010, Gibco), Recombinant Human EGF CF (20ng/ml) (236-EG-200, R&D Systems) Recombinant Human FGF basic CF (233-FB/CF, R&D Systems),	1% penicillin-streptomycin (SV30079.01, Hyclone) or 1% Antibiotic-Antimycotic (15240062, Gibco)
<i>AmnioMAX™ C-100 Basal Medium (17001-07, Gibco)</i>	AmnioMAX™ C-100 Supplement (12556-023, Gibco)	Already included in supplement

Table 2.8-2 Contents of B27 Supplement, adapted from (Brewer and Cotman, 1989, Brewer et al., 1993, Chen et al., 2008).

Component	Conc. / L
<i>Biotin</i>	125mg
<i>DL Alpha Tocopherol Acetate</i>	50mg
<i>DL Alpha Tocopherol</i>	50mg
<i>BSA,</i>	125g
<i>Catalase</i>	125mg
<i>Human Recombinant Insulin</i>	156.25mg
<i>Human Holo-Transferrin</i>	250mg
<i>Superoxide Dismutase</i>	375000 U
<i>Corticosterone</i>	1mg
<i>D-Galactose</i>	750mg
<i>Ethanolamine HCl</i>	50µg
<i>Glutathione (reduced)</i>	50mg
<i>Linoleic Acid</i>	50mg
<i>Linolenic Acid</i>	50mg
<i>Progesterone</i>	315µg
<i>Putrescine 2HCl</i>	805mg
<i>Sodium Selenite</i>	625µg
<i>T3 (triiodo-L-thyronine)</i>	100µg
<i>L-Carnithine HCl</i>	100mg

The contents of Amniomax Basal Media and Amniomax Supplement were not published.

Cells were plated onto Poly-D-Lysine CELLCOAT® dishes (628940, Greiner Bio One) and Collagen Type I CELLCOAT® dishes (628950, Greiner Bio One) or (collagen; 734-0275, Poly-D-Lysine; 734-0284, BD Biocoat, VWR). Alternatively, specific coating methods were developed as described below.

2.8.1. Collagen Coating One

This protocol was used initially for four mouse cell culture models before Collagen Coating Two was established and found to be just as effective. Collagen coating media: 5ml HBSS, 5ul BSA (100mg/ml) (a2153-10g, Sigma-Aldrich), 100ul HEPES (1M at pH6.5, 15630-056, Gibco), 50ul Rat Tail Collagen I (11519816, Gibco). All reagents are gently pipetted together, with 2ml applied to a 6cm dish (10111351, Nunclon Delta) and incubated for two hours at 37°C. Plates are washed with HBSS several times and used immediately.

2.8.2. Collagen Coating Two

The second collagen coating protocol to be developed, but appeared to be just as effective in promoting epithelial cell phenotypes in culture environments. HCl is prepared at 1mM, pH3 and then autoclaved. Rat Tail Collagen I was diluted with the HCl at a ratio of 1:2 and 1ml of the solution is incubated on a 6cm dish (10111351, Nunclon Delta) for 4 hours at 37°C. Plates were rinsed with serum free media immediately before use.

2.8.3. Poly-D-Lysine Coating

Poly-D-Lysine (1mg/ml) (A-003-E, Millipore) was diluted into HBSS to a solution of 50ug/ml. The 6cm dishes were covered with 2ml of solution and incubated overnight at 4°C or for two hours at 37°C. Plates were washed five times with HBSS and used immediately or covered with HBSS and stored for up to 5 days at 4°C.

2.8.4. Passaging Cells

When cells became confluent in a cell culture vessel, the cells were passaged in order to maintain a healthy cell number, preventing excessive nutrient use and cell death. Over-confluent or under-confluent cells may lose their desired phenotype, as some cells prefer to be seeded sparsely on a dish, whilst others like to be confluent, with many cell-cell adhesion junctions to facilitate cell signalling pathways.

During the culture of cells, the medium was removed, and the cells were washed in pre-warmed HBSS. Plates were gently agitated to ensure efficient removal of cellular debris, before aspirating. Each plate then had 1ml of TrypLE (12563-029, Gibco) added and the plates returned to 37°C to incubate. Cells were checked regularly, and agitated by tapping the culture flask, for cellular detachment. Once cells had detached from the dish, the suspension was collected and added to 10ml DMEM 10% FBS in order to neutralise the TrypLE action. The suspension could then be spun in a centrifuge at 1000rcf for 3 minutes. A pellet would form in the tip of the tube and the supernatant could be aspirated. Cells were re-suspended in the desired culture media and plated out again, either onto more plates, or removing some of the cell suspension to the

appropriate cell concentration, cell concentration is calculated using an automatic cell counter.

2.8.5. Freezing Cells

Cell suspensions were achieved by aspirating the culture media, incubating with TrypLE, as above in 2.8.4 Passaging Cells. Cells would dissociate from the culture ware and could be collected in additional DMEM supplemented with 20% FBS, to neutralise the action of the TrypLE. The suspension could then be spun in a centrifuge at 1000rcf for 3 minutes to form a pellet. When the pellet was formed, the supernatant was aspirated and cells were suspended at 1×10^6 cells/ml in FBS (Foetal Bovine Serum, F7524, Sigma) with 10% DMSO (D2660-100ML, Sigma). Cell suspensions were distributed between 1ml aliquots in cryovials and placed in the -80°C freezer overnight, before being transferred to liquid nitrogen tanks for long term storage. Vials of cells stored in liquid nitrogen were carefully catalogued into spreadsheets to ensure accurate stocks.

2.8.6. Thawing Cells

Vials of cells were removed from liquid nitrogen and thawed rapidly. To prevent excess damage to cells, the frozen aliquot was warmed with the addition of DMEM 10% FBS and gently agitated by pipette. The cell suspension was spun in a centrifuge as described previously, and the supernatant removed. Cells could then be suspended in the relevant culture medium and distributed, as desired, between cell culture vessels. Frequently, cells that had been thawed from liquid nitrogen could take a long time to recover back to previously observed behaviour, particularly primary cell lines.

2.8.7.Semi-Solid Organ Culture

Whole mouse SMG were sectioned using a vibratome (VT1200S, Leica) to generate 250µm thick tissue sections. The tissue was either stuck to the mount directly with veterinary superglue, or embedded in dense agar that facilitates accurate cutting of the tissue. The tissue is then submerged in PBS and mounted onto the vibratome for cutting. Alternatively, the tissue was micro-dissected with individual lobules being selected for organ culture. Sections were cultured on a semi-solid, agar-based gel: DMEM/F12 20% FBS 1% antibiotics, 1% multivitamin (MEM Vitamin Solution 100X, M6895, Sigma Life Science) was heated to 37°C in a water bath for 30 minutes. 0.5g low melting point agar (A9414-25G, Sigma Aldrich) was added to 20ml of sterilised distilled water and heated in a microwave-oven at 650W for 90 seconds, until the liquid is clear and colourless. The agar was left to cool for one minute and then 1ml of agar was added for every 10 ml of culture medium. The agar and medium were mixed together, avoiding bubbles, and 2ml of the gel-media was pipetted onto a 3.5cm dish, and were left to set for 30 minutes at room temperature. When the gel set, the tissue was placed on top of the gel, with the option of additional media dripped onto the tissue.

2.9. Primary and Secondary Mouse Organoid Cultures

The sphere culture technique was adapted from previously published and established three-dimensional culture protocols (Nanduri *et al.*, 2014; Ogawa and Tsuji, 2015). The technique had to be optimised, and the process of optimisation, with the corresponding protocols used are described in chapter specific materials and methods sections: section 3.2.1 and section 3.3.1. Primary spheres were cultured on top of Matrigel (Matrigel™ 354234, Corning), suspended in sphere culture medium, this medium changed during the optimisation process and, therefore, is described in more detail in each chapter. Primarily, a volume of Matrigel was gently pipetted into each well being used of a chilled 96 well plate (655090, Greiner BioOne) using chilled pipette tips. The plate and tips must have been cooled in a -20°C freezer for at least 30 minutes before use. Once the gel had been added, the plate was incubated at 37°C for five minutes to allow the gel to set before plating suspended cells in media on top of the gel. The media was changed every two days and images of the spheres recorded using a microscope and camera (DM IL LED Fluo, Leica). Secondary spheres were adapted from the 'Differentiation Assay' set out by Nanduri et al (Nanduri *et al.*, 2014). Wells containing primary spheres in Matrigel were flushed with cold HBSS to dissociate the spheres from the gel matrix. The contents of the well were removed and spun at 500rcf for 5 minutes in a 1.5ml micro-centrifuge tube, with the supernatant containing the majority of the Matrigel being removed. The gel was made as described (Nanduri *et al.*, 2014), by combining Matrigel and Rat Tail Collagen I, neutralised with 1N NaOH added dropwise, incorporating the cell structures into the gel before plating out. The plates were incubated for 30 minutes at 37°C to allow

the gel to set before addition of media on top of the gel. Media was changed every two days and images were recorded using a cell culture microscope (DM IL LED Fluo, Leica).

2.10. Human Organoid Cultures

The sphere culture technique using human tissue derived cells was adapted from previously described protocols for mouse derived cell spheroids. These protocols also required further optimisation, with these stages outlined in the relevant materials and methods section 3.3.1. Primary spheres were cultured on Matrigel (Matrigel™ 354234, Corning) in a spheroid culture media which contained both B27 and Amniomax media, allowing for the promotion of both epithelial and mesenchymal cells. The media components were further modified for the use of human cell cultures, using human epidermal growth factor and human fibroblast growth factor. Secondary spheres followed the same protocol as described previously in section 2.10, with adaptations for human cell cultures, using appropriate human EGF and FGF growth factors.

2.11. Flow Cytometry

This flow cytometry protocol for mouse or human mesenchymal stem cell markers was adapted from the manufacturer's instructions; Mesenchymal Stem Cell Identification Kit (Mouse: SC018, Human: SC017, R&D Systems). Adhered cells were incubated in TrypLE (12563-029, Gibco) or collagenase 1%, causing them to detach as described previously for cell passaging. To quench the TrypLE or collagenase, the cell suspension was incubated in DMEM with FBS 10/20%. Alternatively, whole tissue was digested using 1% collagenase and mechanical mincing, lysate was agitated every 5 minutes for 20 minutes and passed through a series of decreasing sized pipette tips, or pushed through a cell strainer, to generate a single cell suspension. The cells were spun at 1000rcf for 5 minutes and the supernatant removed and the cell pellet suspended in flow cytometry staining buffer (FC001, R&D Systems) to a concentration of 1×10^6 cells/ml. Then, 90ul of cell suspension was incubated in 5ul of primary antibodies or isotype control for 30 minutes at room temperature. Primary antibodies were removed through repeated washes with 500ul flow staining buffer, centrifugation, removal of supernatant and suspending in a final volume of 100ul flow staining buffer. Secondary antibodies were added at a volume of 5ul, using Alexa 488 donkey anti-rat. The suspension was incubated for 30 minutes at room temperature before another washing step, after which, the pellet was suspended in 200ul flow staining buffer for analysis on a flow cytometer (BD Accrui C6, BD Biosciences) and analysed using BD CSampler™ software. To act as positive experimental controls, samples were incubated with a control immunoglobulin that matched the targeted antibodies and provided a background level of IgG binding.

2.12. RNA extraction & cDNA production

RNA was extracted and purified using an acid guanidinium thiocyanate-phenol-chloroform extraction protocol. The total RNA was extracted using Tri-Reagent (93289 25ml, Sigma Aldrich) and incubating for 5 minutes at room temperature before addition of Chloroform (C2432-500ML, Sigma Aldrich) at a ratio of 5:1 (lysate: chloroform). The samples were then incubated for a further 5 minutes before centrifugation for 10 minutes at 13000rpm. The aqueous phase was then collected and added 1:1 with 2-Propanol (34965-1L, Fluka Analytical) with 1ul GlycoBlue (AM9515, Ambion). The sample was incubated at -20°C overnight before centrifugation at 13000rpm for 45min at 4°C. The subsequent pellet was then washed in 1ml 70%Ethanol (20821.321, VWR Chemicals) and centrifuged for 10 minutes at room temperature at 9000rpm. The resulting pellet was suspended in 10ul of 0.1% diethylpyrocarbonate (D5758, Sigma Aldrich) treated distilled water.

Purified RNA was quantified on a NanoDrop 2000 UV-Vis Spectrophotometer (Thermo Scientific). Quality control was assessed by analysis of the 260/230 ratio, which highlights phenol contamination and a 260/280 ratio of more than 1.8 can indicate DNA contamination.

Reverse transcription was performed using High-Capacity cDNA Reverse Transcription Kit (4368814, Applied Biosystems) in accordance with the manufacturers protocol, on a Veriti™ Thermal Cycler 96 well (Applied Biosystems) using the manufacturer's program of 25°C for 10 minutes, 37°C for 120 minutes, 28°C for 5 minutes and 4°C indefinitely

thereafter. Samples were then diluted in 180ul of DEPC treated water, mixed gently and stored at -20°C.

2.13. Q-PCR

Real Time PCR was performed in triplicate for all samples to generate a technical replicate. Samples were combined with LightCycler 480 SYBR Green I master kit (4887352001, Roche Life Science) (diluted 1:1 with the water provided in accordance with the manufacturer's instructions) and appropriate primers in a ratio of 1:8:1 totalling 10µl. This equates to a final primer concentration of 1µM. The samples were analysed with each primer in triplicate as a technical control. Primers were designed against the CDS sequence for each gene, provided by NCBI gene (<http://www.ncbi.nlm.nih.gov/gene/>) using Primer 3 website (http://biotools.umassmed.edu/bioapps/primer3_www.cgi) and validated on UCSC In-SilicoPCR (<http://genome.ucsc.edu/cgi-bin/hgPcr?command=start>).

Primers were designed to give an amplicon length that reduces the risk of dimers and hairpins. The primers were also designed to cross an exon to negate the problems of genomic DNA contaminants being amplified. To reduce the risk of RNA degradation leading to non-binding of primers, primers were designed to bind towards the 5' end of the cDNA. Primers were all validated against cDNA extracted from mouse embryonic fibroblasts, to ensure that they can detect cDNA and that the amplicons produced are of the anticipated length. Primers to the mouse genes used in this study are shown in Table 2.13-1. Primers designed for working with human derived cell lines or tissue derivatives are displayed in Table 2.13-2

Table 2.13-1 Primer Sequences Targeting Mouse RNA Sequences for genes of interest

<i>Abbr.</i>	<i>S Primer</i>	<i>S Sequence</i>	<i>AS Primer</i>	<i>AS Sequence</i>
<i>Amy1</i>	m.Amy1_S1296	AGCTTTTGGCAGAGGAAACA	m.Amy1_AS1503	TGGGTCTTCGGCAGAGTTAC
<i>AQP5</i>	m.Aqp5_S530	TCTACTTCACCGGCTGTTCC	m.Aqp5_AS728	TATGTGCCTTTGACCACAGC
<i>Cdh1</i>	m.CDH1-616	CAGCTGCCCGAAAATGAAAAGG	m.CDH1-861	TCCACCGCTTCCCCATTTGATG
<i>GAPDH</i>	m.GapDH-F	ATCACTGCCACCCAGAAGAC	m.GapDH-R	CAGTGAGCTTCCCGTTCAG
<i>Vim</i>	m.Vim-S1246	CCAACCTTTTCTTCCTGAA	m.Vim-AS1393	GGTCATCGTGATGCTGAGAA

Table 2.13-2 Primer Sequences Targeting Human RNA Sequences for genes of interest.

<i>Abbreviation</i>	<i>S Primer</i>	<i>S Sequence</i>	<i>AS Primer</i>	<i>AS Sequence</i>
<i>36b4</i>	h.36b4_S	GCAATGTTGCCAGTGTCTGT	h.36b4_AS	GCCTTGACCTTTTCAGCAAG
<i>AQP5</i>	h.aqp5_S515	GCCACCTTGTCGGAATCTAC	h.aqp5_AS701	TCACTCAGGCTCAGGGAGTT
<i>β actin</i>	h.bActin_S342	GCACCACACCTTCTACAATGAG	h.bActin_AS507	GGATAGCACAGCCTGGATAGC
<i>β actin</i>	h.bActin_S785	CCTCCCTGGAGAAGAGCTAC	h.bActin_AS951	GATGTCCACGTCACACTTCA
<i>Gli1</i>	h.GLI1_S550	AAGCGTGAGCCTGAATCTGT	h.GLI1_AS750	CATGTGAACCACCAGCATGT
<i>Gli2</i>	h.GLI2_S1271	TGGCTGACCTCAAGGAAGAT	h.GLI2_AS1420	GGATGTGCTCGTTGTTGATG
<i>Gli3</i>	h.GLI3_S883	GGCCATCCACATGGAATATC	h.GLI3_AS1078	TGAAGAGCTGCTACGGGAAT
<i>Glis1</i>	h.GLIS1_S1768	GGTGTGTATCCTGGCTCCAT	h.GLIS1_AS1962	GGGGCTGACTATTGGTGAGA
<i>Glis2</i>	h.GLIS2_S1470	AACGCCAGGTACAAGATGCT	h.GLIS2_AS1668	GCTTAAAGCGGCTCACTGGAG
<i>VIM</i>	h.VIM_S1196	CCTACAGGAAGCTGCTGGAA	h.Vim_AS1393	GGTCATCGTGATGCTGAGAA

The instrument used was a Roche Lightcycler 480 Instrument II 384-well block real-time PCR machine, used according to the manufacturer's instructions. Program details are explained below in Table 2.14-3.

Table 2.13-3 Program of the PCR cycles used for QPCR on the Roche LightCycler.

<i>Program Step</i>	<i>Temperature</i>	<i>Time (hh:mm:ss)</i>	<i>Repeats</i>
<i>Pre-Incubation</i>	95°C	00:05:00	1
<i>Amplification</i>	95°C	00:00:10	40-55
	60°C	00:00:20	
	72°C	00:00:10	
<i>Melting Curves</i>	95°C	00:00:05	1
	65°C	00:01:00	
	97°C	Until reached	
<i>Cooling</i>	95°C	00:00:01	1

Results were analysed using Comparative Ct methods. PCR amplification was checked to ensure appropriate amplification curves and annealing temperature was obtained. Results were exported into Microsoft Excel where basic calculations and analysis was performed.

2.14. Statistics

Experimental data was analysed using PRISM 5 software (Graph Pad Software). For Real-Time PCR analysis, a Two-way ANOVA followed by Bonferroni correction was performed. Two-way ANOVA and Student's t-Test were also used. Statistical significance was set at * $p < 0.05$, ** $p < 0.01$ & *** $p < 0.001$. For QPCR data, each reaction was run in triplicate, to produce experimental controls. For mouse derived tissue work, all cultures were derived by combining the tissues from three littermates in order to diminish individual variation. We performed $\Delta\Delta C_t$ analysis by relating all experimental results to internal controls of housekeeping genes, and also to control samples. Then the expression levels could be compared relatively between experimental samples with the background expression removed.

Statistical analysis of the Laser Capture Microdissection results was performed on the triplicate C_t values produced from the QPCR experiments, using Excel and GraphPad software and using the SciPlot plugin on RStudio, to perform a repeated measures ANOVA (or linear mixed-effects model analysis) and Chi-squared analysis. This analysis examines the impact of multiple variables on the mean C_t values (Galecki and Burzykowski, 2013). Multiway interactions were calculated to compare the ΔC_t change between patient cohorts and tissue regions, whilst also combining ΔC_t values across all regions to compare RNA expression levels purely between cohorts using the student t-test. Sample sizes of $n=4$ were used non-PSS and four PSS positive patient samples and results considered statistically significant at $P < 0.05$.

3. Results

3.1. Characterisation of PSS and non-PSS Patient Labial Salivary Gland Tissue

It was essential to prioritise the characterisation of human salivary gland tissue in a way that could identify different cellular compartments, whilst also highlighting any significant differences in staining distributions between non-PSS and PSS positive patient tissue. In order to achieve this, minor salivary gland biopsies were received from the Sjogren's Registry, a Medical Research Council supported biobank based at Newcastle University. The samples were collected from patients across the UK, who presented with symptoms of PSS and were having labial salivary gland biopsies removed for definitive diagnostic purposes, as is routine. The samples collected were excess material taken during the diagnostic procedure, removed with the informed consent of the patients for the purpose of academic and medical research into the field of Sjogren's Syndrome.

Previous studies have used generic pan-epithelial and pan-mesenchymal markers to denote different regions of the tissue, with significant work being completed to generate a panel of markers that could be used to identify some stem-cell like niches or other sub-populations. For example, work by Lombaert, Brunsting, Weirenga, *et al.*, 2008, isolated Sca-1 and c-kit positive cells from salivary gland tissue to demonstrate their stem cell-like abilities by forming organoid structures and expressing alpha-amylase. Whilst Maimets *et al.*, 2016, demonstrated that the well-established E-cadherin marker was

an accurate marker for epithelial structures, alongside β -catenin, and alternatively using CD29, C-kit and other markers to identify stem cells within their organoid structures. However, there has been little work to characterise the changes to marker expression profiles when comparing the PSS positive and non-PSS patient tissue, particularly the impact on the mesenchymal cell population.

It is known that the salivary gland tissue does not clear the immune lesions of PSS and there is a reduction in salivary flow rate (Speight, Kaul and Melsom, 1992). Therefore, it could be hypothesised that homeostasis of the cell cycle is impacted, along with the activation of quiescent stem cell populations to differentiate into fully functional secretory salivary gland tissue. However, as this work has been investigated previously; we developed an interest in the impact of PSS on the mesenchymal cell niche, as we know the epithelial and mesenchymal cells interact with one another during development and that this interaction is key in directing tertiary structure organ formation. Pathways which could contribute to this change in behaviour within the tissue include the stem cell fate determination pathway, cell cycle control mechanisms, epithelial-mesenchymal cell interactions, and immune response markers.

As shown subsequently, we developed a panel of markers that could be used throughout the research project that would identify our cells of interest. This panel was used through many techniques, such as immunofluorescence, purification through FACS or MACS and relative RNA expression analysis. Furthermore, known mesenchymal cell markers were combined with a variety of stem cell markers to investigate how truly representative some of the established mesenchymal stem cell markers were within the pan-mesenchymal cell population.

For further characterisation of the salivary gland biopsies, it was decided that it would be inaccurate to extract and analyse RNA from the whole bulk tissue to investigate changes to molecular expression in subpopulations of the tissue. Ideally, specific regions of the tissue would be isolated from healthy and diseased patients because the focal infiltrates that occur during PSS form discrete lesions, potentially inducing changes only in the tissue directly surrounding the lesions.

The technique of laser capture microdissection (LCM) was developed to select specific regions of the tissue. Frozen samples from human labial salivary gland tissue were sectioned and stained. Regions were selected based on tissue physiology and staining patterns, and were carefully removed and processed through our standard RNA extraction protocol. From non-PSS patient tissue, regions of acinar epithelial cell structures, ductal epithelial cells were collected, along with mesenchymal cells surrounding these duct structures. From diseased patients, the regions differed; ductal epithelial cells were collected from ducts surrounded by immune lesions, the immune lesions themselves, the peri-lesion region of tissue, and finally a region of non-affected epithelial acinar tissue, distant from prominent lesions; as demonstrated in Figure 3.1-10.

The aim of this chapter was to characterise the different cell populations within the salivary gland tissue, whilst identifying the impact on marker expression in tissue from PSS positive patients. LCM technology was used to investigate regional changes in molecular expression profiles, which was intended to enhance understanding of changes in stem cell proliferation and terminal differentiation pathways that could impact salivary gland tissue regeneration.

3.1.1. Immunofluorescence of PSS versus non-PSS Salivary Gland

Tissue

From the images produced in Figure 3.1-1 and Figure 3.1-2, it was evident that E-cadherin (CDH1) and Vimentin were two markers that discretely identified two discrete cellular populations, with no overlap between the stains. The Vimentin staining appeared fibrous in morphology, staining strongly around ductal regions of the tissue, and around structures that have potential to be neurovascular bundles. Smaller structures staining for Vimentin can also be seen surrounding the secretory E-Cadherin positive stained structures. Because of the fibrotic nature of the staining, it is not possible to see the Vimentin positive cell bodies linked to the fibrous processes that surround the acinar structures. The E-cadherin staining was particularly bright between compacted cells, and highlighted duct structures within the tissue and defined the acinar secretory structures by delineating the apical and basal membranes of the cells. Highlighted in Figure 3.1-1 with white arrows are duct structures, which present as regular-shaped, compacted, E-cadherin positive cells surrounding a hollow lumen structure, surrounded by a thicker layer of Vimentin positive, fibrous cells. This staining pattern of epithelial and stromal tissue is conserved in the H&E histological staining performed in FFPE samples, indicating a very heterogeneous tissue morphology that is preserved across all patient samples. Artefacts were observed within the tissue, gaps that did not stain for any of the markers, suggesting damage to the tissue, or poor tissue quality. Patient DSO 283, which was a non-PSS patient as confirmed by the Sjogren's Registry, presented with staining patterns that could suggest minor immune infiltration

surrounding a prominent duct structure; a high concentration of DAPI or haematoxylin stained nuclei densely surrounding a duct structure, whilst none of the other non-PSS samples presented with this phenotype.

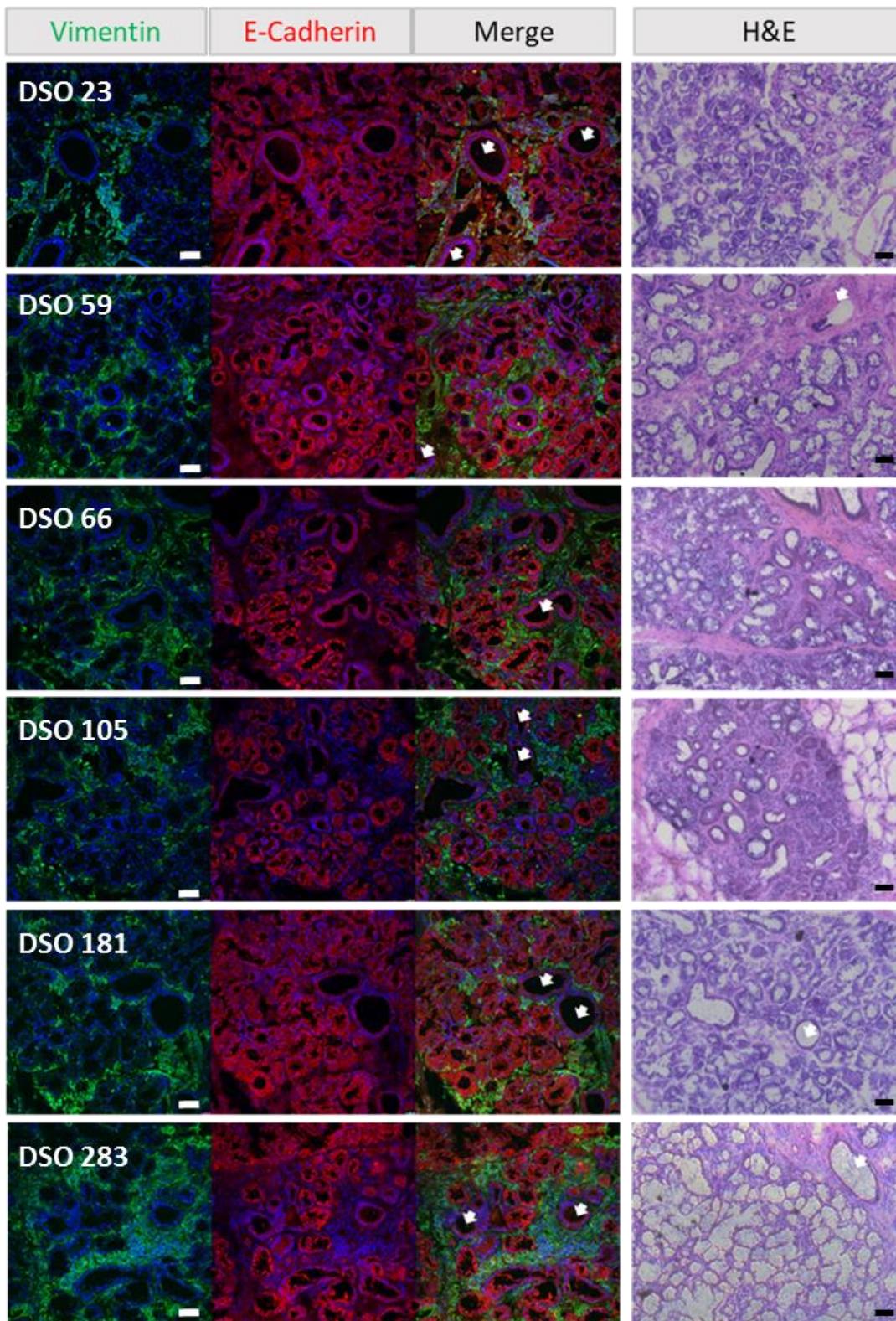


Figure 3.1-1 Labial salivary gland biopsies from six non-PSS patients, characterised by IF staining for E-cadherin (red) and Vimentin (green), sectioned at 10um thickness, visualised with Alexa 568 and Alexa 488 conjugated secondary antibodies respectively. Counterstained with DAPI nuclear stain. Paired with comparable H&E stained tissue sections from the same piece of biopsy. White arrows indicate ducts. Images taken at X20 magnification. Scale bar represents 50um.

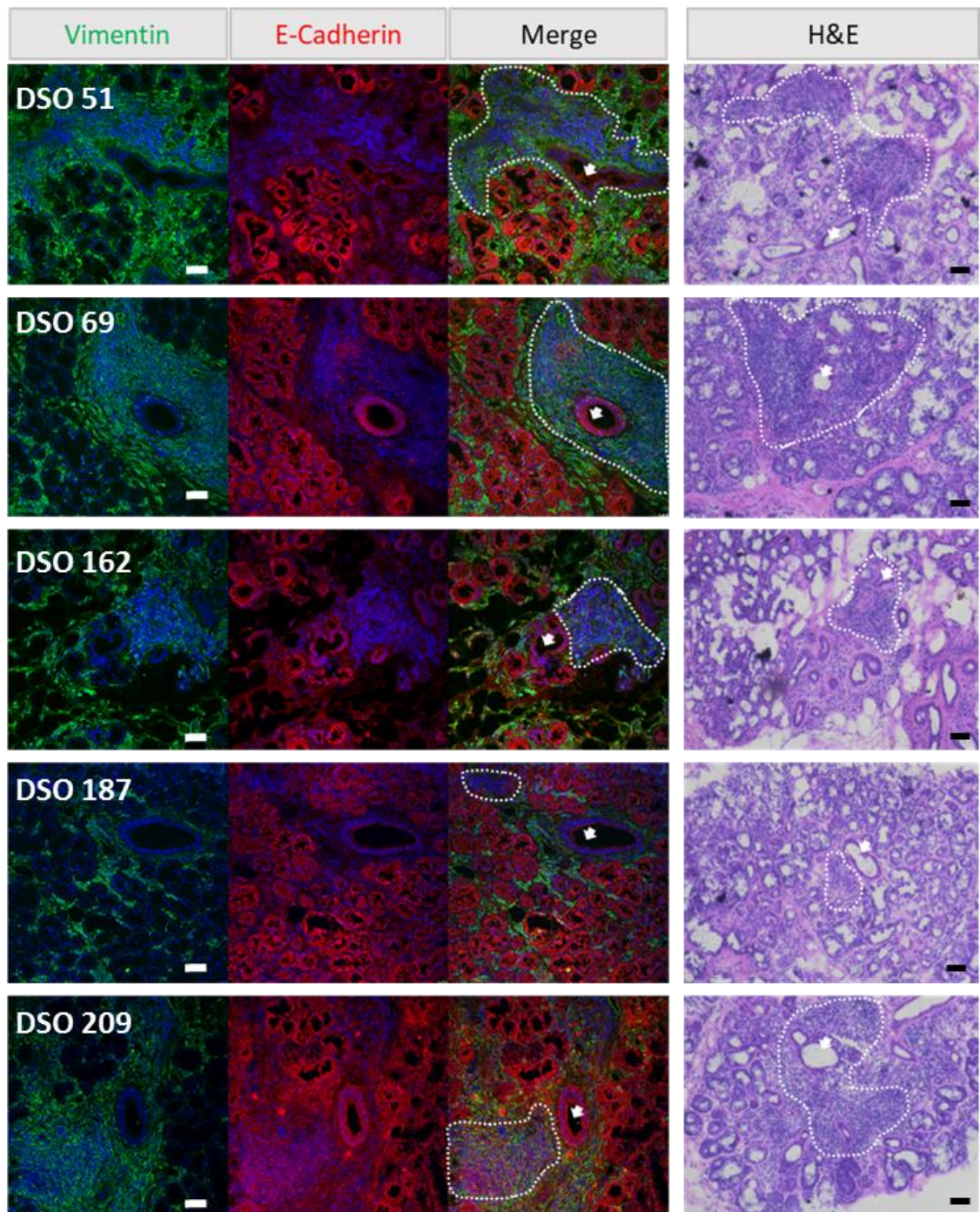


Figure 3.1-2 Immunofluorescence characterisation of PSS patient labial salivary gland biopsies. Five disease positive patients stained with anti-E-cadherin (red) and anti-Vimentin (green) antibodies, counterstained with DAPI nuclear stain. Images taken at 20x magnification. White dotted lines indicate focal lesion boundaries, arrows indicate duct structures. Images paired with corresponding H&E stained tissue sections from the same biopsy. Scale bar represents 50um.

In the PSS positive samples shown in Figure 3.1-2, the two markers stained as before, with DAPI identifying the dense focal lesions of immune infiltrates into the tissue, confirming the disease diagnosis of PSS. The most striking staining pattern difference that we observed in the PSS positive samples was that the focal immune lesions stained strongly for Vimentin. Intense clusters of staining of Vimentin was observed, frequently centred around, or near, a duct structure, penetrating into surrounding tissue. This pattern coincides with the H&E staining performed simultaneously that histologically identifies the immune lesions. However, where the acinar tissue was still intact and unaffected by the lesions, the pattern of staining was retained as in healthy tissue.

The diversity of the lesion sizes across the samples was quite large, with some patient samples presenting with small and focal lesions and others with global and diffuse lesions that majorly disrupted the residual tissue and, in the case of DSO 209, resulted in minimal unaffected tissue remaining. The lesions are highlighted in the images of Figure 3.1-2 by white dotted lines, the white arrows indicate an example of the duct structure.

The immune lesions may cause interference with the Vimentin staining as there appeared to be intense staining for Vimentin in the same locality as the immune lesions. It was concluded that a larger panel of markers would be needed, to identify any molecular changes between the healthy and PSS patient samples, and to identify sub-populations of the cells.

By using markers to identify the immune cell populations, it was possible to observe the distribution patterns in the immune lesions, enabling us to demonstrate the diversity of PSS grades, as advanced lesions would show with more staining for CD19 positive B cells.

Furthermore, we could then use CD19 and CD4 as markers to check if cell cultures had been cross contaminated by immune cells.

In Figure 3.1-3, there appears to be a scattered background expression of immune cell markers CD19 (red) for B cells and CD4 (green) for T cells. However, only the PSS positive samples have large regions of CD4 positive staining, coinciding with the lesions defined in the H&E staining patterns. Within these large lesions, there was also some smaller aggregated staining of CD19, and the ratio between the CD4 and CD19 stain appeared to vary between each patient and is not consistent across the cohort.

The staining in Figure 3.1-4 indicates the discrete staining of AQP5 marker within the salivary glands, highlighting the secretory epithelial structures only. In the PSS-positive samples, where the lesions had destroyed the tissue, there was a complete absence of AQP5 staining, whilst maintaining the expression profile of non-PSS tissue in regions away from the immune infiltrates. Furthermore, ductal tissue stained for CD133, but not with AQP5, whilst acini retained some CD133 staining.

Both CD133 and NSun2 appeared to stain the tissue ubiquitously in Figure 3.1-5, with no discernible pattern of staining that differentiates between the PSS and non-PSS patient samples. However, the NSun2 marker appeared slightly more prevalent within the immune lesions, and was very obvious within the acinar regions, whilst CD133 appeared more prevalent within the supporting stroma.

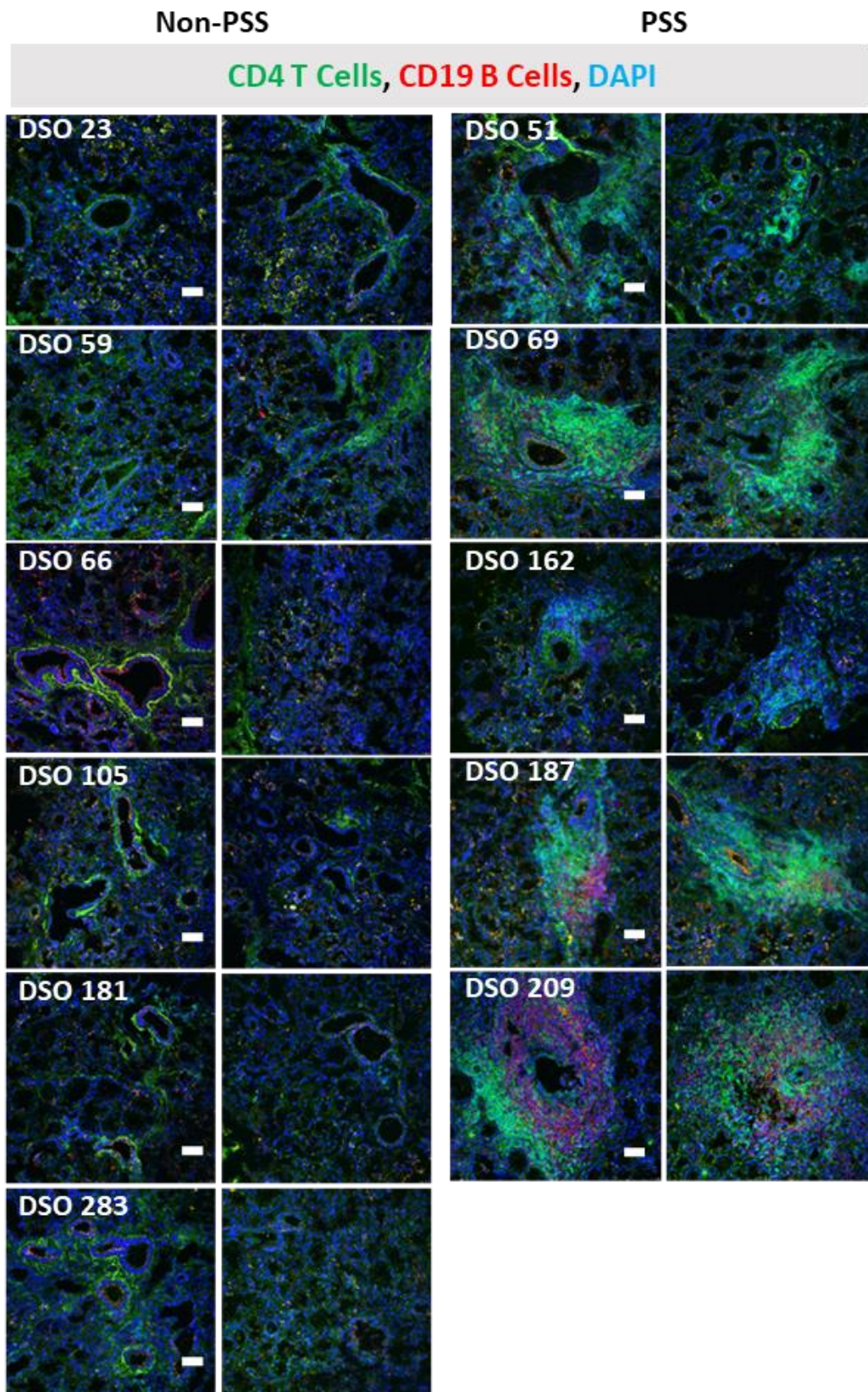


Figure 3.1-3 Immunofluorescence staining of PSS-negative and PSS-positive patient samples, sectioned at 10um, stained with anti-CD4 antibodies for T Cells (Green), anti-CD19 antibodies for B Cells (Red). Experimental duplicates are shown, with images taken at 20x magnification, scale bar represents 50um.

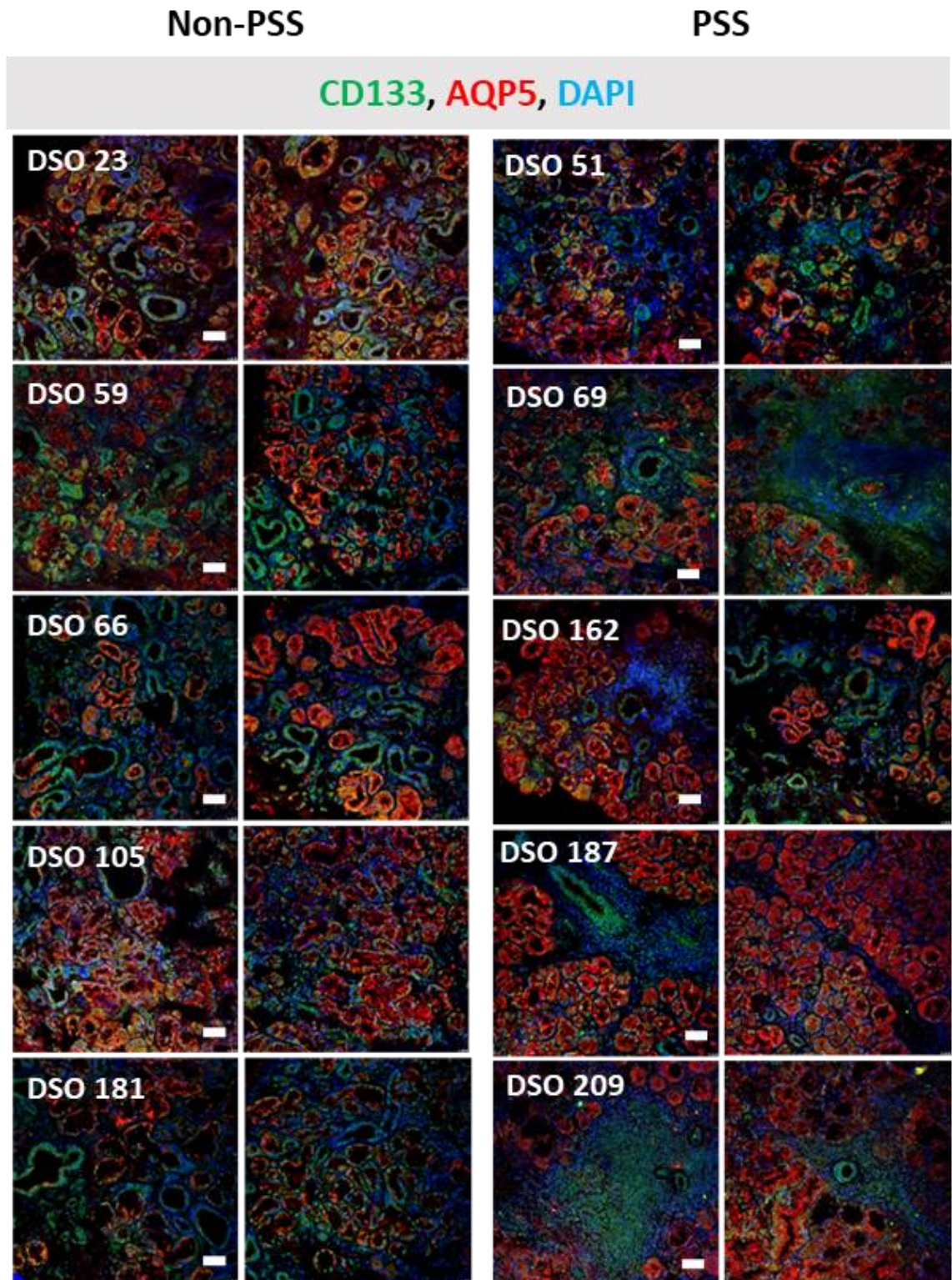


Figure 3.1-4 Immunofluorescence staining of PSS-negative and PSS-positive patient samples, sectioned at 10um, stained with anti-CD133/Prominin1 (green) and anti-AQP5 (red) antibodies. Experimental duplicates are shown with images taken at 20x magnification, scale bar represents 50um.

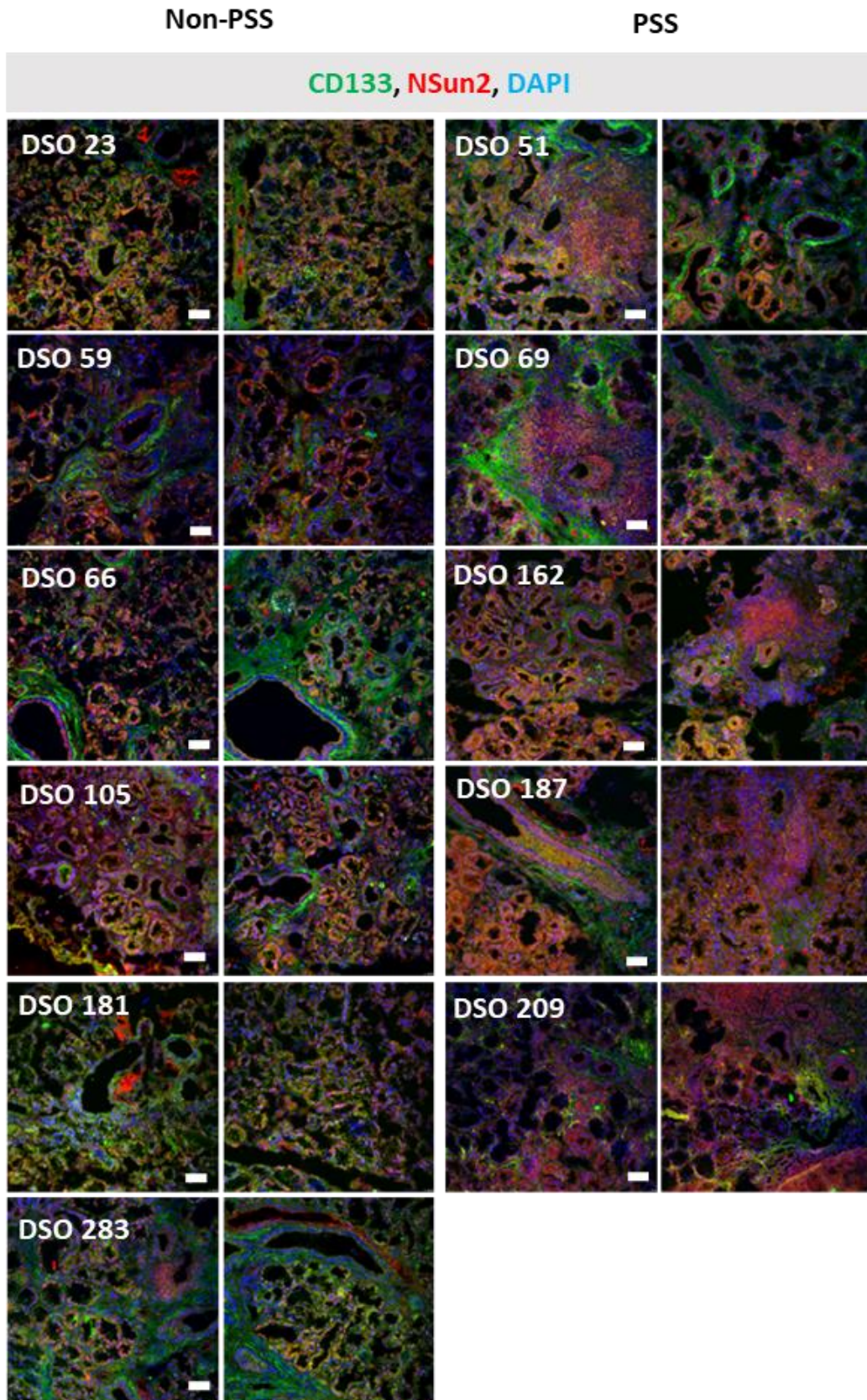
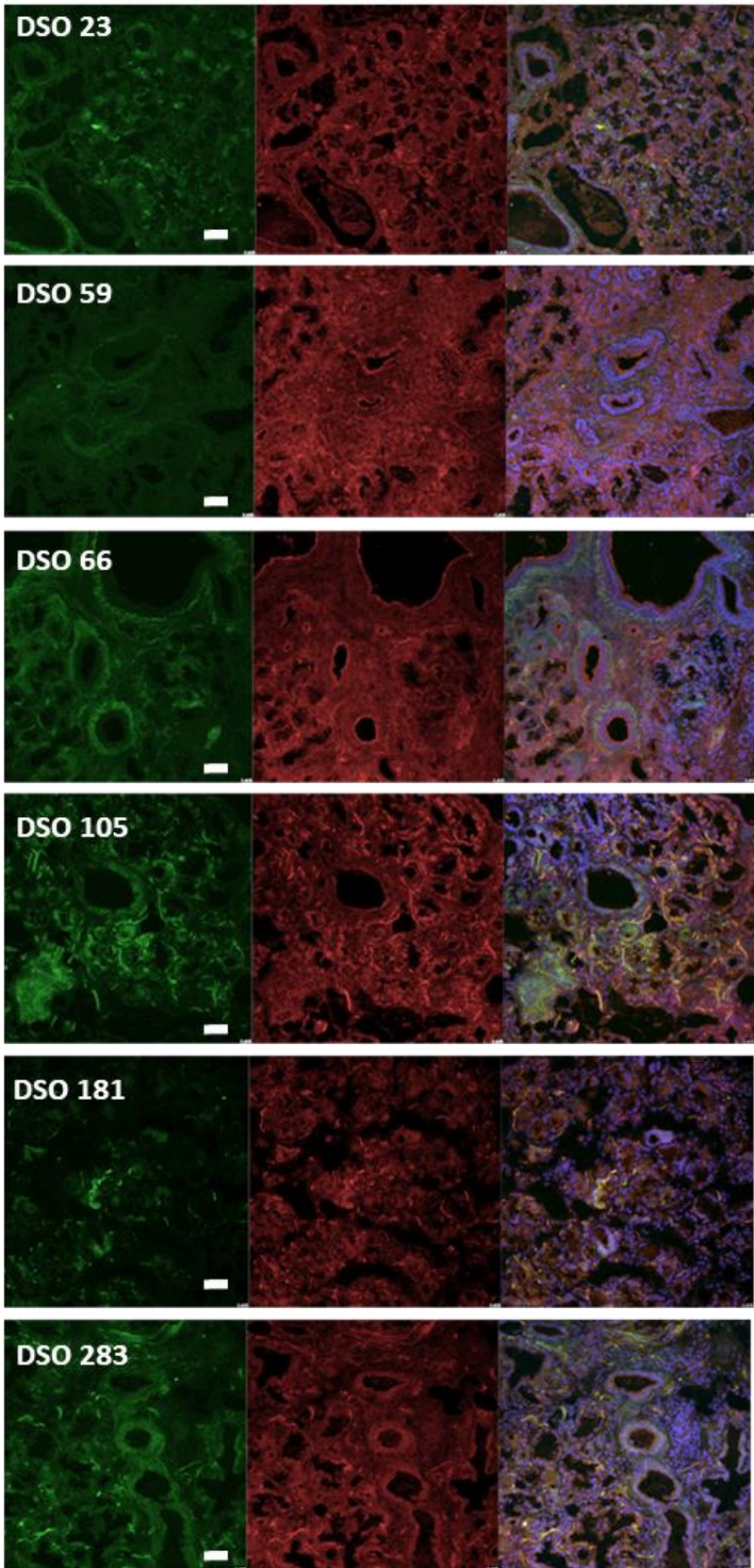


Figure 3.1-5 Immunofluorescence staining on PSS-negative and PSS-positive patient samples, sectioned at 10um, stained with anti-CD133/Prominin1 (green), NSun2 (red) antibodies. Images taken at 20x magnification, scale bar represents 50um.

Non-PSS

A-tubulin (sigma), A-tubulin (Cell Sig.), Merge



PSS

A-tubulin (sigma), A-tubulin (Cell Sig.), Merge

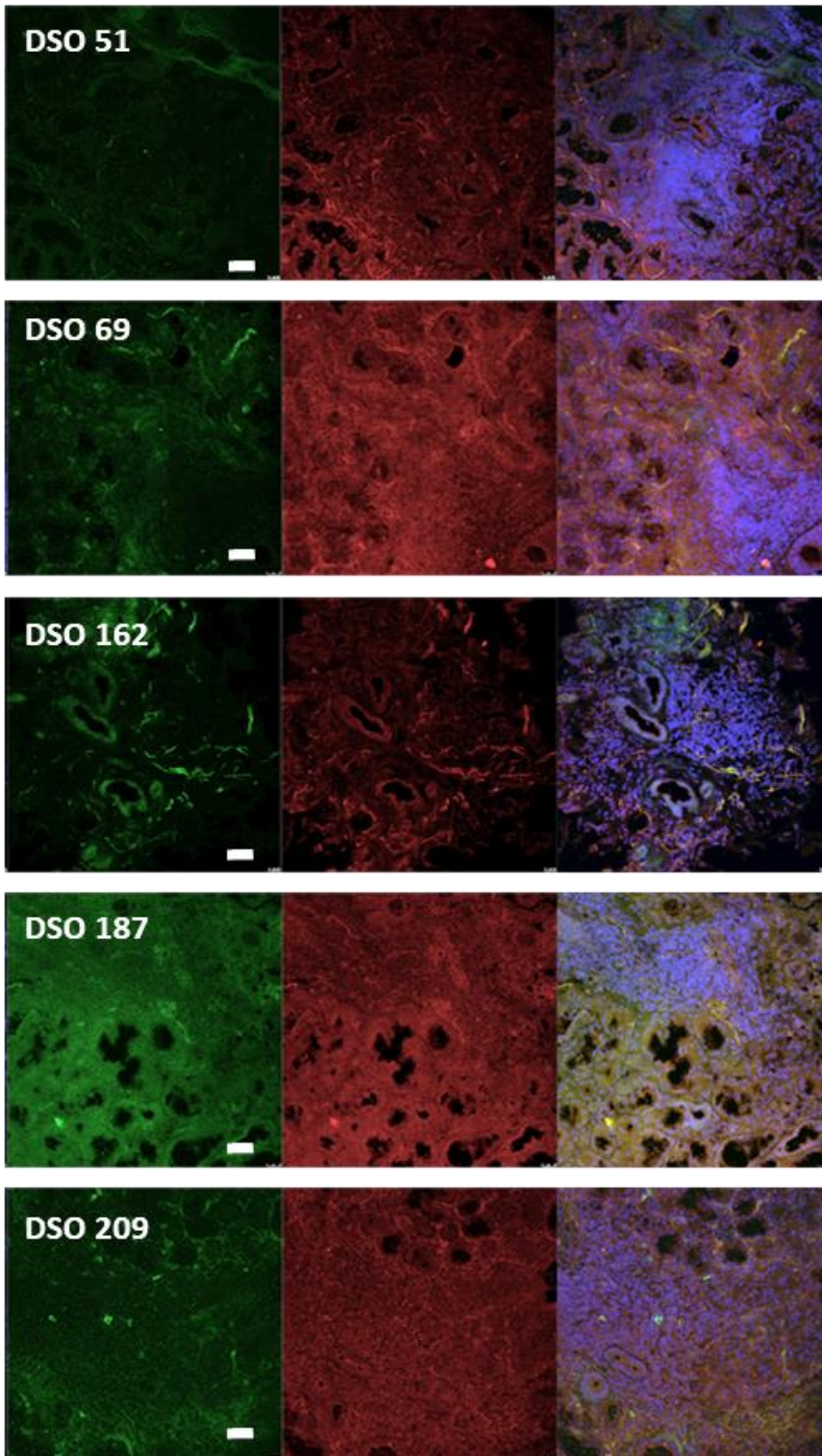


Figure 3.1-6 Immunofluorescence staining on PSS-negative and PSS-positive patient samples, sectioned at 10um, stained for anti-Acetylated Tubulin antibodies (Sigma (red) vs Cell signalling (green)). Images taken at 20x magnification, scale bar represents 50um.

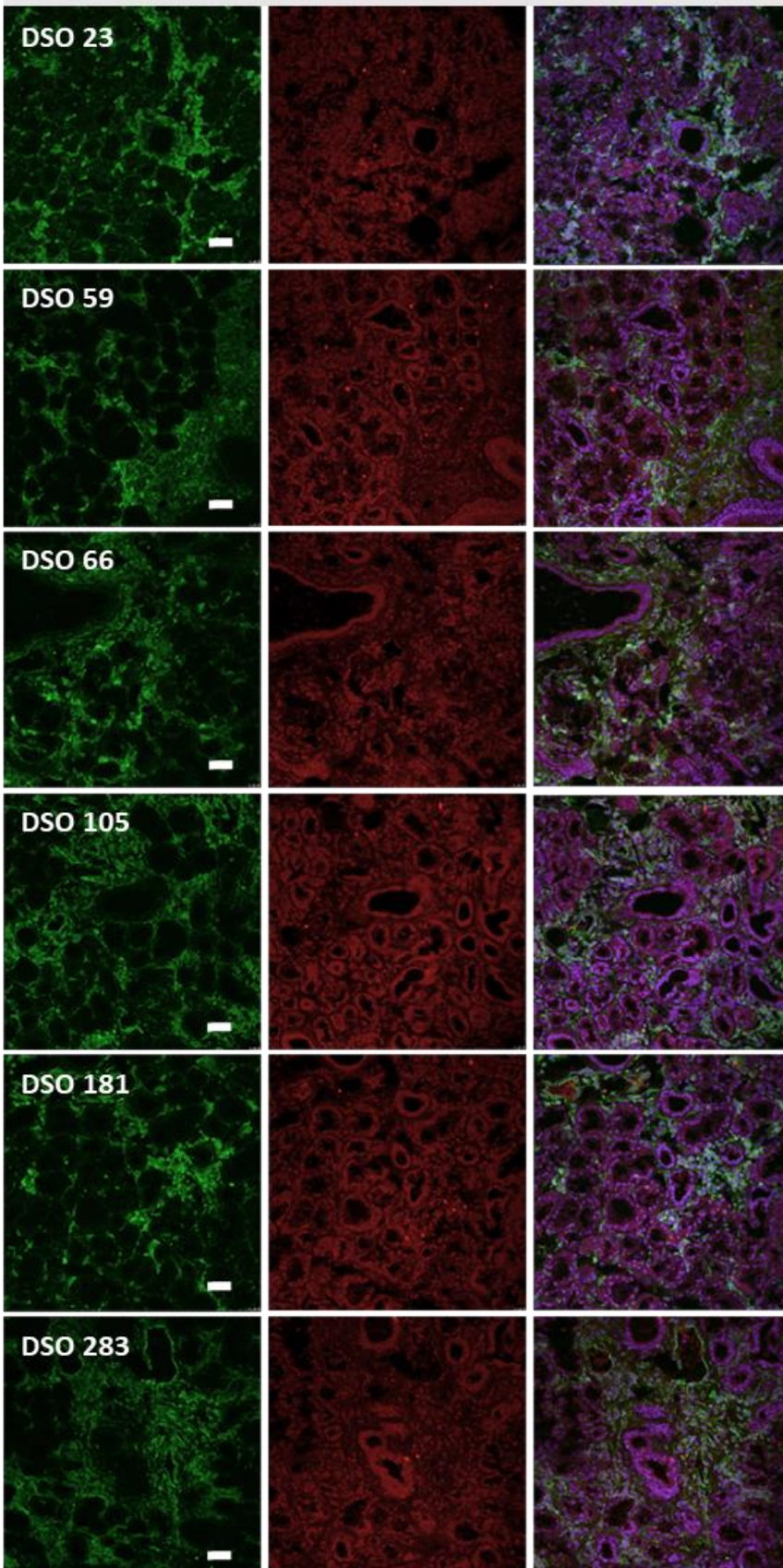
Two different antibodies from different providers were used to stain for acetylated tubulin as they were both used by other members of the research group and we had wanted to corroborate which antibody would be most beneficial for us in this project. In the results shown in Figure 3.1-6, there was considerable background staining, however, thin filamentous structures could be observed in both PSS and non-PSS tissue. The patterns were not consistent across each cohort, and in some patients, minimal staining was observed. Where there was dense nuclear staining of the lesions in PSS samples, the larger fibrous staining was still evident, but the smaller fibres were no longer present.

Despite being a transcription factor involved in the maintenance of neural stem cells, in the labial salivary gland biopsies, it appeared that Sox2 stained every nucleus within the tissue, shown in Figure 3.1-7. There was little difference between the staining distribution of Sox2 and DAPI between the PSS and non-PSS patients, although it had been expected to observe few cells initially and possibly even fewer in PSS patients. The brighter fluorescent specks were deemed to be artefacts of the experiment as they appeared not to be associated to other structures, whilst the Vimentin stained as previously observed.

Figure 3.1-8 demonstrates that CD29 stained the non-PSS tissue in a very similar pattern to Vimentin, in a fibrous nature surrounding structures that appeared epithelial. Alpha-amylase was less effective as a marker for epithelial tissue, as the background fluorescence levels were so high. Although we observed that CD29 staining was very intense in the lesions in the PSS tissue.

Non-PSS

Vimentin, Sox2, Merge



PSS

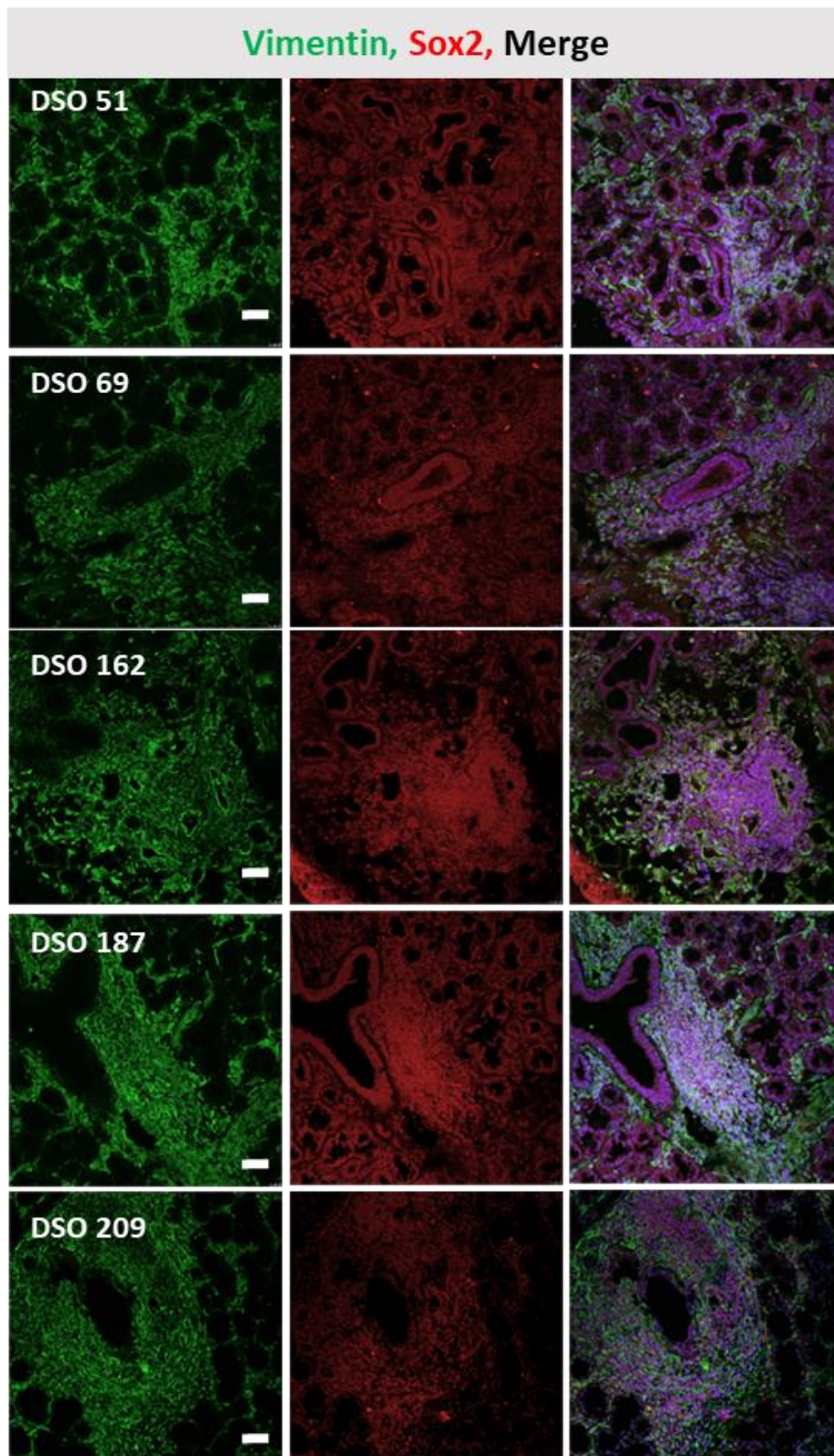
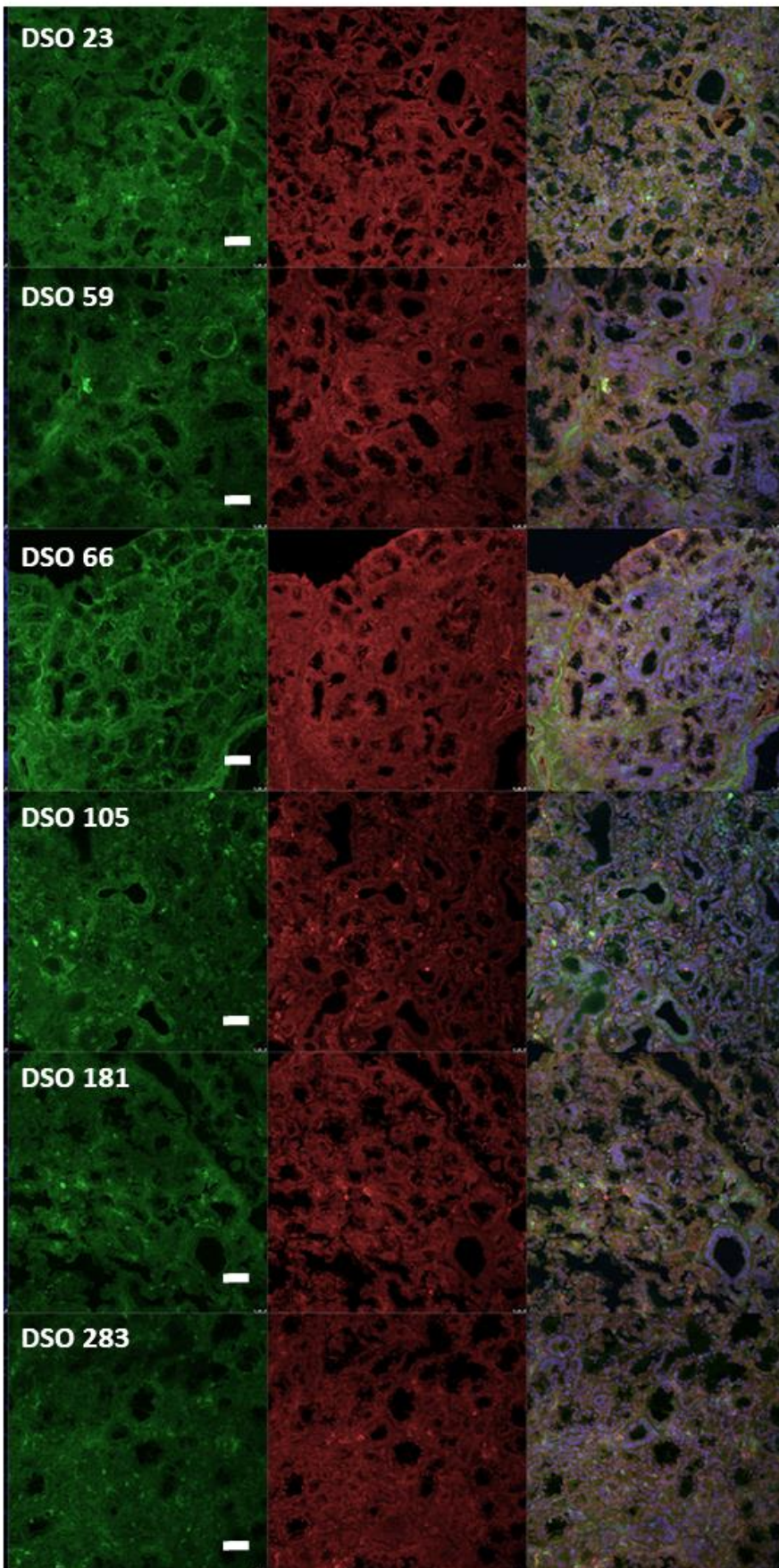


Figure 3.1-7 Immunofluorescent staining for stem cell marker Sox2 (red) and mesenchymal cell marker Vimentin (green) on non-PSS and PSS patient labial biopsies. Sox 2 ubiquitously stains nearly all of the tissue and appears non-specific. Images taken at 20X magnification, scale bars represent 50um.

Non-PSS

CD29, AMY1a, Merge



PSS

CD29, AMY1a, Merge

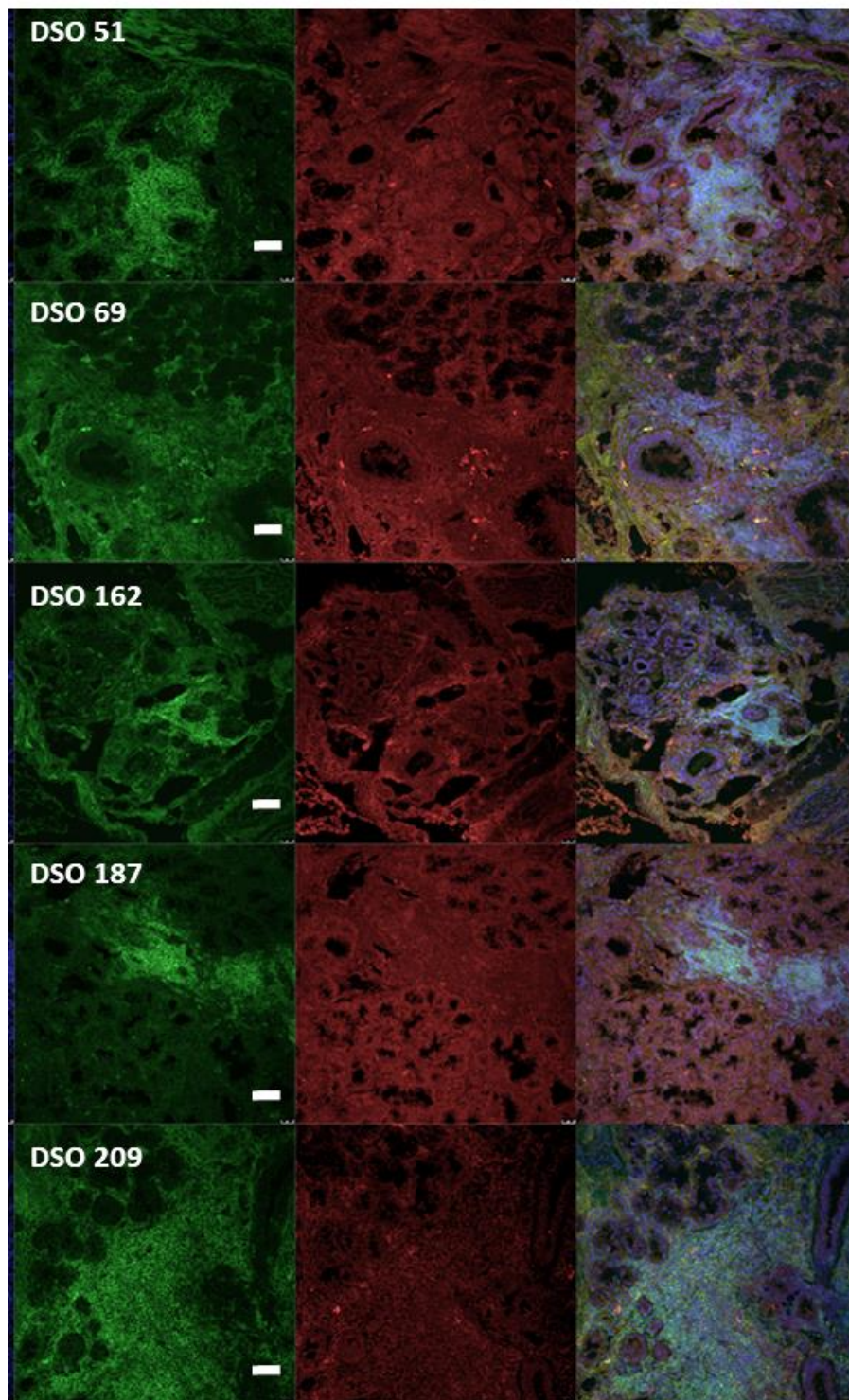
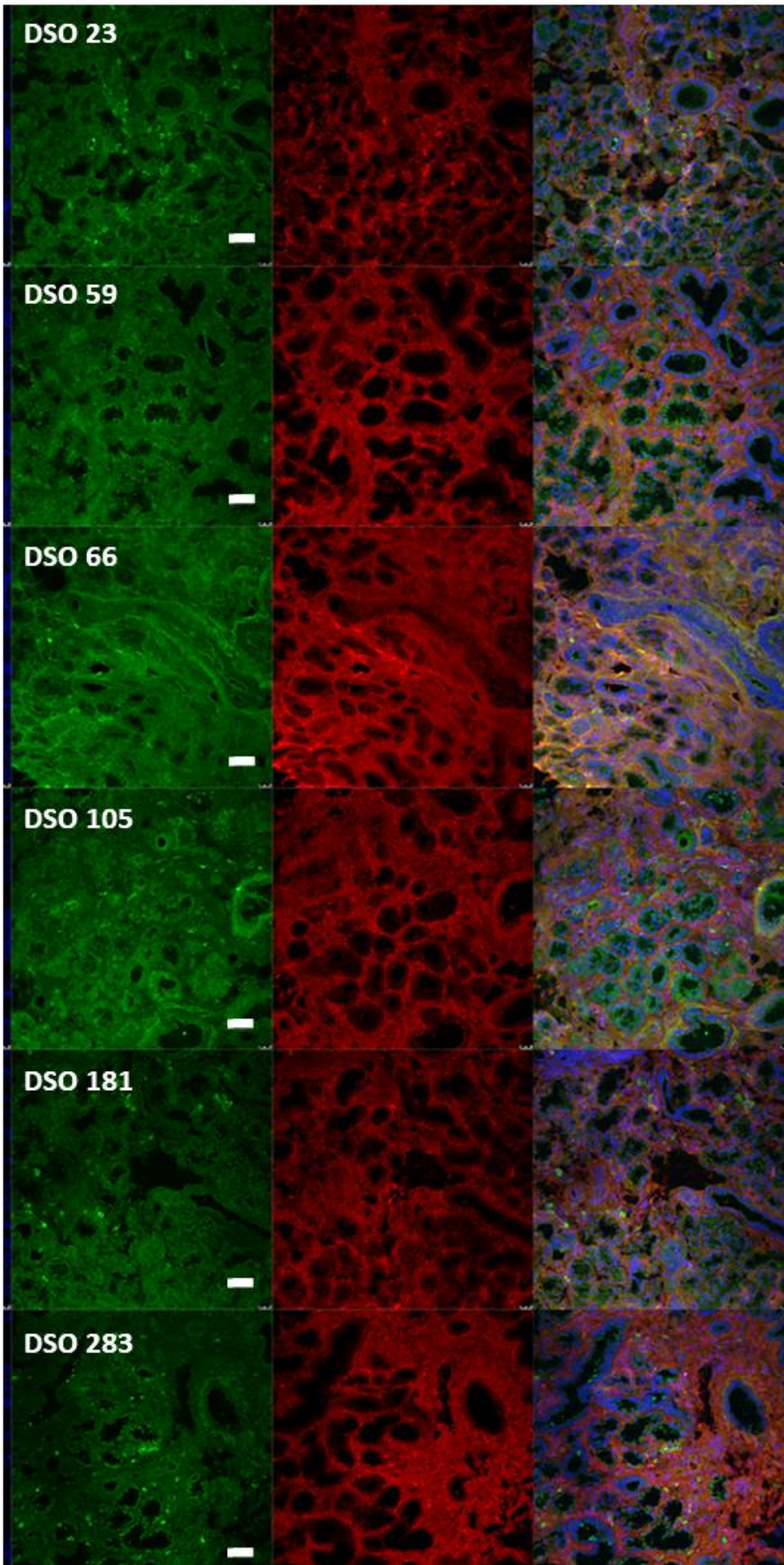


Figure 3.1-8 Immunofluorescent staining of PSS positive and non-PSS patient labial salivary gland tissue for CD29 (green) and AMY1a (red). Nuclei are visualised with DAPI. 10um sections and images taken at 20x magnification, scale bar equal to 50um.

SSB, PDGFRb, Merge

Non-PSS



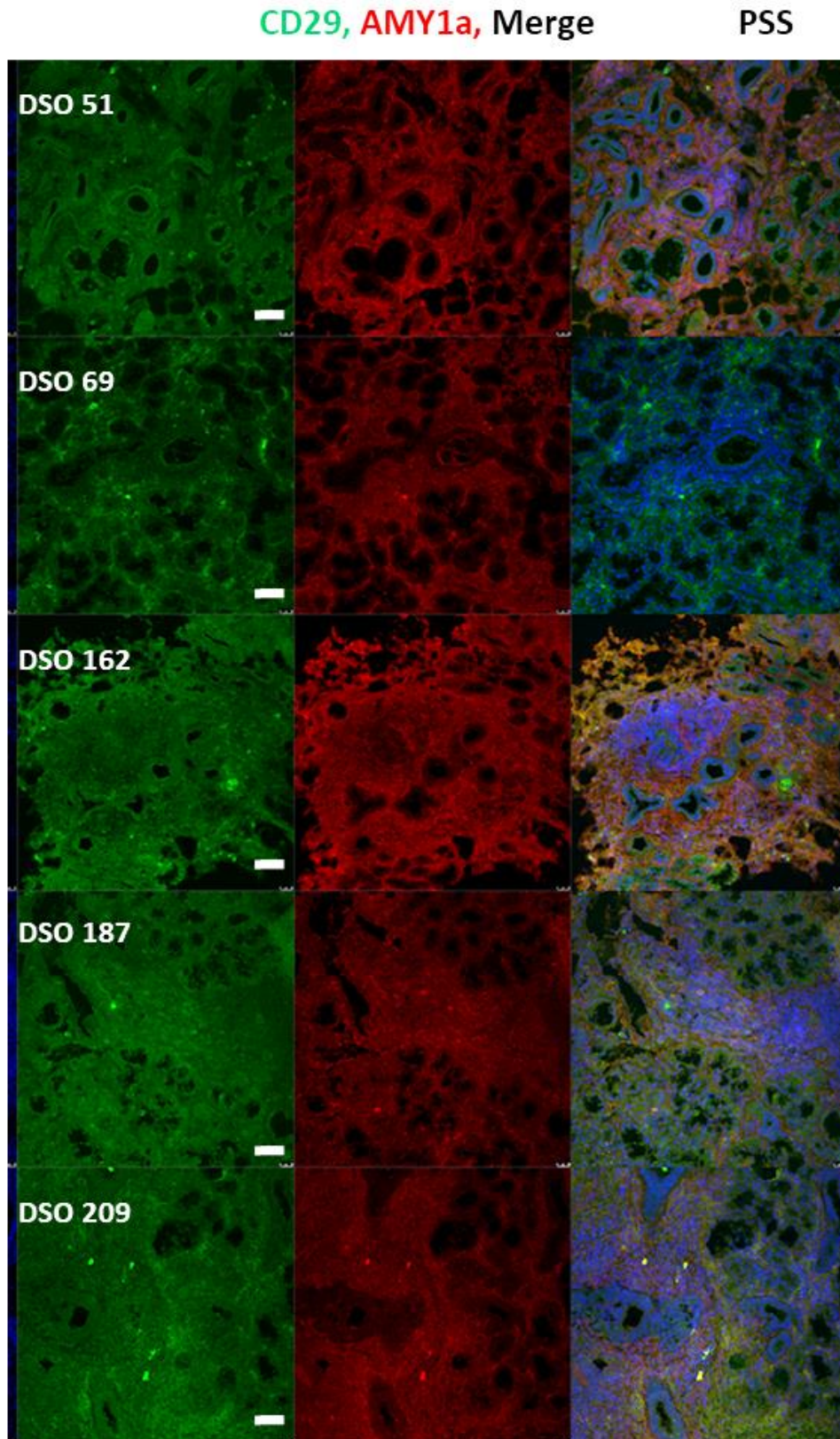


Figure 3.1-9 Immunofluorescent staining for PDGFR β (red) and SSB (green) in labial salivary gland tissue from non-PSS and PSS patients. Nuclei are stained with DAPI. Sections are 10um thick, with images taken at 20x magnification, scale bar is equal to 50um.

From the images in Figure 3.1-9, it appears that the PDGFR β staining highlights a similar mesenchymal cell population to the Vimentin staining. Although there are high levels of background fluorescence, fibrous staining patterns can also be observed around structures that appear to be either ducts or acinar tissue. This coincided with the Vimentin versus E-cadherin staining demonstrated earlier in Figure 3.1-1, with good demonstration of the discrete cellular populations of the salivary gland. The lesions also did not stain for PDGFR β , with reduction of the marker in the areas impacted by the immune infiltrates.

The staining profile of the human salivary gland tissue is outlined in Table 3.1-1, indicating how specific cell populations can be identified by a couple of pan-epithelial or pan-mesenchymal cell markers. However, there are many markers that could be seen across both populations which could interfere later when choosing which markers to use to identify cells in culture environments. By compiling a table such as this, it has enabled us to identify E-cadherin and K14 as ideal candidate markers for epithelial cells, and Vimentin, PDGFR β and CD105 for mesenchymal cells.

To expand on the characterisation of the human biopsy samples, samples were sectioned onto specialised membrane slides for use with laser capture microdissection technology. Regions of tissue were selected as demonstrated in Figure 3.1-10. Initially, tissue was stained using immunofluorescence staining, however this technique produced high background fluorescence on the Arcturus Laser cutting microscope, obscuring the regions of interest. Therefore, tissue was stained using H&E staining, shown in Figure 3.1-10, with a first look establishing the structure of the tissue before regions were collected and analysed for discrete regional differences in markers

involved in stem cell fate determination pathways, Gli1, Gli2, Gli3, Glis1, Glis2, Glis3, Patched1 (Ptch1), Patched2 (Ptch2), and Smoothed (Smo), by quantitative real-time PCR analysis.

Human Tissue	Acinar Secretory Cells	Epithelial Ductal Tissue	Mesenchymal Tissue	Immune Cells	Neurovascular Tissue
Marker					
E-Cadherin	+++	+++			
Vimentin			+++	+++	+
AQP5	+++				
Amylase	++				
PDGFRb			++		
CD105			++		
CD106			+		++
CD4				+++	
CD19				+++	
CD133	+	++	+	+	+
NSun2	+	+	++	+	+
Sox2	+	+	+	+	+
Tubulin	+	+	+	+	+
SSB	++	++			
CD45				++	
K14	+++	++			

Table 3.1-1. An overview of immunofluorescent staining presented in human labial salivary gland biopsies. Staining profiles demonstrate the discrete staining patterns observed in the salivary gland tissue, enabling identification of specific structures in whole tissue, and identifying individual cell populations later on in cell culture conditions.

3.1.2. Regional Analysis of non-PSS versus PSS Tissue by LCM

In order to investigate the molecular changes influence by the presence of PSS associated immune lesions, regions of tissue were selected and removed through the use of Laser capture microdissection, as described in Materials and Methods 2.7. Regions were selected as demonstrated in Figure 3.1-10, and it was possible to remove the regions as demonstrated in Figure 3.1-11, using H&E staining. RNA extraction could then be performed on aggregated tissue sections and analysed against a panel of primers for markers associated with inflammation, stem cell fate determination and quiescence through real-time QPCR.

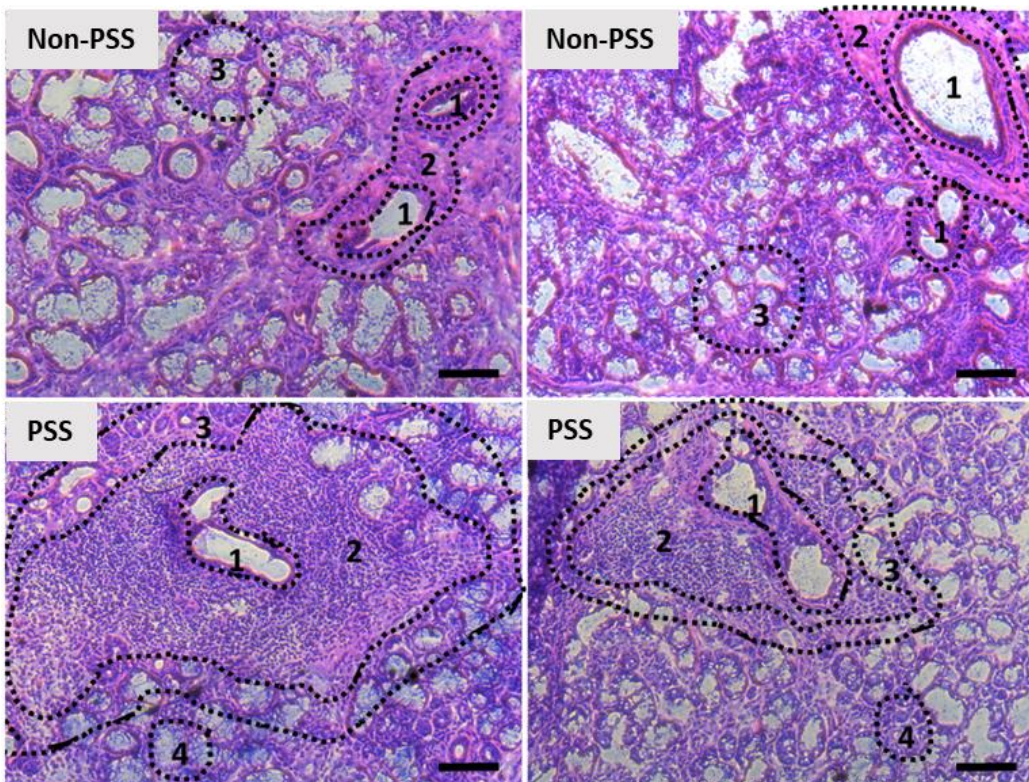
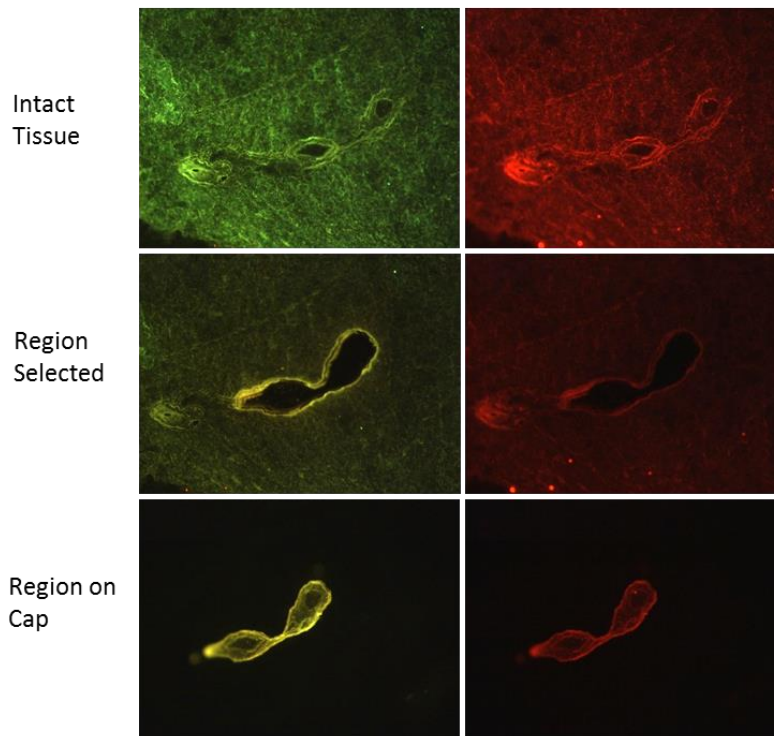


Figure 3.1-10 A diagram demonstrating how the regions of interest to be selected and removed through laser capture microdissection were decided upon. Non-PSS tissue regions include: 1) ductal epithelial cells, 2) surrounding mesenchymal cells structures around ducts, 3) acinar tissue. PSS tissue regions include: 1) immune lesion associated ductal epithelial tissue, 2) immune lesion, 3) peri-lesion region, 4) un-associated acinar tissue. These regions give a good representation of different tissue regions whilst enabling a comparison to be drawn between the cohorts. Scale bar is equal to 100um.

Vimentin and E-Cadherin



Haematoxylin and Eosin

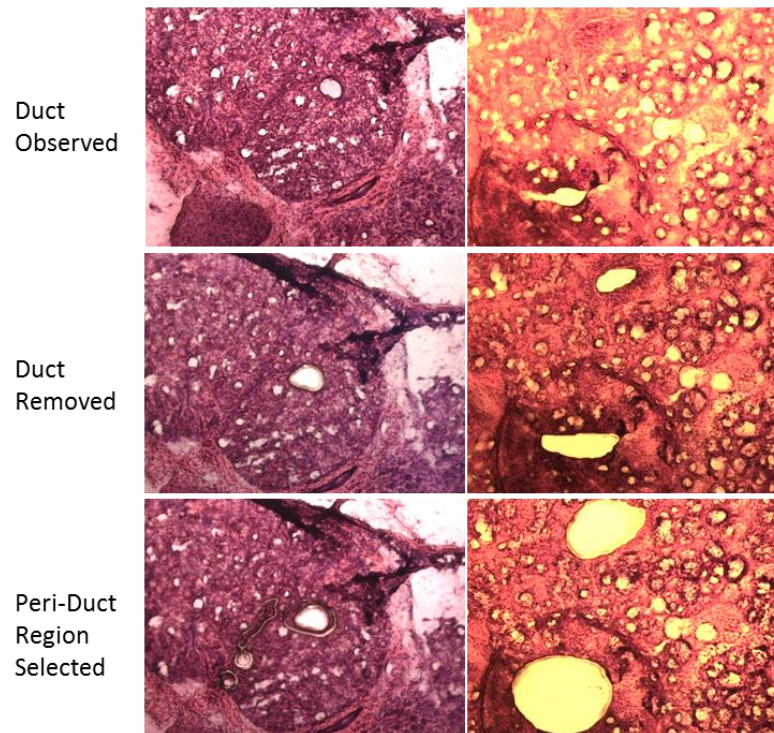
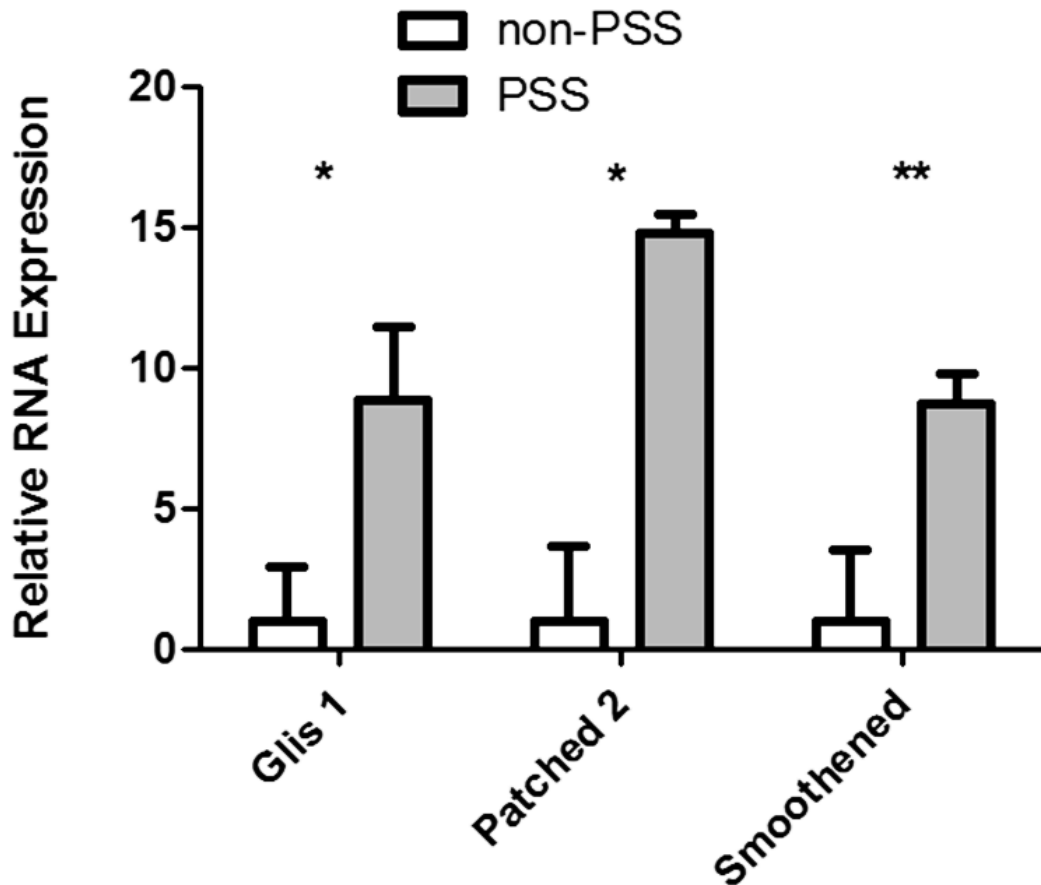


Figure 3.1-11 Representative images of regions of interest , showing which regions were removed from biopsy samples, with IF and H&E staining optimised on non-PSS patient samples. Through each stage, it's clear to see the regions being removed from the tissue, and the UV laser cutting through the issue and membrane. H&E stain gave a better visualisation of tissue structure for removal of regions.



	Normalised Mean of Ct		P Value	Significance
	non-PSS	PSS		
Glis1	9.84	7.07	0.03592	*
Patched 2	8.159778	5.000917	0.007816	*
Smoothened	6.822833	4.002833	0.001892	**

Figure 3.1-12 *Glis1*, *Ptch2* and *Smo* are significantly increased in PSS patient biopsies when Ct values are pooled from all regions collected, across all patients in each cohort. Expression profiles calculated from Ct values from LightCycler SyberGreen QPCR. $\Delta\Delta Ct$ displayed as a value of relative mRNA expression, with P values calculated from student t-test analysis on normalised mean Ct values. (P<0.0005: ***, P<0.005: **, P<0.05: *). Non-PSS n=4, PSS n=4. Variation in RNA expression influenced by the regions selected via LCM did not produce significant difference.

RNA quantity was low, which meant that PCR cycles for many genes tested did not have Ct values that peaked, despite the primers having previously been confirmed to work effectively. Therefore, analysis of primers for *Gli1*, *Gli2*, and *Gli3* did not produce any results, this is explained in Appendix 6.2.3. However, there were significant changes in expression levels of *Glis1*, *Ptch2* and *Smo*, when the mean Δ Ct values were compared across all regions between the two cohorts of patients as shown in Figure 3.1-12. This indicated a global increase in expression levels of *Glis1*, *Ptch2* and *Smo* in the PSS positive patient samples. The normalised mean Ct values were converted into values of relative expression level of the target RNA. Therefore, the lower the relative RNA value, the lower the level of expression. The aggregated $\Delta\Delta$ Ct of all the regions of the same patient tissue were calculated and plotted to generate the graph in Figure 3.1-12, demonstrating the relative RNA expression levels as a direct comparison between the PSS and non-PSS cohorts; effectively a comparison of bulk tissue samples rather than regional comparisons.

Further statistical analysis was performed, using RStudio to perform student t-tests between the expression levels of each marker between each region. The only significant result was that *Smo* was more highly expressed in the non-associated acinar region of PSS positive patients, compared to the matched acinar region in non-PSS tissue ($P=0.04924$), the significance of this will be discussed in 3.3 Discussion. As this statistical test directly compares the Ct values normalised against the background level of the housekeeping genes, the graphs in Figures 3.1-13, 3.1-14, and 3.1-15 appear different to Figure 3.1-12; the larger column signifies a larger Ct value, which signifies a lower level of RNA expression, due to a later peak calling during the QPCR.

Using the same software, a repeated measures ANOVA was performed, which takes into consideration the three variables: three comparable regions of interest, disease phenotype, and gene of interest. In Figure 3.1-13, using normalised mean Ct values, *Glis1* demonstrated no significance between the expression levels between regions and cohorts. *Ptch2* showed that the most significant factor for the differences observed between the variables was caused by the disease status (P= 0.02135(*), 0.03378(*), 0.03527(*)) shown in Figure 3.1-14, whilst *Smo* also indicated that disease status was the most significant factor in the difference between samples (P=0.003212(**), 0.004394(**), 0.009964(**)) Figure 3.1-15.

What these results indicate is that, although there are differences in levels of expression of *Glis1*, *Smoothed* and *Patched* between different regions of the tissue within the same patient, these differences are not significant. We should expect some heterogeneity across tissue as different regions will have different cellular composition and different cellular activity. However, there is significant changes in expression between PSS and non-PSS patients, that even over such a small cohort of samples, due to the nature of repeated measures ANOVAs, present with very high significance.

With an increase in the expression of *Smoothed*, in the future it would be interesting to analyse downstream effectors, such as *Gli* and *SUFU* as described in Figure 1.3-1 and to monitor cell cycle and cell fate determination pathways.

Glis1

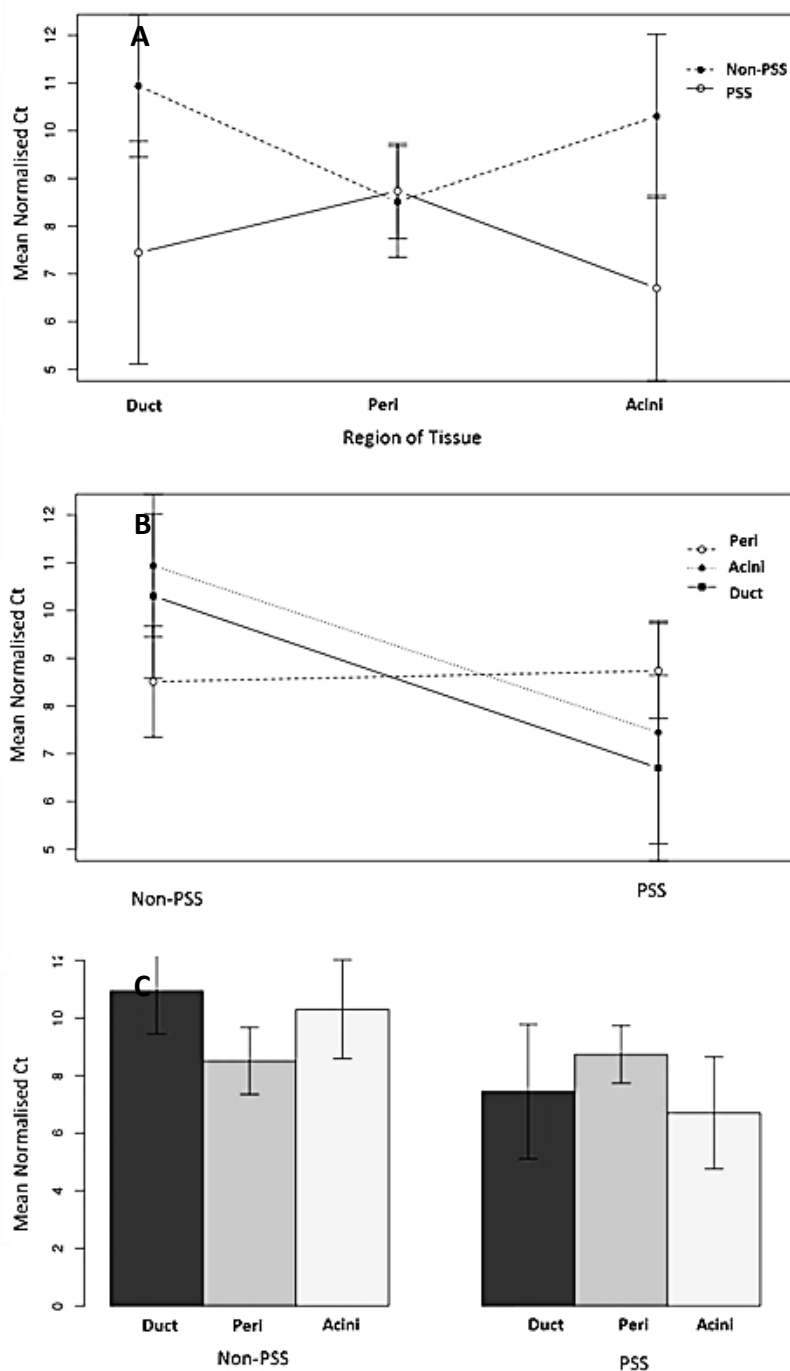


Figure 3.1-13 A) Variance of expression of *Glis1* is not shown to be significant either between the disease cohorts, B) or between the regions of interest. C) Furthermore, Student t-tests did not demonstrate any significance between the Ct values between each region and disease cohort. Graphs generated using repeated measures ANOVA analysis on R Studio, as described in 2.16 Statistics.

Patched 2

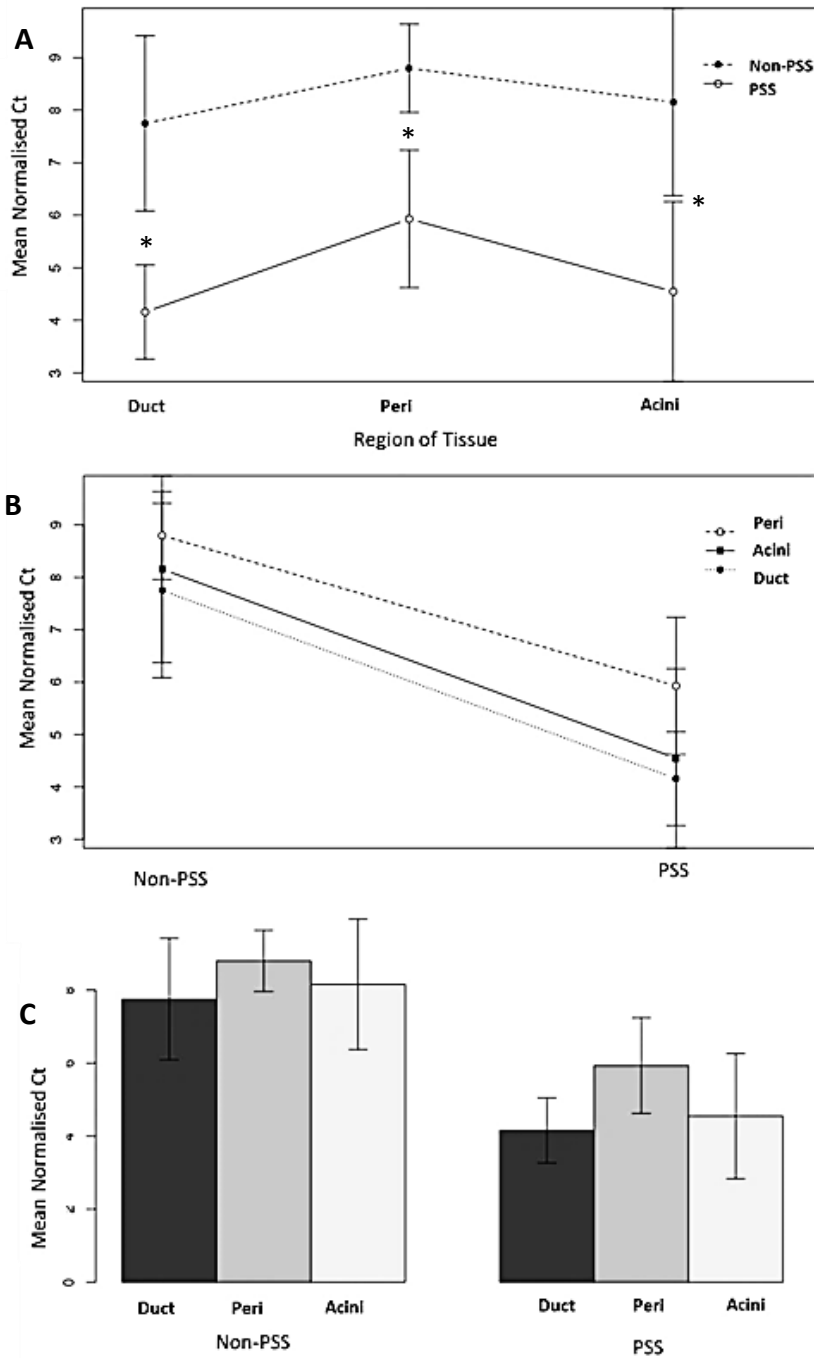


Figure 3.1-14 A) *Ptch2* demonstrates significant differences between the non-PSS and PSS cohort. B) There was no significance between regional differences in mean Ct values. C) There was no significance when performing the Student t-test between each region and disease cohort. ($P < 0.0005$: ***, $P < 0.005$: **, $P < 0.05$: *). Graphs generated using repeated measures ANOVA analysis on R Studio, as described in 2.16 Statistics.

Smoothened

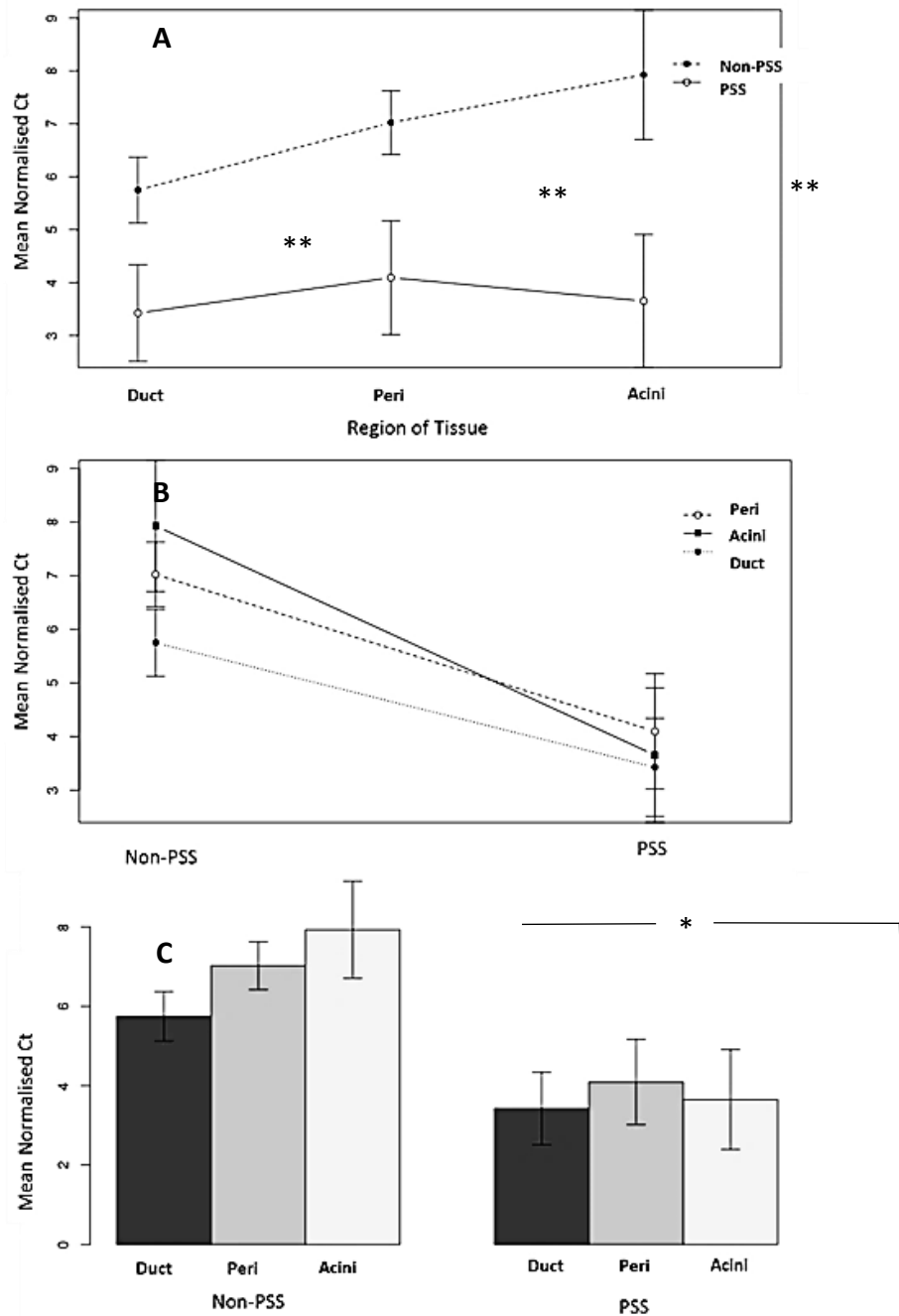


Figure 3.1-15 A) The expression of *Smo* is significantly impacted by disease state, with increased expression in PSS samples. B) The region has no significant impact on expression levels. C) The Student t-test indicates significance in the expression of *Smo* between the acinar regions of the non-PSS and PSS tissue ($P=0.04924$). ($P<0.0005$: ***, $P<0.005$: **, $P<0.05$: *). Graphs generated using repeated measures ANOVA analysis on R Studio, as described in 2.16 Statistics.

3.1.3. Discussion

The results above demonstrated that E-cadherin staining identified epithelial tissue, defining ducts and the sero-mucous acinar structures of the salivary gland, whereas Vimentin stained mesenchymal cells within the tissue, forming the stromal supporting structures surrounding ducts and the acinar cells. This is consistent with the literature that describes these markers as ideal candidates for discriminating between the two cellular niches (Mani *et al.*, 2008; Li *et al.*, 2011). E-cadherin, which is known to be involved in tight-junction complexes between epithelial cells, interacting with β -catenin and the cell cytoskeleton to control cell-cell signalling, maintaining cell structure, and is known to go through moderated changes in cell migration during wound healing and metastasis in cancer progression (Li *et al.*, 2011). The mesenchymal cells are stained positively for the generic pan-mesenchymal cell marker, Vimentin, which is a known mesenchymal cell marker, as the reduction in expression of E-cadherin and the increase of expression of Vimentin is one of the key hallmarks of Epithelial-Mesenchymal cell transition (Mani *et al.*, 2008; Kalluri and Weinberg, 2009). It is a filament protein that can also be integrated with Neurofilament protein in neuronal cells. However, it is also present in the cytoskeleton of mesenchymal cells and, therefore, it was useful for identifying any compartments of the tissue that did not stain for epithelial markers. However, in the PSS-positive patient samples there was less E-cadherin staining in these regions, correlating with the known destructive behaviour of the disease. The staining profiles and comparisons of H&E histological staining were consistent with the diagnoses provided by the pathologists at the Sjogren's Registry, and informed by the

patients, and although chosen for their low-grade status, this still presented a range of phenotypes.

The comparative H&E staining demonstrated the differential staining of different regions of the tissue. The acinar regions appeared darker purple because they contained tightly packed epithelial cells and appeared to stain more intensely for haematoxylin, the nuclear stain. Fibrous regions, made up of the supporting mesenchymal cell populations, stained a light pink colour, indicating low cell density and high concentrations of collagen. This stain allowed confirmation of the established disease phenotype assigned by the tissue bank. The PSS positive patient samples presented with dark and discrete focal lesions of immune cell infiltrates, which defined the PSS disease status. In the images in Figure 3.1-2, these lesions are delineated by dotted white lines and demonstrate the diversity of the lesion presentation. Furthermore, one non-PSS patient, DSO 283, presented with an appearance of dense immune infiltration. There is evidence to suggest healthy patients can present with small focal lesions due to minor infections or non-pathological infiltration (Radfar *et al.*, 2002). Due to this, the negative PSS diagnosis of this patient was re-confirmed with the tissue bank.

In Figure 3.1-3, strongly defined CD4 positive T cells can be observed, which are known to be the major cell type recruited during the initiation of PSS. Smaller discrete populations of CD19 positive B cells within the CD4 positive lesion were also present. These appeared more frequently in the larger, higher grade lesions, but could also be observed in some of the smaller, denser lesions. The CD19 positive B Cells indicated a higher grade of PSS, as they had been recruited through the acquired immune system, through the process of antigen presentation (Kramer, 2014). The presence of these

CD19 B cells could suggest a higher risk of developing conditions such as Non-Hodgkin's Lymphoma, due the formation of granular centres (Le Pottier *et al.*, 2009; Lee *et al.*, 2016). It was imperative to note that, where tissue presented with intense CD19 positive B Cell regions they did not appear to have any further change in the presentation of other markers. In unaffected regions, these patient samples presented in just the same way with E-cadherin and Vimentin.

In comparison to the healthy tissue, the PSS positive tissue had significantly increased presence of immune cells. Here, CD4 positive cells were observed within most samples of the non-PSS cohort, but circulating immune cells in healthy tissue should be expected. Furthermore, this study did not have access to more detailed clinical data, which could have identified additional complications such as infections or other autoimmune conditions that could have detracted from the reliability of a sample.

When other markers as potential identifiers of mesenchymal sub-populations were also investigated, good staining results for CD29 and PDGFR β were achieved; markers, which have previously been established as identifying mesenchymal stem cells (Takahashi *et al.*, 2014; Lu *et al.*, 2015), staining tissue in consistent patterns similar to that of Vimentin but in smaller proportions. However, CD29 highly stained the focal lesions in the PSS positive patients, which made it difficult to differentiate between the non-lesion mesenchymal cells and immune infiltrate lesion areas that stained positive for CD29. On the other hand, PDGFR β became a useful marker to investigate further as the staining appeared to be present in the general secretory tissue and around duct structures, whilst it was not increased in the focal lesions of PSS positive patients. Both these

markers have been shown to present similar distribution patterns to each other and Vimentin, with no overlap between epithelial cell markers such as E-cadherin.

Alternatively, SSB is a marker that is present in normal healthy salivary gland tissue, being normally detected in the nucleosome of glandular epithelial cells in the salivary gland (Human Protein Atlas; Uhlén *et al*, 2015), whilst the detection of auto-anti-SSB is one key method for accurate diagnosis of PSS (Mavragani, Tzioufas and Moutsopoulos, 2000). As with the other markers, in the direct vicinity of the immune lesions, there was an absence of staining for SSB, similar to that seen in the PDGFR β staining. However, a more significant decrease in SSB staining was expected to be observed in the PSS compared to non-PSS samples as it is one of the proteins against which the autoimmune condition is raised.

The functionality of the tissue was also investigated, hoping to demonstrate a reduction of mature differentiation markers within the PSS affected samples. Aquaporin 5 (AQP5), is a known water transport protein (Gresz *et al.*, 2014), described earlier in the introduction, which is involved in the movement of water across the acinar epithelial tissue into the lumen of the salivary glands, and is only found in fully mature functional saliva secreting cells. Our results demonstrated that the AQP5 positive regions were also positive for CD133, whereas the duct structures only stained positive for CD133 but not AQP5, indicating a persistent stem cell-like population. This could correspond to previously published work that demonstrated that stem cell niches of epithelial tissue appear constrained to the intercalated duct and replicate in a conveyor-belt fashion away from the intercalated duct, and that there are no fully differentiated secretory epithelial cells in the ductal tissue (Aure, Arany and Ovitt, 2015). CD133 has an unknown

mode of action but is thought to be involved with cell membrane modification with the formation of cilia structures, and has been shown to stain stem cell niches in other tissues (Corbeil, Fargeas and Jászai, 2014). These patterns remained unaffected in the lesion free areas of the PSS positive tissue, and only exhibited a change in the areas defined as immune lesions, most certainly due to the lack of epithelial tissue remaining in these regions.

Acetylated tubulin is a filamentous protein involved in the formation of cilia processes as part of the cell membrane (Sudo and Baas, 2010). Cilia are important for cell signalling pathways and are involved with cell membrane topography, cell maturation and differentiation (Goetz and Anderson, 2010), particularly the Sonic Hedgehog signalling via the Proliferating Cell Nuclear Antigen Receptor 1 (PCNA1) receptor, which dictates stem cell fate (Jaszai *et al.*, 2007; Corbeil, Fargeas and Jászai, 2014). Currently there is no understanding on the impact of PSS on stem cell fate determination, and there are no publications investigating the role or impact of the disease on SHH or its downstream effectors. Therefore, we hypothesised that processes involved in stem cell fate determination could be impacted and result in the lack of tissue regeneration caused by PSS, including CD133 (Proliferating Cell Nuclear Antigen Receptor 1) and related downstream signalling such as Patched, Smoothed activation of Gli transcription factors, and the association with cilia structure modulation.

Initially, reduced staining frequency of acetylated tubulin had been expected, specifically truncated cilia structures. However, cilia structures are typically between 1 and 10µm in length (Dummer *et al.*, 2016), and we found that, in the arboreal structured salivary gland tissue, it is difficult to orientate the tissue to visualise the cilia effectively. Instead, we observed pronounced structures staining positively for acetylated-tubulin.

There is evidence to show that fibroblasts and peripheral neuronal dendrites have acetylated tubulin rich regions in their microtubules and, as the salivary gland tissue is rich in nervous tissue for stimulation, isolating a discrete staining pattern of cilia using only acetylated tubulin would prove to be difficult (Sudo and Baas, 2010). The staining observed in Figure 3.1-6 can be interpreted as peripheral nervous tissue that is involved in stimulation of the salivary gland tissue, staining positively for acetylated tubulin. However, it would be beneficial to continue this work, so as to compare cilia presentation between PSS and non-PSS patient samples, using higher magnification and possibly electron microscopy images, mimicking similar work established by other members of the research group.

Although the large panel of markers and the histological staining has helped to distinguish the structure of the labial biopsy samples, whilst indicating a very clear phenotype for the PSS and non-PSS patient samples, this study most significantly has observed lesions stained heterogeneous staining throughout the same patient and across cohorts, shown in Table 3.1-1, potentially reflecting the high diversity of immune cells recruited in the immune lesions. To develop a better understanding of stem cell fate during PSS, and impact of PSS on the expression of mature cell markers and cell cycle, other techniques and methods should be used to analyse expression patterns of cell differentiation and maturation markers.

The limitation of this work was that subjective interpretation of staining patterns within the tissue was heavily relied upon. The way in which lesions occur within the tissue prevented consistent images being taken between PSS and non-PSS patients, as we had

to focus on areas impacted by immune lesions within the disease cases. To counteract this, excessive images were taken with a mixture of affected and unaffected regions.

The high affinity of the lesions for many markers distorted the staining profiles, such that it was impossible to accurately analyse or quantify any staining in comparable regions of interest within the non-PSS patients. It was only possible to evaluate the perilesion regions and the unaffected tissue regions from the PSS patients, whilst in the non-PSS tissues, it was possible to characterise the whole tissue. Ideally, it would have been preferable to visualise the ducts that were directly being attacked by the invading immune cells, but frequently they were indiscernible beneath the immune lesion.

What this staining did not demonstrate was any change in generic markers between the non-PSS and PSS positive patient samples. Although a reduced staining pattern was observed in some of the markers directly, where the lesions were, this was accounted for by the fact that the invading immune cells destroyed the tissue. The unaffected regions presented with normal staining patterns for all of the markers, with no suggestion of any impact of the immune infiltration away from the focal lesion site. Due to the heterogeneity of the tissue type and the focal formation of the lesions, it was therefore difficult to accurately quantify how the staining differed between the case and control samples. It is evident from our IF characterisation of the tissue that there is significant impact of PSS on the structure and staining patterns of the tissue, but alternative methods to investigate these changes and more complex mechanisms still need to be considered.

Experimentally, it may be easier to analyse cultured cells, although it is evident that they are not representative of the *in vivo* situation. Purified cell populations in culture appear

to be stem cell enriched, as demonstrated by their continued proliferative ability, and could indicate a change in cell behaviour and marker expression when compared to the *in vivo* case. Furthermore, the epithelial and mesenchymal cells in culture grow at different rates and therefore future experiments would have to coordinate collections to ensure the same passages are analysed from each cell type for each patient. A synchronising experiment, that pushed the cells into the same stage of the cell cycle, could have also been a potential mechanism of study. Regardless, cell cultures can be a good representative model for studying the molecular changes between PSS positive and non-PSS patients, when analysing molecular mechanisms and cell behaviour.

Alternatively, it was thought that Laser Capture Microdissection (LCM) would be able to clarify these mechanisms by selecting very specific regions of the tissue, such as the ductal epithelial tissue associated with immune lesions, to investigate how these cells may have had an inducement in their cell signalling capacity. However, the RNA yield was very low and resulted in many markers being discounted from analysis. However, the LCM results did demonstrate that *Glis1*, *Patched2* and *Smoothed* are globally elevated in the PSS positive patient tissues. By aggregating the patients into two disease phenotype cohorts, and then comparing the normalised mean Ct values across all regions, a significant elevation of expression across all three genes in the PSS cohort was demonstrated.

Further analysis showed that the control acinar regions selected in both PSS and non-PSS tissues had a significant change in *Smo*. This is novel work, as it indicates that the tissue in regions not directly impacted by PSS immune lesions have an alternative phenotype, that is significantly different from comparative regions selected from non-

PSS tissue. This suggests that either, the patients already present with an altered *Smo* phenotype before the disease initiation, or that when the disease is progressing, the tissue is being stimulated to increase *Smo* expression in a way that could facilitate an increased activation of the SHH pathway. However, there is still an observed decrease in salivary flow rate and we were unable to characterise a change within the Gli transcription factor family, making this an area for further research, as Gli proteins can be activated through the Smoothed receptor or indirectly by MAPK/ERK1 signalling (Rovida and Stecca, 2015).

3.1.4. Conclusion

Through immunofluorescent staining, we have developed a panel of markers which identifies the two major cell populations within the salivary gland tissue. We further demonstrated the combination of T and B immune cells which form the immune lesions and how they frequently stain positive for a large number of other markers.

Further to this, CD29 and PDGFR β were used as markers to identify subpopulations within the mesenchymal cell population, the more reliable of which was PDGFR β as it does not stain the immune lesions positively and therefore, can be used with more confidence within the PSS-positive tissue samples. However, both can be used in cell culture work, and are frequently used in the literature. In this study stem cell and cell differentiation markers were used, such as CD133 and AQP5, to help characterise the mature regions of tissue that contained fully differentiated cells, whilst demonstrating the lack of many of these markers in regions where lesions have destroyed the tissue.

Immunofluorescence results produced in this chapter were useful for the rest of the project, as we established a panel of markers that could be used throughout the rest of the experimental plan, investigating the regenerative capacity of our cells of interest. The markers from the IF staining could be used to identify comparative cell cultures, and potentially identify stem cells or functional cell populations *in vitro*.

The LCM experiments were designed to understand the impact of PSS on cell signalling pathways within the tissue, particularly investigating stem cell fate determination and functionality of cells within the diseased tissue environment. Currently there are no publications available that investigate the role of Sonic Hedgehog (*SHH*) and its

associated proteins within Sjogren's Syndrome and very few that discuss *SHH* and its role within salivary glands in general.

This change to the expression pattern of *Smo* between the PSS positive and non-PSS patient samples indicates a potential lead into investigating the molecular changes in PSS and understanding the progression of the disease state. These preliminary findings, using the LCM technique and relative RNA expression analysis, were completed towards the end of the PhD period and have potential for delivering much more significant findings regarding the mechanistic actions underlying the depleted tissue regeneration. To achieve this, the LCM work should be expanded to collect more regions from more tissue sections, increasing the RNA yield and "n- number" of PSS and non-PSS patients, enabling more accurate comparisons of relative RNA expression levels. Furthermore, it is believed that the techniques used here could be developed further, investigating better mechanisms of fixing and staining tissue to collect regions whilst preserving the RNA more efficiently using RNA preservation reagents. With more time and finances, the research group would be able to develop a better understanding of which mechanisms changed within patient tissues, resulting in the reduced repair mechanism.

3.2. Development of Murine Organoid Models to Investigate the Role of Mesenchymal Cells

The fibrotic lesions in radiotherapy exposed tissue or PSS patients, is not removed by the body and the addition of stem cells to the tissue may result in tissue hyper-plasticity and would not necessarily result in an increased ability to secrete saliva, especially if ducts were blocked or damaged. By transplanting a new organoid into the correct area, it could be possible to restore salivary function, and even remove the damaged gland.

One example of this is the research carried out by (Pradhan-Bhatt *et al.*, 2013), who used hydrogel systems to generate small, three-dimensional spheroids that are able to secrete salivary fluids and proteins that are affected by neurotransmitter stimulation. Implants that had been successfully implanted into a rat host could successfully demonstrate staining for amylase and b-catenin, two proteins that are considered examples of functionality in mature salivary gland tissue.

Similarly (Ogawa *et al.*, 2013) have had significant results with their bioengineered salivary and lacrimal glands, generated from embryonic epithelial and mesenchymal tissue, recombined and implanted into a mouse. They took salivary glands from embryonic day 13.5 mice, used dispase to dissociate the epithelial tissue from the mesenchymal tissue surrounding it. They could then digest these elements separately and recombine the cells in a three-dimensional cell culture matrix. The group could successfully develop organoid structures that were re-implanted into adult mice, with the addition of an engineered excretory duct. These organoids then developed further to become fully differentiated and functional salivary gland or lacrimal glands within the

mouse after implantation (Hirayama *et al.*, 2013; Ogawa *et al.*, 2013; Hirayama, Tsubota and Tsuji, 2015). The limitation of this research is that the focus is on using embryonic mouse tissue instead of attempting to regenerate tissue derived from adult mice or human clinical samples. The tissue used above will have a greater population of stem cells or stem-like cells, which would enable a greater regenerative capacity. However, this would not correlate with fully mature tissue, and as both IR and PSS happen predominantly in an adult human population, it could be suggested that concentrating efforts on regenerating diseased human clinical samples would have more impact on the research field.

The common goalposts to demonstrate an effective organoid culture model is to demonstrate cell survival and proliferation, frequently there is the identification of the formation of a lumen, with polarisation of the acinar structures demonstrated with the presence of MUC1, which should only be present on the apical membrane of acinar secretory cells, and the production and secretion of alpha-amylase, one of the key digestive enzymes produced by the salivary glands (Pradhan-Bhatt *et al.*, 2013).

Alternatively, young mice were sacrificed at 8 – 12 weeks old and their salivary gland tissue excised, and enzymatically digested whilst agitated to generate single cell suspensions before being cultured directly into a three-dimensional gel system (Nanduri *et al.*, 2014). This work by Robert Coppes' group generated organoid structures too, but they are subsequently digested and re-plated into fresh gel, to rid the culture environment of cellular debris and to promote cellular differentiation. These secondary organoids were transplanted into radiation induced hyposalivation mice models and were successfully grafted, with an increase in salivary flow rate, improved histology and

elevated staining of AQP5, suggesting the grafting itself also added to the survival and growth of the structures.

The many compartments of cell populations within the salivary gland complicates our understanding of tissue regeneration. Different research groups have attempted to understand the importance of specific cell niches within salivary glands, and how they may aid the development of fully functional salivary gland organoid structures. This can include blood vessels and the peripheral nervous system, both systems that are notoriously difficult to model *in vitro*, but which contribute extensively to the development and expansion of tissue cultures.

Work carried out by the Hoffman lab in the NIDCR has successfully demonstrated the importance of grafting organoids to improve the neural stimulation of the tissue, in order to increase the efficacy of salivary gland tissue regeneration in an IR exposure assay. Stimulation of the salivary glands by the peripheral parasympathetic nervous system will enable the tissue to produce an enhanced regenerative phenotype (Knox *et al.*, 2013). The group could successfully show that embryonic salivary gland rudiments exposed to IR had increased apoptosis, reduced end bud numbers and reduced innervation. This paper also confirms the negative impact of IR on human parasympathetic innervation, with samples presenting an impaired and apoptotic phenotype with less Neurturin staining. However, treatment of the mouse embryonic ex-vivo organ cultures with excess Neurturin, before and post-irradiation, enabled a greater restoration of parasympathetic innervation which led to a greater tissue regeneration, measured by an increased in terminal end buds and E-Cadherin expression (Knox *et al.*, 2013).

Similarly, there has been significant leaps in the ability of researchers to develop neuronal organoid structures that are implanted into the brains of mice (Mansour *et al.*, 2018). They successfully demonstrate the importance of vascularisation on the development of the implanted models, by comparing the developmental reach and the nervous responses of the implant on the host brain tissue. Integration of the nerves, penetrance of host glial cells, and host-model synaptic junctions could also be demonstrated. Whilst the impact on the behaviour of the animals was very limited, and there could be no way of investigating changes or impact on personality or demonstrating distorted motor-control, however, they demonstrated the significant impact of vascularisation to the advanced development of organoid models.

One concern for transplanting organoids would be graft versus host disease. Mice models for the purpose of organogenesis implantation are frequently immune-suppressed and, therefore, non-reactive to invasive cell populations. Whilst designing novel treatments for human patients, it would be ideal to be able to take cells directly from a patient's own salivary glands, regenerate and implant an organoid structure that is then capable of replenishing the damaged tissue, whilst withstanding a potential fresh onslaught of the disease condition, in PSS. Furthermore, as PSS is characterised by autoantigens, implanting a bioengineered salivary gland rudiment into a patient could result in the new organ being similarly attacked by the immune system as before, resulting in no improvement for the patient (Ogawa *et al.*, 2013).

Another variable in the research into organogenesis as a therapy, is the variety of matrices in which cells models can be grown. Matrigel is a very well-established gel matrix, originating from a mouse sarcoma cell line – Engelbreth-Holm-Swarm cells. It is

a basement membrane secretion and will contain a variety of proteins such as laminin, collagen, entactin and heparin sulphate proteoglycans. It is frequently used in small volumes to coat cell culture flasks to enhance adhesion of cells and allow adhesion of normally non-adhesive cell lines. It can also be used in larger volumes to create three-dimensional cell cultures. One established method for studying stem cell niches in intestinal crypts is to generate models using Matrigel (Grabinger *et al.*, 2014; O'Rourke *et al.*, 2016).

Matrigel has limitations in that it is collected in batches and there can be significant variation between the expression levels of different growth factors within the gels. Furthermore, the growth factors are from a mouse cell line and may have significant influence over mouse derived cell cultures grown within the gels, or alternatively limit the translational approach of the gel when using tissue from other origins. However, it has been used quite frequently and is accepted as a viable and effective model for three-dimensional cell modelling.

Matrigel appears to be one of the most frequently used and well-established methods for three-dimensional culture assays, but other types of gels are being developed that could rival Matrigel in the way researchers can control the contents of the gel more, or have less variability between batches. In a Letter to Nature by Gjorevski *et al* 2016, their group compares the efficacy of their previously established ISC organoid models in PEG hydrogels with varying additions of laminin, perlecan, hyaluronic acid (Gjorevski *et al.*, 2016). The advantage of these systems is that they are more easily manipulated for different experimental needs. The group found that with hybrid PEG hydrogels containing both non-degradable and degradable PEG, they could alter matrix stiffness

in the correct way so that Yap proteins could be expressed, a result that the group had not previously been observed with Matrigel. They could establish well-formed intestinal crypt models with polarised cells, positive E-cadherin staining and could demonstrate functional ability with the presence of mucins.

By manipulating the exact composition of extra cellular matrix components in hydrogels, it could be possible to generate an effective organoid model without the use of stromal tissue. Sokol *et al* designed hydrogel components that specifically mimicked the ECM of mammary tissue: fibronectin, hyaluronic acid and laminin (Sokol *et al.*, 2016). Through their work, they could grow an accurate and functional model of mammary tissue, with a leading edge of stem cells driving growth of the terminal buds. The group did compare their results to Matrigel, as the previous standard, but could demonstrate that their organoids were able to reach a much higher level of differentiation and maturation in comparison.

Hydrogels and collagen gels, are more simplistic and can be lacking in many other components. Having to individually add these to culture assays would add an increased sense of control and reduce variability to experimental process, but this might not outweigh a very lengthy process of adding all the variable basement membrane proteins when there is a widely available, prepared alternative.

As an alternative route of research, instead of focusing efforts on the difficulties of implanting organoid structures into animal models, or complicated, hyper-realistic *in vitro* organogenesis, it was realised that the mechanistic interactions between the epithelial and mesenchymal cell types during tissue regeneration are poorly understood.

Therefore, this project rapidly changed direction, and instead of attempting to grow organoids for implantation, the focus changed to investigate how essential the mesenchymal cells were for the tissue regeneration pathways, and how this cell population, and mesenchymal stem cells, are impacted by PSS or exposure to ionising radiation. By adopting established protocols and developing the organogenesis assay as a tool with which to study changes in cell behaviour and molecular expression profiles, a novel use for the technology was created, with an aim to create consistent organoids that demonstrate a significant impact on the mesenchymal cell and mesenchymal stem cell niche.

Although this research is focused on the human condition, and how PSS induces a change to cell morphology and molecular profiles within the human salivary glands, the salivary gland organogenesis models were primarily developed using mouse derived cell cultures. This was concurrent to the characterisation of the human labial gland biopsy samples, and was used as an effort to preserve as much precious human samples as possible, whilst the protocol was established. The technique used was adapted from previously published tissue regeneration studies, and the resultant protocol generated consistent and reproducible organoids which, in the future, could be utilised to model the impact of PSS on human derived primary cells. Initially, the aim was to demonstrate a reliable technique and emphasise the necessity of mesenchymal cells within regeneration and organ development.

3.2.1. Mouse Cell Culture and Organoid Model Methods

Murine Sphere Protocol One

This protocol was adapted from Nanduri *et al*, 2014, as described in materials and methods 2.10. First cells had to be collected following the protocol for passaging cells, 2.8.4. Once cells had been collected and spun to form a pellet, the supernatant could be removed and the cells suspended in 1ml of culture medium in order to count the cells using the automatic cell counter or the haemocytometer. The first incarnation of the technique used 20,000 of each cell type per well, combined into their respective culture medium as a cell suspension. Epithelial cells were suspended in of DMEM F12 B27 supplemented media, and mesenchymal cells were suspended in complete Amniomax media, with sufficient cell suspension prepared to run triplicate experimental repeats simultaneously. 100ul of Matrigel was added to the bottom of each well, using pre-cooled plates and pipette tips, working quickly to avoid the gel setting unevenly and carefully to avoid bubbles which could disrupt efficient oxygen and nutrient exchange. The gel was allowed to set at room temperature before 200ul of each cell suspension was layered on top of it. Images were taken every day and the media gently pipetted off and replaced every two days. When removing the media, care was taken not to disrupt the gel matrix, only removing the superficial media layer before gently replacing the media by pipetting down the side of the well to minimise disturbance.

Murine Sphere Protocol Two

The sphere numbers were excessive in the experiments using Protocol One, so the total cell number was reduced, while the epithelial and mesenchymal cells were combined. From the immunofluorescent staining performed on the mouse and human tissue, it

was observed that the mesenchymal cells make up a significantly smaller proportion of the mature tissue, Therefore, the proportion of the mesenchymal cells used in our model at a ratio of 3:1, that is 7500 epithelial cells and 2500 mesenchymal cells. These cells were recombined and cultured in a culture medium that was made up of equal parts of the B27 supplemented media and Amniomax. In this way, it was assumed that sufficient nutrients would be present for both cell types within the culture environment. Furthermore, only 75ul of Matrigel was layered into the bottom of each well, to ensure sufficient space was left above to allow layering of culture media.

Murine Sphere Protocol Three

The final and most successful iteration of the protocol reduced the number of cells being used even further to a maximum of 5000 cells per well, maintaining the ratio of 3:1 of epithelial to mesenchymal cells in the combined cell condition, 3750 epithelial cells to 1250 mesenchymal cells. We combined cell culture mediums as in Protocol Two but most significantly, the medium was also spiked with 10% Matrigel to maintain the stimulation by growth factors present in the gel. 75ul of Matrigel was first layered in the bottom of each well of a 96 well plate, with triplicate wells prepared for each condition. The conditions ran for this protocol were epithelial cells alone, mesenchymal cells alone, and the 3:1 ratio of epithelial to mesenchymal cells combined. Once the cultures were established, the suspended spheres were washed with pre-warmed HBSS at every change of the media, which happened every two days. This ensured a more efficient removal of cellular debris and promoted better cell growth. This protocol was the one used to generate results from the sphere assays demonstrated in Figures 3.2-14 to 3.2-17.

Sphere Analysis

The spheroids in each well were counted using Image J, with the counts duplicated by a second blind counter. During each experiment, two or three wells were prepared of each condition, so each of these replicate wells was counted. The experiment design was highly replicable, so the counts from across five experimental repeats could be counted and used to generate average sphere numbers. The diameter of the spheres was measured using Image J software, always measuring the spheroids in a diagonal line from south-west to north-east orientation. This maintained consistency and removed bias that could have arisen from subjective measurements.

Mouse cells spheres were isolated from the Matrigel gel through washes in cold HBSS to dissociate the spheres from the gel, before being collected for histological and immunofluorescence staining. Tissue was mounted on microscope slides and taken through the standard H&E or IF protocols. Alternatively, the initial spheres experiments were fixed and stained whilst still within the Matrigel gel culture environment, but this produced high levels of background fluorescence, resulting in the extraction method.

3.2.2. Immunofluorescent Characterisation of Murine SMG

Extensive characterisation of the mouse salivary gland tissue was undertaken, using a similar panel of markers as those used in for the human tissue, confirming that different cell populations can be identified, including potential stem cell niches, as demonstrated in Figures 3.2-4 to -7. To achieve this, the mouse salivary glands were removed from the mouse and the peripheral adipose tissue, lymph tissue removed. The parotid gland and the sublingual gland were also removed under microdissection, to leave the submandibular gland, which is more representative of human salivary gland structures (Maruyama *et al.*, 2018).

After establishing the immunofluorescence characterisation, the mouse submandibular gland tissue was digested and cell culture conditions developed by spontaneously selecting for different cell populations using a variety of culture media and coating methods as described in the materials and methods. Cell phenotypes were confirmed by cell growth patterns and morphology, whilst immunofluorescence confirmed expression profiles of markers that had been confirmed in tissue sections. The relative RNA expression levels of markers were also used to confirm cell types.

An assay was planned that would recombine these primary cell cultures into three-dimensional structures, representative of a developing salivary gland structure. The generation of consistent organoid models was the primary aim, indicating a successful optimisation of the technique, which could then be used to investigate the regenerative potential of human PSS patient derived mesenchymal cells. Furthermore, it was imperative to conclusively demonstrate the importance of mesenchymal cells during salivary gland organoid development.

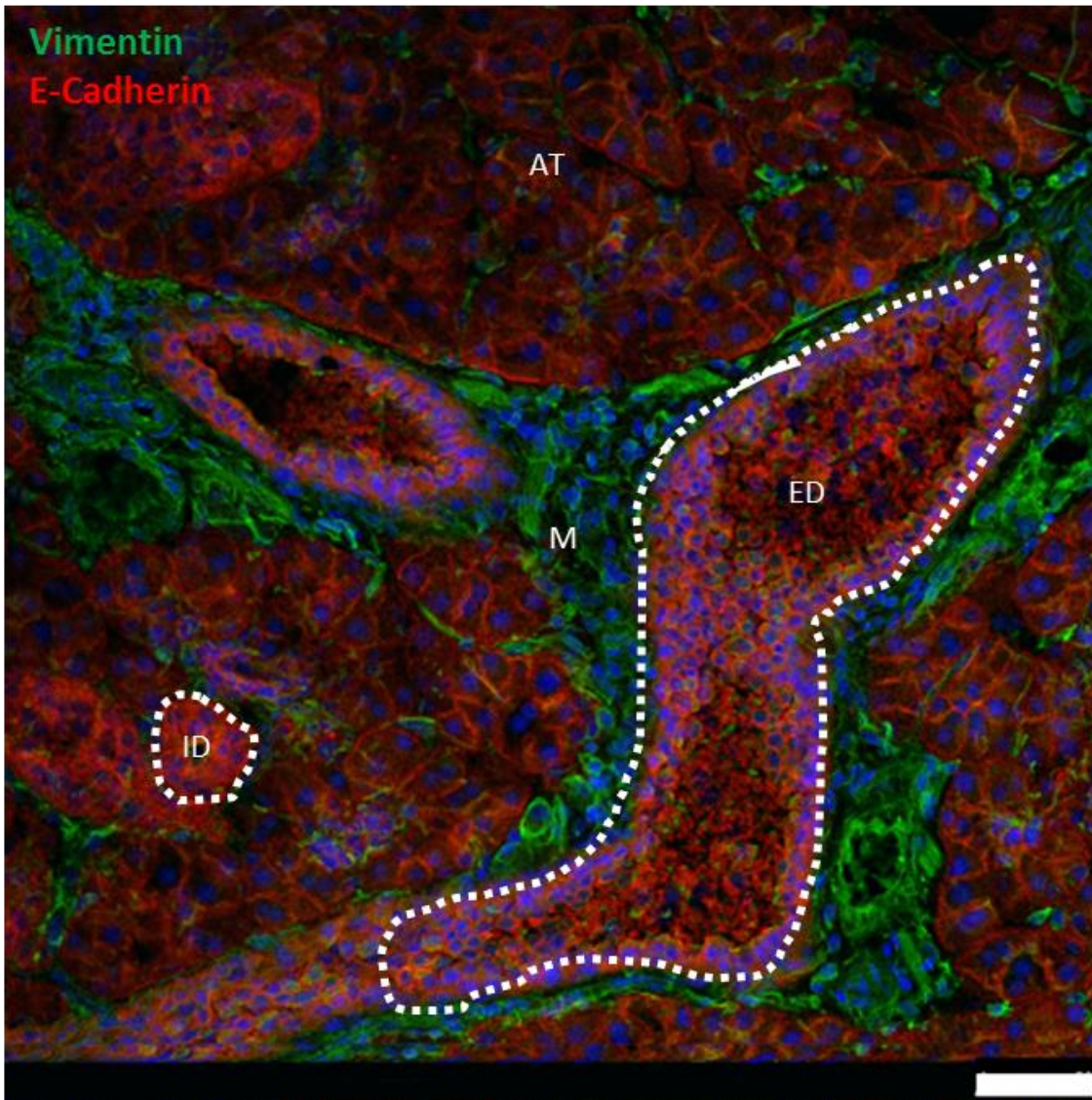


Figure 3.2-1. E-cadherin (CDH1) and Vimentin staining on mouse submandibular gland tissue. A high magnification image demonstrates discrete cellular populations within mouse submandibular gland tissue. E-cadherin visualised with Alexa-568 and Vimentin with Alexa-488. Images were taken at 20X magnification, with the scale bar equivalent to 50um. AT – Acinar Tissue, M – Mesenchyme, ID – Intercalated Duct, ED – Excretory Duct.

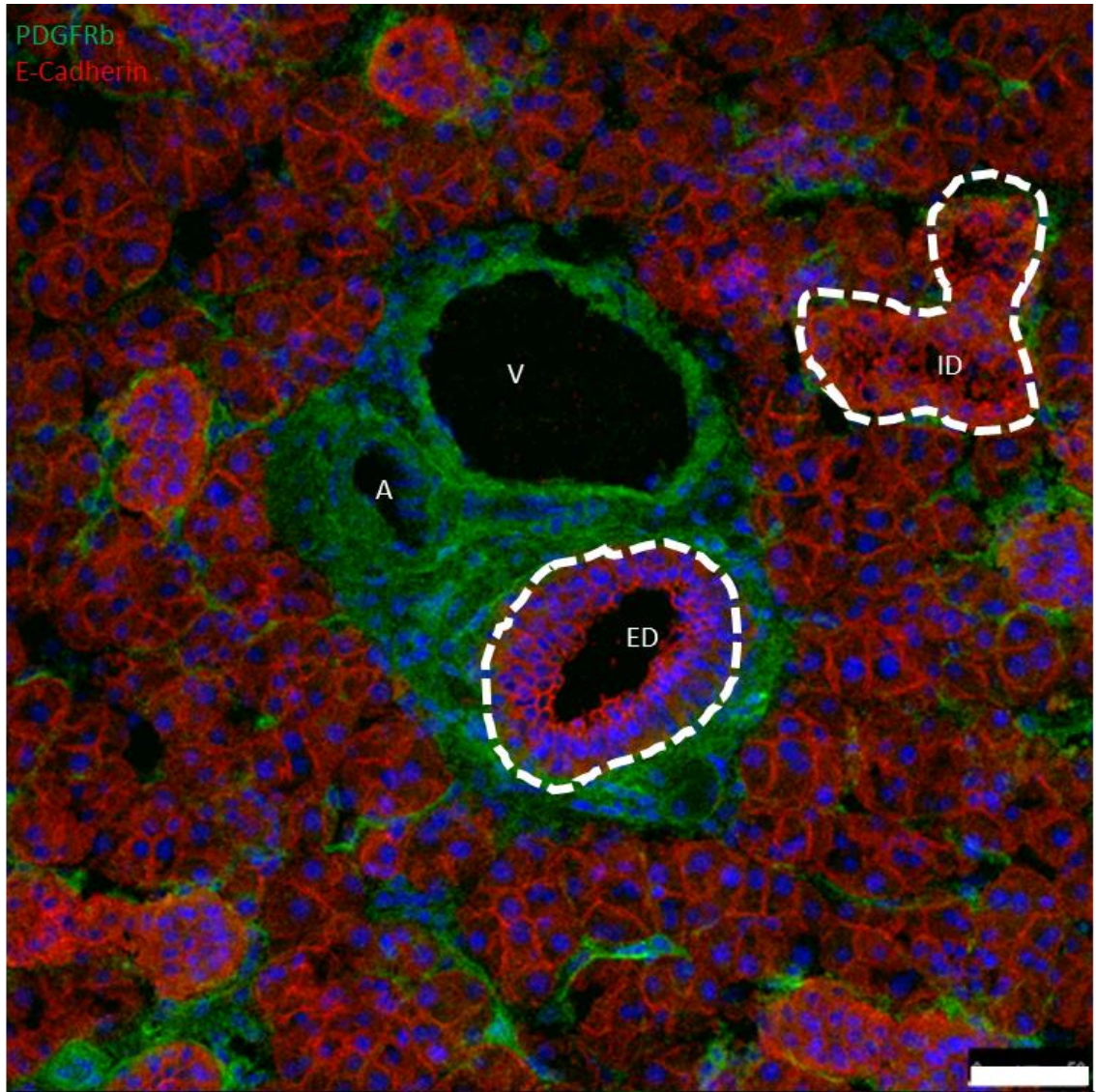


Figure 3.2-2. Immunofluorescent staining of mouse submandibular gland tissue for E-cadherin (CDH1) (red) and PDGFR β (green), demonstrating discrete cellular populations within mouse submandibular gland tissue. Scale bar equivalent to 50 μ m. A – Arterial blood vessel, V – Venous blood vessel, ED – Excretory Duct, ID – Intercalated Duct.

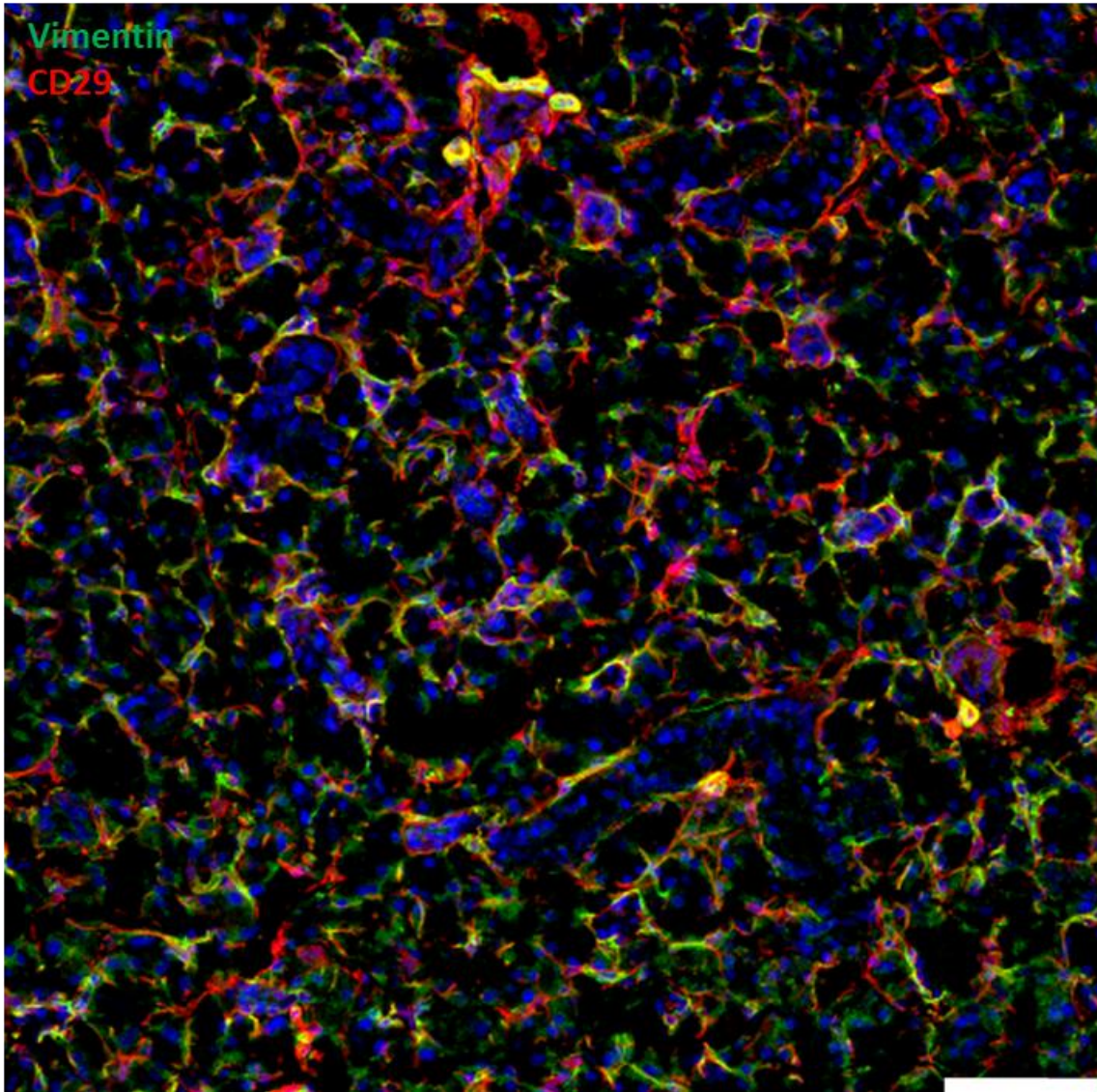


Figure 3.2-3 Immunofluorescent staining of mouse submandibular gland tissue for CD29(red) and Vimentin(green) demonstrated discrete cellular populations within mouse submandibular gland tissue. Scale bar equivalent to 50um. Co-localisation marked in yellow.

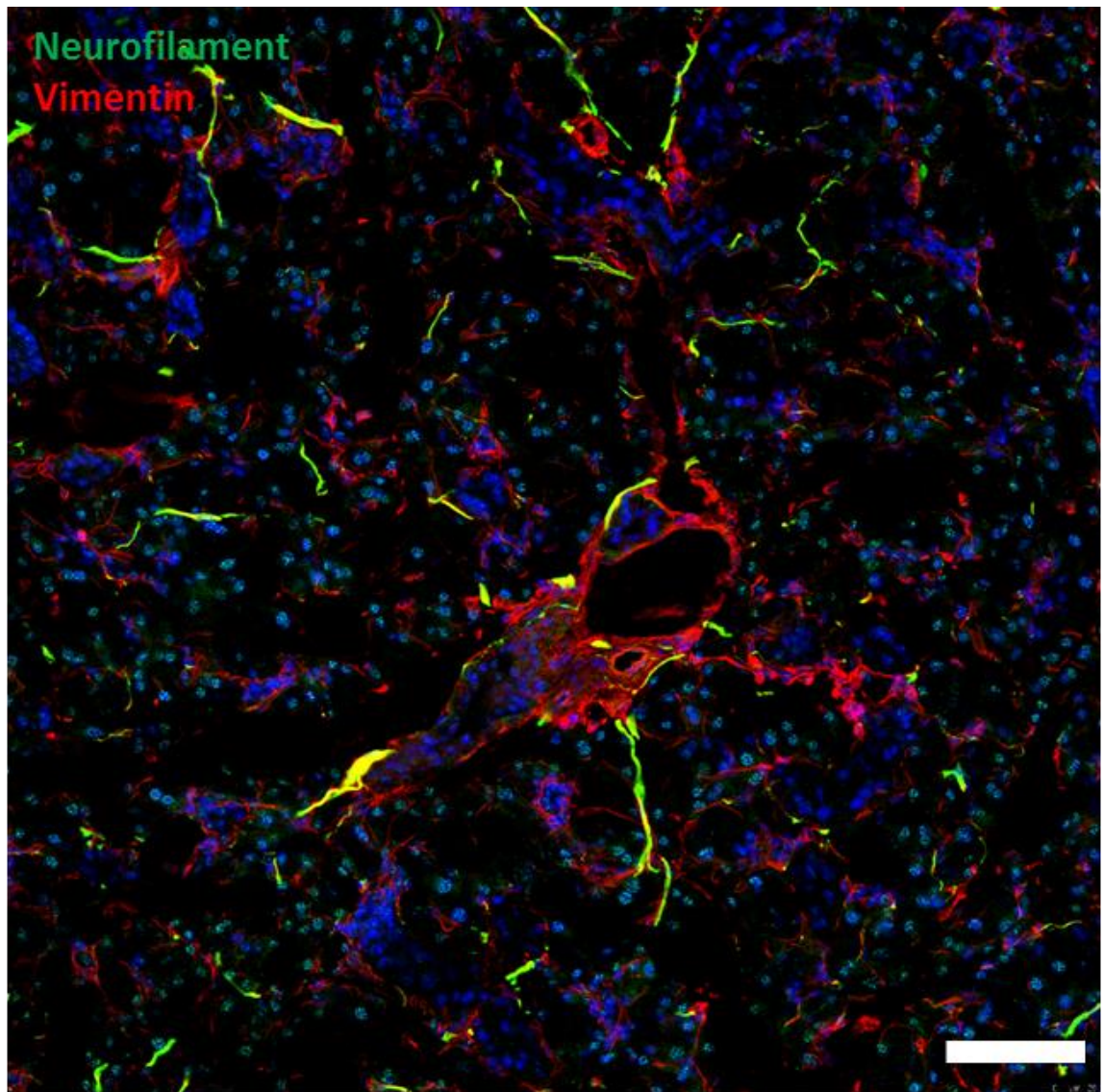


Figure 3.2-4. Immunofluorescent staining of mouse submandibular gland tissue for Vimentin (red) and Neurofilament (green) demonstrated discrete cellular populations within mouse submandibular gland tissue. Scale bar equivalent to 50 μ m. Co-localisation is demonstrated in yellow.

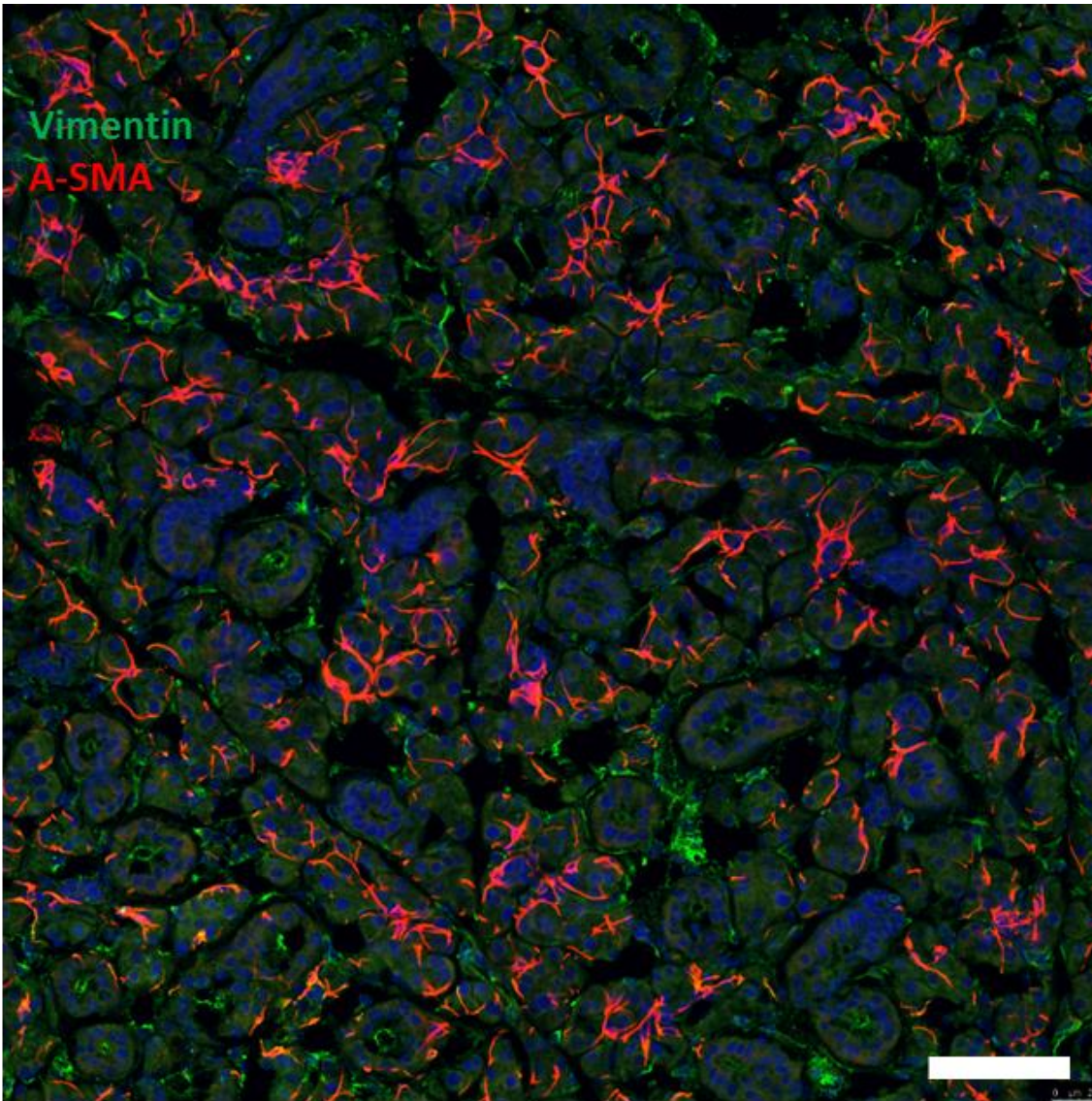


Figure 3.2-5. Immunofluorescent staining of mouse submandibular salivary gland tissue for α -SMA (red) and Vimentin (green). This staining demonstrated discrete cellular populations within mouse submandibular gland tissue. Images were taken at 20X magnification, with the scale bar equivalent to 50um.

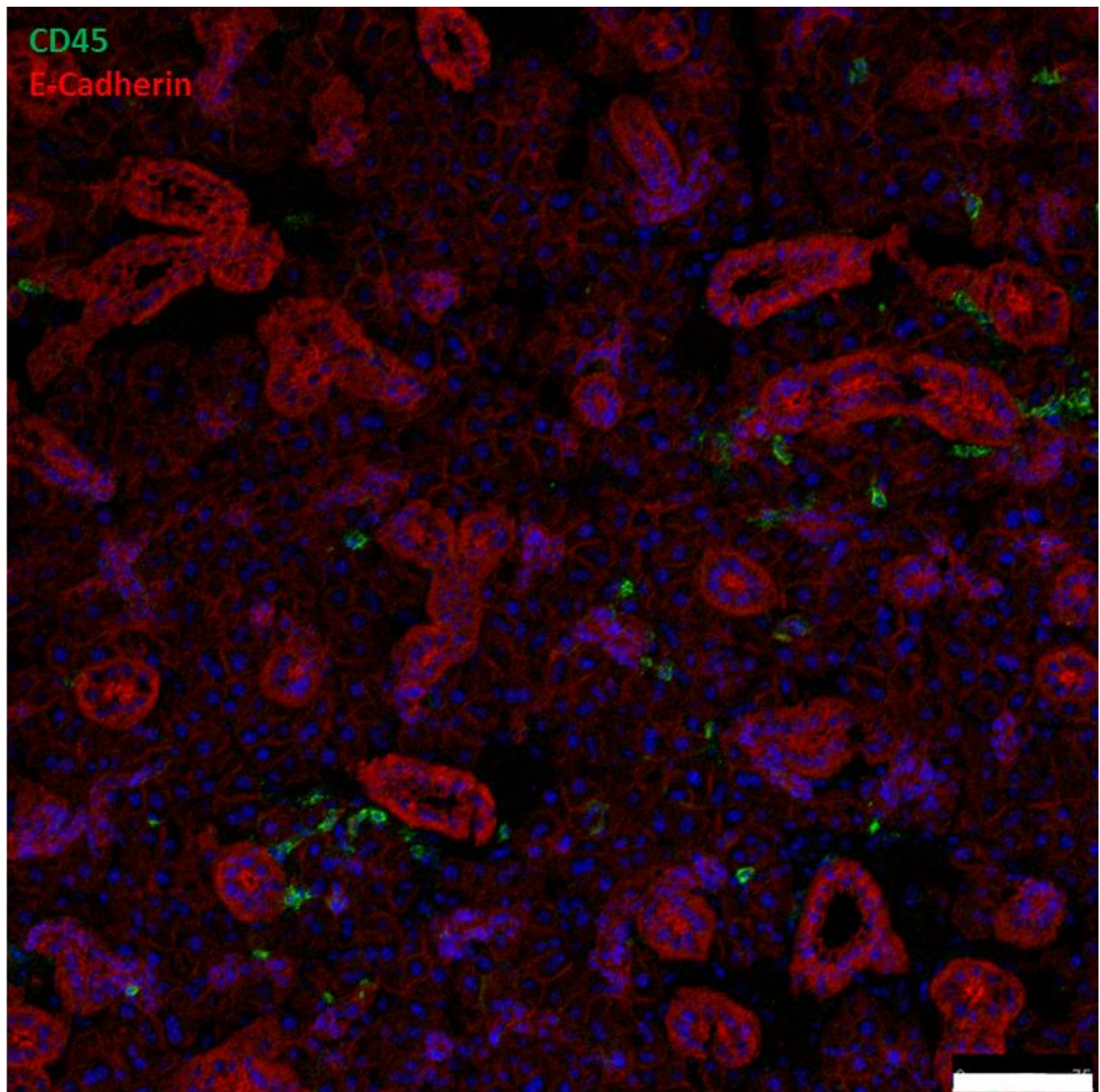


Figure 3.2-6. Immunofluorescent staining of mouse submandibular salivary gland tissue for E-cadherin (CDH1) (red) and CD45 (green) replicates the consistent epithelial tissue structures, acinar and ductal structures, whilst CD45 indicates circulating immune cells. Scale bar equivalent to 50um.

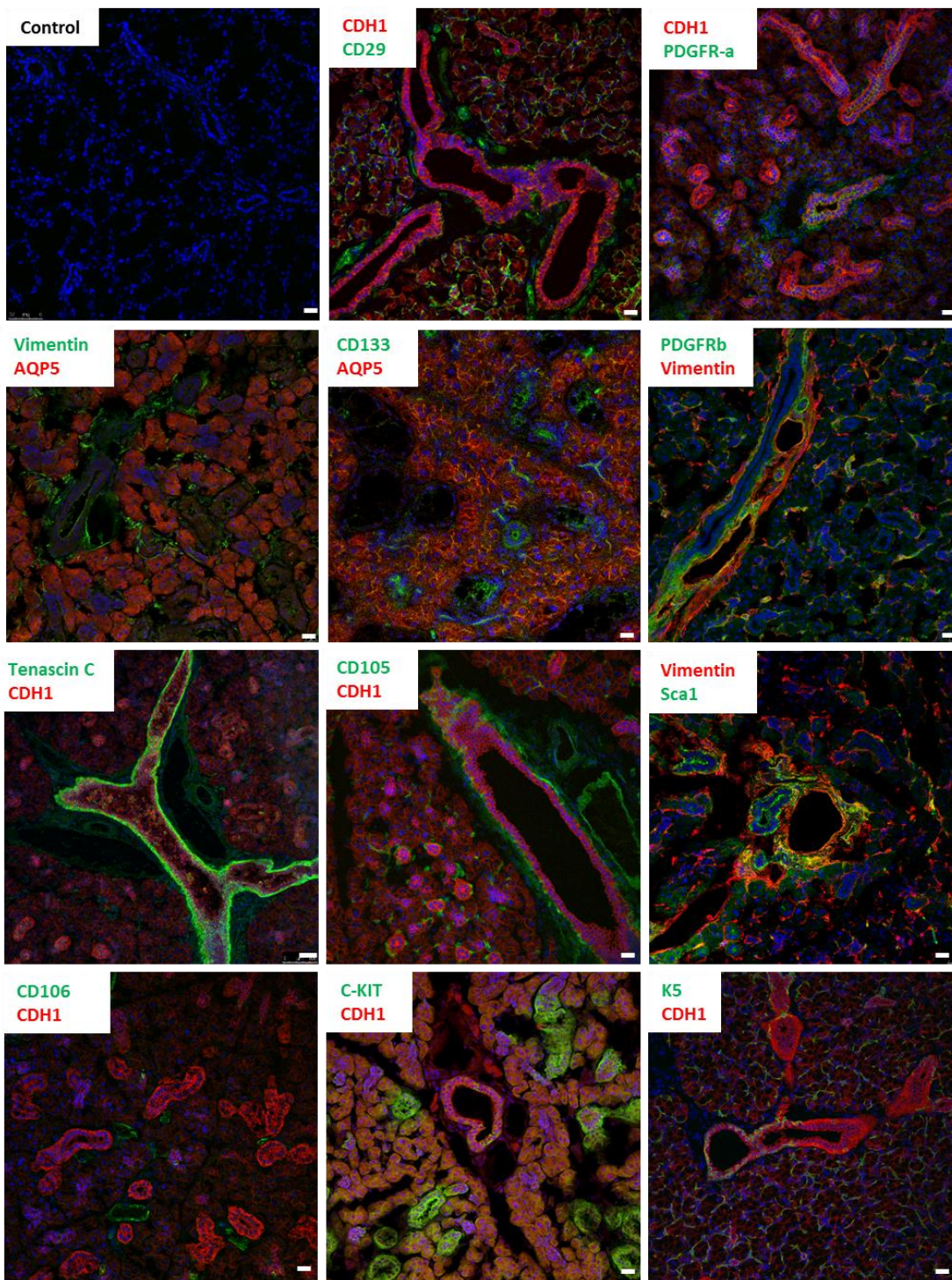


Figure 3.2-7. A panel of general markers was used in immunofluorescence on mouse salivary gland tissue characterising and identifying cell populations within the tissue. P30 WT CD1 mice, sectioned at 10um thickness. Immunofluorescence staining with antibodies raised against E-cadherin (CDH1), Vimentin, PDGFR β , CD133, AQP5, CD105, CD106, Tenascin C, CD45, PDGFR α , K5, C-kit. X20 magnification. Scale bar equal to 50um.

The above immunofluorescent images, from Figures 3.2-1 to Figure 3.2-7, indicate that the same markers of CDH1 and Vimentin, which had been confirmed in the human salivary gland tissue, can be used to identify the epithelial and mesenchymal cell populations within the mouse salivary gland tissue. E-cadherin discretely stains the tight junctions between the epithelial cells and there is no evidence of staining on structures that are thought to be blood vessels, or around the duct structures that would predominantly be mesenchymal tissue. The Vimentin staining appears to stain the residual areas that the E-cadherin does not stain, but in a much more fibrous nature. There is no overlapping of the staining, generating two ideal candidate markers for identifying the two cell populations.

Where Vimentin stained the general mesenchymal tissue, the CD29 and PDGFR β specifically stained smaller populations of these cells, shown in Figures 3.2-3 and 3.2-7, and Figure 3.2-2 and 3.2-7 respectively. These markers could be observed in very similar staining patterns to the Vimentin, but when co-staining was performed, there was not a complete co-localisation of the markers, suggesting only a small subset of the Vimentin positive cells are also CD29 or PDGFR β positive, indicative of MSCs. Although Neurofilament does stain a fraction of the Vimentin positive cells, in Figure 3.2-4, it does not stain the majority. Therefore, it can be stated that the majority of Neurofilament staining is also Vimentin positive, but only a small fraction of Vimentin staining is also Neurofilament positive, this could be suggestive of heterogeneity of the neuronal filament proteins within the neuronal processes in the salivary gland tissue.

An overview of all the markers used to stain the murine salivary gland tissue is provided below in Table 3.2-1. This table demonstrates how discrete the staining of each region

of tissue can be, with only markers associated with stem cell fate being present in both populations, as they would be integral to cell differentiation and cell signalling pathways common to all cell types.

Mouse Tissue	Acinar Secretory Cells	Epithelial Ductal Tissue	Mesenchymal Tissue	Immune Cells	Neurovascular Tissue
Marker					
E-Cadherin	+++	+++			
Vimentin			+++		+
AQP5	+++				
Amylase	++				
PDGFRb			++		
CD105			++		
CD106			+		++
Neurofilament					+++
A-SMA	++				
CD45				++	
PDGFRa		+++			
Tenascin C			+		++
Sca1			++		
K5	+	++			
K14	+++	++			
C-Kit		++			

Table 3.2-1 Overview of staining patterns in mouse salivary gland tissue. An indication of the intensity and location of immunofluorescent staining, extrapolated from images collated for Figures 3.2-1 to 3.2-7.

As described in the literature (Alam *et al.*, 2011), Keratin 14 staining can be an alternative marker for epithelial cells as it appears to globally stain the same regions as CDH1, whilst K5 appears to stain a small fraction of the CDH1 positive cells only within the ductal regions of the epithelial tissue. In the staining of AQP5 in Figure 3.2-7, low intensity but punctate staining was observed in the acinar regions, but no staining

observed in the mesenchymal regions, as expected, and no staining in the ductal regions.

The staining of α -smooth muscle actin (α -SMA) does not co-localise with Vimentin, demonstrated in Figure 3.2-5, which confirms from the literature that α -SMA is a highly conserved marker for the myoepithelial cells that surround the secretory acinar cells. It is known that the myoepithelial cells develop from an epithelial lineage and are unlikely to co-localise. However, Vimentin can integrate into actin filaments in other cell types, and actin filaments control the tension in the myoepithelial cells. Most significantly, the confirmation of this lack of co-localisation was needed so that, when cell culture conditions are generated, the correct cell phenotype can be isolated and confirmed, whilst proving lack of cellular contamination from other cell niches. Critically, the staining profiles are similar to those seen in the human salivary gland tissue, giving greater confidence in the reliability of these markers.

After creating this profile with which to identify cell populations, representative cell cultures were generated which were manipulated into three-dimensional models as an assay to study salivary gland development and model tissue regeneration. As described in the materials and methods, salivary glands were excised from adult CD1 mice, digested and plated into different culture environments to promote specific cell survival.

3.2.3. Developing Murine Cell Culture and Organoid Models

Cell type was initially judged on physical appearance and cell growth patterns, displayed in Figure 3.2-8; both cell populations were adherent whilst properties such as colony shapes, heterogeneity, size and shapes of individual cells were judged to define phenotype. Epithelial cells are known to be polygonal in shape, with regular dimensions and consistency across the population, growing in discrete patches on an adherent surface. Mesenchymal cells appear fibroblastic, elongated in shape with a bi-polar or multi-polar appearance. By observing cell morphology and colony formation patterns, cell types could be estimated, whilst immunofluorescence staining for Vimentin and E-cadherin could confirm cell types using these pan-epithelial and pan-mesenchymal markers (Mani *et al.*, 2008).

As demonstrated in Figures 3.2-8 and Figure 3.2-9, cells cultured in B27 media and collagen coating were observed to be epithelial in phenotype, by their characteristic “cobblestone” colony formations and tightly compacted appearance; they also stained positively for E-cadherin and did not stain for Vimentin, which is sufficient to differentiate between the ecto/endoderm derived epithelial tissue and the neural-crest derived mesenchyme (Patel and Hoffman, 2014). Cells were also stained with Keratin 14 which was present only in the B27 cultured cell population, and is known to be an epithelial cell marker (Alam *et al.*, 2011). Similarly, the cells cultured in Amniomax media with poly-D-lysine coating, presented with a fibroblastic-like appearance and stained positively for Vimentin and had very little staining of E-cadherin. The Amniomax cultured cells were also the only ones that stained positively for CD105, a marker frequently used in the identification of MSCs (Khalili *et al.*, 2012; Cleary *et al.*, 2016).

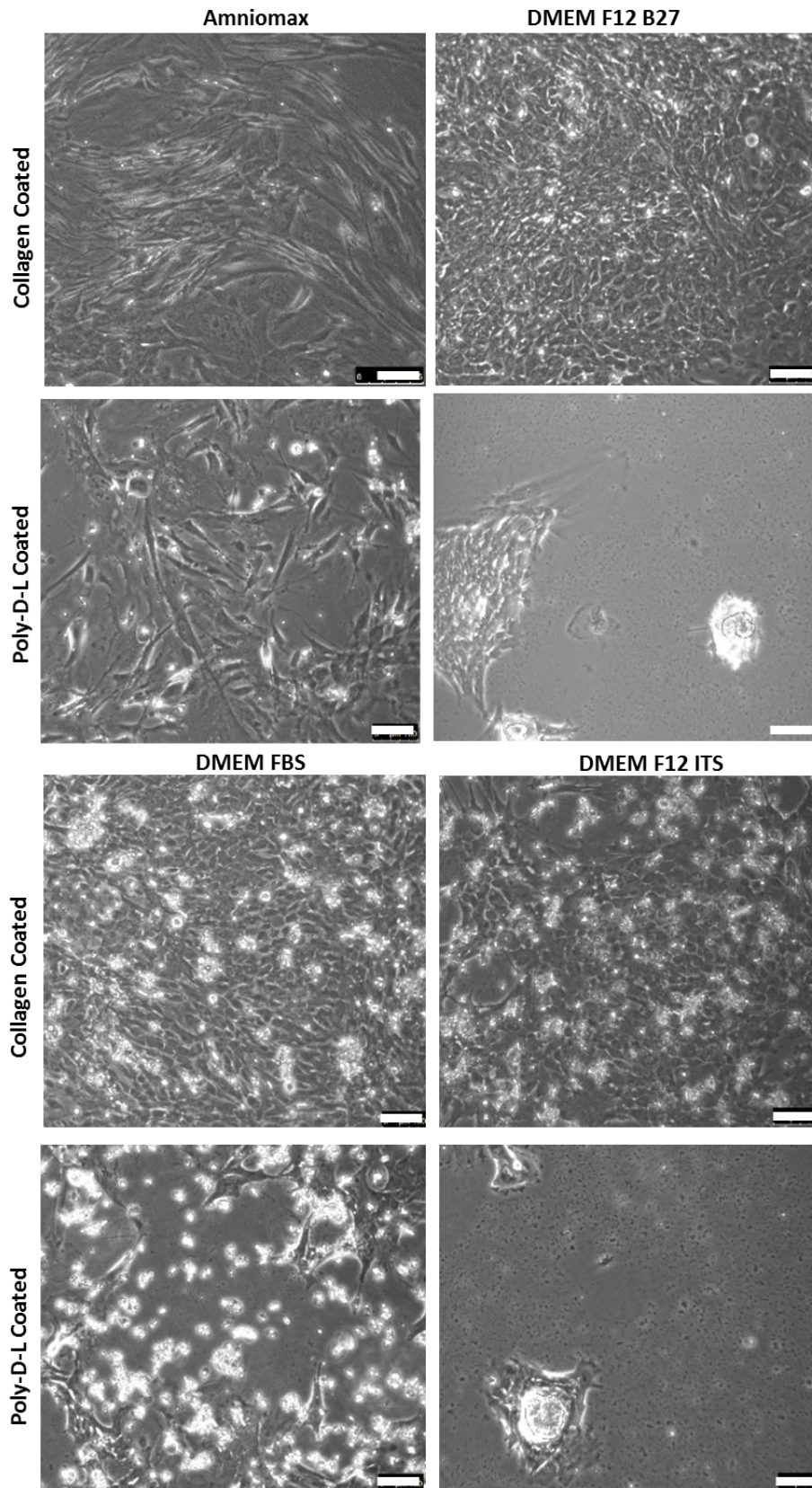


Figure 3.2-8 Establishing cell culture models from mouse submandibular glands. Cultures of cells 4 days post tissue digestion, indicating spontaneous selection of different cell phenotypes through different culture conditions: Amniomax DMEM F12 with B27 supplement, DMEM with FBS and DMEM F12 with ITS and EGF supplementation. Images taken at 20x magnification.

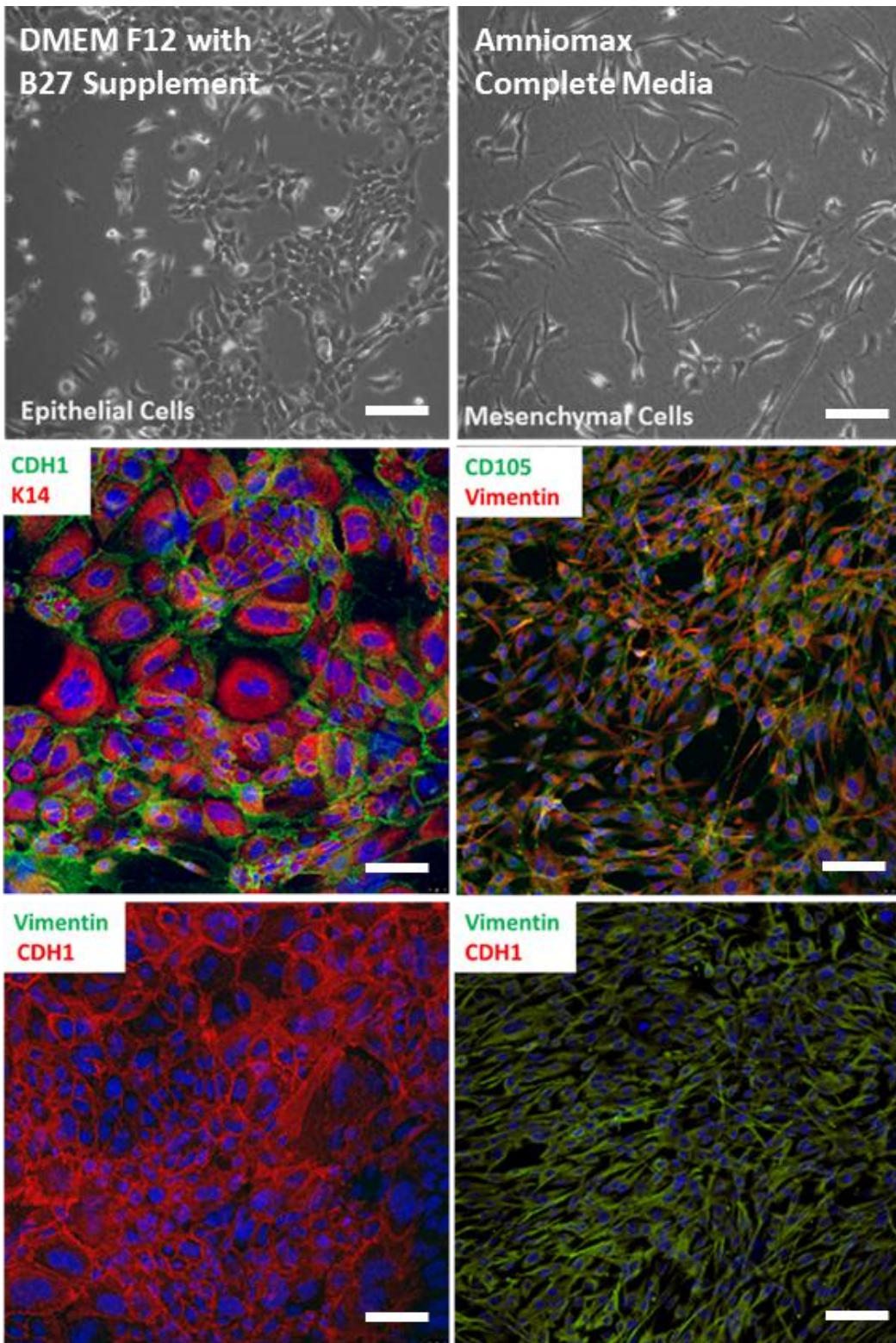


Figure 3.2-9. Optimised cell culture conditions using DMEM F12 B27 with Collagen coated dishes for epithelial cells and Amniomax with Poly-D-Lysine coated dishes for mesenchymal cells have their phenotype through immunofluorescence. Demonstrating E-Cadherin (CDH1) and K14 staining with an absence of Vimentin staining for epithelial cells, and Vimentin and CD105 staining, with an absence of E-cadherin (CDH1) in mesenchymal cells. Scale equivalent to 25um.

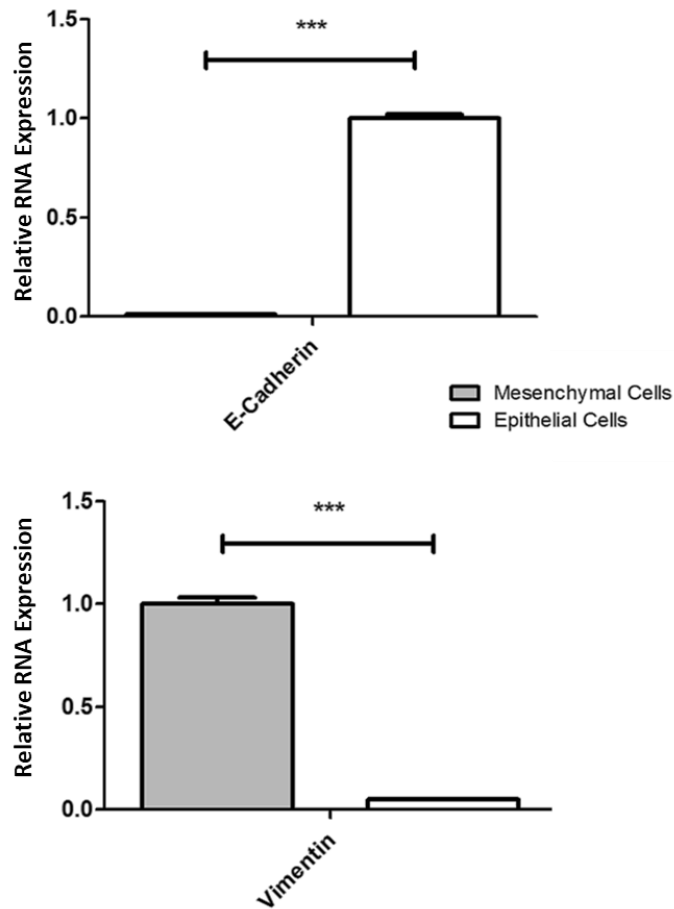


Figure 3.2-10. The optimised cell culture conditions promote growth of two discrete cell populations. Relative mRNA expression levels of E-Cadherin and Vimentin in cells cultured from the P30 CD1 mouse in B27 supplemented DMEM culture medium (white) and Amniomax culture medium (grey). Expression is defined through quantitative-real time-PCR, error bars display the standard error of the mean (P<0.0001: *, P<0.001: **, P<0.01: *)**

The phenotype observed in the cell morphology and immunofluorescence was corroborated with relative RNA expression levels through PCR analysis, which demonstrated that the B27 cultured cells had a significantly higher expression level of E-cadherin and a lower level of Vimentin relative to the expression observed in the Amniomax cultured cells. From these findings, the two primary cell cultures were henceforth named as “Epithelial Cells” and “Mesenchymal Cells”. These Epithelial and Mesenchymal cells were cultured over time to investigate the long-term potential of the

cells to persist. After two or three passages, it was noted that the cells appeared to present with a more uniform, homogeneous phenotype. When the Mesenchymal cells reached passage five, their appearance changed; appearing to proliferate less and becoming more fibrous and less healthy looking, often not surviving at all past passage ten. It is commonly noted that primary cell cultures are only viable for the first ten passages before they are no longer representative of the desired cell type, due to genetic drift, or they have spontaneously become immortalised, which would then not be representative of *in vivo* environments. On the other hand, the epithelial cells maintained a better phenotype up to and beyond passage ten, but for consistency, it was decided that only cell cultures below passage five could be used for further studies, as this should maintain a more consistent cell phenotype. Furthermore, when studying both Epithelial and Mesenchymal cells, the passage number were matched, and ideally the same batch of cultures should be used in order to avoid divergence from the initial cell phenotype in one of the cell populations. In this way, it was easier for the project to preserve a closer representation of the *in vivo* environment.

Having cultured cells as above, the percentage of cells that were positive for mesenchymal stem cell markers was analysed through flow cytometry analysis, whilst the potential for using FACS or MACS technology to purify stem cell populations was considered. Using flow cytometry methods as described in the materials and methods, cells were isolated in aliquots of a single cell suspension and were incubated with antibodies targeting a range of Mesenchymal Stem Cell markers provided by R&D systems. As demonstrated in Figure 3.2-10, identification of stem cell niches within the cultured cells was unsuccessful and attempts to identify populations directly from whole

digested tissue produced even smaller or non-existent populations, shown in Figure 3.2-11. However, Sca-1 and CD29 were consistently elevated within our cell populations, and are known to be mesenchymal cell markers and potential stem cell markers in the salivary gland mesenchymal cell population (Khalili *et al.*, 2012; Maimets *et al.*, 2015).

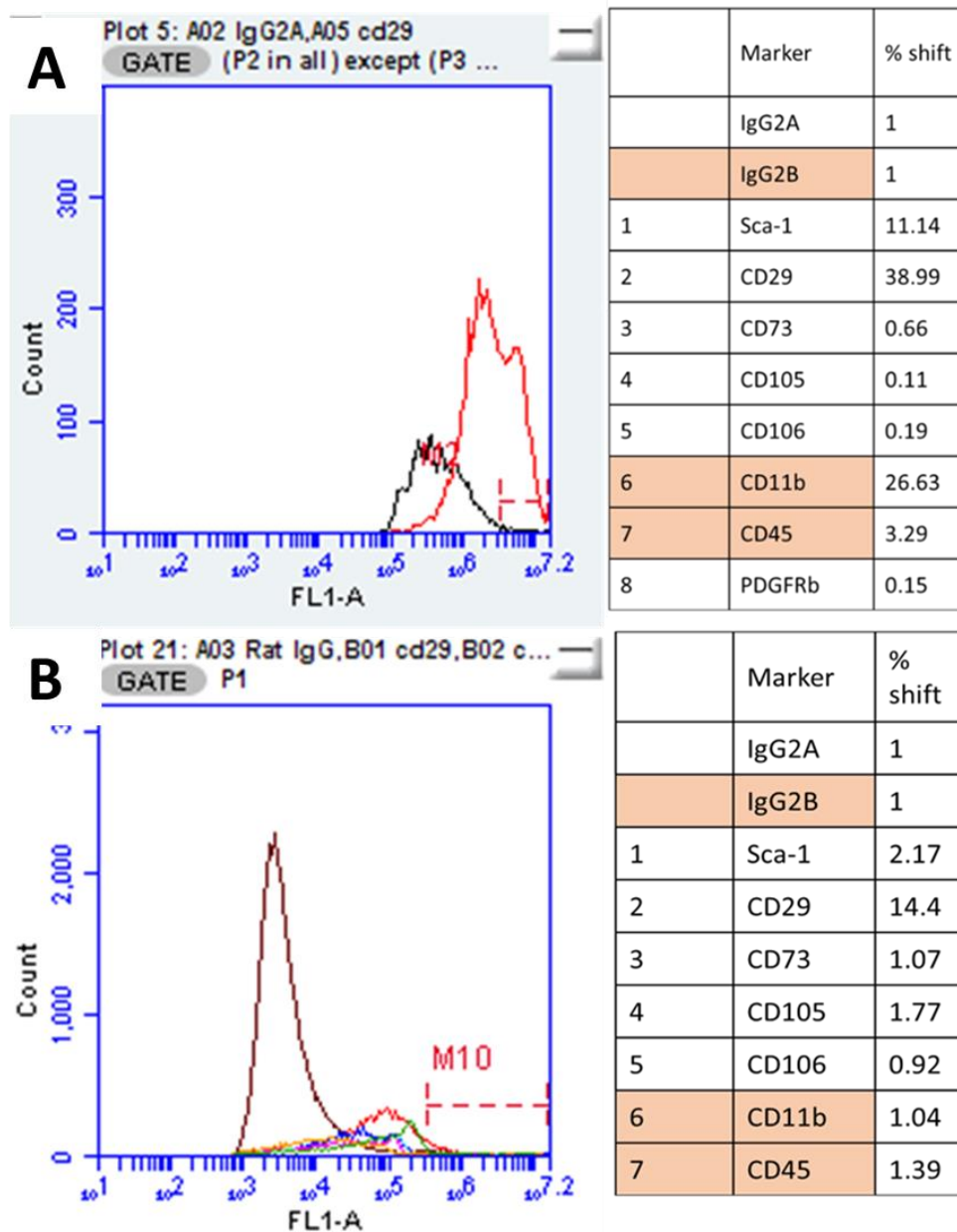


Figure 3.2-11. FACS shows low abundance of MSC markers, with the exception of Sca-1 and CD29 (ITG2b). The top graph A) shows the large proportion of cells identified by CD29, the bottom graph B) depicts all markers in comparison to the IgG control. The percentage increase shift is a relative measure between the numbers of events detected as positive for an IgG binding control compared to the marker of interest. The two tables are repeated experiment outputs.

Cells that had been established as primary cell cultures, as above in Figures 3.2-8 to 3.2-11, were used in three-dimensional cell culture assays. Three conditions were created, one assay with only epithelial cells, another with mesenchymal cells and the third where the two cell types were combined. As described in 3.2.1 Mouse Sphere Culture Methods, cells were combined into Matrigel, which is a secretion from a mouse, sarcoma cell line (Engelbreth-Holm-Swarm sarcoma mice) produced by Corning. There were three stages of protocol optimisation detailed in section 3.2.1 with results displayed in Figure 3.2-12 to Figure 3.2-14.

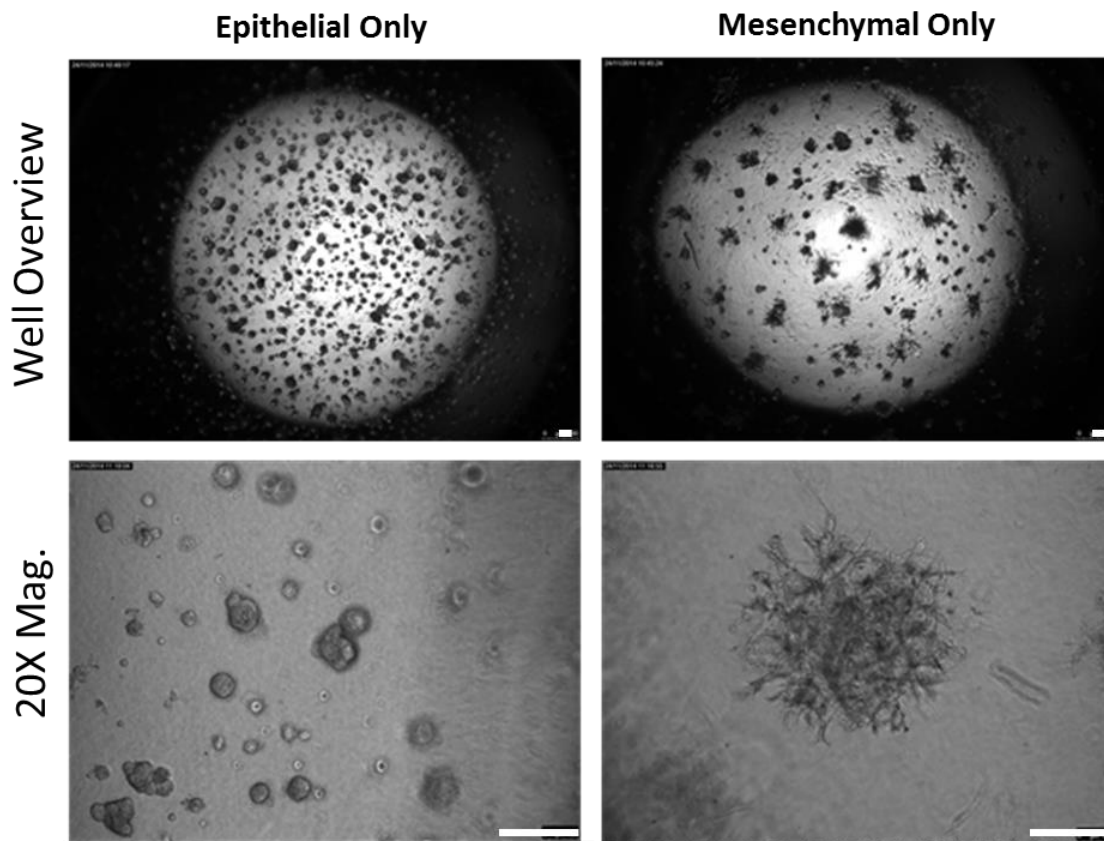


Figure 3.2-12 Protocol One of Spheroid Model Culture, optimising three-dimensional organoid culture conditions from the growth of mouse derived epithelial and mesenchymal cell types. 20,000 cells per well, keeping epithelial and mesenchymal cells separate. Images were recorded 7 days after initiation of the spheroid cultures. Images show an overview of a whole well from a 96 well plate and a 20X magnification image of examples of spheres observed in these conditions. Scale bars represent 200um.

Figure 3.2-12, demonstrates the phenotype of spheres generated using mouse sphere protocol one, which demonstrated that the cells could survive in the three-dimensional culture conditions, resulting in two distinctly different structured types of spheroids. The spheres produced using method one were seen to be inconsistent in size and shape and unreliable between repeated experiments, generating a large range of phenotypes and too many spheres per well, limiting our ability to study one sphere over time. Therefore, it was concluded that both cell types should be combined, at lower concentrations, in to observe the effect each cell type has on the ability of the spheres to grow.

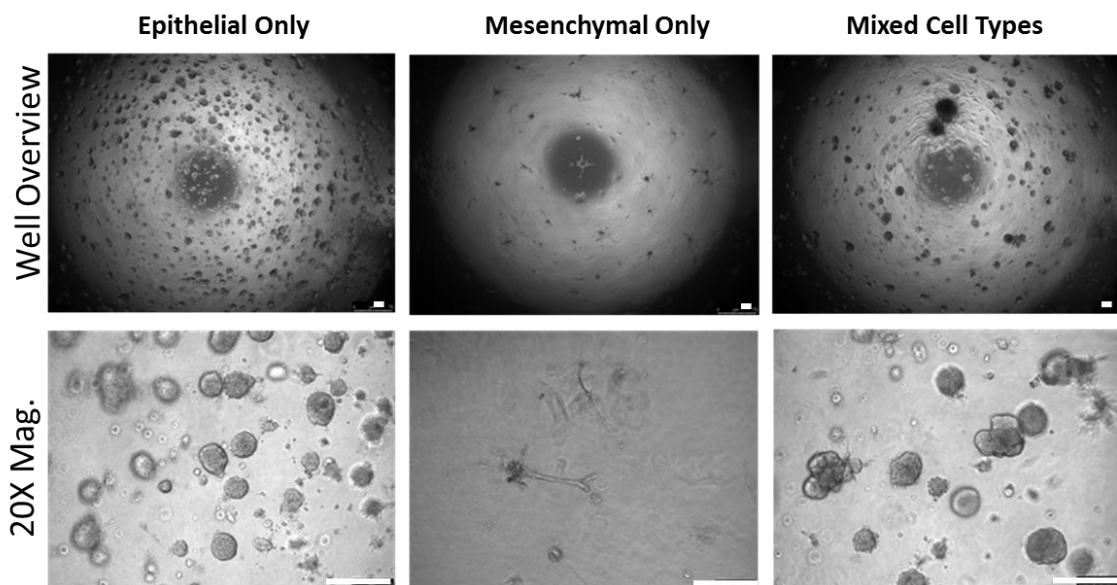


Figure 3.2-13 Protocol Two developed organoid spheres combining mouse epithelial and mesenchymal cell types limited at 10,000 cells per well. Epithelial and mesenchymal cells were each cultured separately as controls but also combined together in a third culture environment demonstrating an enhanced spheroid phenotype when cells were combined. Images were taken 7 days after initiation of the spheroid experiment, with an overview of the culture well and higher magnification of example spheroids observed in each condition. Scale bar equal to 200um .

These cultures, using Protocol Two, shown in Figure 3.2-13, were successful and presented with consistent structures. The spheroids in the mixed condition were consistent and started to present with budding and branching phenotypes more

frequently than in the epithelial alone. However, the number of spheroids in the gel conditions prevented accurate records being taken, and nutrient uptake from the culture environments was rapid, resulting in some cultures dying prematurely due to lack of nutrients in the media.

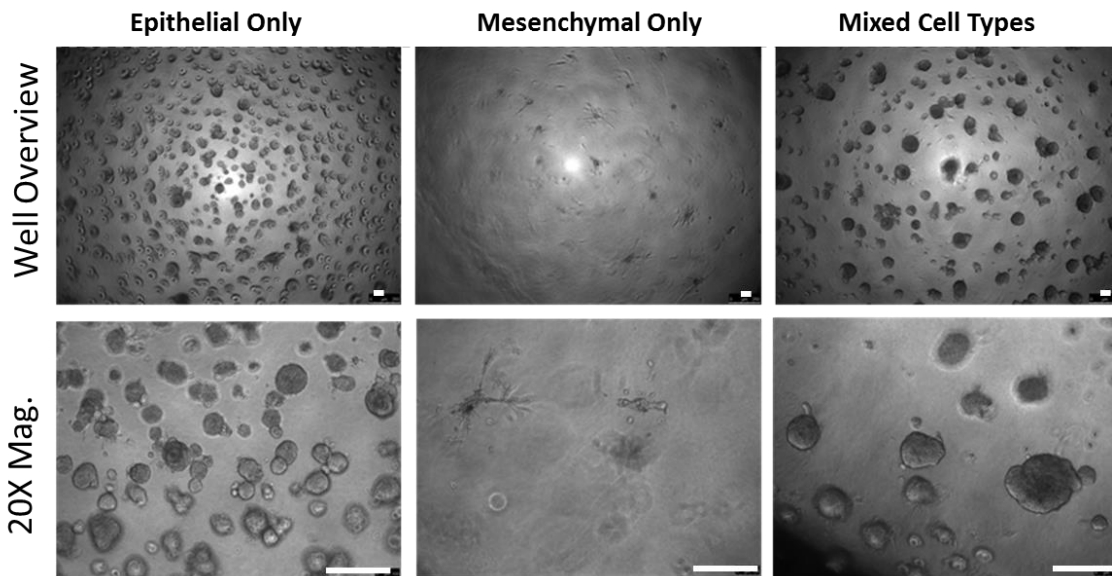


Figure 3.2-14 Spheroids developed using Protocol Three for organoid cultures. Cells were combined again in Matrigel, whilst using single cell type cultures as control environments to compare organoid development, with reduced cell numbers and improved techniques for maintaining cultures. Images were taken at 7 days after spheroid initiation with an overall view of the well and a magnified images of representative spheres within the culture environments. Scale bar equal to 200um.

The fully optimised technique was Protocol Three, with results shown in Figure 3.2-14.

This protocol produced spheres of a consistent size and frequency within each well, and sparse enough to facilitate better long-term observations of spheres. This technique could then be used to analyse how impactful the mesenchymal cells are in defining organoid development. First, we needed to confirm cell phenotype was also maintained throughout the organoid experiments and that both epithelial and mesenchymal cells persisted.

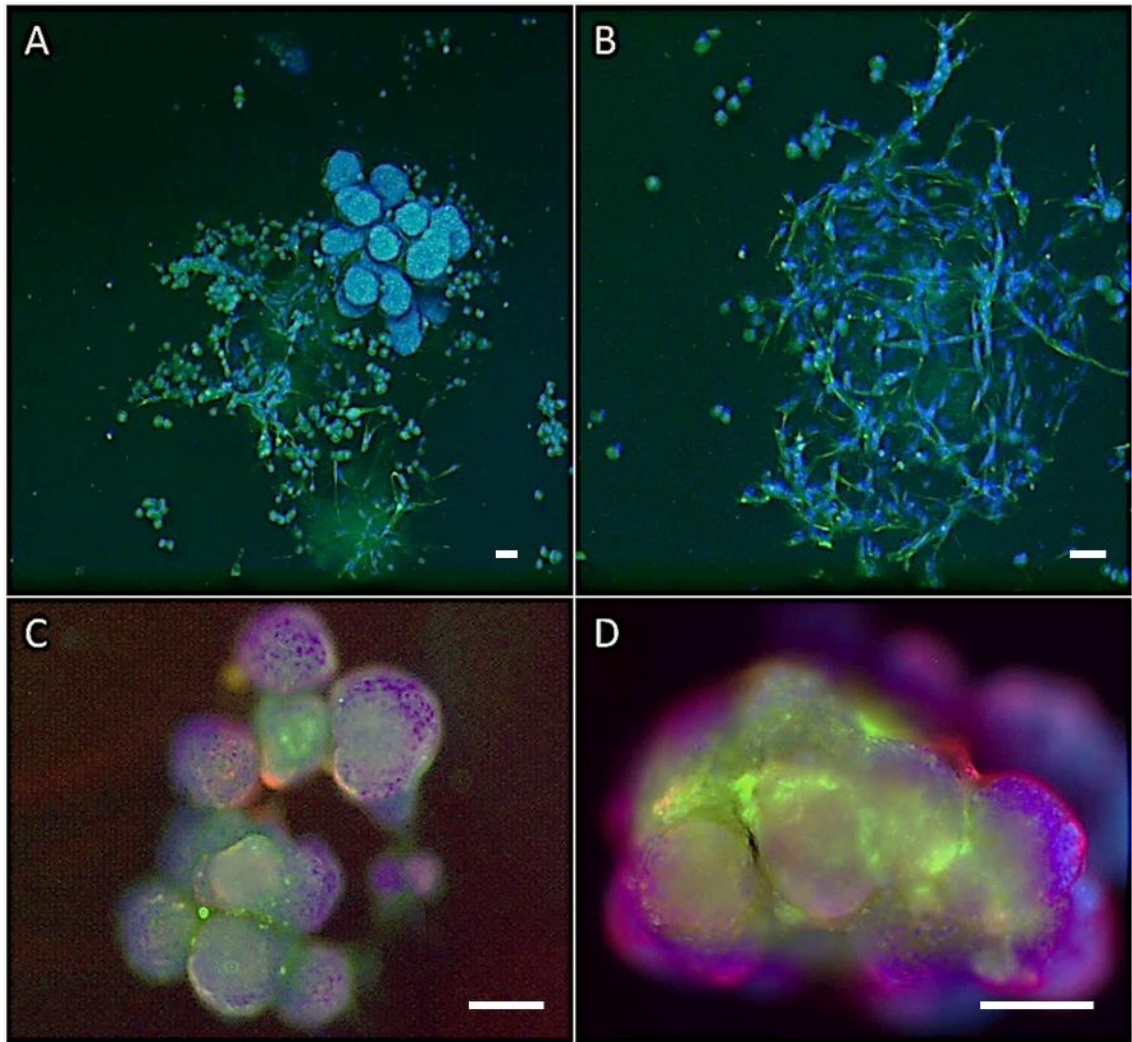


Figure 3.2-15. Organoid models generated from combining epithelial and mesenchymal cells using the third spheroid protocol, demonstrating that epithelial and mesenchymal cells are preserved throughout organogenesis. A) A mixed cell sphere condition stained for Vimentin, B) mesenchymal only sphere condition stained for Vimentin, C&D) mixed cell conditions stained for E-Cadherin (Alexa-568) and Vimentin (Alexa-488). Images captured at various magnifications and images cropped where appropriate, scale bars representative of 75µm.

Spheroid structures were isolated and stained for established generic cell markers. In Figure 3.2-15, A) and B) were images taken of spheres that were still embedded in the gel. The gel had prominent levels of background fluorescence in images taken for the Alexa-568 excitation peaks, due to the phenol red present in media and Matrigel, meaning that red channels could not be visualised. However, the green channel for Alexa-488, representing Vimentin in all four images, could still be clearly imaged. C) and

D) were removed from the gel through successive washing with cold PBS and fixing in cold PFA as described in the materials and methods. Staining for E-cadherin and Vimentin was successful here and both markers could be visualised in the organoids. In A) and B), it is evident that mesenchymal cells persist and generate 'spider web' structures. These cells are not condensed into cell-cell adherent spheroids, but form a skeleton structure, that could suggest an overarching network or scaffold on which epithelial structures could then populate. A) also contains, what appears to be, epithelial cells which have less staining for Vimentin and form dense clusters of cells, reminiscent of budding epithelial structures in the developing salivary gland.

Images C) and D) in Figure 3.2-15 contain both cell types and stain strongly for E-cadherin and Vimentin. The E-cadherin staining appears to be present between the cells, as observed in the tissue characterisation in Figure 3.2-1 to 3.2-7. The majority of Vimentin staining in both images appears to reside predominantly between the spherical formations, suggesting an ability of the cells to organise and form tissue structures rather than aggregate in a random manner.

The aim of the next section of work was to conclusively prove that mesenchymal cells are relevant and necessary for the salivary gland organoids to correctly develop structures which mimic the developing mouse salivary gland *in vivo*, and to investigate if spheres developed with the inclusion of epithelial and mesenchymal cells had an advanced developmental phenotype. Following the visualisation of the protocol in Figure 3.2-16 A, salivary glands were excised, digested and plated out to generate primary cell cultures. These were maintained until passage three, at which point cells were collected and combined to form primary and secondary spheroids for analysis.

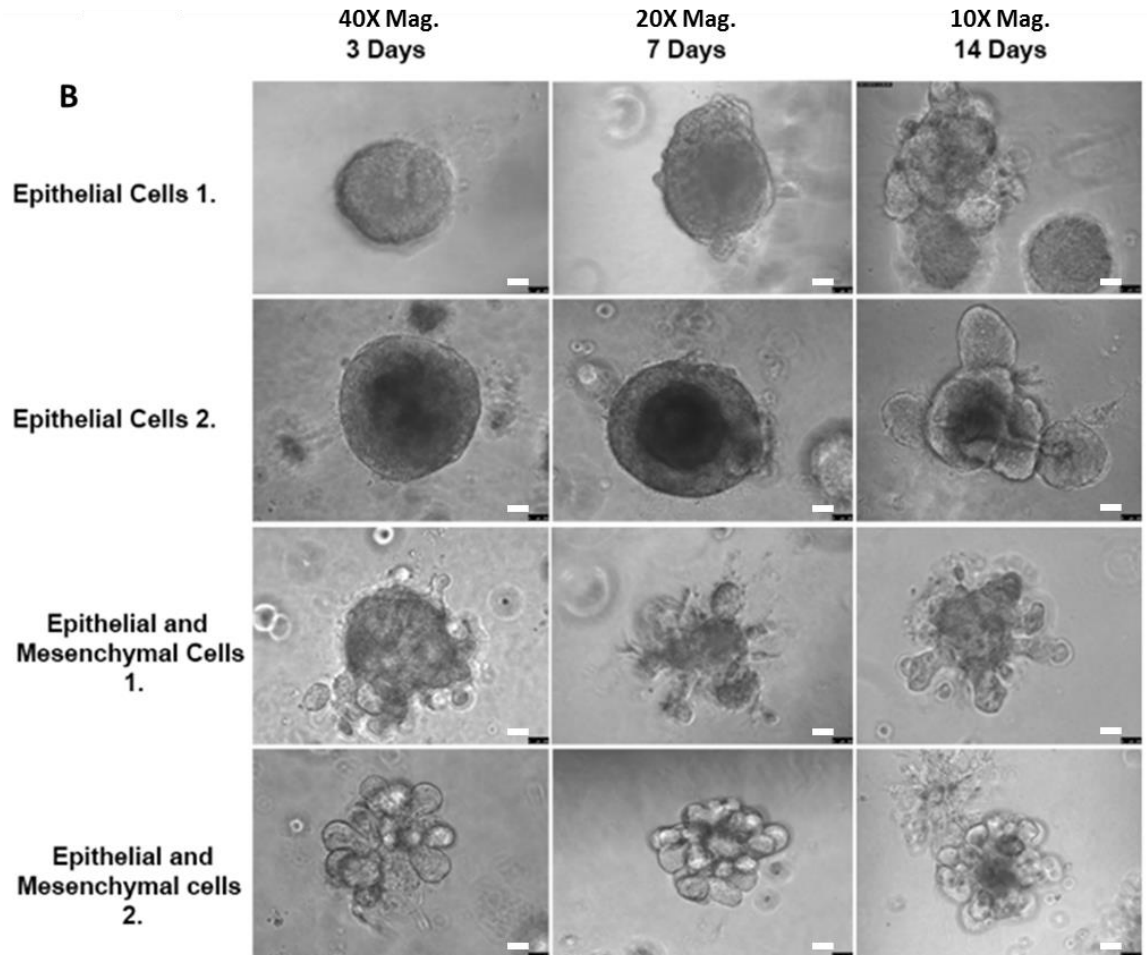
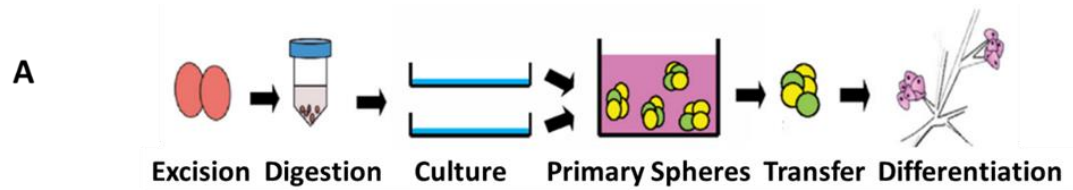


Figure 3.2-16. Optimised sphere assays using protocol three produced consistent spheroids that demonstrate significant changes with the addition of mesenchymal cells. A) A diagrammatic representation of the protocol used to develop sphere protocol. B) Primary sphere cultures, with experimental repeats 1 and 2, demonstrated budding and branching phenotypes as would be observed during developmental stages of organoid structures. Images were taken at various magnification. Scale bar at 40X equal to 100um, scale at 20X equal to 225um, scale bar at 10x, equal to 275um

Using Protocol Three, the regenerative capacity of the spheroids could be quantified by measuring sphere diameter, frequency of spheres in each assay, and counting the number of branches presenting on each sphere structure, shown in Figure 3.2-17. Spheres could be grown in the same Matrigel for a period of 21 days, they could then be

extracted from the gel and spread on slides for staining for immunofluorescence: Figures 3.2-16 and 3.2-18, or processed for PCR analysis of RNA expression: Figure 3.2-19.

It was then shown that, with the inclusion of mesenchymal cells, sphere frequency increased and sphere diameter also increased by an average of 23%. These results can be seen in Figure 3.2-17 and Figure 3.2-19 where the number of spheres in each condition were counted, the number of spheres presenting with a branching phenotype, and also the diameter of the spheres were measured.

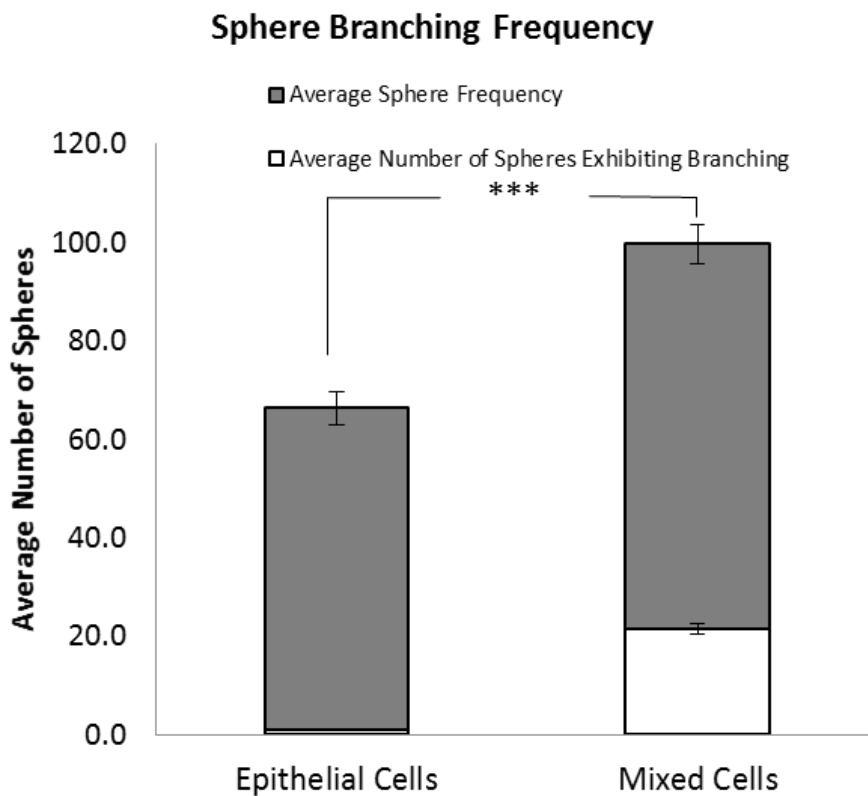


Figure 3.2-17. Sphere assays comprising of mixed epithelial and mesenchymal cells presented with an increase in the number of spheres in total and an increase in spheres that exhibited the budding and branching phenotype compared to epithelial only conditions at the same time point. Statistical analysis of the frequency of spheres and the exhibition of branching phenotype, error bars represent the standard error of the mean (Student's t-test was used as a statistical analysis, where $P < 0.0001$: *).**

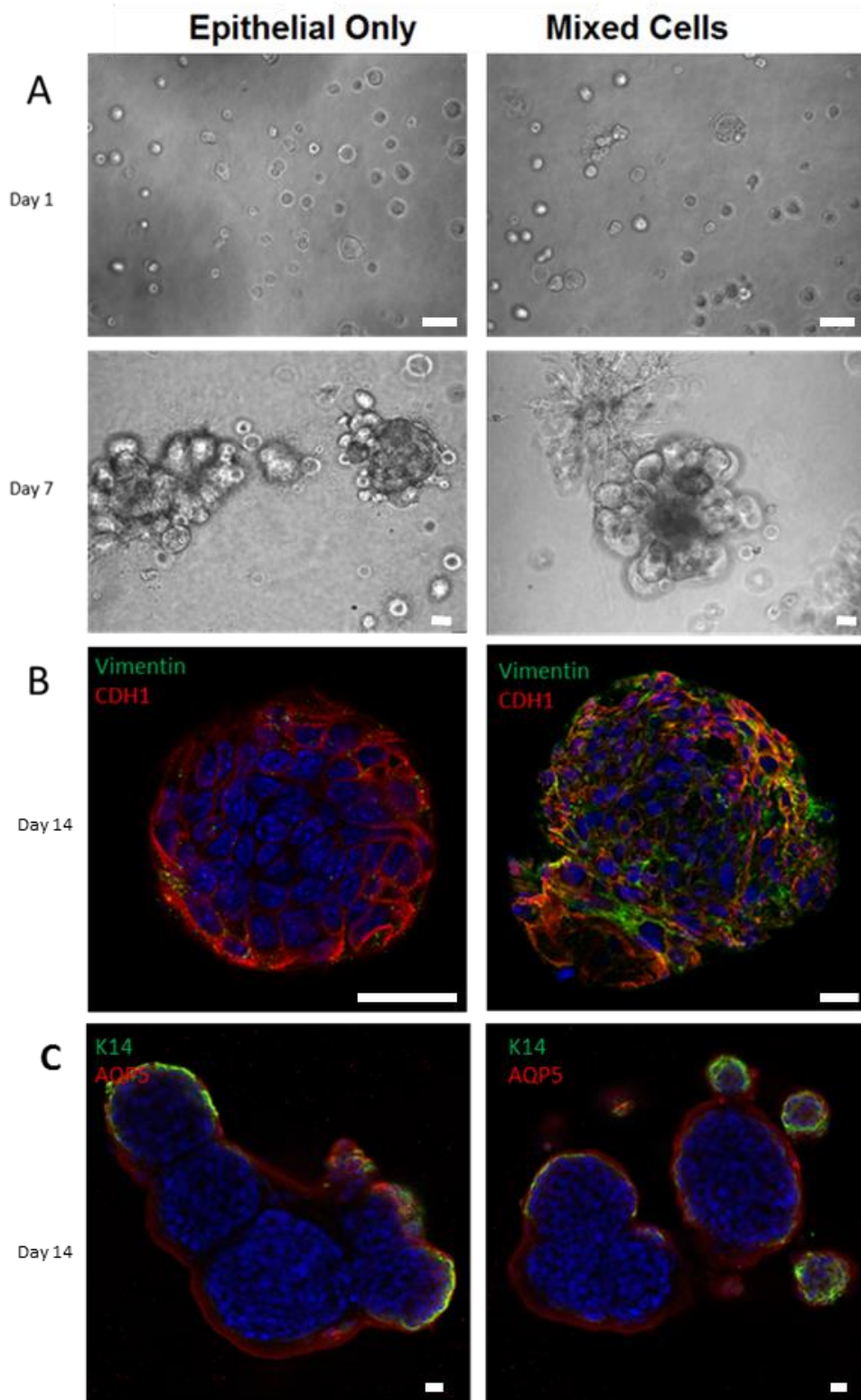


Figure 3.2-18 Established spheroids demonstrate that mesenchymal cells enhance developmental potential of spheroids in culture. A) ECs and MCs combined into three-dimensional organoid structures after 24 hours and 7 days. B) Vimentin and E-Cadherin (CDH1) staining of spheres cultured for 2 weeks. C) IF staining for AQP5 and K14, mature salivary gland tissue markers. Scale bar is equal to 50um.

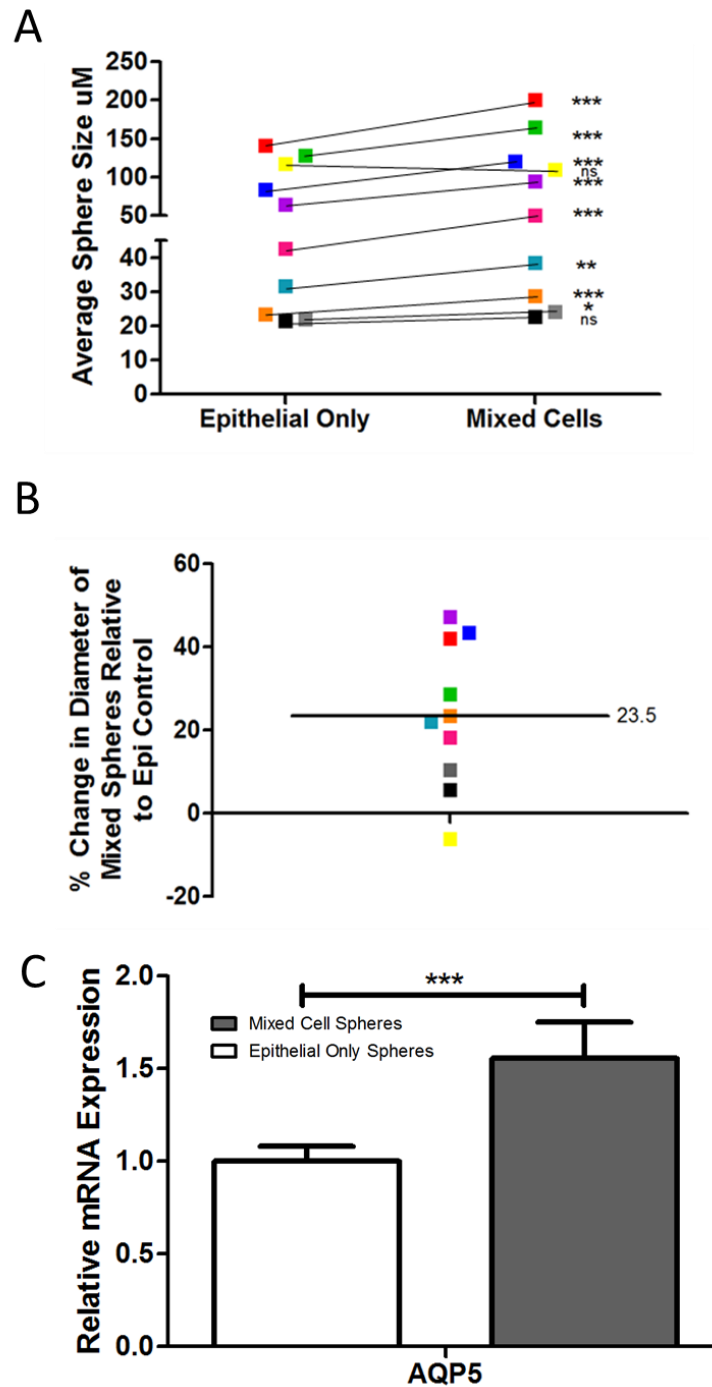


Figure 3.2-19. Analysis shows mixed cell spheres were more developmentally advanced than epithelial only structures. A,B) Spheres over 10 repeated experiments were 23.5% larger with the inclusion of MCs, colours denote paired experimental results. \pm SEM 2.699 for epithelial structures and 4.815 for mixed cell structures. $n=860$ epithelial spheres, $n=822$ mesenchymal spheres. C) Relative RNA expression of one pair of experimental results, $n=2$ internal repeats with combined RNA, demonstrating a higher level of AQP5 expression in mixed cell spheres. Error bars represent SEM (Student's t-test was used as a statistical analysis, where $P<0.0001$: ***)

Immunofluorescence staining of the spheres in Figure 3.2-18, indicated that the epithelial only conditions still only contained epithelial cells at the point of sphere extraction, and the mixed cell spheres did indeed stain positive for both epithelial and mesenchymal cell markers. However, staining was unable to show any changes in the expression patterns of AQP5, used as an indicator of developmental state. However, the relative RNA expression of AQP5 was shown to be significantly increased in spheres containing both epithelial and mesenchymal cells, when compared to epithelial only controls. Furthermore, AQP5 expression can only be attributed to an increase in developmental stage as the same total cell number remains the same between culture conditions, with the only difference attributed to the addition of mesenchymal cells, which do not produce AQP5 protein.

These spheroid structures were then removed from the gel and could be reintroduced to a second culture environment, described in Materials and Methods 2.10, which had additional collagen gel and fresh media added to create a less dense culture environment. The aim of these secondary sphere cultures was to investigate the possibility of inducing further differentiation in the organoids, to develop duct structures, or increase expression levels of differentiation markers. Spheres were observed transforming through extreme changes of morphology with compacted spheres presenting with branching structures and long, duct-like processes extending into the surrounding gel matrix. One key observation is that these processes frequently grew towards, and connected with, other organoids growing in the gel environments.

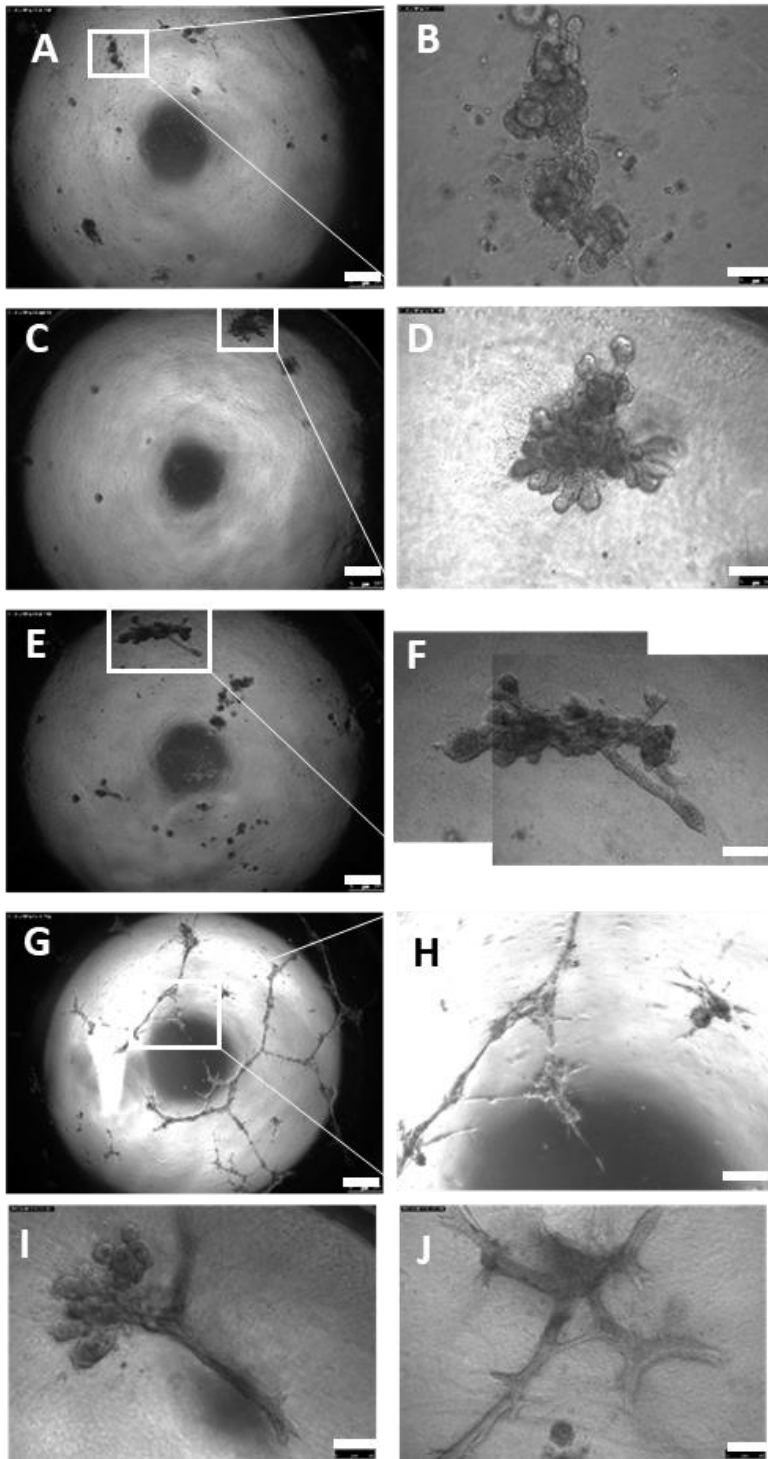


Figure 3.2-20 Overview of a well of secondary sphere culture environment with a high magnification observation of spheroids of interest therein. Primary Spheres were transferred to secondary sphere cultures. Comparisons drawn between A&B) epithelial only cell spheres cultured in a mixed culture medium, C&D) mixed cell spheres in a mixed culture medium E&F) epithelial only spheres in B27 medium, G&H) mesenchymal cell only spheres in Amniomax medium, I) mixed cell spheres first cultured in B27 Primary Sphere culture and then J) transferred to Amniomax. Images taken at various magnification: A, C, E, G at 5x with a scale bar of 250µm, F, H at 10x with a scale bar of 125µm , B, D, I, J at 20x with a scale bar of 50µm.

Spheres that had initially comprised of mesenchymal cells created “spider-web” patterns in the secondary sphere cultures. These structures are reminiscent of epithelial duct structures within the salivary gland, with examples demonstrating a focal point from which these duct-like extensions were primarily emanating. The structures incubated in B27 supplemented basal medium appeared to be more acinar in structure, whilst the cells cultured in Amniomax medium changed significantly to ductal-like structures. When mixed cell spheres are cultured in a mixture of culture mediums, the patterns are a combination of both structures. Alternatively, by taking cultures grown solely in B27 culture environments, which promote epithelial cell growth, and then transferring to a secondary sphere culture containing only Amniomax to promote mesenchymal cell growth, significant changes were observed in the tertiary structures of the organoids. Figure 3.2-20 I) and J) show the preserved acinar-like buds and branches could be observed, with the extended duct-like structures appearing when transferred to the collagen-Matrigel secondary gel culture environment. Attempts to dissociate these structures from gels were unsuccessful, and staining the structures within the gel was impractical due to the high levels of background fluorescence caused by the gels. This background in the collagen and Matrigel gels was higher than seen previously in the Matrigel only cultures.

3.2.4. Discussion

The variety of cells within the salivary gland tissue is diverse and, therefore, any in vitro representations of the salivary gland will have limitations. However, working with mouse salivary gland tissue has enabled the optimisation of staining techniques, the development of cell culture conditions and the manipulation of cells through the generation of three-dimensional models in preparation for working with human patient samples.

The immunofluorescence staining is highly conserved between mouse and human tissue, when comparing between the staining presented in section 3.1 and section 3.2, with E-cadherin and Vimentin being similarly effective for identifying the epithelial and mesenchymal cell populations. Identifying mesenchymal stem cell markers was more successful in the mouse tissue and through the use of IF and FACS, a small population of cells that are positive for stem cell markers such as PDGFR β , Sca-1, CD29 and CD105 was identified. These markers have been discussed in other papers where isolated cell populations are used in therapeutic approaches to conditions such as radiation exposure (Lombaert, Knox and Hoffman, 2011), and are frequently demonstrated as being able to identify mesenchymal stem cell populations (Khalili *et al.*, 2012). However, the panels of markers described in the mesenchymal stem cell isolation kit from R&D systems were developed against bone mesenchymal stem cells, which give rise to different blood cell populations. Cells isolated from blood are easier to process through flow cytometry analysis due to their shape and size, and the panel may not be as relevant for the material we are using as there are always regional differences between markers expressed in tissues around the body. For example, CD106 is also known as VCAM1

(Vascular Cell Adhesion Molecule-1), and not only is it used as a stem cell marker in bone mesenchymal cells, but it's also relevant for identifying endothelial cells, and therefore it could distort the accuracy of our results. Furthermore, it was not an option to duplex the antibodies from the MSC kit due to the same host being used to raise the antibodies, the project was unable to confirm the degree to which these markers are presented in the same cell population.

As discussed previously in section 3.1, Vimentin can be integrated with other filamentous proteins within neurones such as Neurofilament. These filamentous proteins are responsible for facilitating the migration of cells, and enabling the structure of fibrous processes, such as dendrites, that are involved in cell signalling and peripheral nervous systems. Neurofilament could have been targeted to negatively select population of cells through FACS/MACS. However, it is notoriously difficult to select fibrous cell types through these methods as it is important to generate single cell suspensions, otherwise there is a risk of cross-contaminated cell populations, although specific kits have now been developed, specifically for isolating single cell suspensions of fibroblasts, such as one provided by Miltenyi Biotec. Furthermore, FACS technology was developed for analysing blood cell populations, and the technology does not translate well to digested tissues or adherent cell cultures.

As expected, AQP5 may be used as a marker to identify the acinar, secretory cells, as AQP5 is a water channel protein found only on the apical membrane of cells to facilitate secretion of saliva through a hypertonic salt gradient, as discussed in section 1.2. This is because only mature, fully differentiated acinar cells will express AQP5, so therefore, it can also be used as a marker for fully differentiated secretory tissue. This marker was

used in a similar manner to work done by (Chan *et al.*, 2011), to demonstrate the developmental progression of the organoid structures. Ideally, it would be preferable to check a panel of markers such as Chan *et al.*, using alpha-amylase and ZO-1 too, as this would ensure a specific salivary gland maturity phenotype.

The development of cultured cells through spontaneous selection provided a population of cells that accurately represented the tissue niches of epithelial and mesenchymal cells. These cells could be shown to express discrete panels of markers, confirmed by comparing the staining profiles to the previously stained tissue sections, whilst they also grew in established patterns and phenotypes that aided the clarification of the cell type. These cells grew well in culture but were limited in the number of passages as they are primary cell cultures.

Retrospectively, it would have been preferable to spend more time optimising the growth conditions and performing further analysis using IF of the cells to confirm phenotype. It also would have been preferable to have completed more work on the flow cytometry analysis of the expression profiles of the cells. Although the limitations of this technology have previously been discussed. Through the use of FACS or MACS, it could have been possible to generate a purified stem cell population before returning these cells to culture in single cell environments to amplify pure colonies of undifferentiated stem cells. A long-term aim of encouraging single cells to generate a colony spheroid structure could have been developed to ensure cellular uniformity, whilst hopefully observing some of the population undergoing differentiation down a mature secretory cell lineage.

However, even with these very simplistic methods, this research conclusively showed that cells could be developed from mouse salivary glands and that these heterogeneous cells could be recombined in a three-dimensional gel model to create organoid type structures, representative of the developing salivary gland structure. Although the process of sphere formation was indiscernible; the project was keen to demonstrate that a clonal expansion of cells was responsible for the production of the spheroid structures, rather than aggregation, it wasn't possible using the techniques used here.

A few limitations to this area of study were encountered, in that when tissue derived from two-month-old mice was used, the yields of cells were very low, and the proliferative capacity made the culture not viable. Alternatively, the use of mice younger than post-natal day 21 was avoided, as the salivary glands have not reached maturity in mice until they have passed through the adolescent stages to become fully grown adults (Melnick *et al.*, 2001). As the intention was to model a human autoimmune disease that predominantly affects older individuals, the use of mice at postnatal day 30 was maintained, as they are considered adult mice at this point and have undergone complete salivary gland formation and differentiation. Younger mice, with developing salivary glands, would have disproportionately higher levels of stem cells, higher levels of growth factor signalling, and more disparity in expression of differentiation markers than a fully mature adult mouse.

The process of optimising the organoid technique required a few stages of experimenting with various protocols. Through the initial preliminary experiments, it was demonstrated that combining the epithelial and mesenchymal cells produced organoid structures that resembled early stages of salivary gland development.

However, the culture conditions were the limiting factor, as the culture media had not been combined. The spheroids that grew in the B27 media stopped growing after a few days and were very rounded in structure with some branching and budding. Alternatively, the spheroids grown in Amniomax media did not form spheres but formed branching fibrous structures that were not representative of any developmental structures. This suggested that the Amniomax culture medium did not contain the correct nutrients to maintain both phenotypes and that, by combining the media together, the persistence of both cell populations was ensured.

When the number of cells used in the experiments was reduced for Sphere Protocol Two, with results shown in Figure 3.2-13, the ratio of epithelial and mesenchymal cells was also altered, as there has been suggestion in the literature, that incubating cells with an epithelial to mesenchymal cell ratio of 2:1 increases the developmental structures of the organoids (Farahat *et al.*, 2017). It is believed that this is meant to be more representative of the ratio of cells within the salivary gland tissue.

Despite these changes, the number of cells in each well remained too high which caused the spheres to become very dense and nutrient uptake from the media to be very rapid, indicated by a change in the pH, detected by the Phenol red dye in the media. We also observed some necrotic spheroids and some disintegration, leading to reduced lifespan of the sphere experiments, adding a further limitation to the technique. However, it was observed that the early structures that formed, did resemble early stages of salivary gland development, and that some internal lumen formation and potentially significant branching and budding of these structures could be observed. When transferred to secondary culture conditions, a mixture of Matrigel and Collagen, these cultured

spheroids could generate large, extended duct like structures that resembled the intercalated ducts of the developing salivary gland.

In addition to previous limitations, Matrigel is an expensive reagent, requiring the use of small volumes in the 96 well plates, and reduced experimental repeats. This could be counteracted by the spiking of culture medium with very small quantities of Matrigel, which ensured the sphere cultures were exposed to relevant growth factors over their experimental lifespan. Matrigel is an extracellular basement membrane secretion, containing laminins and collagens and a variety of growth factors. It has been well established for use within tissue regeneration assays, frequently seen as a gold-standard for organogenesis or none 2-D cell culture methods, and several of these published works were adapted into a new protocol for generating organ-like structures (Feng *et al.*, 2009; Maria *et al.*, 2011; O'Rourke *et al.*, 2016). Other organoid gel model alternatives were considered, such as PEG hydrogels, but the use of Matrigel is well established in the field of salivary gland regenerative studies and has been shown to be effective in sphere cultures, despite restrictions in the ability to specifically moderate components.

Although spheres were extracted and fixed for immunofluorescent analysis, the volume of RNA yielded from the cultures was very small and at the time it was not considered relevant to extract RNA from all of the experiments and this could have added further dimensions to the study. Extracting proteins would have also been impractical for these experiments, due to the yield again, but also the Matrigel is comprised of basement membrane proteins and could have masked any smaller protein expression levels.

Regarding the analysis of sphere development, other groups have used a variety of other potential dimensions or attributes to define and measure the proliferative capacity or developmental potential of the organoids such as (Sokol *et al.*, 2016) who measure the volume of the structures that they generate and also the frequency of structures formed per standard number of cells in the initial culture. Although the measurement of sphere diameter is sufficient to demonstrate an increase in proliferation, many assumptions had to be made which may reduce the reliability of the results. It was assumed that, even if the spheroids are not completely spherical in shape, the measurement of the diameter is a consistent indicator of total sphere size. It was also assumed that one single measurement, maintained at a consistent direction of measurement across all spheres in each condition is a sufficient, reliable and representative measurement. From the experience of working with these spheres, the structures were observed to not be perfectly spherical, with many examples of flattened or hollow organoids, and attempting to calculate sphere volume would be less reliable than a single indicator of size such as diameter or circumference. Circumference was also disregarded for the purposes of this project, as those structures that may have exhibited budding and branching would have an exponentially larger circumference than their control counterparts and would negatively impact the accuracy of the results.

An alternative method may have been to count the number of nuclei present in each spheroid as this would have given a more accurate representation of the number of cells involved in each structure and could be measured over time as a dimension of proliferative ability. However, the structures can be very dense, making counting the nuclei difficult.

Once the primary spheres were cultured, extraction for IF staining was also problematic; it was difficult to find a suitable method for visualising these structures. Gently extracting, with many washes of cold HBSS, and plating onto microscope slides was the only method that would reliably reduce the background fluorescence of the gel matrices, enabling a decent visualisation of the structures and distribution of generic and developmental markers. However, damaged structures were frequently observed and many structures were lost during the washing stages, and became stuck inside pipette tips and microcentrifuge tubes. With hindsight, more effort should have been made to find alternative methods of evaluating the developmental potential of the tissues, such as inclusion of GFP labelled cells, which could identify and longitudinally follow stem cell populations throughout development of the organoid models (Emmerson *et al.*, 2017). Alternatively, in situ hybridisation techniques could be used to identify each cell population with a different colour, to reduce the amount of background fluorescence observed at the end of the experiments. Co-staining with other markers could then also be performed, which would allow the visualisation of any epithelial-mesenchymal transition between each of the populations (Okumura *et al.*, 2003; Okumura, Shinohara and Endo, 2012).

The experimental results clearly indicate an enhanced developmental phenotype with the addition of mesenchymal cells. The reason behind this is thought to be because of the epithelial-mesenchymal cell-cell signalling that is known to occur *in vivo*, and is now being mirrored in the organoid models. As explained in the introduction, during very early developmental stages of salivary gland development, the mesenchymal cells play an important role through their physical presence, but also through FGF signalling, to

direct the proliferation and branching of the epithelial tissue. The incorporation of mesenchymal cells has allowed epithelial cells to progress down their specific lineages where they start to express differentiation markers and exhibit tissue organisation.

3.2.5. Conclusion

In conclusion, mouse submandibular gland tissue was characterised with markers comparable to the panel used on human tissue in section 3.1. A fraction of the mesenchymal tissue was shown to stain positively for mesenchymal stem cell markers and it was possible to identify both generic and stem cell populations within cell culture populations through analysis by QPCR, IF and FACS. Cell cultures were successfully combined into three-dimensional organoid culture models that were optimised successfully and were reliable and reproducible. These spheroids displayed a more significant role played by mesenchymal cells in the formation of these organoid models by consistently producing spheroids that were larger and more developmentally advanced. Finally, this model was considered mature enough to be taken forward for work with human derived cell cultures.

Alternatively, this model could be used as a model for investigating the effect of dysregulation of molecular pathways. Because this model uses cultured cells, it would be possible to modulate the expression levels of proteins involved in pathways such as cell differentiation, cell cycle, or salivary secretion, using transfection or CRISPR technology (Sander and Joung, 2014). With more time and resources, this investigative route should be pursued, investigating the stem cell fate determination pathways, as there has already been some suggestion that these pathways could be impacted in PSS positive patient samples. Without the confounding disease condition, it could be possible to manipulate cells into presenting with the same impaired regenerative potential and to investigate ways in which this could be reversed.

3.3. Establishing 3D Organogenesis Assays Derived from Human Patient Biopsies

Techniques were developed from the success of establishing mouse cell lines and organoid models that could be used to investigate the regenerative potential of human derived cell lines. Culture condition parameters were maintained from the mouse culture system, whilst adapting the growth factors for use with human cells.

Where other groups are investigating the use of regenerative tissue engineering to recover structure and function of salivary gland tissue, very little work has involved isolating human patient derived cell cultures and further dividing the cells into sub-populations of different cell types and functions or investigating the very specific role of mesenchymal cells in the regeneration models. There have been successful attempts at using adipose derived, induced stem cells to represent a mesenchymal stem cell population, as they're seen to be enriched within adipose tissue when compared to bone marrow. Work done by Lim (Lim *et al.*, 2013) injected these adipose MSCs into the tail of rats which had been exposed to a dose of irradiation. They could demonstrate the efficacy of the cells to migrate to the salivary glands and significantly repair the inflicted damage, demonstrated by an increase in salivary flow rates and a decrease in the lag time of secretion when compared to untreated controls.

Alternatively, other research groups have grown organoid structures using salivary gland acinar progenitor cells (Srinivasan *et al.*, 2017). Srinivasan *et al* isolated cells directly from tissue that were enriched for progenitor markers through culture environments. The panel they used coincide with similar markers which were tested during the mouse

and human characterisation studies during our research: CD105, CD90, K5 and c-Kit. Although Srinivasan *et al* hadn't divided the cell population into different subpopulations, they could successfully grow organoid structures reminiscent of the developing salivary gland structures, with cells that they identified as being salivary gland precursors. It is hoped that any organoid model that was developed through the course of this research project could also have translational applications when studying other conditions that could affect salivary gland structure and function other than PSS, such as exposure to ionising radiation, or extrapolated into the regenerative potential of other tissues.

Although it has already been established that spheroids are very diverse and can be developed from cultured cells (McCall *et al.*, 2013), from directly isolated single cell suspensions (Grabinger *et al.*, 2014), from mouse (Maruyama *et al.*, 2018), and from human origins (Pradhan-Bhatt *et al.*, 2013), it is believed that this project is unique in that it is generating primary cells direct from PSS affected individuals, providing an ability to directly monitor the effect of the disease on the behaviour of cells in culture.

The aim of this experiment was to produce primary cell cultures that represented epithelial and mesenchymal cell populations as had been achieved previously in section 3.2 with the mice salivary gland cultures. The protocol was optimised for use with human patient tissue, starting with the isolation of epithelial and mesenchymal cell populations from labial salivary gland tissue removed as excess diagnostic material. Then these cells were combined into three-dimensional cultures, as before, with the aim of understanding the mechanistic impact of PSS on the mesenchymal cell population.

3.3.1. Human Cell Culture and Organoid Methods

Human Primary Cell Cultures

Human labial glands were digested and plated out into culture conditions as described in the Materials and Methods 2.8. DMEM F12 media was supplemented with B27 supplement and human EGF and human FGF to be applicable for human cell culture work. To promote the growth of epithelial cells, tissue lysate was suspended in B27 supplemented media and plated onto collagen coated dishes using Collagen Coating Protocol Two, described in Materials and Methods 2.8.1. Alternatively, the promotion of the growth of mesenchymal cells was achieved by plating the tissue lysate in Amniomax complete media, on Poly-D-Lysine coated cell culture dishes, as described previously. When cells had been passaged three times, they were collected for organoid model cultures. Passage three cell cultures were also fixed for immunofluorescence staining and collected for RNA collection using the standard phenol-chloroform RNA extraction technique detailed in Materials and Methods 2.13; both these techniques were used to aid characterisation of the cells and confirm the protocol could successfully work in human cultures as it did in mice.

Human Sphere Culture Protocol One

Initially, Protocol Three, as demonstrated in section 3.2.3, was adapted for use with human derived tissue. Thawed Matrigel was pipetted into pre-cooled 96 well plates and allowed to set. The cells were collected from culture dishes, washed, and suspended in 1ml fresh media and the cell concentration calculated. In the epithelial only cultures and the mesenchymal only cultures, 5,000 cells per well were mixed with media spiked with 10% Matrigel. In the combined culture conditions, 3750 epithelial cells and 1250

mesenchymal cells were combined with the media to a volume of 200ul. The cell suspension was then layered on top of the Matrigel base. These cultures were imaged every day, with the media changed every two days. This technique was optimised on cells isolated from DSO135, a non-PSS patient sample.

Human Sphere Culture Protocol Two – Mouse and Human Combination

The Human Sphere Culture Protocol One was adapted further with the combining of mouse derived primary cell cultures and human derived primary cell cultures together in the same three-dimensional culture environment. 3750 mouse epithelial cells were combined with 1250 human mesenchymal cells in one well of a 96 well plate, mixed in a media combination suitable for both mouse and human culture conditions. Cells were collected at passage three, as before, and suspended in a media that contained both: DMEM F12 B27, plus mouse EGF and mouse FGF, and Complete Amniomax Medium with human EGF and human FGF, all spiked at 10% with Matrigel. Control wells contained either 5000 epithelial cells only, or 5000 mesenchymal cells only; also in the mixed media cocktail. The cell suspension was layered over 75ul of Matrigel, as described before, with the cells being imaged every day and media changed every two days, with washes of warm HBSS after media removal.

Analysis of Human-Mouse Spheres

Spheres were monitored and imaged every day, with the diameter being measured at 14 days after the initiation of the sphere experiment. The diameter was measured diagonally across the spheres from a South West to North East direction in order to maintain consistency and to completely remove subjective measurements being taken. The diameter of spheroids was recorded, with the student t-test and ANOVA used to indicate statistical significance between cohorts.

Mouse-Human spheres were isolated from the Matrigel gel for histological and immunofluorescence staining. Spheroids were carefully isolated and fixed in PFA before being added to OCT compound and sectioned at 5 or 10um thickness. Tissue was mounted on microscope slides and taken through the standard H&E or IF protocols. Unfortunately, spheres appeared to be seriously damaged when sectioned. Therefore, an alternative method was developed, in which spheres were fixed whilst in the gel before dissociating from the gel with cold HBSS. Once spheroids were obtained, they were transferred to microscope slides and allowed to dry until adhered; IF staining could then be performed with reduced risk of damage or sample loss, using the same Immunofluorescence staining protocol established in section 2.3.

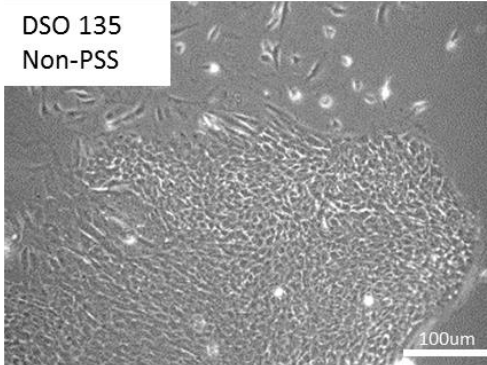
3.3.2. Optimising Cell Cultures of Human Derived Epithelial and Mesenchymal Cells

Cell cultures generated from human tissue mimicked the phenotype of cells produced in the mouse cell cultures. They produced compacted, 'cobble stone' cells that appear to represent an epithelial population, and a fibroblast-like, non-tight junction forming mesenchymal looking population. These cell morphologies are very well-preserved characteristics of the epithelial and mesenchymal cell populations and are frequently used to determine cell type when developing cultures. It was possible to generate cell lines from patient samples representing PSS positive and non-PSS populations.

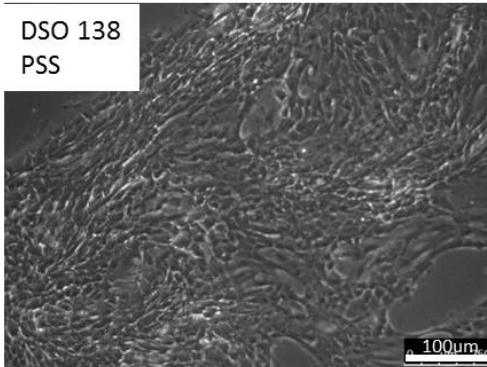
Cell phenotype was more accurately confirmed with IF staining and it was demonstrated that the cells developed in the B27 culture medium and collagen coated plates stained strongly for E-Cadherin and not for Vimentin, whilst the other population, cultured in Amniomax medium and with Poly-D-Lysine coated plates, stained strongly for Vimentin and weakly with E-Cadherin, as shown in Figure 3.3-1. These phenotypes were doubly confirmed with relative mRNA expression levels, showing relatively low levels of Vimentin and elevated levels of E-cadherin expression in the B27 cultured cells, and high Vimentin with low E-cadherin in the Amniomax cultured cells. These cells represented the desired populations of epithelial and mesenchymal cells as previously described in section 3.2. It was then possible to use these optimised culture conditions to develop three-dimensional organoid assays.

**Epithelial,
B27 Culture**

DSO 135
Non-PSS

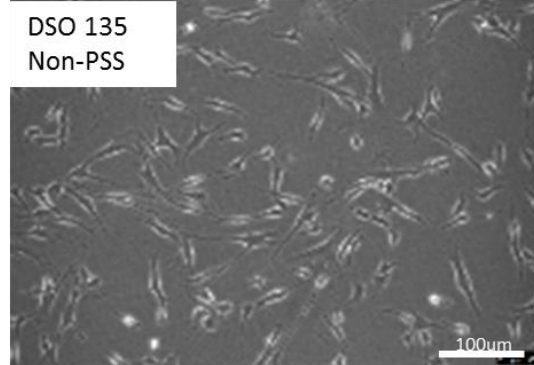


DSO 138
PSS

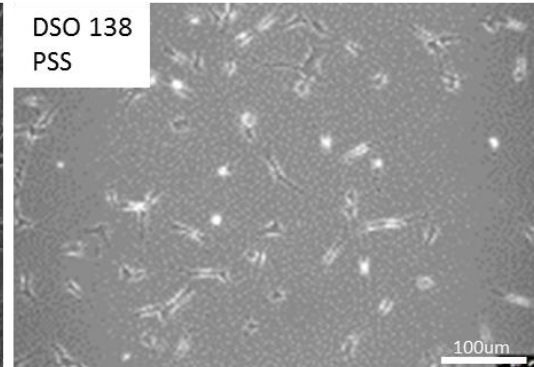


**Mesenchymal,
Amniomax Culture**

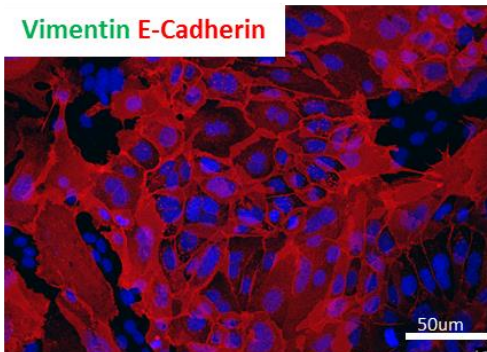
DSO 135
Non-PSS



DSO 138
PSS



Vimentin E-Cadherin



Vimentin E-Cadherin

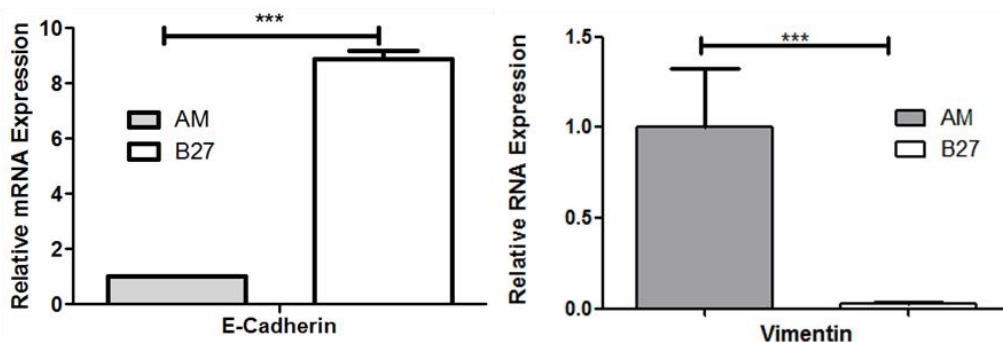
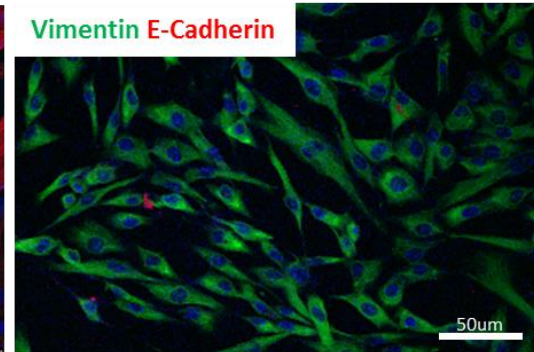
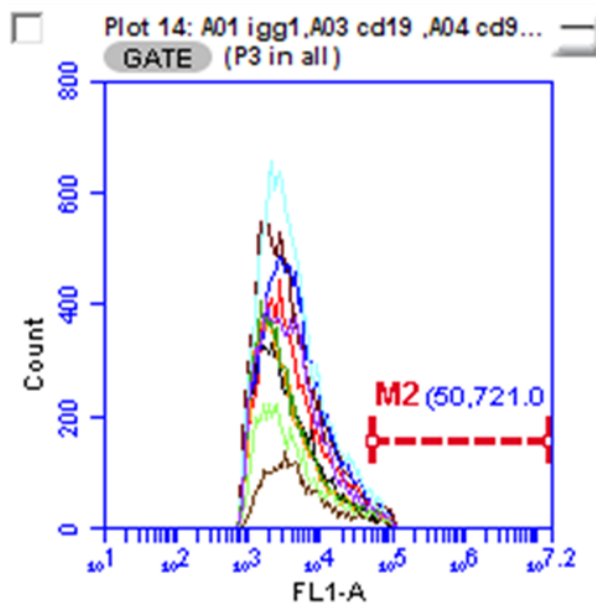


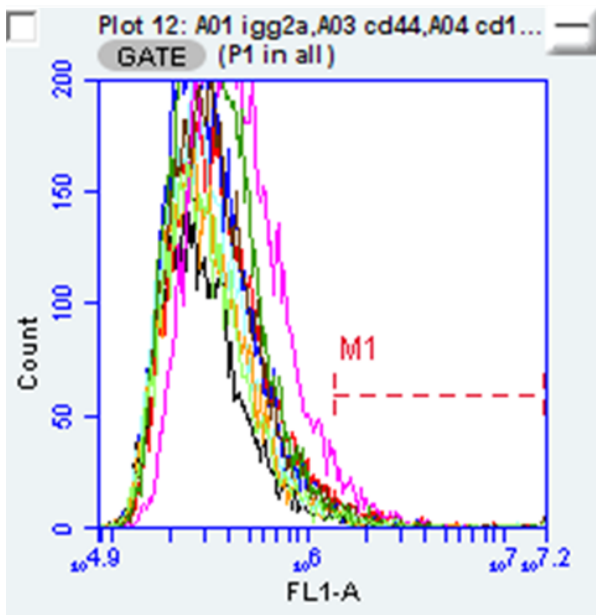
Figure 3.3-1 The development of human primary cell cultures that represent epithelial and mesenchymal cell populations. Non-PSS DSO 135 and PSS positive DSO 138 are shown to both produce discrete phenotypes of cells in the two culture environments, with phenotype confirmed by immunofluorescent staining with anti-Vimentin and anti-E-cadherin antibodies, and by QPCR analysis of RNA. Scale bars are described in the figure at 100µm in cell culture brightfield images, and 50µm in the IF images. Error bars display the standard error of the mean (P<0.0001: ***, P<0.001: **, P<0.01: *)

Once the culture conditions were optimised and confirmed to present the desired cellular phenotype in non-PSS DSO 135 and PSS positive DSO 138, the assumption was made that this should be sufficient across other patient samples, and further confirmation of cell phenotype would not be required for each cell line generated, so long as the growth pattern and shapes were maintained and monitored for each new cell batch created.

Further analysis of the marker expression profiles was attempted using flow cytometry, shown in Figure 3.3-2, to detect an established panel of markers provided by R&D Systems that was designed to identify mesenchymal stem cells. Due to the scarcity of sample material, the project relied on performing flow cytometry analysis on cultured cells that had been passaged to single cell suspension, as opposed to digesting fresh tissue for the assay.



DSO 116	Marker	% Shift in Expression
	IgG1	1.00
1.	CD90	1.66
2.	CD19	1.86
3.	CD105	1.88
4.	CD106	1.65
5.	CD146	1.94
6.	CD166	2.51
7.	CD44	2.14
8.	CD45	2.04



DSO 147	Marker	% Shift in Expression
	IgG1	1.00
1.	CD90	1.76
2.	CD19	1.54
3.	CD105	3.65
4.	CD106	1.29
5.	CD146	1.28
6.	CD166	1.05
7.	CD44	2.84
8.	CD45	1.16

Figure 3.3-2. Mesenchymal stem cell populations were identified in cultured cell populations through flow cytometry analysis. DSO116, a non-PSS patient, and DSO 147, a PSS positive patient, derived cell lines were taken through the flow cytometry protocol as developed for mice cells. All the markers delivered a higher number of events than the relative IgG control, which is identified by the percentage shift of the peak of events over 1%, although all of these shifts in expression were minimal.

These experiments indicate that both the non-PSS and PSS positive samples present with MSC markers in very low abundance. The markers used in each experiment each reached a profile over 1%, indicating a true positive staining above the background levels detected by IgG alone, although none of the markers identified a large proportion of the cells. As multiplexing experiments were not performed, no comment could be made on which proportion of the cells is being identified by the same markers, or if each of these markers identified a unique proportion of the cells. It could also suggest that these cell populations in culture are definitely of mesenchymal cell origin and that these markers could be used to isolate, or purify, cell populations through FACS or MACS technology.

The primary outcome of this experiment was to confirm cell phenotype and to calculate the percentage of stem cells within our cell cultures. The project aims to investigate the role of mesenchymal cells within the tissue regeneration model, however, these findings suggest that future work could attempt to isolate MSCs and compare the efficacy of this purified population against mature MCs. Once cell phenotypes had been confirmed through flow cytometry, morphology, immunofluorescence and relative mRNA expression levels, these cell populations could then be taken to develop the spheroid models by following the methods optimised on murine cell culture models and developed for us with human tissue as described in section 3.3.1 Human Cell Culture and Organoid Methods.

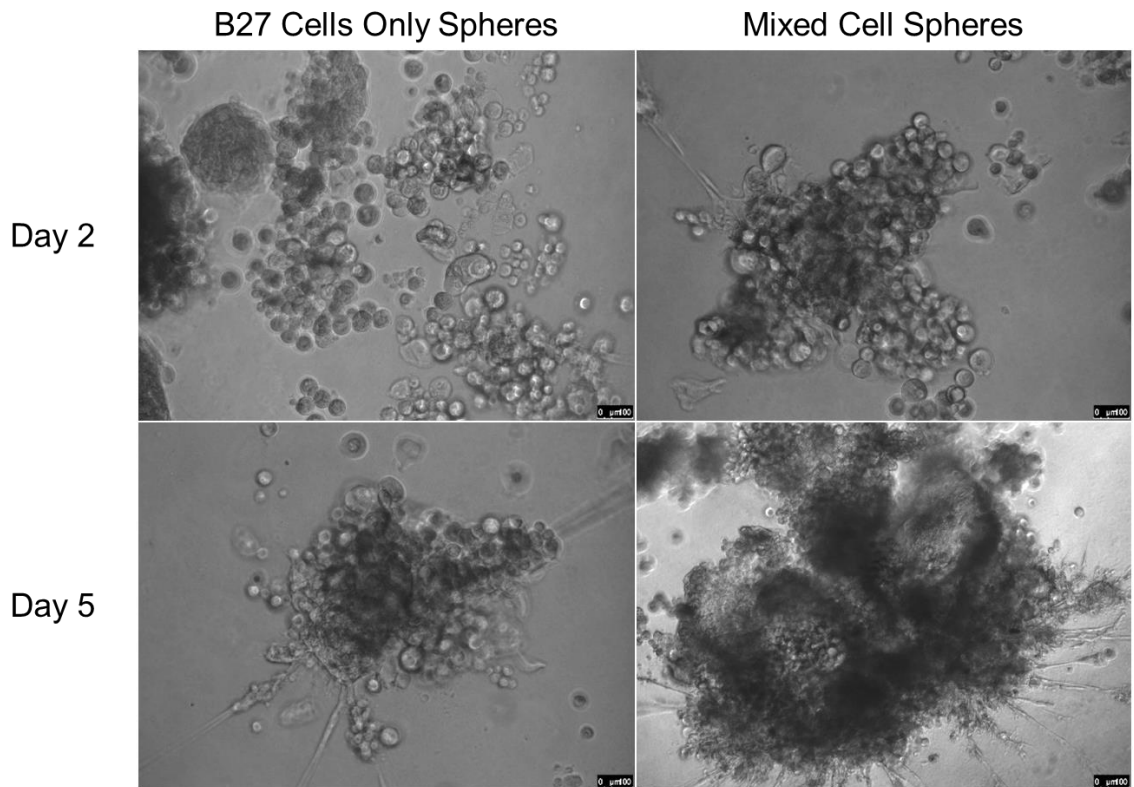


Figure 3.3-3 Human cells from DSO 135 (non-PSS) were combined to generate three-dimensional organoids. Human epithelial and mesenchymal cell combined in Matrigel do not form condensed colony spheres after five days in culture. Records taken two days after initial implantation into Matrigel, and five days after. Images taken at 20x magnification, scale bar represents 100µm.

The human cells were viable and proliferated within the Matrigel cell culture environment as shown in Figure 3.3-3, using Human Sphere Culture Protocol One. However, the growth pattern was not comparable to the mice culture conditions observed in section 3.2.3. From visual observations, the epithelial cells did not compact into large spherical-like structures, they appear to remain single cellular and produce a large amount of cellular debris, which cluttered the gel culture environments. These observations were noted consistently through repeated experiments, indicating that the human epithelial cells were not reliable and could not be used in the same manner as the mouse epithelial cells. From the results displayed in Figure 3.3-3, it was evident that the human cells were unable to independently form consistent organoid structures.

An idea was developed to overcome the issue of the human epithelial cells, by combining human cells with mouse cells, Human Sphere Protocol Two; this reduced variability in each human epithelial cell culture by replacing the defective human epithelial cells with the well-established mouse epithelial cells from section 3.2.3. This also enabled a clearer focus on the role played by mesenchymal cells only on directing the development of epithelial cells in organoid growth. When each non-PSS and PSS positive human mesenchymal cells were combined with mouse epithelial cells, in Figure 3.3-4, the spheroid structures formed as previously seen in the mouse assay. Sphere structures with budding and initial stages of lumen formation could be seen, and variation in the size and structure was observed in assays using cells from PSS versus non-PSS derived cells.

The mesenchymal cells generated from the DSO 135, non-PSS biopsy sample combined with the mouse epithelial cells to form regular and consistent structures reminiscent of the mouse spheroid models in section 3.2.3; these are shown in Figure 3.3-4. When cells were used from DSO 138, 140 and 147, which were all PSS positive patient samples, significant changes in the presentation of the spheroid structures were observed, with fewer regular spheres being formed, changes in sphere uniformity and size. These spheres were further developed in a secondary sphere assay, where we did observe some lumen formation and elongation of duct-like structures. However, many of the spheres were lost in the transition to this culture environment and, once in this environment, they become incredibly susceptible to contamination and necrosis, similar to the limitations on secondary spheres performed on mouse derived cell cultures.

Despite this, images were recorded 24 hours after the spheres had been transplanted and 12 days later in culture, as shown in Figure 3.3-4.

By removing the variability introduced by patient primary epithelial cell cultures, this technique of using human mesenchymal cells and mouse epithelial cells could allow the direct comparison of the ability of human mesenchymal cells from PSS and non-PSS patients to direct, or influence, spheroid structure formation, whilst the expression patterns of mature salivary gland or differentiation markers can be monitored throughout.

In Figure 3.3-4, it's evident to see that there were visually significant differences in the structures generated by cells derived from PSS and non-PSS patients. DSO 135 produced small, consistent spheroid structures that grew at a steady rate, developing concise and regular buds, with evidence to suggest internal lumen formation. When transplanted to secondary sphere cultures, duct-like appendages were observed to form, with the suggestion of lumen formation. These structures would appear to grow towards other spheroid structures within the gel, creating a network of a super-structure, indicative of successful growth factor signalling between organoids. However, the spheroids generated from PSS-positive patient samples presented with varying phenotypes. The mouse epithelial cells persist during the growth of the spheroid structures, but the variation caused by human patient mesenchymal cells is clear. DSO 147, as a low-grade PSS patient, appears to grow similarly to the non-PSS control. Whilst the higher-grade DSO 140 patient derived cells grew out and away from the spheroids, in a fibrous fashion, whilst the epithelial tissue aggregated in larger bodies with less orientation, higher density, and no suggestion of lumen formation or budding phenotypes.

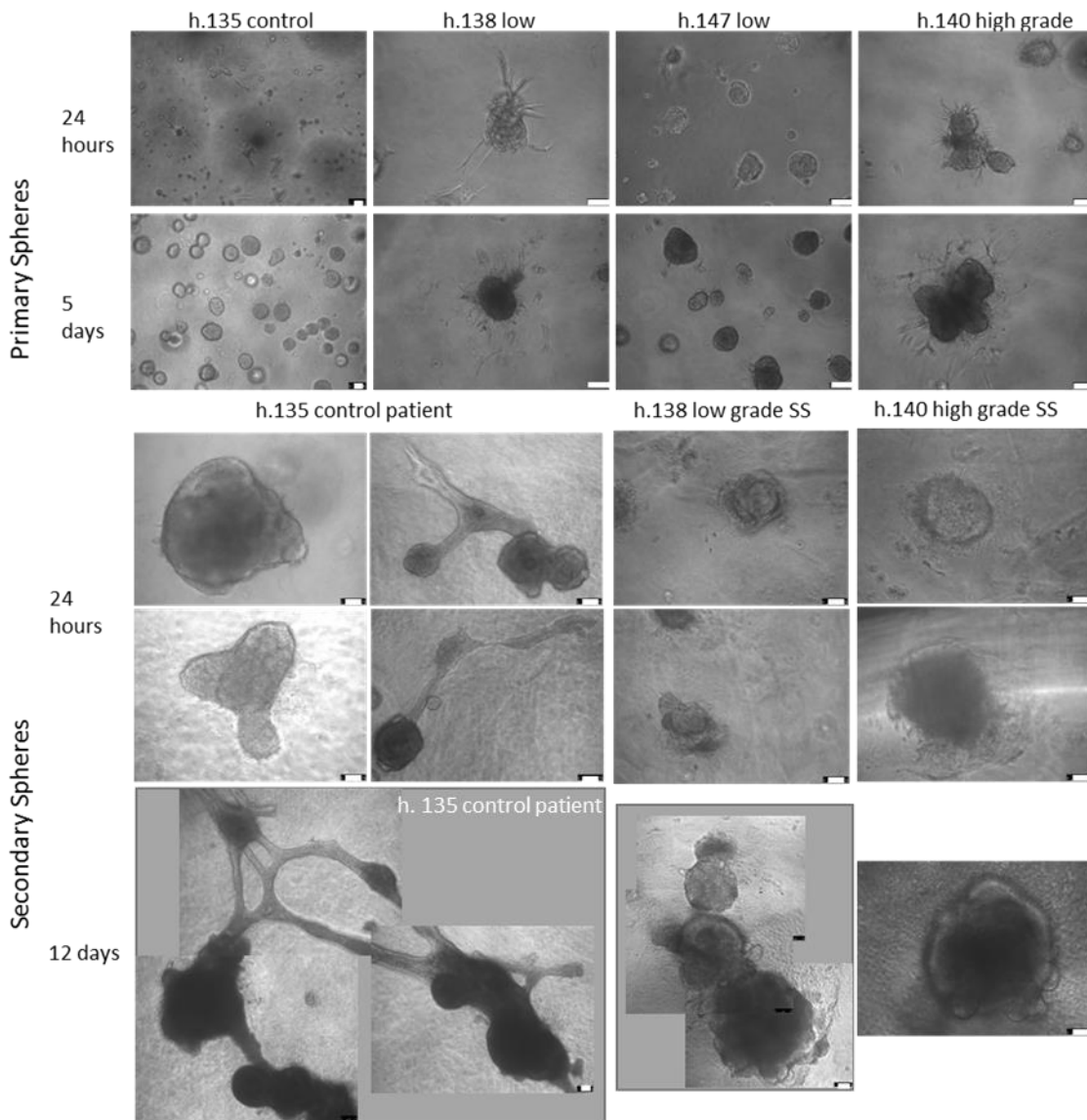


Figure 3.3-4. Three-dimensional culture models combining both human mesenchymal cells and mouse epithelial cells in a recombination experiment have been optimised successfully to represent tissue development. Recombination organoids grew in a repeatable and reliable pattern. Scale bar is equivalent to 50uM. Primary spheres were transferred to a secondary gel environment after 5 days and were cultured for a further 12 days.

When the PSS spheroids were transported to secondary gels, the Matrigel and collagen combination conditions, all the PSS patient cell lines displayed reduced capabilities in generating spheroids compared to the healthy samples: the DSO 147 spheroids did not survive the transition and were damaged or would break soon after implantation or were lost during the process. Many spheres from the DSO 140 population would

disintegrate after 24 hours, with a lot of cellular debris preventing further visualisation of the structures. The DSO 138 spheroids did persist and appeared to present with a budding phenotype consistent with control samples, but no extensive duct-like structures were observed as seen in the DSO 135 population. Once established, analysis of the regenerative capacity of the PSS MCs could be performed using these novel human-mouse recombination organoids.

3.3.3. Case/Control Cohorts Present with Different Regenerative Potentials in Human-Mouse Organoids.

Mesenchymal cells generated from four different patient samples were combined into three-dimensional assays with mouse epithelial cells using 3.3.1 Human Sphere Protocol Two. The spheres were monitored over a period of time with the diameter measured after seven days in culture, with results displayed in Figure 3.3-5. The size of the spheres were used as a quantifiable variable in the regenerative capacity of the cells in culture. Spheres generated with high grade PSS positive patient derived mesenchymal cells produced smaller sphere structures with a more fibrous appearance and no appearance of 'hollowing out' on the inside of the spheres. The high-grade PSS patient DSO 147 consistently produced significantly smaller spheres than non-PSS control cells.

Figure 3.3-5, B), displays the four experimental results with paired case and control results, each point represents a single sphere diameter measurement. These graphs show that the distribution of diameter size was consistent for each condition, and that the PSS-positive cells produced significantly smaller spheres than the non-PSS control spheroids. These results could then be displayed as an average diameter and compared across experiments, whilst also generating a graph that represents the average diameter of PSS-positive spheroids as a relative % of the average control spheroids. Overall, mesenchymal cells isolated from PSS positive patients (DSO117, 138 and 147) generated spheres that were 58.83% of the size of their corresponding experimental controls, suggestive of a reduced proliferative and regenerative capacity observed in the PSS derived mesenchymal cells when compared to non-PSS derived mesenchymal cells.

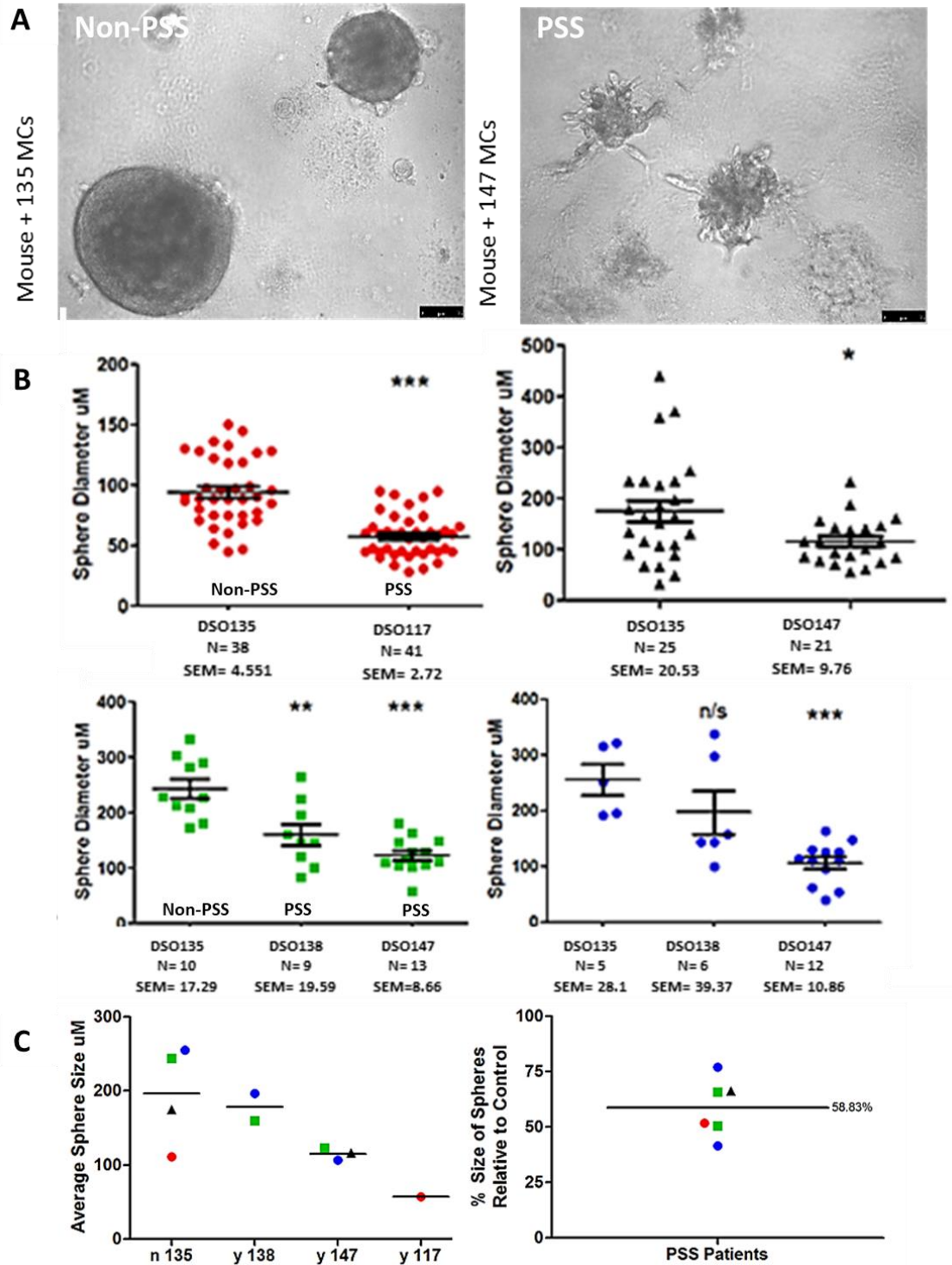


Figure 3.3-5. Cells isolated from PSS positive patient samples had a reduced regenerative potential when compared to control samples over a 14 day incubation. A) 135 (non-PSS) cells compared to 147 (PSS positive) cells when combined with the same mouse epithelial cells. B) Sphere diameter was significantly reduced in disease positive organoids. ($P < 0.0001$: ***, $P < 0.001$: **, $P < 0.01$: *) C) This trend was consistent across subsequent repeated experiments, paired experimental samples are colour coordinated, 135 is non-PSS, 138 and 147 are low grade PSS, 117 is high grade PSS.

As demonstrated in the H&E staining in Figure 3.3-6, the spheres after five days of incubation had a defined outer layer and a heterogeneous inner layer of cells. This already suggests a level of polarisation and rudimentary tissue organisation; however, the samples were damaged through the sectioning protocol, so observers couldn't be certain of lumen formation or the degree of development. The IF staining indicates expression of epithelial and mesenchymal cell markers, condensed nuclei in spheroid structures, but no indication of discrete cellular compartments or polarisation of structures. All of the antigens targeted by IF appear evenly distributed across the structures and staining patterns overlap considerably, suggesting no division between the epithelial and mesenchymal cell populations within the organoid structures. Although, the presence of both markers evenly distributed throughout the organoids suggests that both cell populations have persisted through the culture environment.

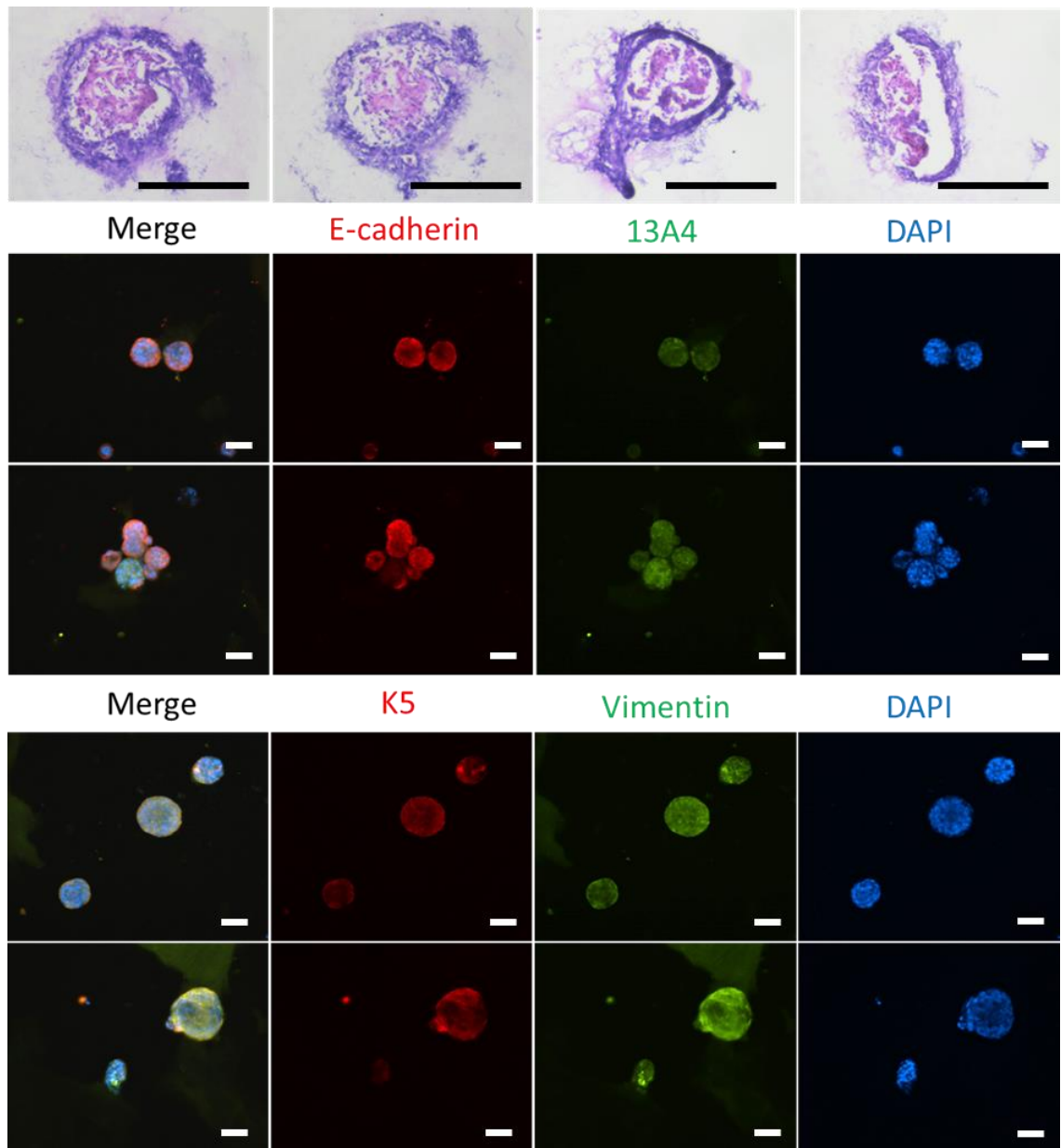


Figure 3.3-6. Histological and Immunofluorescence staining of DSO 135 derived non-PSS patient mesenchymal cells combined with mouse epithelial cells. Primary spheres were collected at seven days post gel implantation, fixed and isolated before mounting on slides, or embedded in OCT and sectioned into slides for Haematoxylin and Eosin staining. Samples are stained with antibodies raised against E-cadherin, K5, Vimentin and 13A4 (mouse-specific CD133/Prominin 1 extracellular loop). Fluorescent images taken at X20 magnification, scale bar represents 100um, H&E images taken at 40X magnification, Scale bars represent 150um.

3.3.4. Discussion

Using the same culture conditions established during the mouse cell culture environments, we could generate epithelial and mesenchymal cell populations that expressed similar marker profiles to representative regions within tissue, established in section 3.1. This has recapitulated the efficacy of the culture environments to produce reliable cell culture outputs of consistent phenotype, despite using cells derived from both PSS and non-PSS patient tissue. Immunofluorescent staining and QPCR analysis also demonstrated the two discrete cell populations being positive for epithelial markers and negative for mesenchymal cell markers, and *vice versa*. However, when we analysed the cell cultures by FACS, we were unable to confidently declare that our cell populations possessed any stem cell populations.

It was hoped that the cells *in vitro* would be enriched for MSC markers due to the effect of culture environments on maintaining a proliferative phenotype in cells. However, the human mesenchymal cells could only be maintained over a smaller number of passages, indicating an already differentiated, mature mesenchymal cell phenotype, with only a small proportion of stem-like cells. The panel of markers used in Figure 3.3-2 was originally described in bone marrow mesenchymal stem cells (BMSCs) and the flow cytometry technology is designed to work on circulating blood cells. Therefore, the process of detaching the cells with enzymes may have cleaved some of the surface markers, reducing the detected levels of MSCs. Alternatively, the panel may be specific for the BMSCs and would not be truly representative of the MSC populations extracted from other tissues.

From these experiments we can show that organoid structures can be grown to resemble the mouse three-dimensional culture experiments in section 3.2. We have demonstrated the same level of influence on organoid growth patterns as indicated by the mouse spheroid experiments through the addition of mesenchymal cells, reinforcing the conclusion that mesenchymal cells are relevant and important for directing salivary gland tissue regeneration. Simultaneously, the conditions that compare the effect of PSS vs non-PSS derived mesenchymal cells on sphere growth pattern has indicated a smaller sphere diameter across the organoid structures in diseased patient samples, the structures were anecdotally observed to have less branching and budding, suggesting a less advanced developmental phenotype.

The presence of budding and branching sub-structures was used as evidence of a more advanced developmental phenotype whilst developing the mouse spheroid structures. However, this phenotype was less pronounced in the human experiments, but in the future, it would be beneficial to consider using a larger range of physical dimensions, including the formation of a lumen as demonstrated in other organoid studies (Pradhan-Bhatt *et al.*, 2013; Maruyama *et al.*, 2018).

Immunofluorescence staining has indicated that both epithelial and mesenchymal cell phenotypes persisted through the sphere protocol. However, the technique has limitations, and damaged structures paired with high background fluorescence levels limited our ability to analyse the organoids sufficiently. Although the organoid structures were positive for E-cadherin, K5, 13A4 (CD133) and Vimentin, it was difficult to identify individual cells or to see any stratifying or polarisation of cell structures, or to discern discrete populations of cells within the organoids. Similarly, H&E staining of sections of

the organoids could not show us whether the structures had formed lumen-like structures after a period of incubation. Although, two layers of tissue were observed, suggesting strong differentiation and polarisation of the spheroids, indicative of early stages of glandular development.

This is in contrast to recently published work that indicates an ability of spheroid structures from mouse and human origin to form well organised organoid structures with visible lumen formation that can be visualised through the lack of nuclei and positive F-actin staining on apical membranes of cells, as indicated in Figure 3 of the paper published by (Maruyama *et al.*, 2018). Similar staining was undertaken by Leigh *et al.*, who used partially dissociated salivary glands and monitored the structural formations to demonstrate lumen formation with F-actin (Leigh *et al.*, 2014). These papers demonstrated that the process of growing advanced organoid structures *in vitro* and extracting these structures from the gels for observation through histological and immunofluorescence staining is possible. Potentially future work on my project could use the staining techniques with F-actin to indicate the initial stages of lumen formation. However, these studies both used whole digested salivary gland tissue from mouse and human origin, and avoided an intermediate cell culture or cell selection stage, maintaining cell diversity and decreasing the number of passages cells have to endure. It would be a future aim, if this project were to be continued, to achieve spheroid structures as conserved and as advanced in developmental phenotype as are presented by Maruyama *et al.* Although, it was desirable to establish a method in which cell cultures could be manipulated and controlled before recombination in a tissue model, and the benefit of our system is that cells could be purified via FACS, induced down cell

lineages, or exposed to RNAi technology or transfection overexpression experiments before being introduced to an organoid model.

The development of organoid cultures was based on a variety of published work, adapting protocols and optimising for our cell culture conditions. Protocols were followed which extracted cells from tissue, cultured to generate a purified cell population and recombined to generate organoid structures (Nanduri *et al.*, 2014). But Nanduri *et al* also struggled to isolate and stain their Matrigel embedded structures with immunofluorescent staining due to the high background fluorescence and difficulty removing organoids from the gel without damaging the structures. However, the technique of using three-dimensional cultures is a specialised skill, particularly the handling and manipulating of tissues once they have been grown in gels. This limited the ability to successfully analyse the samples, and could have contributed to the poor quality of extracted spheroids used for immunofluorescence staining.

However, in our study spheroids were used as an assay and showed a significant decrease in the size of spheroids when using cells from PSS positive patients, indicating a reduced regenerative capacity of the cells. Unfortunately, due to the difficulty of extracting the spheroid structures from the gels, and the low RNA yields of the conditions, there could be no categorical definition of the mechanistic change that has altered this behaviour. It would have been ideal to identify alterations in signalling pathways and conclusively prove that stem cell fate determination pathways have been impacted by the disease state.

An alternative method to investigate the effect of PSS on only the mesenchymal tissue, would have been to use embryonic salivary gland explants. By removing the developing

salivary gland from mice as early as embryonic day 13, and dissociating the epithelial structures from the mesenchymal structures using enzymatic digestion such as dispase, it is possible to grow the epithelial structures in three-dimensional cultures (Patel and Hoffman, 2014). Using this model, it would be possible to introduce PSS or non-PSS derived mesenchymal cells and to monitor the impact on the development of the explant structures. In this instance, more variables could be removed whilst starting with established and consistent epithelial structures. The study by Patel *et al*, also used BrdU experiments to demonstrate the location of the proliferative cells, which could also be used in our models to comparably quantify the proliferative capacity of PSS and non-PSS structures *in vitro*.

3.3.5. Conclusion

In conclusion, human only derived cell cultures could be generated that were representative of PSS-positive and non-PSS conditions. The initial human organoids did not behave as expected and could not form reliable and repeatable spheroid structures that recapitulated developmental stages of the salivary gland. Primarily, this was because the epithelial cells did not grow in compacted spheroid structures as seen in the mouse organoid work and as published in the literature (Leigh *et al.*, 2014).

However, through the recombination experiment with mouse epithelial cells and human patient derived mesenchymal cells, novel structures were formed that incorporated both cell types. Once optimised, these structures clearly demonstrated that the inclusion of PSS derived mesenchymal cells resulted in diminished spheroid structures in comparison to healthy controls. Although the mechanism behind this reduced proliferative and regenerative potential is not yet understood, it has been successfully shown that it is not only the epithelial structures that are affected by PSS. As the mesenchymal cells are vital during embryonic stages of salivary gland development, it is evident that they are impacted by the exposure to PSS and have undergone a pivotal change in their mechanistic behaviour that impedes the epithelial-mesenchymal cell interaction, preventing structure formation and regeneration. The research group aims to expand in this success by identifying the key changes that have occurred in the mesenchymal cell population, and confirming this phenotype is responsible for a reduced proliferative ability by manipulating cells used within the organoid models, and investigating ways in which these modifications can be reversed in the search for a potential therapeutic target.

This is the point at which work should continue; investigating the effect of the PSS condition on the Sonic Hedgehog signalling pathway. As demonstrated in section 3.1.2, the PSS positive patient samples had an overall increase in expression profiles of specific proteins, Patched and Smoothed, which are involved in SHH signalling. As yet, it is not known why these proteins have elevated profiles in the disease condition. However, now that the organoid models are established, and the mesenchymal cells from disease patients can be confirmed to have a reduced regenerative capacity, it is the optimal opportunity to investigate any mechanistic changes.

However, the primary aim should be to further characterise the expression of SHH and Gli transcription factors directly because, as the downstream effectors, Gli proteins can be activated directly or indirectly. Meaning that even if there were changes to the SHH, Ptch or Smo proteins, transcriptional activation can still occur. It would be imperative to compare the expression profiles in LCM tissue, whole biopsies, cultured cells and these organoid structures before moving on to attempting to “fix” the tissue through manipulation experiments such as RNAi and Crispr technology.

4. Overall Discussion

4.1. Review of Project Aims

The main aim of this project was to investigate the changes to mesenchymal cells within PSS-positive salivary gland tissues, to better understand the molecular impact of this condition through changes to RNA and protein expression, and to identify the possibilities of recovering these cells to be proliferative once again, to aid tissue recovery and regeneration.

4.2. Characterising and Investigating Molecular Changes of PSS Tissue

Through this research, it was possible to demonstrate a clear panel of markers that distinguished discreet cell populations within the labial salivary glands of healthy and diseased patients. This panel of markers also translated well into the mouse tissue and subsequent *in vitro* models. The definitive diagnosis for PSS is the presence of the immune cells which resulted in reduced staining expression for general markers in the immune lesion areas because the healthy histoarchitecture has been destroyed (Mavragani and Moutsopoulos, 2014b). Specifically, an absence of mature, fully differentiated and functional epithelial markers such as E-cadherin and AQP5 was observed. The immune lesion stains strongly with Vimentin and CD29, but not at all for PDGFR β , which identified PDGFR β as a marker for the mesenchymal cell niche within the tissue that does not coincide with the immune infiltrates. Furthermore, it was

confirmed that the cells that formed the lesions were immune cells by staining for CD4 and CD19, which stains T cells and B cells respectively.

Lower grade stages of PSS disease patient samples were specifically requested, so that the residual, unaffected tissue could still be visualised. Therefore, when performing immunofluorescence for the CD4 and CD19 markers, it was clear to see the progression stages of the disease across the variety of the patients. Primarily there is the aggregation and recruitment of the T cells to the tissue, before the size and intensity of the CD4 lesion increases and we start to observe CD19 positive B cells forming intense centres within the T cell population. In some patients, this is known to lead to the formation of a germinal centre, which can be the first stages of the development of lymphomas as discussed in the Introduction (Awasthi *et al.*, 2011; Voulgarelis *et al.*, 2012).

Whereas previous studies may have chosen to study the staining profiles of a singular marker for each tissue compartment, by using a large panel, a novel approach was taken and could demonstrate that several markers identify similar regions of tissue, and that it's possible to subdivide the previously established cell categories. One example of this, has been to use Vimentin, which has already been established in the literature as a pan-mesenchymal cell marker (Larsen *et al.*, 2003). However, it was demonstrated that, with the use of the markers PDGFR β , CD29 and CD105, there are other subpopulations of these cells that could possibly represent mesenchymal stem cells. Previously, these cells may have been identified using flow cytometry in salivary gland tissue (Lv *et al.*, 2014). However, using a panel of markers can generate a much greater understanding of different cell subpopulations within the tissue and leads to better identify the mesenchymal stem cell population.

In general, mesenchymal stem cells are not identifiable by one very specific marker alone, hence the reason for using a panel of different markers, which are demonstrated in Figure 4.2-1. These markers identify MSCs in a variety of different tissue origins, and only a few of them were seen to be positive in our cell populations.

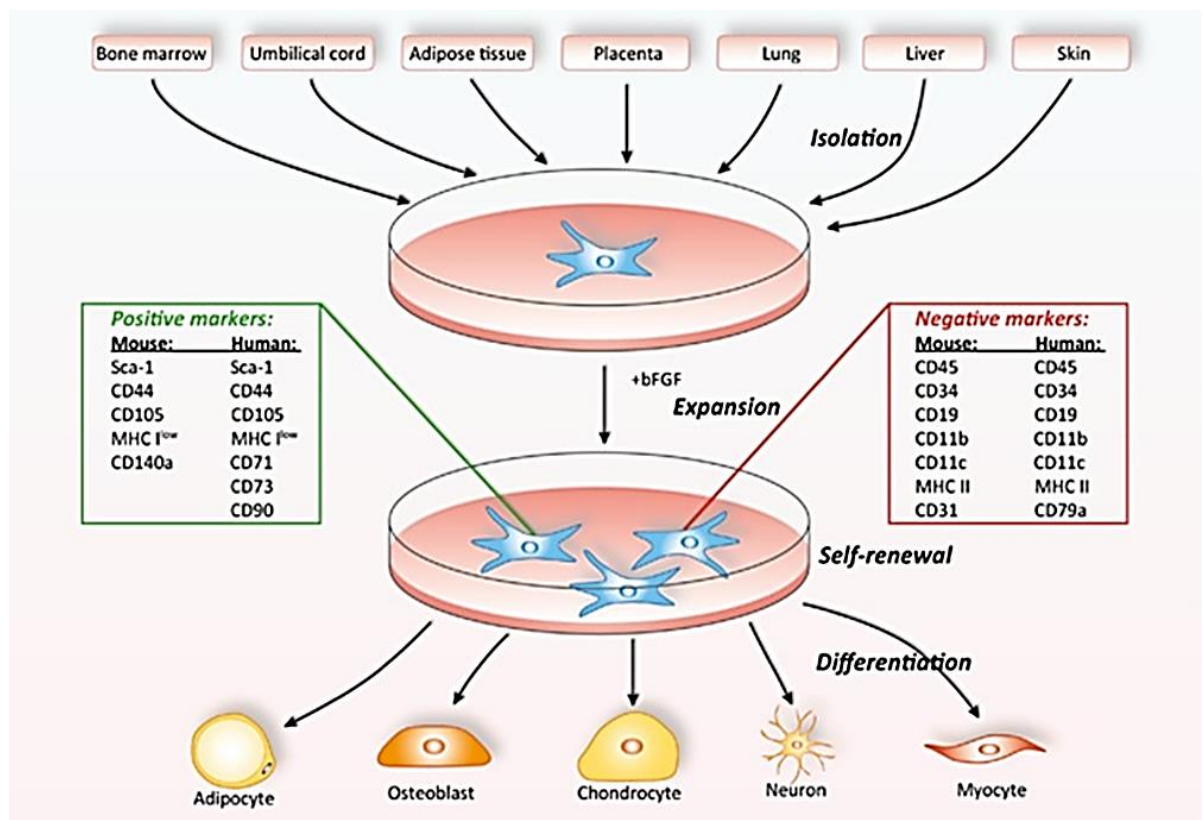


Figure 4.2-1 Representation of the isolation and characterisation of mesenchymal stem cell populations derived from different tissue origins, with a conserved panel of markers with which they can be identified (Chen et al., 2016).

The selection of markers that were used in this project was taken from the literature (Khalili *et al.*, 2012; Takahashi *et al.*, 2014; Lee, Park and Roh, 2015; Chen *et al.*, 2016) and can demonstrate an MSC population within mouse and human tissue sections, and digested tissue analysed through flow cytometry. Although many of these markers may have been initially identified through the analysis of cells extracted from bone marrow

and other tissue origins, it was possible to demonstrate the positive expression of some of these markers within the salivary gland samples.

Through the considerable work of optimising the culture conditions and performing IF staining, flow cytometry and QPCR analysis, the above markers were shown to persist through cell cultures and organoid models. However, a stronger presentation of the stem cell properties could have been demonstrated by the transition through differentiation to one of three mature cell phenotypes; chondrocytes, osteoblasts and adipocytes (Pittenger *et al.*, 1999b; Chen *et al.*, 2016). The motivation behind declining these experiments was that some of these lineage experiments can be incredibly costly, and to perform them once would have meant performing them every time for every batch of cells. Furthermore, they would have been particularly time consuming and disrupted the process of cell culture and sphere generation that we employed, with the cells performing best when in passage three to five and without having undergone a freeze-thaw process.

However, the investigations into molecular changes through LCM extraction methods had demonstrated a very significant finding that implicates the SHH signalling pathway, which is responsible for cell proliferation and preventing apoptosis. It was challenging to find papers discussing SHH and PSS and very few papers were available discussing SHH in the salivary gland in general, suggesting a novel field of research for the future. This is a very promising field of research and should certainly be continued, with effort focussed on the expression of Patched, Smoothed and the downstream Gli transcription factors. Currently, there has been no work to identify how the residual tissue is reacting to the disease process in PSS, or how the mesenchymal cell population

is impacted. Whilst these results could be indicative of a mechanistic attempt to recover tissue functionality or limit further tissue degradation.

4.3. Generating Organoid Models Using Mouse and Human Tissue

The initial aim, with the development of culture models, was to generate rudimentary salivary glands, in a regenerative capacity, with the potential for re-implantation into rodents, recapitulating work from the literature (Hirayama *et al.*, 2013; Nanduri *et al.*, 2014; Ogawa and Tsuji, 2015). Further aims were to investigate the role and importance of different cell types in the efficacy of the tissue regeneration, however, the initial experiments required more optimisations than expected.

During the transfer process, after 12 months of PhD work, it was decided that this research would aim less towards regenerating functional salivary glands for re-implantation, and instead, it would pursue the investigations into cell populations within the salivary glands and how their interactions influence the potential for regeneration. This could then lead towards the development of an experimental process that could be used as an assay, comparing the regenerative potential from cells retrieved from human patients presenting with or without PSS.

Three dimensional organoid models have been developed by many groups, investigating a variety of organs and are not novel concepts. A variety of studies have investigated the regeneration of mammary gland tissue (Sokol *et al.*, 2016), lacrimal glands (Hirayama *et al.*, 2013), or salivary glands (Nanduri *et al.*, 2014) in a similar manner to which organoids were developed throughout this project. These models have been implanted

into host animals, to demonstrate how the inclusion of innervation of vascularisation improve organoid development, whilst demonstrating functional properties such as the increased secretion of saliva or tears. Furthermore, these models have been implanted into rodent models as a method with which to improve salivation and tissue repair in the hosts (Ogawa *et al.*, 2013).

However, the technique was adapted into an experimental assay, and the results produced in section 3.2 and 3.3 reinforce the importance of mesenchymal cells in the fate determination of the epithelial structures. Without the ability of the mesenchymal tissue to direct and form the epithelial structures, as demonstrated in previous studies regenerating mammary tissue (Veltmaat *et al.*, 2003; Jimenez-Rojo *et al.*, 2012), the tissue would lack organisation, polarity and functionality. It is also known that there is a reduced proliferative capacity in the salivary gland tissue suffering from PSS, and a reduced cell differentiation (Herrera-Esparza *et al.*, 2008), which coincides with the results from this study; this study also demonstrated a reduced regenerative capacity of mesenchymal cells isolated from PSS patient tissue.

However, one key area that this research didn't cover was the established process of epithelial to mesenchymal transition (EMT) that occurs between epithelial and mesenchymal cells *in vivo* and in *in vitro* models (Mani *et al.*, 2008; Li *et al.*, 2011). This process could, theoretically, be happening within the organoid models, and impact the accuracy of our, and other published models. The way to tackle this conundrum would be to stain cells with lineage tracing agents, such as CMDiI, before the cells are recombined into the culture models. This way, it would be possible to track the cells and observe how they integrate in the three-dimensional gels, and which other markers the

cells express to confirm their cell phenotype. Unfortunately, the limitations to this work prevented the confirmation of mechanistic changes within the experimental model. But it is hoped that with this well-established method, and the documentation of significant changes in growth patterns in PSS positive samples will be used to confirm mechanistic changes within the patient tissue. In the future, the model will also facilitate investigations into ways to repair mechanistic alterations and return the tissues to “normal” homeostasis.

4.4. Identifying the Radiotherapy Impact on Mesenchymal Cells.

Although the group attempted to generate models of irradiation therapy exposure on cell cultures, as shown in Appendix 6.1, the impact of the x-rays could not be detected by the methods employed. This project arose due to deterioration in contact with the tissue bank and, therefore, there was an attempt to broaden the scope of the project by developing the organoid model in another direction. By using human derived salivary gland mesenchymal cells, developed from the non-PSS labial biopsies received from the Sjogren’s Registry, and using mouse mesenchymal cells and human gingival epithelial cells, the group hoped to demonstrate a significant impact of radiation exposure on cells in culture that could then be combined into the three-dimensional organoid models, as a way of investigating regenerative potential of these exposed cells. As demonstrated in section 6.1 in the Appendix, this was unsuccessful, which could be seen as contradicting the literature as exposure to even low level IR has frequently been shown to affect cells and organ cultures (Ribeiro, 2012; Truong *et al.*, 2018).

As discussed previously, the type of machinery that was used to generate the x-rays was insufficient for the role (Shah, Bansal and Logani, 2014), and there was no method to accurately control and monitor the exposures. This research project has genuine potential to be of benefit to the field of irradiation exposure and its short-term impact on the regenerative capacity of cells. If the research group were to continue optimising this experimental design and use more relevant technology for the exposure of cultures, it should be possible to demonstrate a significant phenotypical change within the exposed cells, whilst confirming the molecular and mechanistic changes within different cell populations that are inhibiting the effective growth, repair and regeneration of the exposed salivary gland tissue. However, other groups have demonstrated how nuclear aberrations are not the best phenotypical change to observe in IR exposed tissues (Ribeiro and Angelieri, 2008), and double stranded DNA breaks only start to be observed at higher levels of IR exposure (Rothkamm and Löbrich, 2003). The further work in this area should identify changes to cell cycle components and fate determination pathways, as this would coincide with the work on PSS tissue by Truong *et al* (2018).

4.5. Limitations of this Investigation

The aim of the project had great potential and, although most of the aims were achieved, the conclusions that have been drawn could have been taken much further. Better structure and management of the project could have increased the efficiency and increased data output. Unfortunately, the assumption was made that the techniques would be easy to master and the outcomes would have been exactly as predicted. Therefore, the questions being asked in each chapter were answered concurrently

without due regard for the previous conclusions, which may have provided better direction for subsequent experiments.

Furthermore, the project did change direction in response to results being produced, with an initial aim of attempting to develop an organoid assay for re-implantation into a host animal model, whilst also investigating the role played by sebaceous cells within the salivary gland tissue on the initiation of PSS. However, during the transition from MPhil to PhD, it was discussed that the re-implantation model would be unfeasible due to restrictions on access to animal models, ethical approval of the research, time constraints, and novelty of the research aims. Therefore, a new aim of generating the organoids into an assay of proliferative capacity was developed, particularly responding to results demonstrating the increased proliferative capacity of spheroids with the combination of both mesenchymal and epithelial cells.

The availability of tissue was the largest obstacle faced during this research project, and the group had to rely on a small number of frozen tissue samples, and even fewer freshly excised samples. This was due to the preliminary nature of the research project, which prevented collaborators from sending larger quantities of tissue. Furthermore, freshly excised tissue was sent directly from diagnostic surgery, and many patients did not consent for tissue removal for research purposes.

Immunofluorescence staining was heavily relied upon to identify populations within the tissue. Ideally, it would have been beneficial to improve the flow cytometry work and use FACS sorting techniques to isolate and quantify subpopulations of cells within the tissue. However, we experienced difficulty when extracting single cell suspensions from the heterogeneous and complex tissue of the salivary gland. It is notoriously difficult to

generate single cell suspensions when using cells such as fibroblasts as their fibrous processes resist separation. If this FACS technique could have been applied to the bulk salivary gland samples rather than cultured cells, multiplexing experiments could have been attempted, generating sorts that could identify the epithelial/mesenchymal ratio and then identify the percentage of events in each subpopulation. This would have been an ideal way to quantify and characterise the staining profiles of the tissues, but then it may also have been confounded by the extreme phenotype shift observed in the lesion areas of the tissue, with PSS positive tissue presenting with a significantly increased proportion of immune cells.

Overall, the decision to focus on immunofluorescence staining was the correct one as it has aided the understanding of the physical location of cells and how they have changed around the lesion. A direct impact on the number of secretory epithelial cells secreting saliva has been shown, with a significant change in the distribution of mesenchymal cells surrounding the immune lesions. Furthermore, whilst other research groups have frequently used cell sorting techniques to isolate cells (Lawson *et al.*, 2007; Pringle *et al.*, 2011; Nanduri *et al.*, 2014; Emmerson *et al.*, 2017), this group gave clear evidence for the location and changes to staining patterns within the tissue, which gives a novel perspective on diseased tissue phenotypes.

The last limitation in the characterisation of the tissue was that laser capture microdissection was unable to provide a high enough RNA yield to reliably analyse all of the pathways of interest. Although significant changes in expression levels of proteins associated with the Sonic Hedgehog signalling pathway were demonstrated using this technique. However, this preliminary data has not elucidated what the increase in

Smoothened or Patched means for the tissue, and further investigations must be performed to consider downstream signalling pathways that are affected by this change in molecular expression. This does indicate that this technique could certainly work if more regions of tissue were collected, and if steps were taken to improve RNA yield and to prevent RNA degradation.

Although this research has identified changes to molecular pathways, this was not indicative of the reasons or causation behind the initiation stages of primary Sjogren's syndrome. The results produced through laser capture microdissection has indicated ways in which the residual, unaffected tissue is responding to the disease condition, and could be suggestive of pathways that are ideal for therapeutic targeting, or inducing within our organoid models.

Ultimately, this field of research was entirely new to the research group, and therefore, this project should be perceived as a preliminary research project which started off with a large research remit before focussing on areas that offered genuine promise and results. The optimised spheroid technique is now well established and has been used to identify key behavioural differences between diseased cell cultures and can be used to extend this research and increase our cohort size.

4.6. Future Work

All areas of the project have provided novel and exciting results, which should provide ample support for the research direction to continue. In the future, it is hoped that the group will attempt to collect more biopsy samples so that the sample number can increase, improving the power of the statistical analysis performed. With the expansion

of the project, there needs to be an increase in responsibility and optimising the experimental plan of the research project, because the samples are so precious, wasting samples should be avoided completely when possible. Certainly, more effort should be done to perform the LCM work again, by taking more regions and limiting RNA degradation as much as possible.

It would be desirable in the future to extrapolate the success of the three-dimensional models by investigating the introduction of a disease phenotype *in vitro*. Potentially, non-PSS derived patient cells could be cultured in a three-dimensional assay, with the introduction or co-culture with immune cells, mimicking the effect of the CD4+ T cells invasion, allowing the study of the inducement of change in the organoids. Alternatively, once the mechanistic change within the PSS derived mesenchymal cells has been established, PSS positive cells could be manipulated and recovered to a 'control' phenotype, investigating a way in which to reverse the damage caused by the immune infiltration.

To improve the output of the project, the group could have used alternative techniques, such as mass spectrometry, or gene sequencing, to develop a better understanding of the pathways being modulated between the PSS positive and control tissues. A lot of research is now heading towards a multi-omics approach to research (Rotroff and Motsinger-Reif, 2016; Tasaki *et al.*, 2017), as RNA expression profiles do not always guarantee fluctuations in protein expression levels. By developing a shortlist of genes and proteins that are altered between PSS and non-PSS patients, the group would have more success when attempting to identify therapeutic targets and being able to modulate expression changes in culture models.

4.7. Concluding Remarks

There appears to be a lack of connection between basic sciences, developing the understanding of using isolated cells to push tissue regeneration models, through to the practical and clinical application of implanting these models into animals or human hosts. Salivary gland organoid model work has occasionally been the victim of scepticism from clinical based academics, who claim that there could already be sufficient methods to treat and manage symptoms of PSS. This is certainly true to a degree, and methods as described in the introduction such as the use of pilocarpine or other stimulants to aid secretion of saliva, or other secretory liquids, are imperative for the symptomatic treatment for many patients.

However, the long-term aim of the research group is to identify pathways impacted by PSS with the intention of targeting them as part of a therapeutic treatment for patients suffering from the condition. As there are existing techniques for implantation of organoid models within host animals (Nanduri *et al.*, 2013; Mansour *et al.*, 2018), it is hoped that the results discovered through the spheroid assay developed in this PhD will aid in the adaptation of allografting technology, by manipulating signalling pathways that could contribute to complete recovery of the salivary gland tissue and, therefore, interrupt the reliance on salivary stimulatory drugs and symptomatic management.

Although this work may have very specific implications for PSS, there are also the translational applications for other regenerative tissue research areas in other organs, thereby allowing the complete recovery and cessation of treatment for patients who suffer from long-term, chronic health conditions such as diabetes. Ultimately, this research will enable researchers to develop a better understanding of the impact of PSS

and the disease processes, and facilitate the development of better tissue implantation models to alleviate hyposalivation and replace the treatment of symptoms rather than the disease condition itself.

5. References

Agarwal, P. *et al.* (2015) 'Genotoxic and cytotoxic effects of X-ray on buccal epithelial cells following panoramic radiography: A pediatric study', *J Cytol*, 32(2), pp. 102–106. doi: 10.4103/0970-9371.160559.

Alam, H. *et al.* (2011) 'Novel function of keratins 5 and 14 in proliferation and differentiation of stratified epithelial cells.', *Molecular biology of the cell*. American Society for Cell Biology, 22(21), pp. 4068–78. doi: 10.1091/mbc.E10-08-0703.

Alessandri, C. *et al.* (2017) 'CD4 T lymphocyte autophagy is upregulated in the salivary glands of primary Sjögren's syndrome patients and correlates with focus score and disease activity.', *Arthritis research & therapy*. BioMed Central, 19(1), p. 178. doi: 10.1186/s13075-017-1385-y.

Amano, O. *et al.* (2012) 'Anatomy and Histology of Rodent and Human Major Salivary Glands'—Overview of the Japan Salivary Gland Society-Sponsored Workshop', *Acta Histochemica Et Cytochemica*, 45(5), pp. 241–250. doi: 10.1267/ahc.12013.

Ambort, D. *et al.* (2012) 'Calcium and pH-dependent packing and release of the gel-forming MUC2 mucin', *Proceedings of the National Academy of Sciences*, 109(15), pp. 5645–5650. doi: 10.1073/pnas.1120269109.

Anderson, L. G. and Talal, N. (1972) 'The spectrum of benign to malignant lymphoproliferation in Sjögren's syndrome.', *Clinical and experimental immunology*, 10(2), pp. 199–221. Available at: <http://www.pubmedcentral.nih.gov/articlerender.fcgi?artid=1713180&tool=pmcentrez&rendertype=abstract>.

Antoniazzi, R. P. *et al.* (2009) 'Periodontal conditions of individuals with Sjogren's syndrome', *J Periodontol*, 80(3), pp. 429–435. doi: 10.1902/jop.2009.080350.

Aure, M. H., Arany, S. and Ovitt, C. E. (2015) 'Salivary Glands: Stem Cells, Self-duplication, or Both?', *J Dent Res*, 94(11), pp. 1502–1507. doi: 10.1177/0022034515599770.

Aure, M. H., Konieczny, S. F. and Ovitt, C. E. (2015) 'Salivary Gland Homeostasis Is Maintained through Acinar Cell Self-Duplication', *Developmental Cell*. NIH Public Access, 33(2), pp. 231–237. doi: 10.1016/j.devcel.2015.02.013.

Aure, M. H., Ruus, A. K. and Galtung, H. K. (2014) 'Aquaporins in the adult mouse submandibular and sublingual salivary glands', *J Mol Histol*, 45(1), pp. 69–80. doi: 10.1007/s10735-013-9526-3.

Awasthi, N. P. *et al.* (2011) 'Sjogren's syndrome complicated by non-Hodgkin's lymphoma: spectrum of lymphoid proliferations and associated hepatitis C virus

infection', *Indian J Pathol Microbiol*, 54(2), pp. 430–431. doi: 10.4103/0377-4929.81621.

Baer, A. N. and Walitt, B. (2017) 'Sjögren Syndrome and Other Causes of Sicca in Older Adults', *Clinics in Geriatric Medicine*. Elsevier, pp. 87–103. doi: 10.1016/j.cger.2016.08.007.

Baker, O. J. (2010) 'Tight junctions in salivary epithelium', *Journal of Biomedicine and Biotechnology*. Hindawi, 2010, p. 278948. doi: 10.1155/2010/278948.

Barbe, A. G. (2017) 'Long-term Use of the Sialogogue Medications Pilocarpine and Cevimeline Can Reduce Xerostomia Symptoms and Increase Salivary Flow in Head and Neck Cancer Survivors After Radiotherapy', *Journal of Evidence Based Dental Practice*, 17(3), pp. 268–270. doi: 10.1016/j.jebdp.2017.06.013.

Barbeau, J. and Deslauriers, N. (1995) 'Murine autoimmune exocrinopathy: the minor salivary gland network shows a dichotomous pattern of histopathologic involvement', *Journal of Oral Pathology and Medicine*. Wiley/Blackwell (10.1111), 24(2), pp. 49–55. doi: 10.1111/j.1600-0714.1995.tb01138.x.

Bardow, A. *et al.* (2000) 'The buffer capacity and buffer systems of human whole saliva measured without loss of CO₂.', *Archives of oral biology*, 45(1), pp. 1–12. Available at: <http://www.ncbi.nlm.nih.gov/pubmed/10669087> (Accessed: 7 November 2017).

Berk, L. (2008) 'Systemic pilocarpine for treatment of xerostomia', *Expert Opinion on Drug Metabolism & Toxicology*, 4(10), pp. 1333–1340. doi: 10.1517/17425255.4.10.1333.

Berthod, F. *et al.* (2006) 'Extracellular matrix deposition by fibroblasts is necessary to promote capillary-like tube formation in vitro', *Journal of Cellular Physiology*. Wiley-Blackwell, 207(2), pp. 491–498. doi: 10.1002/jcp.20584.

Blanpain, C. *et al.* (2011) 'DNA-damage response in tissue-specific and cancer stem cells', *Cell Stem Cell*, 8(1), pp. 16–29. doi: 10.1016/j.stem.2010.12.012.

Bolstad, A. I. and Skarstein, K. (2016) 'Epidemiology of Sjögren's Syndrome-from an Oral Perspective.', *Current oral health reports*. Springer, 3(4), pp. 328–336. doi: 10.1007/s40496-016-0112-0.

Braam, P. M. *et al.* (2005) 'Long-term parotid gland function after radiotherapy', *International Journal of Radiation Oncology Biology Physics*. Elsevier, 62(3), pp. 659–664. doi: 10.1016/j.ijrobp.2004.12.015.

Brasser, A. J. *et al.* (2011) 'Presence of wax esters and squalene in human saliva', *Archives of Oral Biology*. Elsevier Ltd, 56(6), pp. 588–591. doi: 10.1016/j.archoralbio.2010.12.002.

Āuhring, H. J. *et al.* (2007) 'Novel markers for the prospective isolation of human MSC', in *Annals of the New York Academy of Sciences*, pp. 262–271. doi:

10.1196/annals.1392.000.

Bundgaard, M., Møller, M. and Poulsen, J. H. (1977) 'Localization of sodium pump sites in cat salivary glands.', *The Journal of physiology*, 273(1), pp. 339–53. Available at: <http://www.ncbi.nlm.nih.gov/pubmed/146078> (Accessed: 7 November 2017).

Burlage, F. R. *et al.* (2001) 'Parotid and submandibular/sublingual salivary flow during high dose radiotherapy', *Radiotherapy and Oncology*, 61(3), pp. 271–274. doi: 10.1016/S0167-8140(01)00427-3.

Burlage, F. R. *et al.* (2009) 'Enhanced proliferation of acinar and progenitor cells by prophylactic pilocarpine treatment underlies the observed amelioration of radiation injury to parotid glands', *Radiotherapy and Oncology*, 90(2), pp. 253–256. doi: 10.1016/j.radonc.2008.11.011.

Carubbi, F. *et al.* (2014) 'Is minor salivary gland biopsy more than a diagnostic tool in primary Sjogrens syndrome? Association between clinical, histopathological, and molecular features: a retrospective study', *Semin Arthritis Rheum*, 44(3), pp. 314–324. doi: 10.1016/j.semarthrit.2014.05.015.

Casciola-Rosen, L. a, Anhalt, G. and Rosen, a (1994) 'Autoantigens targeted in systemic lupus erythematosus are clustered in two populations of surface structures on apoptotic keratinocytes.', *The Journal of experimental medicine*, 179(4), pp. 1317–1330. doi: 10.1084/jem.179.4.1317.

Cassolato, S. F. and Turnbull, R. S. (2003) 'Xerostomia: Clinical Aspects and Treatment', *Gerodontology*. Blackwell Publishing Ltd., 20(2), pp. 64–77. doi: 10.1111/j.1741-2358.2003.00064.x.

Cha, S. *et al.* (2004) 'A Dual Role for Interferon-gamma in the Pathogenesis of Sjogren's Syndrome-Like Autoimmune Exocrinopathy in the Nonobese Diabetic Mouse', *Scandinavian Journal of Immunology*, 60(6), pp. 552–565. doi: 10.1111/j.0300-9475.2004.01508.x.

Chan, Y. H. *et al.* (2011) 'Human salivary gland acinar cells spontaneously form three-dimensional structures and change the protein expression patterns', *Journal of Cellular Physiology*, 226(11), pp. 3076–3085. doi: 10.1002/jcp.22664.

Chen, Q. *et al.* (2016) 'Fate decision of mesenchymal stem cells: adipocytes or osteoblasts?', *Cell death and differentiation*. Nature Publishing Group, 23(7), pp. 1128–39. doi: 10.1038/cdd.2015.168.

Chibly, A. M. *et al.* (2014) 'Label-retaining cells in the adult murine salivary glands possess characteristics of adult progenitor cells', *PLoS ONE*. Edited by J. A. Chiorini, 9(9), p. e107893. doi: 10.1371/journal.pone.0107893.

Cleary, M. A. *et al.* (2016) 'Expression of CD105 on expanded mesenchymal stem cells does not predict their chondrogenic potential', *Osteoarthritis and Cartilage*, 24(5), pp. 868–872. doi: 10.1016/j.joca.2015.11.018.

Cohen-Jonathan, E. *et al.* (1997) 'Radioresistance induced by the high molecular forms of the basic fibroblast growth factor is associated with an increased G2 delay and a hyperphosphorylation of p34CDC2 in HeLa cells.', *Cancer research*, 57(7), pp. 1364–70. Available at: <http://www.ncbi.nlm.nih.gov/pubmed/9102225> (Accessed: 6 October 2017).

Coppes, R. P. and Stokman, M. A. (2011) 'Stem cells and the repair of radiation-induced salivary gland damage', *Oral Diseases*, 17(2), pp. 143–153. doi: 10.1111/j.1601-0825.2010.01723.x.

Corbeil, D., Fargeas, C. a and Jászai, J. (2014) 'CD133 might be a pan marker of epithelial cells with dedifferentiation capacity.', *Proceedings of the National Academy of Sciences of the United States of America*, 111(15), pp. E1451-2. doi: 10.1073/pnas.1400195111.

Delanian, S. *et al.* (2005) 'Kinetics of Response to Long-Term Treatment Combining Pentoxifylline and Tocopherol in Patients With Superficial Radiation-Induced Fibrosis', *Journal of Clinical Oncology*, 23(34), pp. 8570–8579. doi: 10.1200/JCO.2005.02.4729.

Delanian, S. and Lefaix, J. L. (2004) 'The radiation-induced fibroatrophic process: Therapeutic perspective via the antioxidant pathway', *Radiotherapy and Oncology*. Elsevier, pp. 119–131. doi: 10.1016/j.radonc.2004.08.021.

Delli, K. *et al.* (2016) 'Towards personalised treatment in primary Sjögren's syndrome: baseline parotid histopathology predicts responsiveness to rituximab treatment', *Annals of the Rheumatic Diseases*, 75(11), pp. 1933–1938. doi: 10.1136/annrheumdis-2015-208304.

Denny, P. C. *et al.* (1993) 'Parenchymal cell proliferation and mechanisms for maintenance of granular duct and acinar cell populations in adult male mouse submandibular gland', *Anat Rec*, 235(3), pp. 475–485. doi: 10.1002/ar.1092350316.

Denny, P. C., Ball, W. D. and Redman, R. S. (1997) 'Salivary Glands: A Paradigm for Diversity of Gland Development', *Critical Reviews in Oral Biology & Medicine*, 8(1), pp. 51–75. doi: 10.1177/10454411970080010301.

Dirix, P., Nuyts, S. and Van Den Bogaert, W. (2006) 'Radiation-induced xerostomia in patients with head and neck cancer: A literature review', *Cancer*, 107(11), pp. 2525–2534. doi: 10.1002/cncr.22302.

Do, R. *et al.* (2009) 'Squalene synthase: A critical enzyme in the cholesterol biosynthesis pathway', *Clinical Genetics*, pp. 19–29. doi: 10.1111/j.1399-0004.2008.01099.x.

Dominici, M. *et al.* (2006) 'Minimal criteria for defining multipotent mesenchymal stromal cells. The International Society for Cellular Therapy position statement', *Cytotherapy*, 8(4), pp. 315–317. doi: 10.1080/14653240600855905.

Dummer, A. *et al.* (2016) 'Measuring the primary cilium length: improved method for

unbiased high-throughput analysis', *Cilia*. BioMed Central, 5(1), p. 7. doi: 10.1186/s13630-016-0028-2.

Elmore, S. (2007) 'Apoptosis: a review of programmed cell death.', *Toxicologic pathology*. NIH Public Access, 35(4), pp. 495–516. doi: 10.1080/01926230701320337.

Emmerson, E. *et al.* (2017) 'SOX2 regulates acinar cell development in the salivary gland.', *eLife*. eLife Sciences Publications, Ltd, 6. doi: 10.7554/eLife.26620.

Epstein, J. B. *et al.* (1999) 'Quality of life and oral function following radiotherapy for head and neck cancer.', *Head & neck*, 21(1), pp. 1–11. Available at: <http://www.ncbi.nlm.nih.gov/pubmed/9890345> (Accessed: 6 November 2017).

Evans, R. D. R. *et al.* (2016) 'Tubulointerstitial nephritis in primary Sjögren syndrome: clinical manifestations and response to treatment.', *BMC musculoskeletal disorders*. BMC Musculoskeletal Disorders, 17(1), p. 2. doi: 10.1186/s12891-015-0858-x.

Evans, R. L. and Turner, R. J. (1998) 'New insights into the upregulation and function of the salivary Na⁺-K⁺-2Cl⁻ cotransporter.', *European journal of morphology*, 36 Suppl, pp. 142–6. Available at: <http://www.ncbi.nlm.nih.gov/pubmed/9825910> (Accessed: 7 November 2017).

Ewert, P. *et al.* (2010) 'Disruption of tight junction structure in salivary glands from Sjögren's syndrome patients is linked to proinflammatory cytokine exposure', *Arthritis and Rheumatism*, 62(5), pp. 1280–1289. doi: 10.1002/art.27362.

Farahat, M. *et al.* (2017) 'MSCs feeder layers induce SMG self-organization and branching morphogenesis'. doi: 10.1371/journal.pone.0176453.

Featherstone, J. D., Behrman, J. M. and Bell, J. E. (1993) 'Effect of whole saliva components on enamel demineralization in vitro.', *Critical reviews in oral biology and medicine : an official publication of the American Association of Oral Biologists*, 4(3–4), pp. 357–62. Available at: <http://www.ncbi.nlm.nih.gov/pubmed/8373991> (Accessed: 6 November 2017).

Feng, J. *et al.* (2009) 'Isolation and characterization of human salivary gland cells for stem cell transplantation to reduce radiation-induced hyposalivation', *Radiotherapy and Oncology*. Elsevier Ireland Ltd, 92(3), pp. 466–471. doi: 10.1016/j.radonc.2009.06.023.

Festjens, N., Vanden Berghe, T. and Vandenabeele, P. (2006) 'Necrosis, a well-orchestrated form of cell demise: Signalling cascades, important mediators and concomitant immune response', *Biochimica et Biophysica Acta - Bioenergetics*. Elsevier, pp. 1371–1387. doi: 10.1016/j.bbabi.2006.06.014.

Fox, R. I. (2005) 'Sjögren's syndrome', *The Lancet*, 366(9482), pp. 321–331. doi: 10.1016/S0140-6736(05)66990-5.

Franzén, L. *et al.* (1992) 'Parotid gland function during and following radiotherapy of

- malignancies in the head and neck. A consecutive study of salivary flow and patient discomfort', *European Journal of Cancer*, 28(2–3), pp. 457–462. doi: 10.1016/S0959-8049(05)80076-0.
- Gałecki, A. and Burzykowski, T. (2013) 'Linear Mixed-Effects Model', in: Springer, New York, NY, pp. 245–273. doi: 10.1007/978-1-4614-3900-4_13.
- Garcia, A. B. A. *et al.* (2016) 'Asymptomatic Atherosclerosis in Primary Sjögren Syndrome: Correlation Between Low Ankle Brachial Index and Autoantibodies Positivity.', *Journal of clinical rheumatology : practical reports on rheumatic & musculoskeletal diseases*, 22(6), pp. 295–8. doi: 10.1097/RHU.0000000000000413.
- Gervais, E. M. *et al.* (2015) 'Changes in the Submandibular Salivary Gland Epithelial Cell Subpopulations During Progression of Sjogren's Syndrome-Like Disease in the NOD/ShiLtJ Mouse Model', *Anat Rec (Hoboken)*, 298(9), pp. 1622–1634. doi: 10.1002/ar.23190.
- Ghisolfi, L. *et al.* (2012) 'Ionizing radiation induces stemness in cancer cells.', *PloS one*. Public Library of Science, 7(8), p. e43628. doi: 10.1371/journal.pone.0043628.
- Gjorevski, N. *et al.* (2016) 'Designer matrices for intestinal stem cell and organoid culture', *Nature*. Nature Publishing Group, 539(7630), pp. 560–564. doi: 10.1038/nature20168.
- Glick, D., Barth, S. and Macleod, K. F. (2010) 'Autophagy : cellular and molecular mechanisms', *Journal of Pathology The. NIH Public Access*, 221(1), pp. 3–12. doi: 10.1002/path.2697.Autophagy.
- Goetz, S. C. and Anderson, K. V (2010) 'The primary cilium: a signalling centre during vertebrate development.', *Nature reviews. Genetics*. NIH Public Access, 11(5), pp. 331–44. doi: 10.1038/nrg2774.
- Gorr, S.-U., Venkatesh, S. G. and Darling, D. S. (2005) 'Parotid Secretory Granules: Crossroads of Secretory Pathways and Protein Storage', *Journal of Dental Research*, 84(6), pp. 500–509. doi: 10.1177/154405910508400604.
- Grabinger, T. *et al.* (2014) 'Ex vivo culture of intestinal crypt organoids as a model system for assessing cell death induction in intestinal epithelial cells and enteropathy.', *Cell death & disease*. Nature Publishing Group, 5(5), p. e1228. doi: 10.1038/cddis.2014.183.
- Gresz, V. *et al.* (2001) 'Identification and localization of aquaporin water channels in human salivary glands.', *American journal of physiology. Gastrointestinal and liver physiology*, 281(1), pp. G247-54. Available at: <http://www.ncbi.nlm.nih.gov/pubmed/11408278> (Accessed: 7 November 2017).
- Gresz, V. *et al.* (2004) 'Immunolocalization of AQP-5 in rat parotid and submandibular salivary glands after stimulation or inhibition of secretion in vivo', *Am J Physiol Gastrointest Liver Physiol*, 287(1), pp. G151-61. doi: 10.1152/ajpgi.00480.2003.

- Gresz, V. *et al.* (2014) 'Immunolocalization of AQP5 in resting and stimulated normal labial glands and in Sjögren's syndrome', *Oral Dis*, 21(1), pp. e114–e120. doi: 10.1111/odi.12239.
- Grundmann, O., Mitchell, G. C. and Limesand, K. H. (2009) 'Sensitivity of Salivary Glands to Radiation: from Animal Models to Therapies', *Journal of Dental Research*, 88(10), pp. 894–903. doi: 10.1177/0022034509343143.
- Guggenheimer, J. and Moore, P. A. (2003) 'Xerostomia: etiology, recognition and treatment', *Journal of the American Dental Association*. Elsevier, 134(1), pp. 61–69. doi: 10.14219/jada.archive.2003.0018.
- Guo, C.-Y. *et al.* (2015) 'Sensitivity and dose dependency of radiation-induced injury in hematopoietic stem/progenitor cells in mice.', *Scientific reports*. Nature Publishing Group, 5, p. 8055. doi: 10.1038/srep08055.
- Hai, B. *et al.* (2014) 'Transient activation of hedgehog pathway rescued irradiation-induced hyposalivation by preserving salivary stem/progenitor cells and parasympathetic innervation.', *Clinical cancer research : an official journal of the American Association for Cancer Research*. NIH Public Access, 20(1), pp. 140–150. doi: 10.1158/1078-0432.CCR-13-1434.
- Han, I. *et al.* (2017) 'Differentiation Potential of Mesenchymal Stem Cells Is Related to Their Intrinsic Mechanical Properties', *International Neurourology Journal*. Korean Continence Society, 21(Suppl 1), p. S24. doi: 10.5213/INJ.1734856.428.
- Haneji, N. *et al.* (1994) 'A new animal model for primary Sjögren's syndrome in NFS/sld mutant mice.', *Journal of immunology (Baltimore, Md. : 1950)*, 153(6), pp. 2769–77. Available at: <http://www.ncbi.nlm.nih.gov/pubmed/8077681> (Accessed: 3 November 2017).
- Herrera-Esparza, R. *et al.* (2008) 'Apoptosis and cell proliferation: the paradox of salivary glands in Sjogren's disease', *Acta Reumatol Port*, 33(3), pp. 299–303. Available at: <https://www.ncbi.nlm.nih.gov/pubmed/18846009>.
- Hirayama, M. *et al.* (2013) 'Functional lacrimal gland regeneration by transplantation of a bioengineered organ germ', *Nature Communications*, 4, p. 2497. doi: Artn 2497Doi 10.1038/Ncomms3497.
- Hirayama, M., Tsubota, K. and Tsuji, T. (2015) 'Bioengineered Lacrimal Gland Organ Regeneration in Vivo', *Journal of Functional Biomaterials*, 6(3), pp. 634–649. doi: 10.3390/jfb6030634.
- Holmberg, K. V and Hoffman, M. P. (2014) 'Anatomy, biogenesis and regeneration of salivary glands', *Monogr Oral Sci*, 24, pp. 1–13. doi: 10.1159/000358776.
- Holsinger D. T., F. C. . B., Holsinger, F. C. and Bui, D. T. (2007) 'Anatomy, Function and Evaluation of the Salivary Glands', in Eugene N. Myers, R. L. F. (ed.) *Salivary Gland Disorders*. Berlin, Heidelberg: Springer Berlin Heidelberg, pp. 1–16. doi: 10.1007/978-3-

540-47072-4_1.

Hu, K. X. *et al.* (2010) 'The radiation protection and therapy effects of mesenchymal stem cells in mice with acute radiation injury.', *The British journal of radiology*. British Institute of Radiology, 83(985), pp. 52–8. doi: 10.1259/bjr/61042310.

Huangfu, D. and Anderson, K. V (2006) 'Signaling from Smo to Ci/Gli: conservation and divergence of Hedgehog pathways from Drosophila to vertebrates', *Development*, 133(1), pp. 3–14. doi: 10.1242/dev.02169.

Human Protein Atlas (no date) 'Cell atlas - PLXNA4 - The Human Protein Atlas'. Available at: <https://www.proteinatlas.org/ENSG00000138385-SSB/cell#human> (Accessed: 19 September 2018).

Humphries, M. J. *et al.* (2006) 'Suppression of Apoptosis in the Protein Kinase C δ Null Mouse *in Vivo*', *Journal of Biological Chemistry*, 281(14), pp. 9728–9737. doi: 10.1074/jbc.M507851200.

Jaskoll, T. *et al.* (2004) 'Sonic hedgehog signaling plays an essential role during embryonic salivary gland epithelial branching morphogenesis', *Developmental Dynamics*, 229(4), pp. 722–732. doi: 10.1002/dvdy.10472.

Jaskoll, T. and Melnick, M. (1999) 'Submandibular gland morphogenesis: stage-specific expression of TGF- α /EGF, IGF, TGF- β , TNF, and IL-6 signal transduction in normal embryonic mice and the phenotypic effects of TGF- β 2, TGF- β 3, and EGF-r null mutations', *Anat Rec*, 256(3), pp. 252–268. Available at: <http://www.ncbi.nlm.nih.gov/pubmed/10521784> (Accessed: 5 October 2017).

Jaszai, J. *et al.* (2007) 'Differential expression of Prominin-1 (CD133) and Prominin-2 in major cephalic exocrine glands of adult mice', *Histochem Cell Biol*, 128(5), pp. 409–419. doi: 10.1007/s00418-007-0334-2.

Jimenez-Rojo, L. *et al.* (2012) 'Stem Cell Fate Determination during Development and Regeneration of Ectodermal Organs', *Front Physiol*, 3, p. 107. doi: 10.3389/fphys.2012.00107.

Jones, E. A. *et al.* (2002) 'Isolation and characterization of bone marrow multipotential mesenchymal progenitor cells', *Arthritis and Rheumatism*, 46(12), pp. 3349–3360. doi: 10.1002/art.10696.

Jorkjend, L. *et al.* (2003) 'Periodontitis, caries and salivary factors in Sjögren's syndrome patients compared to sex- and age-matched controls', *Journal of Oral Rehabilitation*, 30(4), pp. 369–378. doi: 10.1046/j.1365-2842.2003.01088.x.

Kalluri, R. and Weinberg, R. A. (2009) 'The basics of epithelial-mesenchymal transition.', *The Journal of clinical investigation*. American Society for Clinical Investigation, 119(6), pp. 1420–8. doi: 10.1172/JCI39104.

Kang, M. *et al.* (2017) 'Facilitated saliva secretion and reduced oral inflammation by a

novel artificial saliva system in the treatment of salivary hypofunction.', *Drug design, development and therapy*. Dove Press, 11, pp. 185–191. doi: 10.2147/DDDT.S121254.

Kasper, M. *et al.* (2006) 'GLI transcription factors: Mediators of oncogenic Hedgehog signalling', *European Journal of Cancer*. Pergamon, 42(4), pp. 437–445. doi: 10.1016/J.EJCA.2005.08.039.

Katsiogiannis, S. *et al.* (2006) 'Salivary gland epithelial cells: A new source of the immunoregulatory hormone adiponectin', *Arthritis and Rheumatism*, 54(7), pp. 2295–2299. doi: 10.1002/art.21944.

Katsiogiannis, S., Tenta, R. and Skopouli, F. N. (2015) 'Endoplasmic reticulum stress causes autophagy and apoptosis leading to cellular redistribution of the autoantigens Ro/Sjögren's syndrome-related antigen A (SSA) and La/SSB in salivary gland epithelial cells', *Clinical and Experimental Immunology*, 181(2), pp. 244–252. doi: 10.1111/cei.12638.

Khalele, B. A. E. O. E. O. (2016) 'Sjögren's syndrome in a 25-year-old female: A case study', *Future Dental Journal*. Elsevier, 2(2), pp. 94–98. doi: 10.1016/j.fdj.2016.10.001.

Khalili, S. *et al.* (2012) 'Mesenchymal stromal cells improve salivary function and reduce lymphocytic infiltrates in mice with Sjögren's-like disease', *PLoS ONE*, 7(6), pp. 1–11. doi: 10.1371/journal.pone.0038615.

Kim, B. M. *et al.* (2015) 'Therapeutic Implications for Overcoming Radiation Resistance in Cancer Therapy.', *International journal of molecular sciences*. Multidisciplinary Digital Publishing Institute (MDPI), 16(11), pp. 26880–913. doi: 10.3390/ijms161125991.

Knox, S. M. *et al.* (2013) 'Parasympathetic stimulation improves epithelial organ regeneration', *Nature Communications*. Nature Publishing Group, 4, p. 1494. doi: 10.1038/ncomms2493.

Konings, A. W. T., Coppes, R. P. and Vissink, A. (2005) 'On the mechanism of salivary gland radiosensitivity', *International Journal of Radiation Oncology*Biophysics**, 62(4), pp. 1187–1194. doi: 10.1016/j.ijrobp.2004.12.051.

Korff, T. and Augustin, H. G. (1999) 'Tensional forces in fibrillar extracellular matrices control directional capillary sprouting.', *Journal of cell science*, 112 (Pt 1, pp. 3249–3258.

Kramer, J. M. (2014) 'Early events in Sjögren's Syndrome pathogenesis: The importance of innate immunity in disease initiation', *Cytokine*. Elsevier Ltd, 67(2), pp. 92–101. doi: 10.1016/j.cyto.2014.02.009.

Krysko, D. V. *et al.* (2008) 'Apoptosis and necrosis: Detection, discrimination and phagocytosis', *Methods*, 44(3), pp. 205–221. doi: 10.1016/j.ymeth.2007.12.001.

Larsen, M. *et al.* (2003) 'Role of PI 3-kinase and PIP3 in submandibular gland branching

morphogenesis', *Dev Biol*, 255(1), pp. 178–191. Available at:
<https://www.ncbi.nlm.nih.gov/pubmed/12618142>.

Larsen, M., Yamada, K. M. and Musselmann, K. (2010) 'Systems analysis of salivary gland development and disease', *Wiley Interdiscip Rev Syst Biol Med*, 2(6), pp. 670–682. doi: 10.1002/wsbm.94.

Lawson, D. a *et al.* (2007) 'Isolation and functional characterization of murine prostate stem cells', *Proceedings of the National Academy of Sciences of the United States of America*, 104(1), pp. 181–186. doi: 10.1073/pnas.0609684104.

Lee, J., Park, S. and Roh, S. (2015) 'Transdifferentiation of mouse adipose-derived stromal cells into acinar cells of the submandibular gland using a co-culture system', *Experimental Cell Research*. Elsevier, 334(1), pp. 160–172. doi: 10.1016/j.yexcr.2015.03.006.

Lee, K. E. *et al.* (2016) 'The significance of ectopic germinal centers in the minor salivary gland of patients with Sjögren's syndrome', *Journal of Korean Medical Science*, 31(2), pp. 190–195. doi: 10.3346/jkms.2016.31.2.190.

Lee, S. *et al.* (2010) 'Disrupting circadian homeostasis of sympathetic signaling promotes tumor development in mice', *PLoS ONE*, 5(6). doi: 10.1371/journal.pone.0010995.

Leigh, N. J. *et al.* (2014) 'Three-dimensional cultures of mouse submandibular and parotid glands: a comparative study', *J Tissue Eng Regen Med*. doi: 10.1002/term.1952.

Li, B. *et al.* (2011) 'Evidence for mesenchymal-epithelial transition associated with mouse hepatic stem cell differentiation', *PLoS ONE*, 6(2). doi: 10.1371/journal.pone.0017092.

Li, J. *et al.* (2010) 'Mutation of inhibitory helix-loop-helix protein Id3 causes T-cell lymphoma in mice', *Blood*. American Society of Hematology, 116(25), pp. 5615–5621. doi: 10.1182/blood-2010-03-274506.

Li, J. *et al.* (2016) 'Epithelial stratification and placode invagination are separable functions in early morphogenesis of the molar tooth.', *Development (Cambridge, England)*. Company of Biologists, 143(4), pp. 670–81. doi: 10.1242/dev.130187.

Liang, C.-C., Park, A. Y. and Guan, J.-L. (2007) 'In vitro scratch assay: a convenient and inexpensive method for analysis of cell migration in vitro', *Nature Protocols*, 2(2), pp. 329–333. doi: 10.1038/nprot.2007.30.

Lim, J.-Y. *et al.* (2013) 'Systemic Transplantation of Human Adipose Tissue-Derived Mesenchymal Stem Cells for the Regeneration of Irradiation-Induced Salivary Gland Damage', *PLoS ONE*, 8(8), p. e71167. doi: 10.1371/journal.pone.0071167.

Limesand, K. H., Schwertfeger, K. L. and Anderson, S. M. (2006) 'MDM2 Is Required for Suppression of Apoptosis by Activated Akt1 in Salivary Acinar Cells', *Molecular and*

Cellular Biology, 26(23), pp. 8840–8856. doi: 10.1128/MCB.01846-05.

Lindholm, J. S. *et al.* (1981) 'Variation of skin surface lipid composition among mammals', *Comparative Biochemistry and Physiology -- Part B: Biochemistry and*, 69(1), pp. 75–78. doi: 10.1016/0305-0491(81)90211-X.

Lombaert, I., Knox, S. M. and Hoffman, M. P. (2011) 'Salivary gland progenitor cell biology provides a rationale for therapeutic salivary gland regeneration', *Oral Diseases*, 17(5), pp. 445–449. doi: 10.1111/j.1601-0825.2010.01783.x.

Lombaert, I. M. A., Brunsting, J. F., Wierenga, P. K., *et al.* (2008) 'Cytokine treatment improves parenchymal and vascular damage of salivary glands after irradiation', *Clinical Cancer Research*, 14(23), pp. 7741–7750. doi: 10.1158/1078-0432.CCR-08-1449.

Lombaert, I. M. A., Brunsting, J. F., Weirenga, P. K., *et al.* (2008) 'Rescue of Salivary gland function after stem cell transplantation in irradiated glands', *PLoS ONE*, 3(4), pp. 1–13. doi: 10.1371/journal.pone.0002063.

Lu, L. *et al.* (2015) 'Characterization of a Self-renewing and Multi-potent Cell Population Isolated from Human Minor Salivary Glands.', *Scientific reports*. Nature Publishing Group, 5(March), p. 10106. doi: 10.1038/srep10106.

van Luijk, P. *et al.* (2009) 'Bath and Shower Effects in the Rat Parotid Gland Explain Increased Relative Risk of Parotid Gland Dysfunction After Intensity-Modulated Radiotherapy', *International Journal of Radiation Oncology*Biophysics*, 74(4), pp. 1002–1005. doi: 10.1016/j.ijrobp.2009.03.039.

van Luijk, P. *et al.* (2015) 'Sparing the region of the salivary gland containing stem cells preserves saliva production after radiotherapy for head and neck cancer', *Sci Transl Med*, 7(305), p. 305ra147. doi: 10.1126/scitranslmed.aac4441.

Lv, F.-J. *et al.* (2014) 'Concise Review: The Surface Markers and Identity of Human Mesenchymal Stem Cells', *Stem Cells*, 32(6), pp. 1408–1419. doi: 10.1002/stem.1681.

Maimets, M. *et al.* (2015) 'Similar ex vivo expansion and post-irradiation regenerative potential of juvenile and aged salivary gland stem cells', *Radiotherapy and Oncology*. Elsevier Ireland Ltd, 116(3), pp. 443–448. doi: 10.1016/j.radonc.2015.06.022.

Maimets, M. *et al.* (2016) 'Long-Term in Vitro Expansion of Salivary Gland Stem Cells Driven by Wnt Signals', *Stem Cell Reports*. The Authors, 6(1), pp. 150–162. doi: 10.1016/j.stemcr.2015.11.009.

Mandal, P. K., Blanpain, C. and Rossi, D. J. (2011) 'DNA damage response in adult stem cells: pathways and consequences', *Nat Rev Mol Cell Biol*, 12(3), pp. 198–202. doi: 10.1038/nrm3060.

Mani, S. A. *et al.* (2008) 'The Epithelial-Mesenchymal Transition Generates Cells with Properties of Stem Cells', *Cell*, 133(4), pp. 704–715. doi: 10.1016/j.cell.2008.03.027.

- Mansour, A. A. *et al.* (2018) 'An in vivo model of functional and vascularized human brain organoids', *Nature Biotechnology*, 36(5), pp. 432–441. doi: 10.1038/nbt.4127.
- Maréchal, A. and Zou, L. (2013) 'DNA damage sensing by the ATM and ATR kinases.', *Cold Spring Harbor perspectives in biology*. Cold Spring Harbor Laboratory Press, 5(9). doi: 10.1101/cshperspect.a012716.
- Maria, O. M. *et al.* (2011) 'Matrigel improves functional properties of human submandibular salivary gland cell line', *International Journal of Biochemistry and Cell Biology*. Elsevier Ltd, 43(4), pp. 622–631. doi: 10.1016/j.biocel.2011.01.001.
- Martinet, W. *et al.* (2006) 'Detection of autophagy in tissue by standard immunohistochemistry: Possibilities and limitations', *Autophagy*, 2(1), pp. 55–57. doi: 10.4161/auto.2217.
- Martinet, W. *et al.* (2013) 'Immunohistochemical analysis of macroautophagy: Recommendations and limitations', *Autophagy*, 9(3), pp. 386–402. doi: 10.4161/auto.22968.
- Maruyama, C. *et al.* (2018) 'Comparing human and mouse salivary glands: A practice guide for salivary researchers', *Oral Diseases*. Wiley/Blackwell (10.1111). doi: 10.1111/odi.12840.
- Mavragani, C. P., Fragoulis, G. E. and Moutsopoulos, H. M. (2012) 'Endocrine alterations in primary Sjogren's syndrome: An overview', *Journal of Autoimmunity*. Elsevier Ltd, 39(4), pp. 354–358. doi: 10.1016/j.jaut.2012.05.011.
- Mavragani, C. P. and Moutsopoulos, H. M. (2010) 'The geoepidemiology of Sjogren's syndrome', *Autoimmunity Reviews*. Elsevier B.V., 9(5), pp. A305–A310. doi: 10.1016/j.autrev.2009.11.004.
- Mavragani, C. P. and Moutsopoulos, H. M. (2014a) 'Sjogren's syndrome', *Annu Rev Pathol*, 9, pp. 273–285. doi: 10.1146/annurev-pathol-012513-104728.
- Mavragani, C. P. and Moutsopoulos, H. M. (2014b) 'Sjogren syndrome', *CMAJ*. doi: 10.1503/cmaj.122037.
- Mavragani, C. P., Moutsopoulos, N. M. and Moutsopoulos, H. M. (2006) 'The management of Sjogren's syndrome', *Nat Clin Pract Rheumatol*, 2(5), pp. 252–261. doi: 10.1038/ncprheum0165.
- Mavragani, C. P., Tzioufas, A. G. and Moutsopoulos, H. M. (2000) 'Sjogren's syndrome: autoantibodies to cellular antigens. Clinical and molecular aspects', *Int Arch Allergy Immunol*, 123(1), pp. 46–57. doi: 24423.
- McCall, A. D. *et al.* (2013) 'Growth Factors Polymerized Within Fibrin Hydrogel Promote Amylase Production in Parotid Cells', *Tissue Engineering Part A*, 19(19–20), pp. 2215–2225. doi: Doi 10.1089/Ten.Tea.2012.0674.

- Melnick, M. *et al.* (2001) 'Embryonic mouse submandibular salivary gland morphogenesis and the TNF/TNF-R1 signal transduction pathway', *Anat Rec*, 262(3), pp. 318–330. Available at: <http://www.ncbi.nlm.nih.gov/pubmed/11241200>.
- Meng, Z. *et al.* (2017) 'Interferon- γ treatment in vitro elicits some of the changes in cathepsin S and antigen presentation characteristic of lacrimal glands and corneas from the NOD mouse model of Sjögren's Syndrome.', *PloS one*. Public Library of Science, 12(9), p. e0184781. doi: 10.1371/journal.pone.0184781.
- Mettler, F. A. (2012) 'Medical effects and risks of exposure to ionising radiation', *Journal of Radiological Protection*, 32(1), pp. N9–N13. doi: 10.1088/0952-4746/32/1/N9.
- Minakawa, Y. *et al.* (2016) 'Gamma-irradiated quiescent cells repair directly induced double-strand breaks but accumulate persistent double-strand breaks during subsequent DNA replication', *Genes to Cells*, 21(7), pp. 789–797. doi: 10.1111/gtc.12381.
- Mizukoshi, K. *et al.* (2016) 'Shh/Ptch and EGF/ErbB cooperatively regulate branching morphogenesis of fetal mouse submandibular glands', *Developmental Biology*. Academic Press, 412(2), pp. 278–287. doi: 10.1016/j.ydbio.2016.02.018.
- De Moerlooze, L. *et al.* (2000) 'An important role for the IIIb isoform of fibroblast growth factor receptor 2 (FGFR2) in mesenchymal-epithelial signalling during mouse organogenesis.', *Development (Cambridge, England)*, 127(3), pp. 483–92. Available at: <http://www.ncbi.nlm.nih.gov/pubmed/10631169> (Accessed: 5 October 2017).
- Morgan-Bathke, M. *et al.* (2015) 'The Role of Autophagy in Salivary Gland Homeostasis and Stress Responses', *J Dent Res*, 94(8), pp. 1035–1040. doi: 10.1177/0022034515590796.
- MORGAN, W. S. and CASTLEMAN, B. (1953) 'A clinicopathologic study of Mikulicz's disease.', *The American journal of pathology*. American Society for Investigative Pathology, 29(3), pp. 471–503. Available at: <http://www.ncbi.nlm.nih.gov/pubmed/13040489> (Accessed: 17 October 2017).
- Nagler, R. M. (2002) 'The enigmatic mechanism of irradiation-induced damage to the major salivary glands.', *Oral diseases*, 8(7), pp. 141–146. doi: 10.1034/j.1601-0825.2002.02838.x.
- Nanduri, L. S. Y. *et al.* (2013) 'Salisphere derived c-Kit⁺ cell transplantation restores tissue homeostasis in irradiated salivary gland', *Radiotherapy and Oncology*. Elsevier Ireland Ltd, 108(3), pp. 458–463. doi: 10.1016/j.radonc.2013.05.020.
- Nanduri, L. S. Y. *et al.* (2014) 'Purification and Ex vivo expansion of fully functional salivary gland stem cells', *Stem Cell Reports*. The Authors, 3(6), pp. 957–964. doi: 10.1016/j.stemcr.2014.09.015.
- Nelson, D. A. *et al.* (2013) 'Quantitative single cell analysis of cell population dynamics

during submandibular salivary gland development and differentiation.’, *Biology open*, 2(5), pp. 439–47. doi: 10.1242/bio.20134309.

Nicolay, N. H. *et al.* (2013) ‘Mesenchymal stem cells retain their defining stem cell characteristics after exposure to ionizing radiation’, *Int J Radiat Oncol Biol Phys*, 87(5), pp. 1171–1178. doi: 10.1016/j.ijrobp.2013.09.003.

Nicolay, N. H., Lopez Perez, R., Debus, J., *et al.* (2015) ‘Mesenchymal stem cells - A new hope for radiotherapy-induced tissue damage?’, *Cancer Lett*, 366(2), pp. 133–140. doi: 10.1016/j.canlet.2015.06.012.

Nicolay, N. H., Lopez Perez, R., Saffrich, R., *et al.* (2015) ‘Radio-resistant mesenchymal stem cells: mechanisms of resistance and potential implications for the clinic’, *Oncotarget*, 6(23), pp. 19366–19380. Available at: <http://www.ncbi.nlm.nih.gov/pubmed/26203772>.

Nocturne, G. and Mariette, X. (2013) ‘Advances in understanding the pathogenesis of primary Sjogren’s syndrome’, *Nat Rev Rheumatol*, 9(9), pp. 544–556. doi: 10.1038/nrrheum.2013.110.

Nüsslein-Volhard, C. and Wieschaus, E. (1980) ‘Mutations affecting segment number and polarity in *Drosophila*.’, *Nature*, 287(5785), pp. 795–801. Available at: <http://www.ncbi.nlm.nih.gov/pubmed/6776413> (Accessed: 4 September 2018).

O’Rourke, K. P. *et al.* (2016) ‘Isolation, Culture, and Maintenance of Mouse Intestinal Stem Cells.’, *Bio-protocol*. NIH Public Access, 6(4). Available at: <http://www.ncbi.nlm.nih.gov/pubmed/27570799> (Accessed: 9 November 2017).

Ogawa, M. *et al.* (2013) ‘Functional salivary gland regeneration by transplantation of a bioengineered organ germ’, *Nature Communications*, 4, p. 2498. doi: Artn 2498Doi 10.1038/Ncomms3498.

Ogawa, M. and Tsuji, T. (2015) ‘Functional salivary gland regeneration as the next generation of organ replacement regenerative therapy’, *Odontology*. Springer Japan, 103(3), pp. 248–257. doi: 10.1007/s10266-015-0210-9.

Okumura, K. *et al.* (2003) ‘Salivary gland progenitor cells induced by duct ligation differentiate into hepatic and pancreatic lineages’, *Hepatology*, 38(1), pp. 104–113. doi: 10.1053/jhep.2003.50259.

Okumura, K., Shinohara, M. and Endo, F. (2012) ‘Capability of tissue stem cells to organize into salivary rudiments’, *Stem Cells International*. Hindawi, 2012, pp. 1–11. doi: 10.1155/2012/502136.

Paardekooper, G. M. *et al.* (1998) ‘Radiation-induced apoptosis in relation to acute impairment of rat salivary gland function.’, *International journal of radiation biology*, 73(6), pp. 641–8. Available at: <http://www.ncbi.nlm.nih.gov/pubmed/9690682> (Accessed: 10 November 2017).

- Pan, L. *et al.* (1999) 'Impaired immune responses and B-cell proliferation in mice lacking the Id3 gene.', *Molecular and cellular biology*, 19(9), pp. 5969–80. doi: 10.1128/mcb.19.9.5969.
- Parambil, J. G. *et al.* (2006) 'Interstitial Lung Disease in Primary Sjögren Syndrome', *Chest*, 130(5), pp. 1489–1495. doi: 10.1378/chest.130.5.1489.
- Patel, V. N. *et al.* (2007) 'Heparanase cleavage of perlecan heparan sulfate modulates FGF10 activity during ex vivo submandibular gland branching morphogenesis', *Development*, 134(23), pp. 4177–4186. doi: 10.1242/dev.011171.
- Patel, V. N. and Hoffman, M. P. (2014) 'Salivary gland development: A template for regeneration', *Seminars in Cell and Developmental Biology*. Elsevier Ltd, 25–26, pp. 52–60. doi: 10.1016/j.semcdb.2013.12.001.
- Patel, V. N., Rebutini, I. T. and Hoffman, M. P. (2006) 'Salivary gland branching morphogenesis', *Differentiation*, 74(7), pp. 349–364. doi: 10.1111/j.1432-0436.2006.00088.x.
- Peters, B. M. *et al.* (2010) 'Protection of the oral mucosa by salivary histatin-5 against *Candida albicans* in an ex vivo murine model of oral infection', *FEMS Yeast Research*. Blackwell Publishing Ltd, 10(5), p. no-no. doi: 10.1111/j.1567-1364.2010.00632.x.
- Pijpe, J. *et al.* (2007) 'Parotid gland biopsy compared with labial biopsy in the diagnosis of patients with primary Sjögren's syndrome.', *Rheumatology (Oxford, England)*, 46(2), pp. 335–41. doi: 10.1093/rheumatology/kel266.
- Pijpe, J. *et al.* (2009) 'Clinical and histologic evidence of salivary gland restoration supports the efficacy of rituximab treatment in Sjögren's syndrome', *Arthritis and Rheumatism*, 60(11), pp. 3251–3256. doi: 10.1002/art.24903.
- Pispa, J. and Thesleff, I. (2003) 'Mechanisms of ectodermal organogenesis.', *Developmental biology*, 262(2), pp. 195–205. Available at: <http://www.ncbi.nlm.nih.gov/pubmed/14550785> (Accessed: 6 November 2017).
- Pittenger, M. F. *et al.* (1999a) 'Multilineage potential of adult human mesenchymal stem cells.', *Science (New York, N.Y.)*, 284(5411), pp. 143–7. Available at: <http://www.ncbi.nlm.nih.gov/pubmed/10102814> (Accessed: 13 September 2018).
- Pittenger, M. F. *et al.* (1999b) 'Multilineage potential of adult human mesenchymal stem cells.', *Science (New York, N.Y.)*, 284(5411), pp. 143–7. Available at: <http://www.ncbi.nlm.nih.gov/pubmed/10102814> (Accessed: 9 June 2018).
- Le Pottier, L. *et al.* (2009) 'Ectopic germinal centers are rare in Sjögren's syndrome salivary glands and do not exclude autoreactive B cells.', *Journal of immunology (Baltimore, Md. : 1950)*, 182(6), pp. 3540–3547. doi: 10.4049/jimmunol.0803588.
- Pradhan-Bhatt, S. *et al.* (2013) 'Implantable Three-Dimensional Salivary Spheroid

Assemblies Demonstrate Fluid and Protein Secretory Responses to Neurotransmitters', *Tissue Engineering Part A*, 19(13–14), pp. 1610–1620. doi: 10.1089/ten.tea.2012.0301.

Pringle, S. *et al.* (2011) 'Isolation of Mouse Salivary Gland Stem Cells', *Journal of Visualized Experiments*, (48), pp. 9–10. doi: 10.3791/2484.

Pringle, S., Van Os, R. and Coppes, R. P. (2013) 'Concise review: Adult salivary gland stem cells and a potential therapy for xerostomia', *Stem Cells*, 31(4), pp. 613–619. doi: 10.1002/stem.1327.

Proctor, G. B. (2016) 'The physiology of salivary secretion', *Periodontology 2000*, 70(1), pp. 11–25. doi: 10.1111/prd.12116.

Proctor, G. B. and Carpenter, G. H. (2014) 'Salivary secretion: Mechanism and neural regulation', in *Saliva: Secretion and Functions*, pp. 14–29. doi: 10.1159/000358781.

Radfar, L. *et al.* (2002) 'Prevalence and clinical significance of lymphocytic foci in minor salivary glands of healthy volunteers', *Arthritis & Rheumatism*, 47(5), pp. 520–524. doi: 10.1002/art.10668.

Rebustini, I. T. *et al.* (2007) 'Laminin alpha5 is necessary for submandibular gland epithelial morphogenesis and influences FGFR expression through beta1 integrin signaling.', *Developmental biology*, 308(1), pp. 15–29. doi: 10.1016/j.ydbio.2007.04.031.

Ree, A. H. *et al.* (2006) 'DNA damage responses in cell cycle G2 phase and mitosis - Tracking and targeting', *Anticancer Research*, 26(3 A), pp. 1909–1916. Available at: <http://www.ncbi.nlm.nih.gov/pubmed/16827124> (Accessed: 16 November 2017).

Ribeiro, D. A. (2012) 'Cytogenetic biomonitoring in oral mucosa cells following dental X-ray', *Dentomaxillofacial Radiology*, 41(3), pp. 181–184. doi: 10.1259/dmfr/14555883.

Ribeiro, D. A. and Angelieri, F. (2008) 'Cytogenetic biomonitoring of oral mucosa cells from adults exposed to dental X-rays', *Radiat Med*, 26(6), pp. 325–330. doi: 10.1007/s11604-008-0232-0.

Roesink, J. M. *et al.* (2001) 'Quantitative dose-volume response analysis of changes in parotid gland function after radiotherapy in the head-and-neck region', *International Journal of Radiation Oncology Biology Physics*. Elsevier, 51(4), pp. 938–946. doi: 10.1016/S0360-3016(01)01717-5.

Roguedas, A. M. *et al.* (2010) 'Memory B-cell aggregates in skin biopsy are diagnostic for primary Sjögren's syndrome', *Journal of Autoimmunity*. Elsevier Ltd, 35(3), pp. 241–247. doi: 10.1016/j.jaut.2010.06.014.

Romanenko, V. G. *et al.* (2010) 'Tmem16A Encodes the Ca²⁺-activated Cl⁻ Channel in Mouse Submandibular Salivary Gland Acinar Cells', *Journal of Biological Chemistry*, 285(17), pp. 12990–13001. doi: 10.1074/jbc.M109.068544.

- Rothkamm, K. and Löbrich, M. (2003) 'Evidence for a lack of DNA double-strand break repair in human cells exposed to very low x-ray doses.', *Proceedings of the National Academy of Sciences of the United States of America*, 100(9), pp. 5057–62. doi: 10.1073/pnas.0830918100.
- Rotroff, D. M. and Motsinger-Reif, A. A. (2016) 'Embracing Integrative Multiomics Approaches.', *International journal of genomics*. Hindawi Limited, 2016, p. 1715985. doi: 10.1155/2016/1715985.
- Roussa, E. (2011) 'Channels and transporters in salivary glands', *Cell and Tissue Research*, 343(2), pp. 263–287. doi: 10.1007/s00441-010-1089-y.
- Rovida, E. and Stecca, B. (2015) 'Mitogen-activated protein kinases and Hedgehog-GLI signaling in cancer: A crosstalk providing therapeutic opportunities?', *Seminars in Cancer Biology*. Academic Press, 35, pp. 154–167. doi: 10.1016/J.SEMCANCER.2015.08.003.
- Rubin, P. and Casarett, G. W. (1968) 'Clinical radiation pathology as applied to curative radiotherapy', *Cancer*, 22(4), pp. 767–778. doi: 10.1002/1097-0142(196810)22:4<767::AID-CNCR2820220412>3.0.CO;2-7.
- Sánchez Alvarado, A. and Yamanaka, S. (2014) 'Rethinking differentiation: stem cells, regeneration, and plasticity.', *Cell*. NIH Public Access, 157(1), pp. 110–9. doi: 10.1016/j.cell.2014.02.041.
- Sander, J. D. and Joung, J. K. (2014) 'CRISPR-Cas systems for editing, regulating and targeting genomes', *Nature Biotechnology*. Nature Publishing Group, 32(4), pp. 347–355. doi: 10.1038/nbt.2842.
- Sandhya, P. *et al.* (2015) 'Clinical Characteristics and Outcome of Primary Sjogren's Syndrome: A Large Asian Indian Cohort.', *The open rheumatology journal*. Bentham Science Publishers, 9, pp. 36–45. doi: 10.2174/1874312901409010036.
- Schwarz, S. *et al.* (2014) 'Bone marrow-derived mesenchymal stem cells migrate to healthy and damaged salivary glands following stem cell infusion.', *International journal of oral science*, 6(3), pp. 154–61. doi: 10.1038/ijos.2014.23.
- Schwarz, S. and Rotter, N. (2012) 'Human salivary gland stem cells: isolation, propagation, and characterization', *Methods Mol Biol*, 879, pp. 403–442. doi: 10.1007/978-1-61779-815-3_25.
- Shah, N., Bansal, N. and Logani, A. (2014) 'Recent advances in imaging technologies in dentistry.', *World journal of radiology*. Baishideng Publishing Group Inc, 6(10), pp. 794–807. doi: 10.4329/wjr.v6.i10.794.
- Shi, Y. *et al.* (2017) 'Induced pluripotent stem cell technology: a decade of progress', *Nature Reviews Drug Discovery*. Nature Publishing Group, 16(2), pp. 115–130. doi: 10.1038/nrd.2016.245.

- Siqueira, W. L. *et al.* (2007) 'Identification of Protein Components in *in vivo* Human Acquired Enamel Pellicle Using LC-ESI-MS/MS', *Journal of Proteome Research*, 6(6), pp. 2152–2160. doi: 10.1021/pr060580k.
- Siqueira, W. L. *et al.* (2010) 'Evidence of intact histatins in the *in vivo* acquired enamel pellicle.', *Journal of dental research*. International Association for Dental Research, 89(6), pp. 626–30. doi: 10.1177/0022034510363384.
- Skopouli, F. N. *et al.* (1998) 'Association of mast cells with fibrosis and fatty infiltration in the minor salivary glands of patients with Sjögren's syndrome.', *Clinical and experimental rheumatology*, 16(1), pp. 63–5. Available at: <http://www.ncbi.nlm.nih.gov/pubmed/9543564> (Accessed: 17 November 2017).
- Skopouli, F. N. *et al.* (2000) 'Clinical evolution, and morbidity and mortality of primary Sjögren's syndrome.', *Seminars in arthritis and rheumatism*. W.B. Saunders, 29(5), pp. 296–304. doi: 10.1016/S0049-0172(00)80016-5.
- Slomiany, B. L. *et al.* (1996) *Salivary mucins in oral mucosal defense, General Pharmacology*. Pergamon. doi: 10.1016/0306-3623(95)02050-0.
- Sokol, E. S. *et al.* (2016) 'Growth of human breast tissues from patient cells in 3D hydrogel scaffolds', *Breast Cancer Research*. Breast Cancer Research, 18(1), p. 19. doi: 10.1186/s13058-016-0677-5.
- Speight, P. M., Kaul, A. and Melsom, R. D. (1992) 'Measurement of whole unstimulated salivary flow in the diagnosis of Sjögren's syndrome.', *Annals of the rheumatic diseases*. BMJ Publishing Group, 51(4), pp. 499–502. Available at: <http://www.ncbi.nlm.nih.gov/pubmed/1586248> (Accessed: 19 September 2018).
- Srinivasan, P. P. *et al.* (2017) 'Primary Salivary Human Stem/Progenitor Cells Undergo Microenvironment-Driven Acinar-Like Differentiation in Hyaluronate Hydrogel Culture', *Stem Cells Transl Med*, 6(1), pp. 110–120. doi: 10.5966/sctm.2016-0083.
- Stramandinoli-Zanicotti, R. T. *et al.* (2013) 'Effect of fractionated radiotherapy on the parotid gland: An experimental study in Brazilian minipigs', *International Archives of Otorhinolaryngology*, 17(2), pp. 163–167. doi: 10.7162/S1809-9772013000200008.
- Sudo, H. and Baas, P. W. (2010) 'Acetylation of microtubules influences their sensitivity to severing by katanin in neurons and fibroblasts.', *The Journal of neuroscience : the official journal of the Society for Neuroscience*. NIH Public Access, 30(21), pp. 7215–26. doi: 10.1523/JNEUROSCI.0048-10.2010.
- Tabak, L. A. *et al.* (1982) 'Role of salivary mucins in the protection of the oral cavity.', *Journal of oral pathology*, 11(1), pp. 1–17. Available at: <http://www.ncbi.nlm.nih.gov/pubmed/6801238> (Accessed: 9 October 2017).
- Tabak, L. A. L. A. (2006) 'In Defence of the Oral Cavity: The Protective Role of the Salivary Secretions', in. Available at: <http://www.ncbi.nlm.nih.gov/pubmed/16708785> (Accessed: 9 October 2017).

- Takahashi, K. and Yamanaka, S. (2006) 'Induction of Pluripotent Stem Cells from Mouse Embryonic and Adult Fibroblast Cultures by Defined Factors', *Cell*, 126(4), pp. 663–676. doi: 10.1016/j.cell.2006.07.024.
- Takahashi, M. *et al.* (2014) 'Identification of gene expression profile of neural crest-derived cells isolated from submandibular glands of adult mice', *Biochemical and Biophysical Research Communications*. Elsevier Inc., 446(2), pp. 481–486. doi: 10.1016/j.bbrc.2014.02.130.
- Takakura, K. *et al.* (2007) 'Effect of Cevimeline on Radiation-Induced Salivary Gland Dysfunction and AQP5 in Submandibular Gland in Mice', *The Bulletin of Tokyo Dental College*. Tokyo Dental College, Japan, 48(2), pp. 47–56. doi: 10.2209/tdcpublication.48.47.
- Tasaki, S. *et al.* (2017) 'Multiomic disease signatures converge to cytotoxic CD8 T cells in primary Sjögren's syndrome', *Annals of the Rheumatic Diseases*, 76(8), pp. 1458–1466. doi: 10.1136/annrheumdis-2016-210788.
- Teshima, T. H. N. *et al.* (2016) 'Apoptosis in Early Salivary Gland Duct Morphogenesis and Lumen Formation', *Journal of Dental Research*. SAGE PublicationsSage CA: Los Angeles, CA, 95(3), pp. 277–283. doi: 10.1177/0022034515619581.
- Thelin, W. *et al.* (2008) 'The oral mucosa as a therapeutic target for xerostomia', *Oral Diseases*. Blackwell Publishing Ltd, 14(8), pp. 683–689. doi: 10.1111/j.1601-0825.2008.01486.x.
- Tobón, G. J. *et al.* (2011) 'Skin biopsy as a routine diagnostic tool for primary Sjögrens syndrome', *International Journal of Clinical Rheumatology*, 6(3). doi: 10.2217/ijr.11.19.
- Tomsic, M. *et al.* (1999) 'Prevalence of Sjögren's syndrome in Slovenia.', *Rheumatology (Oxford, England)*, 38(2), pp. 164–70. Available at: <http://www.ncbi.nlm.nih.gov/pubmed/10342631> (Accessed: 6 November 2017).
- Toné, S. *et al.* (2007) 'Three distinct stages of apoptotic nuclear condensation revealed by time-lapse imaging, biochemical and electron microscopy analysis of cell-free apoptosis.', *Experimental cell research*. NIH Public Access, 313(16), pp. 3635–44. doi: 10.1016/j.yexcr.2007.06.018.
- Toufektchan, E. and Toledo, F. (2018) 'The Guardian of the Genome Revisited: p53 Downregulates Genes Required for Telomere Maintenance, DNA Repair, and Centromere Structure', *Cancers*, 10(5), p. 135. doi: 10.3390/cancers10050135.
- Truong, K. *et al.* (2018) 'The effect of well-characterized, very low-dose x-ray radiation on fibroblasts', *PLOS ONE*. Edited by G. E. Woloschak. Public Library of Science, 13(1), p. e0190330. doi: 10.1371/journal.pone.0190330.
- Tsunawaki, S. *et al.* (2002) 'Possible function of salivary gland epithelial cells as nonprofessional antigen-presenting cells in the development of Sjögren's syndrome.', *The Journal of rheumatology*, 29(9), pp. 1884–96. Available at:

<http://www.ncbi.nlm.nih.gov/pubmed/12233883>.

Tucker, A. S. (2007) 'Salivary gland development.', *Seminars in cell & developmental biology*, 18(2), pp. 237–44. doi: 10.1016/j.semcd.2007.01.006.

Uhlén, M. *et al.* (2015) 'Proteomics. Tissue-based map of the human proteome.', *Science (New York, N.Y.)*. American Association for the Advancement of Science, 347(6220), p. 1260419. doi: 10.1126/science.1260419.

Valdez, I. H. *et al.* (1993) 'Use of pilocarpine during head and neck radiation therapy to reduce xerostomia and salivary dysfunction.', *Cancer*, 71(5), pp. 1848–51. Available at: <http://www.ncbi.nlm.nih.gov/pubmed/8448748> (Accessed: 3 November 2017).

Valim, V. *et al.* (2016) 'Atherosclerosis in Sjogren's syndrome: evidence, possible mechanisms and knowledge gaps.', *Clinical and experimental rheumatology*, 34(1), pp. 133–142. Available at: <http://www.ncbi.nlm.nih.gov/pubmed/26812164> (Accessed: 16 November 2017).

Veltmaat, J. M. *et al.* (2003) 'Mouse embryonic mammaryogenesis as a model for the molecular regulation of pattern formation', *Differentiation*. Blackwell Verlag, 71, pp. 1–17. doi: 10.1046/j.1432-0436.2003.700601.x.

Vissink, A. *et al.* (2015) 'Current ideas to reduce or salvage radiation damage to salivary glands', *Oral Diseases*, 21(1), pp. e1–e10. doi: 10.1111/odi.12222.

Voulgarelis, M. *et al.* (2012) 'Prognosis and outcome of non-Hodgkin lymphoma in primary Sjogren syndrome', *Medicine (Baltimore)*, 91(1), pp. 1–9. doi: 10.1097/MD.0b013e31824125e4.

Voulgarelis, M. and Tzioufas, A. G. (2010) 'Pathogenetic mechanisms in the initiation and perpetuation of Sjogren's syndrome', *Nat Rev Rheumatol*, 6(9), pp. 529–537. doi: 10.1038/nrrheum.2010.118.

Wells, K. L. *et al.* (2014) 'Dynamic relationship of the epithelium and mesenchyme during salivary gland initiation: the role of Fgf10', *Biol Open*, 3(7), p. 677. doi: 10.1242/bio.20149084.

Zhang, N. Z. *et al.* (1995) 'Prevalence of primary Sjögren's syndrome in China.', *The Journal of rheumatology*, 22(4), pp. 659–61. Available at: <http://www.ncbi.nlm.nih.gov/pubmed/7791159> (Accessed: 6 November 2017).

6. Appendix

6.1. Impact of X-Ray Irradiation on the Regenerative Potential of Salivary Gland Mesenchymal Cells

Head and neck cancer patients will frequently undergo radiation therapy with the aim of reducing the size of the tumour for easier excision, with the inadvertent side effect of exposing the salivary gland tissue (amongst other tissues) to dangerous levels of ionising X-Ray radiation. It was discussed in the introduction how exposure to ionising radiation can cause significant cell death, cell cycle arrest, reduced cell proliferation and a reduction in cell-cell signalling pathways. If cells could be exposed to ionising radiation, inducing a change in their phenotype, it would be possible to incorporate these cells into the three-dimensional assays established previously and characterise the changes in cell behaviour and tissue regeneration potential.

It is now a standard technique that, as a measurement of chromosomal damage, it's possible to count micronuclei (Agarwal *et al.*, 2015) and other nuclear abnormalities, such as nuclear condensation, or nuclear blebbing (Krysko *et al.*, 2008), in order to demonstrate radiation impact on cells.

The primary research aim was to investigate the impact of IR on established cultured cell populations. Once confirmation of a significant impact of ionising irradiation (IR) was confirmed, the group aimed to combine the exposed cells into organoid models so that the mechanistic changes in the regenerative potential of these cells could be monitored.

Simultaneously, organ cultures were developed, which could also be exposed to IR to give a more relatable ex-vivo representation of IR impact. It was hypothesised that cells exposed to IR would have a reduced regenerative capacity due to cell cycle arrest and would produce spheres of limited size and less developed phenotype in comparison to unexposed controls.

6.1.1.X-Ray exposure Methods

Cell cultures were exposed to low levels of irradiation using diagnostic X-Ray equipment (Kodak 2200 Intraoral X-Ray System, Kodak). The starting exposure levels were of 0, 25 and 50 mGy on mouse salivary gland derived epithelial and mesenchymal cells, non-PSS patient derived cells and HGEPP cells. As the samples were cells in culture or tissue sections on semi solid agar cultures, the assumption was made that the exposures were relative and measuring the radiation with Grays for all of the samples would be sufficient, as opposed to calculating estimated Sieverts received by each sample.

The units for measuring radiation are either Grays, which were used in our experiments, or Sieverts. One Gray (1Gy) is equivalent to the absorption of one joule of radiation energy into 1Kg of material and is an estimate based on the emission from the radiation source, whilst one Sievert is a measurement of the equivalent radiation dose received by the sample; meaning the value of Gray multiplied by a tissue specific algorithm that would calculate the actual impact of ionising radiation. However, the machinery that was used to generate the X-Ray exposures is a clinical device that is pre-set to exposures measured in Grays.

After these initial experiments, dosage was increased 10-fold, to 500mGy and then again to 1Gy. These doses were based on clinically relevant doses for irradiation therapy (Burlage *et al*, 2001) . Evidence indicates that the impact of 2Gy is sufficient to develop acute radiation sickness, and that less than 500mGy is sufficient to induce a phenotypic change within exposed cell populations (Dirix, Nuyts and Van Den Bogaert, 2006; Mettler, 2012; Truong *et al.*, 2018). The higher doses were achieved by increasing the frequency of exposures to each sample, as the Kodak system only produces low level X-Ray doses. Exposing the samples every day over a five-day period was also trialled, in an attempt to increase exposure levels to 2Gy. This time-line of exposure did increase the risk of cells being exposed to un-sterile environments, cells also became more confluent, losing their fibroblast cell phenotype. After the four days of exposure and 24 hours of lag time, cells were fixed and stained using standard IF protocols.

Cells were exposed on Day 0, after which the cells were washed with pre-cooled sterile HBSS, and the media replaced following the standard protocol. The cells were then left for 24 hours before the media was removed and the cells fixed with cold 4% PFA for 30 minutes, washed with PBS and stained following the standard immunofluorescence staining protocol as described previously.

Further immunofluorescent staining was performed on the mouse mesenchymal primary cells using a panel of our mesenchymal cell markers, in the hope that the IR was still impacting the cells. The mesenchymal stem cell markers used were PDGFR β , CD29 and Sca1.

6.1.2. Exposure of Cell Cultures to Low Level X-Ray Irradiation Has No Visible Impact on Cell Morphology or Cell Death.

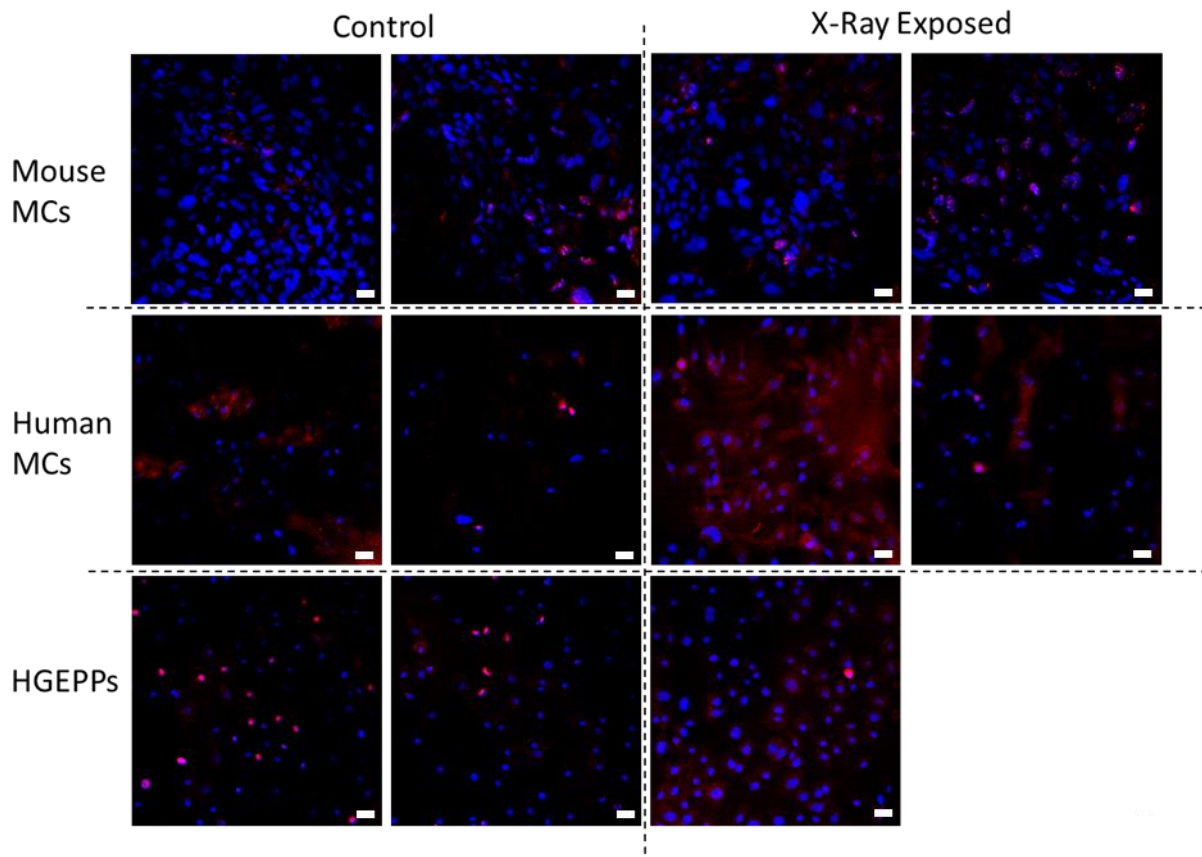


Figure 6.1-1. The impact of 50mGy of irradiation on cell morphology and nuclear changes. Paired images are replicates to demonstrate heterogeneity in culture conditions. Primary mouse mesenchymal cells, primary human mesenchymal cells and established human gingival epithelial cell line, HGEPP, were exposed to varying levels of ionising radiation. Nuclei stained with DAPI and cells stained with NSun2, visualised with Alexa-568 conjugated secondary antibody. Images taken at 20 X magnification, Scale bars represent 50uM.

All cells in culture appear to stain as expected for DAPI, these are shown above in Figure 6.1-1, with consistent patterns of nuclear staining between the control and exposed samples. Instances of abnormal nuclei were observed, for example, there are instances of cells undergoing mitosis, and occasionally there appear to be some instances of micronuclei and apoptosis, where the cytoplasm is very condensed, and the nucleus is a less defined structure (Toné *et al.*, 2007).

However, it was clear from these primary experiments that the low-level dosage of 50mGy was not affecting the cells as desired, as shown in Figure 6.1-1. The dosage was increased by increasing the number of exposures given to each sample. Unfortunately, no significant nuclear aberrations were observed at these higher exposures either, nor any obvious change to cell growth rates or cell phenotype. Any of the aberrations were observed in both the control and exposed samples and were at levels that are expected to be observed in normal cell culture conditions as part of homeostasis (Grundmann, Mitchell and Limesand, 2009).

The addition of staining for the marker Ki67, in Figure 6.1-2, was an attempt to study impact on proliferation of cells that had been exposed to IR. Ki67 was expressed sparsely in all the cell cultures and was not changed between control or treated conditions. There appeared to be very low levels of the marker in the HGEPP (Primary Human Gingival Epithelial Cells (pooled)) cells across both conditions. Cells appeared quite confluent, which could reduce the cell proliferation. The lack of any significant change within the exposed samples when compared to the controls led to the increase in exposure of IR again to 1Gy.

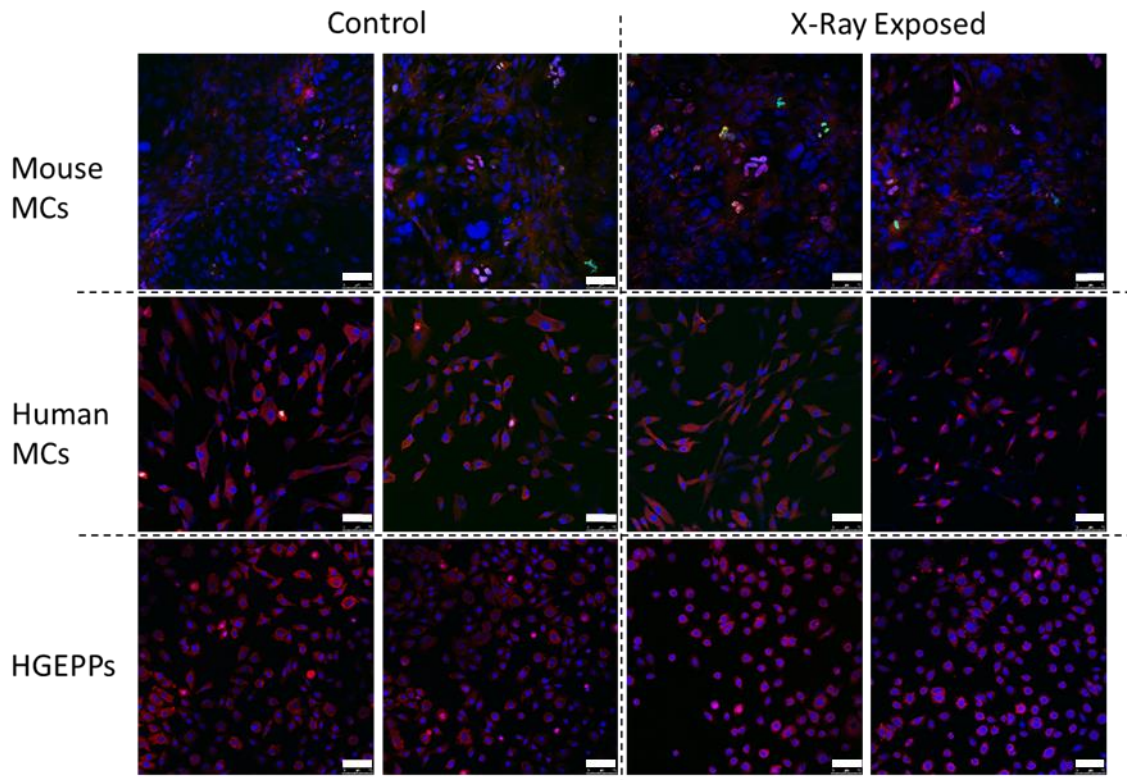


Figure 6.1-2 Increased dosage 500mGy of ionising irradiation also does not induce change on cell morphology. Mouse mesenchymal cells, human mesenchymal cells and human epithelial cell line HGEPPs were exposed and stained with Ki67 and NSun2, visualised with Alexa-488 and Alexa-568 respectively, nuclei are visualised with DAPI nuclear stain. Images were taken at 20X magnification, the scale bar represents 75uM.

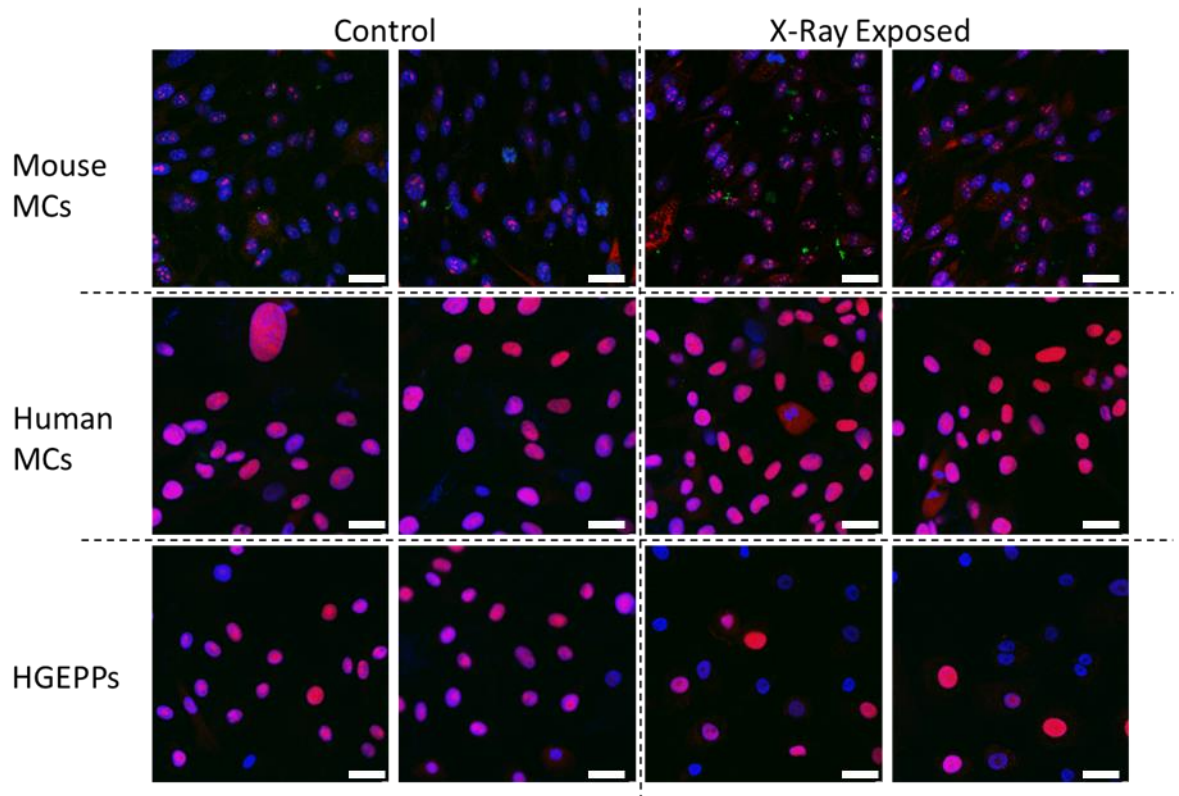


Figure 6.1-3. Further increase to 1Gy of IR dose still did not impact cell culture phenotype. Mouse MCs, human MCs and HGEPPs were exposed and stained for Ki67 and NSun2, the staining was visualised with Alexa-488 and Alexa-568 respectively, and DAPI for nuclear visualisation. Images were taken at 63X magnification, scale bar represents 15uM.

When the cells were exposed to 1Gy, as shown in Figure 6.1-3, more variety of cellular and nuclear phenotypes was anecdotally observed. However, the cells were seeded more sparsely in the culture environment and this allowed more mitosis and cell proliferation to occur. However, there was no observation of any Ki67 staining in the human primary cells or the HGEPP cells, and very few cells stained positive for Ki67 in the mouse MCs. Furthermore, there was no observation of any nuclear blebbing, or micronuclei, excessive cell death, or reduced cell proliferation. Attempts were then made to investigate molecular changes to the cells by staining for a panel of mesenchymal markers that would give an indication of stemness within the cell populations.

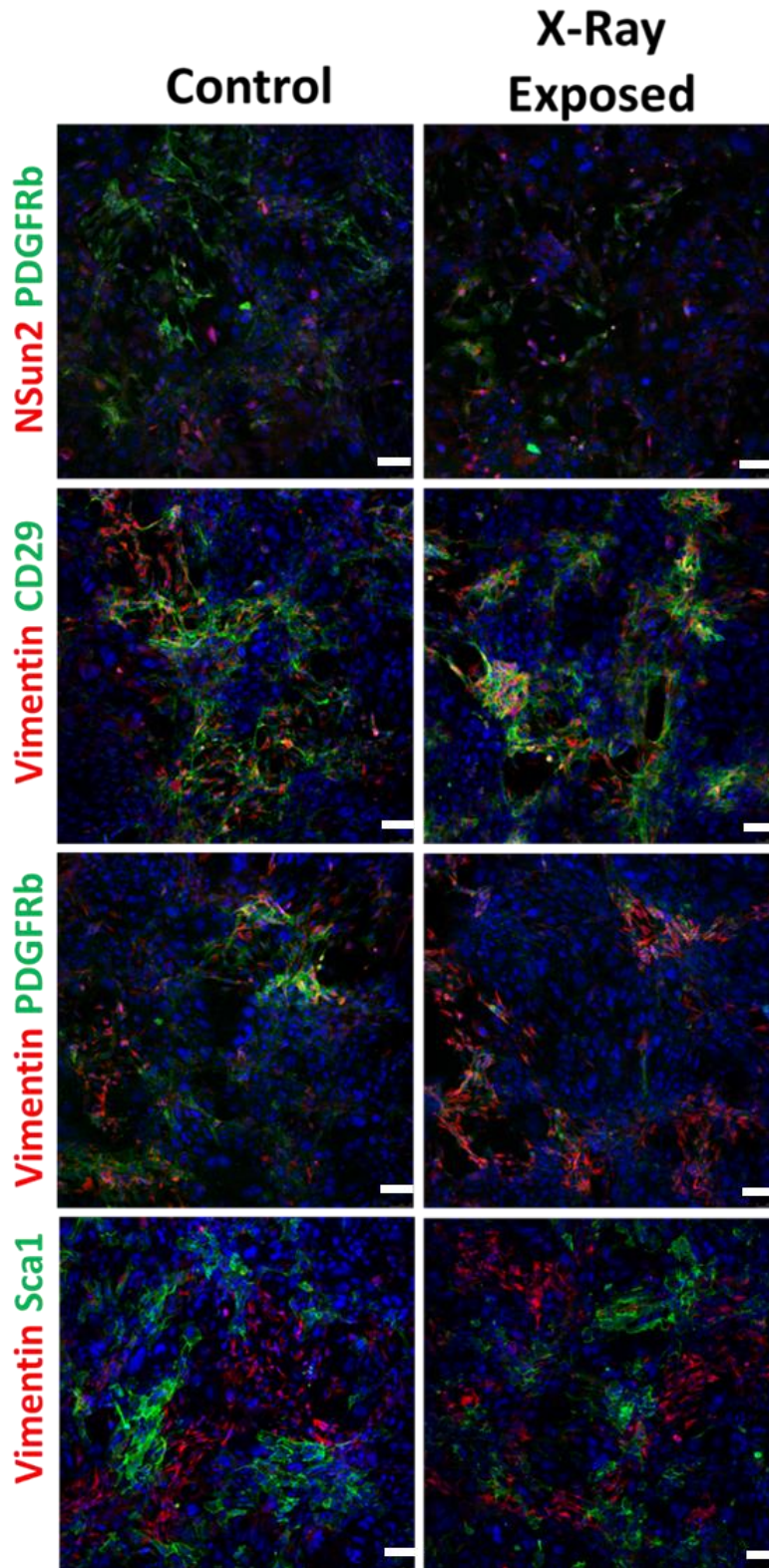


Figure 6.1-4. Immunofluorescent staining on 2Gy exposed mouse mesenchymal cell populations. Mesenchymal cells were exposed to IR over a four-day period. The cells were fixed and stained for NSun2, PDGFR β , Vimentin, CD29, and Sca1, visualised with Alexa-488 and Alexa-568 secondary antibodies, and DAPI staining for nuclear identification. Images were taken at 20X magnification, scale bars represent 75uM.

Despite the longer time frame of exposures, NSun2, Vimentin, CD29 and Sca1 did not appear to have any significant decrease in staining profiles. However, PDGFR β did not stain as ubiquitously in the exposed sample as in the controls. As demonstrated in Figure 6.1-4, less Alexa-488 positive staining was observed, showing reduced PDGFR β .

In all of the samples, due to the length of time that the cells were being cultured, the cells became very confluent and this generated a very heterogeneous population of cells, with great disparity in the staining pattern of the cells. Figure 6.1-4 shows that only small regions of the cells would stain positively for the mesenchymal cell markers, suggesting that a transition may have been undertaken by some of the mesenchymal cells, or a depletion of a specific subset of mesenchymal cells.

To get a better idea of the changes to marker expression profiles, higher magnification images of the same experiment were taken. In these high magnification images, it was easier to compare the staining pattern across the samples. In the top four images, Vimentin and CD29 staining was consistent across the exposed and control samples, indicating that the CD29 marker stained the mesenchymal cell population consistently and that there was no impact on the CD29 expression when exposed to IR. However, when the PDGFR β staining was compared between the exposed and control samples, the control sample staining pattern was very similar to that of the Vimentin and CD29. Whilst the cells exposed to 2Gy of IR had PDGFR β staining that was less fibrous in appearance, with the staining condensing to cytoplasmic punctate staining, with less dendritic-like processes being highlighted by the staining, as seen in the control samples. This was the only marker that appeared to have any significant phenotypical change in appearance due to the exposure to X-Ray irradiation.

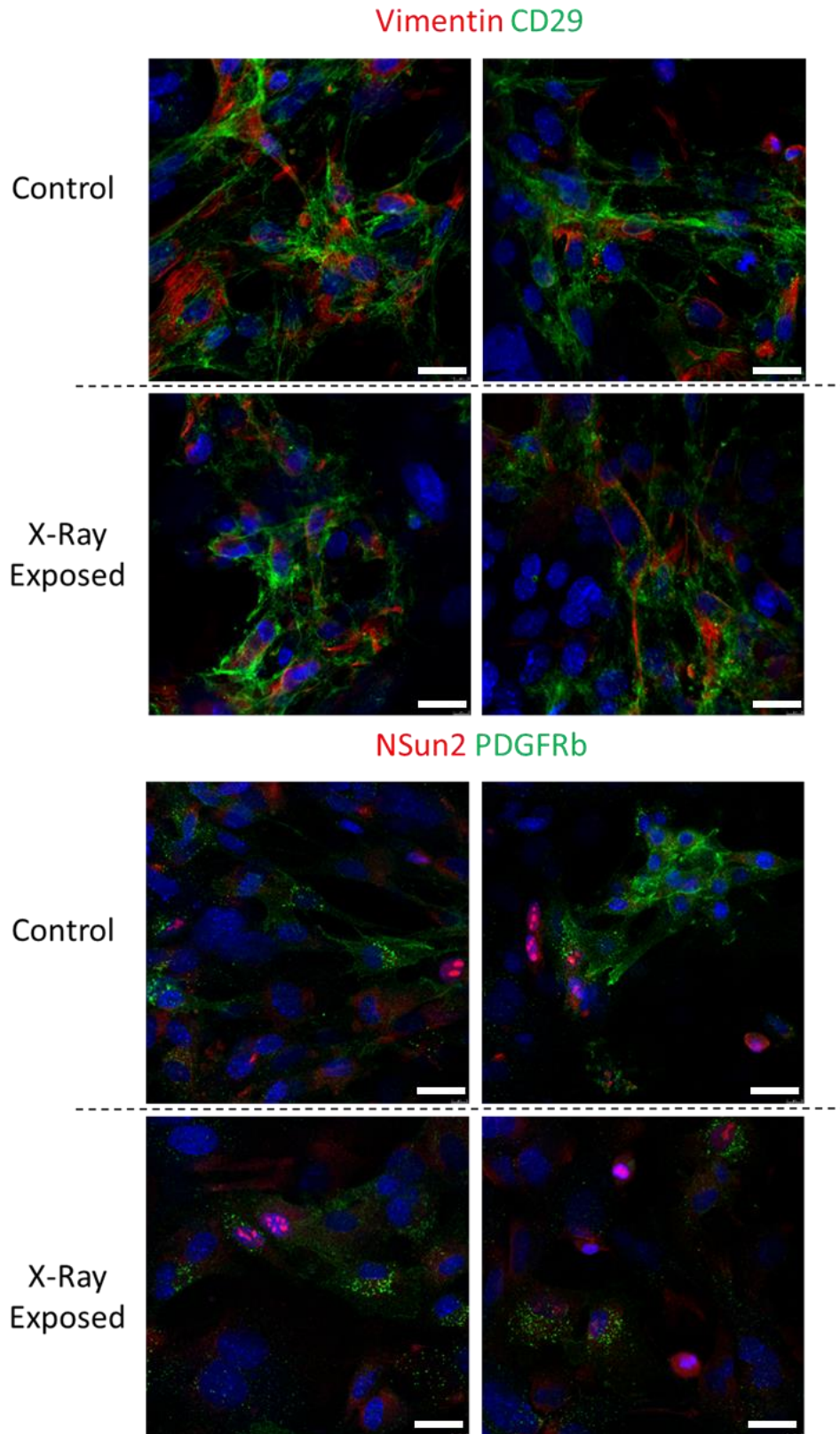


Figure 6.1-5 High magnification images of 2 Gy exposed mouse mesenchymal cells. Cells were prepared as described in Figure 3.3-4, with cells stained for Vimentin (Alexa 568, red) and CD29 (Alexa 488, green). Images taken at 63 X magnification with oil immersion with scale bars representing 10uM.

Simultaneous to the attempt to develop the X-Ray exposure model, experiments were designed for the culture of salivary gland tissue. Sections of 50uM to 250uM thickness were taken from mouse salivary gland samples using a vibratome and small lobules were dissected at the same time. These pieces of tissue were either floated on top of culture media at the air-liquid interface using Whatman filter papers or placed on top of semi-solid agar culture medium, with additional media added on top.

The plan was to expose ex-vivo cultures to ionising radiation in an equivalent manner to which the cells had been exposed. However, these cultures failed to survive 24 hours after placing in culture. A small ring of tissue was seen to persist around the edge of the explants, but there was no positive DAPI or haematoxylin staining within the centre of the tissue when performing staining analysis. These techniques were repeated, and significant attempts were made to optimise the conditions, to no avail. Furthermore, despite incubating the tissue in PBS with antibiotics, antimycotics and fungizone, these cultures would very rapidly develop contaminations; yeast and mould contaminations would permeate all the culture conditions at once. These results are not shown, and both the attempt to expose cells to IR and developing organ cultures were discontinued.

6.1.3. Discussion

When cells were cultured and exposed to X-Ray irradiation, no significant changes to the nuclei of cells could be observed. This was consistent across all the cell types that were exposed and, although there may have been some nuclear aberrations, there was no significance in the distribution of these artefacts between treated and controls, that would suggest any impact of ionising radiation. There are also other known phenotypes of ionising radiation exposure, indicative of apoptosis of the cells, which were not present at all. These include nuclear condensation, ring and necklace formation, complete nuclear collapse, and cell cycle dysregulation or halting (Toné *et al.*, 2007; Truong *et al.*, 2018). Other physical phenotypes that could have been used as measures of IR impact could have included the rate of proliferation by the wound healing “scratch” test, which is a reliable assay for demonstrating cell proliferation and migration (Liang, Park and Guan, 2007).

The Kodak 2200 machines are specially designed to emit very low-level X-Ray irradiation, and, when they are calibrated to detect with digital detecting software instead of physical detection plates, the intensity required for diagnostic purposes is even lower. Certainly, the level of radiation required for radiotherapy is significantly higher than diagnostic purposes, with patients receiving 2Gy every day for five days for a period of two months, with sometimes an initial exposure of 15Gy (Dirix, Nuyts and Van Den Bogaert, 2006). Therefore, to achieve higher exposures, the dose frequency had to be increased, which took longer and had the potential to overheat the machines, despite still being under therapeutic dosage. It was because of this side effect that the decision was taken not to pursue this aim further, as the machines are an integral part of the

dental teaching clinics and damage to them would have impacted the teaching of dental students and the treatment of patients. Throughout the period of this PhD, it was unfeasible to access therapeutic irradiation machinery in the Plymouth University NHS Trust Derriford Hospital, despite attempts to set up access, and it was unfeasible to source alternative X-Ray generating technology within other departments of the university. Furthermore, the protocols and timescales which would have had to be followed to access facilities in the hospital would have been prohibitive for the experimental work and could have resulted in inconsistencies and variability in the samples; obviously patients come first, and the flexibility required would have resulted in cells being out of culture for a long period of time, and risky transportation between sites.

When starting this work, the group was aware of the limitations of using diagnostic X-Ray machinery to expose samples; the level of dosage is purposefully small in order to limit the impact of x-rays on patients, whilst the accuracy of the exposure is variable due to the cone shape used for dispersal and the distance away from the sample. However, there is sufficient evidence to suggest that even small doses can impact cells, such as reduced repair of double stranded breaks (Rothkamm and Löbrich, 2003), changes to cell cycle and cell proliferation rates (Truong *et al.*, 2018). It's also known that IR can induce stem cell-like phenotypes in tissue, and therefore, we could equally expect an increase in stem cell markers, or a more quiescent-like cell population (Ghisolfi *et al.*, 2012).

Primarily, the machinery used to generate the X-Ray doses were not appropriate for the experimental design, as they were diagnostic X-Ray machinery which are designed to

produce very small levels of radiation in order to minimise patient exposure. With great advances being made in all aspects of dental imaging technology, the sensitivity and speed of equipment is greatly reducing the radiation exposure for patients and improving the visual output at a fraction of the IR required previously (Shah, Bansal and Logani, 2014). This resulted in one of the greatest limitations for this research direction, potentially inhibiting the group from delivering doses of radiation that could impact the target tissue or cells of interest. Furthermore, as diagnostic machinery was being used, rather than a bespoke machine, the group was unable to accurately record the dosage received by each experimental sample. If this direction of study were to be continued, it would be preferable to gain access to an X-Ray generating machine that was enclosed and had the capacity to detect and measure the received dosage of irradiation, as opposed to the estimated relative dosage given, as described by Truong et al in their recent publication (Truong *et al.*, 2018).

Alternatively, the impact of X-Ray irradiation on the displayed physical phenotype of the nuclei in cultured cells was investigated, whilst previous studies have suggested that low level doses of radiation may not induce any physical abnormalities or changes to the nucleus or collagen production (Truong *et al.*, 2018), but changes in the cell cycle stage and proliferation rates could be detected immediately after exposure, which could suggest a protective reaction to the damaging radiation environment, followed by a synchronised recovery and proliferation of the cells after a brief period of energy conservation. Therefore, if the expression levels of various house-keeping proteins within our cell cultures had been investigated, valuable insight into how the radiation exposure has maybe interfered on a molecular biology level could have been gained.

These very preliminary studies of changes to mesenchymal cell markers, in Figure 6.1-4 and Figure 6.1-5, demonstrate that there is an impact on the expression pattern of PDGFR β , and that this can logically be attributed to the exposure to IR. This is ideal pilot data to allow the extrapolation of this research; to do more detailed and quantifiable analysis of the expression of the MC markers during exposure.

Contrastingly, there has been work carried out that could suggest that mesenchymal stem cells retain their phenotype, and marker expression profile, despite exposure to IR (Nicolay *et al.*, 2013; Nicolay, Lopez Perez, Saffrich, *et al.*, 2015). These papers suggest that, due to the quiescent state of the MSCs, in their *in vitro* models, the cells will have limited direct DNA damage, as DNA is more likely to be damaged whilst cells are proliferating (Nicolay, Lopez Perez, Debus, *et al.*, 2015), and will present with an increased expression of components of the DNA repair pathways whilst retaining their “stemness” and ability to differentiate into different cell lineages. Whilst comparing this to our work, if higher concentrations of MSCs were being used than initially anticipated, the impact of the IR would be negligible, and no observations of visual differences between our populations would be recorded. However, from previous chapters, where cell culture phenotypes have been established and characterised, there is scepticism that this would apply to our cell populations, and the group believes that the failure of IR exposure experiment resides with the inability to reliably expose to high enough doses of IR, and the variety of alternative analysis methods that could have been used if there were less limitations on time, such as extracting RNA for more detailed analysis of the relative marker expression profiles, and using a panel of markers for IF analysis of cell cycle and DNA repair mechanism regulation.

Most significantly, organ cultures could not be developed in which the tissue would survive for more than 3 days. Tissue sections, or small lobes of the mouse salivary gland tissue that had been cultured on the semi-solid agar would see considerable attrition and tissue degradation within a very short time frame. The tissue culture method was one that had been established within our research group by Dr Bing Hu, and Jemma Walker, for use on developing mouse incisor teeth (unpublished), however, the salivary gland tissue did not survive, despite several attempts at optimising the protocol. Furthermore, as the tissue is being maintained at an organ level and not digested to a single cellular suspension, there is an increased risk that the tissue contained residual microbes that would normally have been removed through the digestion and incubation with antibiotics and antimycotics. This, along with the agar-based culture medium, led to the organ cultures becoming particularly prone to contaminations, despite extra precautions and stringent aseptic techniques being used to protect the cultures.

If the model for X-Ray IR exposure could be established, with confirmed phenotypical change observed within our cell populations, the project should proceed by introducing these exposed cells into three-dimensional cultures, as established in section 3.2 and 3.3, providing a more detailed analysis of the regenerative potential of these mesenchymal cells. This process could be taken further by using patient derived primary cell lines, from patients who have received IR treatment. However, this tissue is rare as few biopsies are taken before and after treatment, and many patients will also be on considerably severe chemotherapy which would affect other cellular process, impacting results.

6.1.4. Conclusion

With more time and resources, this channel of research would have been beneficial to pursue, as ionising radiation has significant impact on the salivary glands of head and neck cancer patients and, therefore, on their quality of life. With greater expertise in this field within our research group, and better access to X-Ray generating technology, these pertinent questions being asked could have provided important and relevant answers to understanding how IR can impact the regenerative potential of mesenchymal cells within the salivary gland.

However, it can be concluded that the cells exposed to ionising radiation possess a level of resilience that appears to prevent them from developing any indications of IR exposure, other than changes to PDGFR β expression patterns. The decrease in PDGFR β expression levels could be the physical manifestation of stem cells being driven into a differentiated state. As cells will undergo a brief pause in the cell cycle before an increased drive of proliferation, as a mechanism of recovery of functionality, post IR exposure (Truong *et al.*, 2018). This research has also shown that even diagnostic levels of IR exposure do not induce a physical manifestation of IR impact in our cell cultures, and any further research in these areas will have to focus on identifying double stranded DNA breaks, elevated DNA repair mechanisms and cellular proliferation rates as subtle measurement of phenotype change due to exposure to ionising radiation.

6.2. Primer Validation and Further QPCR Analysis.

For every PCR experiment, primers were used to amplify the cDNA for specific markers of interest. In this way, relative RNA expression for a range of markers could be quantified between different samples. For establishing whether the primers worked, they had to be validated through semi-quantitative PCR, (SQPCR) which amplifies the cDNA product with fluorescently labelled primers that can be detected when excited with UV light. This technique was planned to be used for the characterisation of the cell cultures produced in section 3.2 and 3.3 for mouse and human cell lines, also the primers were used in analysing the organoid culture models and for the characterisation of the human tissue in section 3.1, by use of Laser Capture Microdissection. In this section, we describe how primers were validated using the semi-quantitative PCR technique, and give examples of relative levels of RNA expression in mouse and human derived cell cultures, in human LCM experiments and spheroid models. We also explain why some of the PCR results were not included in the main body of the thesis, either because the experiments didn't work, the results were challenging to develop further using our techniques, or because there were no significant conclusions to be drawn.

6.2.1. Semi-quantitative PCR Method

Semi-quantitative PCR was used to confirm primers functioned and were expressed in cDNA samples. Most primers had been established by other members of the research group and are, therefore, not shown. Bulk tissue was used to extract RNA from each mouse and human tissue for validation with their appropriate primers. RNA was extracted and cDNA prepared as described in Materials and Methods 2.12 and 2.13.

Samples to run on a gel, 2ul of cDNA sample was placed in a PCR tube with 18ul of primer master mix: 2ul of primer, 10ul LightCycler 480 SYBR Green I master kit (4887352001, Roche Life Science), 6ul DEPC water. The PCR tubes were processed in a Veriti™ Thermal Cycler 96 well (Applied Biosystems) using manufacturers program of 90°C for 5 minutes, 90°C for 30 seconds, 60°C for 30 seconds, 72°C for 45 seconds - repeat steps 2 to 4 approximately 40 times - heat to 72°C for 5 minutes and then 8°C infinitely.

The PCR products were run on an agarose gel, which was prepared by microwaving 200ml TAE buffer and 4g agarose until the solution is clear. The gel was allowed to cool before adding 20ul of gel stain and then poured into a mould, with a comb, and allowed to set at room temperature for 30 minutes. Once set, the gel was placed in an electroplate reader and submerged in TAE buffer. The comb was removed and each well flushed with buffer before adding 12ul of each sample (10ul of sample with 2ul of DNA dye) with wells at either end containing DNA ladder. The gel ran at 125 volts at room temperature for approximately 15 minutes. The gel was visualised, and images taken in a JPEG format, using a UV light chamber (Bio doc-it Imaging System 8" LCD/ML-20, UVD).

Table 6.2-1 Primers designed against mouse tissue derived RNA sequences.

<i>Abbr.</i>	<i>S Primer</i>	<i>S Sequence</i>	<i>AS Primer</i>	<i>AS Sequence</i>
<i>Amy1</i>	m.Amy1_S1296	AGCTTTTGGCAGAGGAAACA	m.Amy1_AS1503	TGGGTCTTCGGCAGAGTTAC
<i>AQP5</i>	m.Aqp5_S530	TCTACTTCACCGGCTGTTC	m.Aqp5_AS728	TATGTGCCTTTGACCACAGC
<i>CD45</i>	m.CD45_S2320	CACTCGGGCTTTCAAAGATA	m.CD45_AS2607	GAAGTTTGAGGAGCAGGTGA
<i>Cdh1</i>	m.CDH1-616	CAGCTGCCCCGAAAATGAAAAGG	m.CDH1-861	TCCACCGCTTCCCCATTTGATG
<i>GAPDH</i>	m.GapDH-F	ATCACTGCCACCCAGAAGAC	m.GapDH-R	CAGTGAGCTTCCCGTTTCCAG
<i>Hes1</i>	m.Hes1-S452	CCAAGCTAGAGAAGGCAGACA	m.Hes1-AS599	GTCACCTCGTTCATGCACTC
<i>Hes1</i>	m.Hes1-S218	CCAAGCTAGAGAAGGCAGACA	m.Hes1-AS365	GTCACCTCGTTCATGCACTC
<i>Hes1</i>	m.Hes1_S325	GCCTCTGAGCACAGAAAGTC	m.Hes1_AS479	TCCAGAATGTCTGCCTTCTC
<i>Hes5</i>	mHes5_S981	AGG GTA GCA GCT TTC AGG AT	mHes5_AS1229	AGC CTC TGG GAT CTC CTC TA
<i>Hey1</i>	m.Hey1-S393	GGTACCCAGTGCCTTTGAGA	m.Hey1-AS547	ACCCCAAACCTCCGATAGTCC
<i>Hey2</i>	m.Hey2-S252	TGCCAAGTTAGAAAAGGCTGA	m.Hey2-AS388	AGCACTCTCGGAATCCAATG
<i>IL18</i>	m. IL18_S414	ACGTGTTCCAGGACACAACA	m.IL18_AS494	TCATCTTCCTTTTGCCAAGC
<i>ITGA1</i>	m.Itga1_S1914	CCACAATTGACATCGACAAA	m.Itga1_AS2158	AGCAACTGCTGTTCAAAAC
<i>ITGB1</i>	m.Itgb1_S1952	CTGGAAAATTCTGCGAGTGT	m.Itgb1_AS2101	ATGGACCAGTGTCCAAAGAA
<i>Ki67</i>	m.Mki67-S9322	AGCAAACCAGCTGCAGAAAT	m.Mki67-AS9515	TTCTTGGTGCATACAATGTCTT
<i>Kit</i>	m.Kit_S2692	CCTGCCGAAATGTATGACG	m.Kit_AS2885	GAGTTGACCTCACGGAATG
<i>Kitl</i>	m.Kitl_S624	TGAAGACTCGGGCTACAAT	m.Kitl_AS705	TAAGGCTCCAAAAGCAAAGC
<i>Krt14</i>	m.Krt14_S1218	CCTGCTGGATGTGAAGACAA	m.Krt14_AS1407	ATCGTGACATCCATGACCT
<i>Krt5</i>	m.Krt5_S1274	AGCTGACAGAGCTGGAGGAG	m.Krt5_AS1494	TCCTCCGTAGCCAGAAGAGA
<i>Myc</i>	m.Myc_S1182	CCAGATCCCTGAATTGGAAA	m.Myc_AS1274	TCGTCTGCTTGAATGGACAG
<i>Nes</i>	m.Nes-S923	AGGCTGAGAACTCTCGCTTG	m.Nes-AS1073	GAGAAGGATGTTGGGCTGAG
<i>Notch1</i>	m.Notch1-S6102	TGTTGTGCTCCTGAAGAACG	m.Notch1-AS6251	TCCATGTGATCCGTGATGTC
<i>Notch2</i>	m.Notch2_S767	TGTTCTACAGATGCCAAT	m.Notch2_AS990	CCACACAAACTCCTCCATTC
<i>Notch2</i>	m.Notch2-S5974	GAGGCGACTCTTCTGCTGTT	m.Notch2-AS6130	CCATGTGGTCAGTGATGTC
<i>NSUN2</i>	m.NSUN2_S1244	ACCTACCATGTTCCACCAA	m.NSUN2_AS1443	TGGATACCCTGGGTTCTCTG
<i>P63</i>	m.p63_S4708	TCTGTGGCATTTCAGACTA	m.p63_AS4921	CACCACCAAGTGAAGGAATC
<i>PDGFA</i>	m.Pdgfa_S288	CAAGACCAGGACGGTCATTT	m.Pdgfa_AS510	CCTCACCTGGACCTCTTTCA
<i>PDGFB</i>	m.Pdgfb_S503	CCACAGTGACCTTGAGGAC	m.Pdgfb_AS697	CCTTGTCATGGGTGTGCTTA
<i>PDGFRα</i>	m.Pdgfra_S2397	TGAAGCAAGCTGATACCACA	m.Pdgfra_AS2611	TCCTCGAGCAACTTGATAGG

<i>PDGFRβ</i>	m.PDGFRβ_S3241	CAGAAATGCTGGGAAGAAAA	m.PDGFRβ_AS3450	AACAGAGCTGGTGCCAGAG
<i>RBP</i>	m.RBP-jk_S5114	TTTCAGGACCGAGCTGTATT	m.RBP-jk_AS5283	AACCCCTTAAGGACTGGATG
<i>Rbp-Jk</i>	m.RBPex2_S37054	CCTCCACCCAAACGACTC	m.RBPex2_AS37227	CCCACCTCACACCTTTTAG
<i>Sca1</i>	m.Sca1_S184	CTGATGGAGTCTGTGTAC	m.Sca1_AS612	ATTAGAGCACCTACCTACC
<i>Sca1</i>	m.Sca1_S204	CAGGAGGCAGCAGTTATTG	m.Sca1_AS450	AGGACCATCAGAGCAAGG
<i>SHH</i>	m.SHH-F	TTCATAGTAGACCCAGTCGAAACC	m.SHH-R	GAGGACGGCCATCATTAGAG
<i>SHH</i>	m.Shh_S883	TCCACTGTTCTGTGAAAGCA	m.Shh_AS1070	GTCCAGGAAGGTGAGGAAGT
<i>Sox2</i>	m.Sox2_S1522	CACCAATCCCATCCAAATTA	m.Sox2_AS1729	GCGCCTAACGTACCTACTAGA
<i>SSB</i>	m.SSb_S1130	CGGAAAAAGAAGCATTGAAA	m.SSb_AS1358	CGACGATCATCATCATCAAA
<i>Tlr2</i>	m.TLR2_S2157	CTCCCACTTCAGGCTCTTTG	m.TLR2_AS2327	ACCCAAAACACTTCCTGCTG
<i>Tlr2</i>	m.TLR2_S1882	AAGAGGAAGCCCAAGAAAGC	m.TLR2_AS2080	CGATGGAATCGATGATGTTG
<i>Tlr4</i>	m.TLR4_S2099	GCTTTCACCTCTGCCTTAC	m.TLR4_AS2272	GAAACTGCCATGTTTGAGCA
<i>Tlr4</i>	m.TLR4_S2333	GGCAGCAGGTGGAATTGTAT	m.TLR4_AS2496	TGCCGTTTCTTGTCTTCTCT
<i>Vcam</i>	m.Vcam1_S1597	ACCCAGGTGGAGGTCTACTC	m.Vcam1_AS1701	GGACTTTATGCCCATTTCTCT
<i>Vim</i>	m.Vim-S1246	CCAACCTTTTCTCCCTGAA	m.Vim-AS1393	GGTCATCGTGATGCTGAGAA

Table 6.2-2 Primers designed for analysis of human tissue derived RNA.

<i>Abbreviation</i>	<i>S Primer</i>	<i>S Sequence</i>	<i>AS Primer</i>	<i>AS Sequence</i>
<i>36b4</i>	h.36b4_S	GCAATGTTGCCAGTGTCTGT	h.36b4_AS	GCCTTGACCTTTTCAGCAAG
<i>AQP5</i>	h.aqp5_S515	GCCACCTTGTCGGAATCTAC	h.aqp5_AS701	TCACTCAGGCTCAGGGAGTT
<i>β actin</i>	h.bActin_S342	GCACCACACCTTCTACAATGAG	h.bActin_AS507	GGATAGCACAGCCTGGATAGC
<i>β actin</i>	h.bActin_S785	CCTCCCTGGAGAAGAGCTAC	h.bActin_AS951	GATGTCCACGTCACACTTCA
<i>CD105</i>	h.CD105_S1960	CAACTGTGTGAGCCTGCTGT	h.CD105_AS2157	GACAGGTCAGGGCTGATGAT
<i>CD133</i>	h.CD133_S407	CCTCTGGTGGGGTATTTCTT	h.CD133_AS616	CAGTTTCCGACTCCTTTTGA
<i>CD133</i>	h.CD133_S1403	TCAGCGTCTTCTATTTCAGG	h.CD133_AS1565	AAAAATCACGATGAGGGTCA
<i>CD133</i>	h.CD133_S3309	GAGAACTGCGTAACTCCA	h.CD133_AS3482	TCATGTTAGTGCCTCCAA
<i>CD19</i>	h.CD19_S720	AAGGGCCTAAGTCATTGCT	h.CD19_AS917	CAGCAGCCAGTGCCATAGTA
<i>CD44</i>	h.CD44_S426	CCGGACACCATGGACAAG	h.CD44_AS576	CCGTCCGAGAGATGCTGT
<i>CD45</i>	h.CD45_S3150	GGTTCCACATTCAGAGCAAT	h.CD45_AS3354	TTCAGCCTGTTCTTTGCTT
<i>CD45</i>	h.CD45_S24	ACTTCTGGCATTGGCTTTG	h.CD45_AS220	AGTGGTTTGTGAGGGGCTCT
<i>CD90</i>	h.CD90_S673	CTCCGAACCAACTCACC	h.CD90_AS870	GAGGTGTTCTGAGCCAGCAG
<i>CDH1</i>	h.CDH1_S2270	AAGAAGGAGGCGGAGAAGAG	h.CDH1_AS2472	GGCTGTGGGGTCAGTATCAG
<i>cKit</i>	h.cKit_S119	TCTGCGTTCTGCTCTAC	h.cKit_AS330	TTCATTCTGCTTATTCTATTTCG
<i>cKit</i>	h.cKit_S306	AACGAATGAGAATAAGCAGAATG	h.cKit_AS637	GACAGAGCCGATGGTAGG
<i>Gli1</i>	h.GLI1_S550	AAGCGTGAGCCTGAATCTGT	h.GLI1_AS750	CATGTGAACCACCAGCATGT
<i>Gli2</i>	h.GLI2_S1271	TGGCTGACCTCAAGGAAGAT	h.GLI2_AS1420	GGATGTGCTCGTTGTTGATG
<i>Gli3</i>	h.GLI3_S883	GGCCATCCACATGGAATATC	h.GLI3_AS1078	TGAAGAGCTGCTACGGGAAT
<i>Glis1</i>	h.GLIS1_S1768	GGTGTGTATCCTGGCTCCAT	h.GLIS1_AS1962	GGGGCTGACTATTGGTGAGA
<i>Glis2</i>	h.GLIS2_S1470	AACGCCAGGTACAAGATGCT	h.GLIS2_AS1668	GCTTAAAGCGGCTACTGGAG
<i>HES1</i>	h.HES1-S161	TGAGCCAGCTGAAAACACTG	h.HES1-AS320	AGCACACTTGGGTCTGTGC
<i>HES5</i>	h.Hes5_S112	CTCAGCCCCCAAAGAGAAAAA	h.Hes5_AS362	CACGAGTAGCCTTCGCTGTA
<i>Hey1</i>	h.Hey1_S2096	CTTTTGGTGCATGGAAGTGT	h.Hey1_AS2247	CAGTTCAGTGGAGGTCGTTT
<i>Hey2</i>	hHey2_S369	CGTCGGATCGGATAAATAA	hHey2_AS578	GCACTCTCGGAATCCTATGC
<i>ICAM1</i>	h.ICAM1_S610	TGATGGGCAGTCAACAGCTA	h.ICAM1_AS871	GAAATTGGCTCCATGGTAT
<i>IL10</i>	h.IL10_S168	CTGCCTAACATGCTTCGAGA	h.IL10_AS366	GGTCTTGGTTCTCAGCTTGG
<i>IL-1β</i>	h.IL 1b_S258	GGAGAATGACCTGAGCACCT	h.IL 1b_AS442	GGAGGTGGAGAGCTTTCAGT

<i>IL6</i>	h.il-6_F HZ	AGTCCTGATCCAGTTCCTGC	h.il-6_R HZ	AAGCTGCGCAGAATGAGATG
<i>IL8</i>	h.il-8_F HZ	TCCAAACCTTTCCACCCCAA	h.il-8_R HZ	CCAGTTTTCTTGGGGTCCA
<i>ITGB1</i>	h.ITGB1_S855	AACTGCACCAGCCATTAG	h.ITGB1_S1057	TCTGTGGAAAACACCAGCAG
<i>K4</i>	h.K4_S1377	CATCTCTGGTTCAGCGGTA	h.K4_AS1556	CTCTTGTTCAGGGTGGTGGT
<i>K4</i>	h.K4_S1266	CCAGGAGCTCATGAGTGTGA	h.K4_AS1463	AAGCCACTACTCAGGCCAAA
<i>Kitl</i>	h.Kitl_S179	GGATGGATGTTTTGCCAAGT	h.Kitl_AS350	TCTTTCACGCACTCCACAAG
<i>KRT5</i>	h.krt5_S1030	GCCCAGTATGAGGAGATTGC	h.krt5_AS1229	AGATTGGCGCACTGTTTCTT
<i>Nestin</i>	h.Nestin_S2823	CATGGAACCTGGAGAATTTG	h.Nestin_AS3019	AGCCAGTCTTGGTCTCTCT
<i>NSUN2</i>	h.NSUN2_S910	ATTGCGAATGATGTGGACAA	h.NSUN2_AS1108	TCATAGTGCCGTCTCCACTG
<i>PDGFR-6</i>	h.PDGFR-b_S3007	GACACCAGCTCCGTCCTCTA	h.PDGFR-b_AS3187	GGCTGTCACAGGAGATGGTT
<i>TLR2</i>	h.TLR2_S	CTGCATTCCAAGACTGG	h.TLR2_AS	GGGAGGCATCTGGTAGAGTC
<i>TLR4</i>	h.TLR4_s152	ACCTCCCCTTCTCAACCAAG	h.TLR4_AS301	GGCTCTGATATGCCCATCT
<i>TLR4</i>	h.TLR4_S152	ACCTCCCCTTCTCAACCAAG	h.TLR4_AS301	GGCTCTGATATGCCCATCT
<i>TLR4</i>	h.TLR4_S	CAAAATCCCCGACAACCTCC	h.TLR4_AS	CCTGCAGTCTGGGAAATG
<i>VCAM1</i>	h.Vcam1_S1616	GGCAGAGTACGCAAACTT	h.Vcam1_AS1846	CCCCAGAATCTTCCATTTT
<i>VIM</i>	h.VIM_S1196	CCTACAGGAAGCTGCTGGAA	h.Vim_AS1393	GGTCATCGTGATGCTGAGAA

6.2.2. Results of Primer Validation

Tables 6.2-1 and -2 display large lists of primers that were accrued for analysis of mouse and human salivary gland tissues, cell cultures and organoid models. These primers were validated to confirm they could be used in experiments by myself or other members of the research team using semi-quantitative PCR analysis on agarose gels. Figure 6.2-1 and 6.2-2 display representative results from this primer validation technique in mouse salivary gland tissue and human salivary gland tissue respectively, with most of the primers being effective and amplifying the gene sufficiently to be detected.

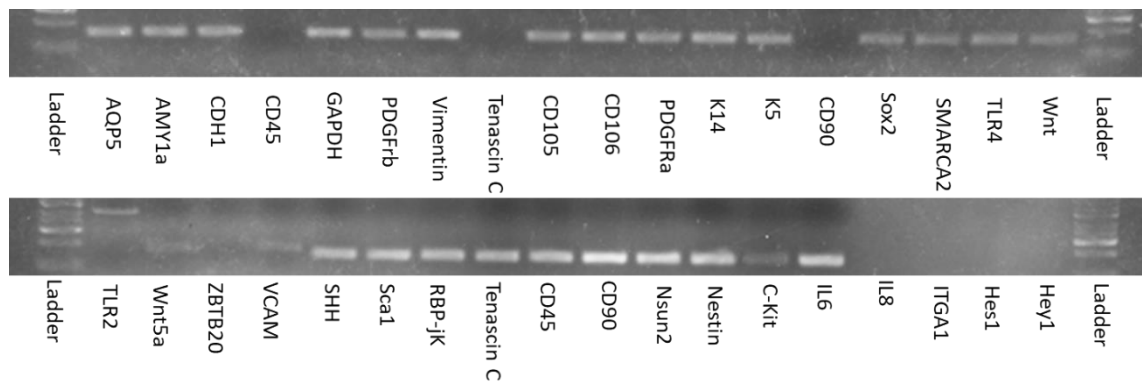


Figure 6.2-1 Example of SQPCR agarose gel image of primers being validated within mouse salivary gland bulk tissue. White bars indicate that the cDNA sequence of interest was amplified and can be detected by the UV scanning camera. Blank spaces indicate that this primer was not effective in amplifying the gene of interest.

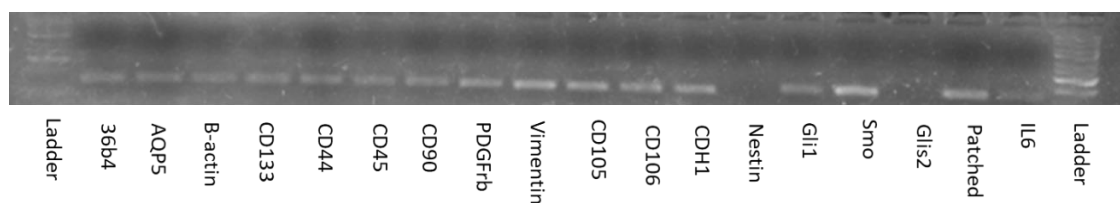


Figure 6.2-2 Example of SQPCR agarose gel image of primers being validated on cDNA produced from human labial salivary gland biopsy tissue. White bars indicate the presence of cDNA that has been accurately amplified and gaps indicate primers that did not successfully amplify the cDNA.

6.2.3. Results of Further QPCR Analysis

Laser Capture Microdissection

As described in the discussion of section 3.1, when regions of tissue were collected from sections of human labial salivary gland tissue, the amount of tissue collected was physically small, and the quality of the RNA may have been impacted. Initially, Gli family primers were ran on the LightCycler as a test of functionality, using RNA extracted from control material that should express these markers; in this case HGEPP cell line and a human keratinocyte cell line, these results are shown in Figure 6.2-3. All of the Gli family markers appear to be expressed in these two cell lines, with the primers enabling the amplification of the target RNA to reach detectable Ct peaks.

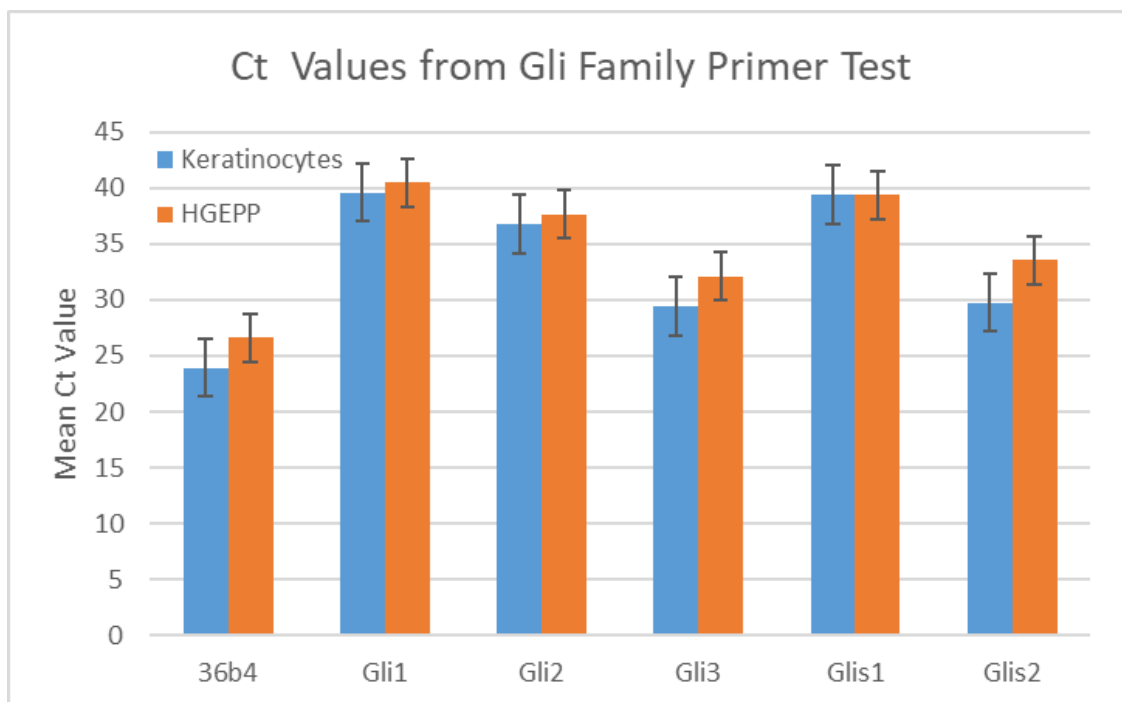


Figure 6.2-3 Gli family member primers were tested using Human Gingival Epithelial Cells and Human Keratinocytes. All primers produced a Ct peak before cycle 45, which was the total number of cycles ran during this QPCR experiment. Error bars represent the standard error of the mean.

However, when the LCM regions were collected, extracted and ran through a QPCR, using the Syber Green and Roche LightCycler technology, the RNA quantity and quality was so low that most of these markers did not produce a detectable peak. Even markers that are expressed very sparsely should amplify to produce a peak, especially with additional cycles added to the QPCR protocol. These markers were removed from the experimental design until only those with noted changes in expression levels in concordance with disease status remained; these are described and presented in section 3.1.2 Regional Analysis of non-PSS versus PSS tissue by LCM.

Human Cell Culture Characterisation

Further to the analysis of the human labial salivary gland sections using LCM, large panels of markers were collated in order to pick a shortlist of markers that could accurately describe the cell type and the disease status of the cell lines. These samples produced a good yield of RNA when extracting using the standard protocol, although few markers exhibited any significant differences, as indicated in Figure 6.2-4 on patient derived mesenchymal cells. These figures show a representative selection of the larger panel of markers initially employed to investigate the phenotype of the human cultures.

Some markers do suggest a trend, for example Stat3 and Hey1, shown in Figure 6.2-5, with all of the PSS positive samples expressing lower levels of markers than the non-PSS patient derived cells. But the majority of the markers in Figure 6.2-4, -5 and -6 follow no pattern of change to expression levels, with both the PSS positive and non-PSS patient derived cells being discordant in their expression levels of these markers across disease status.

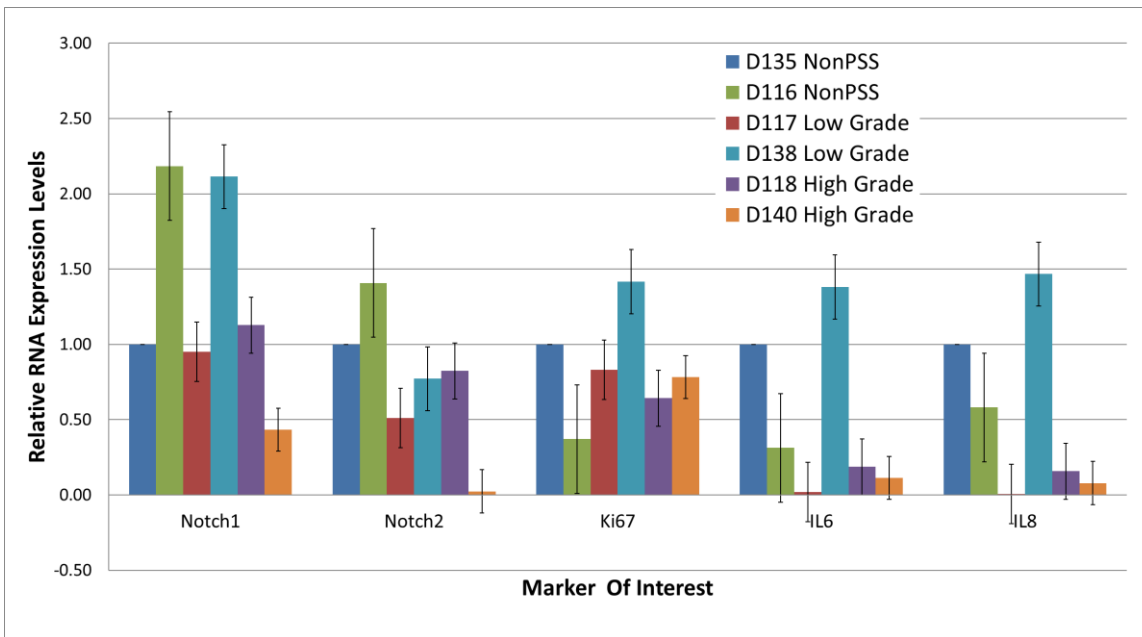


Figure 6.2-4 Relative RNA expression levels for a small panel of markers in human derived mesenchymal cell culture lines from PSS and non-PSS patient salivary gland tissue. Error bars are representative of Standard Error of the Mean, with no trend being displayed between the case/control samples.

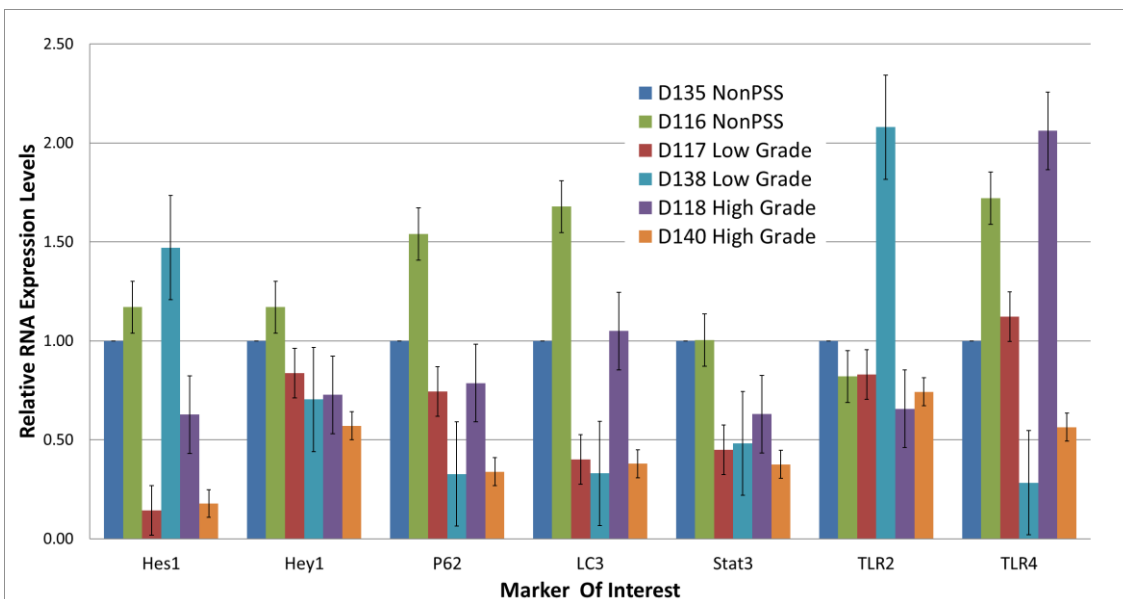


Figure 6.2-5 Relative RNA expression levels for a small panel of markers in human derived mesenchymal cell culture lines from PSS and non-PSS patient salivary gland tissue. Error bars are representative of Standard Error of the Mean.

The markers displayed in Figure 6.2-6 are mostly associated with immune response pathways, however, none of these display consistent patterns across disease status, with the Toll-Like Receptor proteins and Interleukins varying greatly across the cohort.

Furthermore, the stem cell associated markers Kitl and c-kit also do not show any change due to disease status and none of the paired PSS status samples expressing comparative levels of the markers.

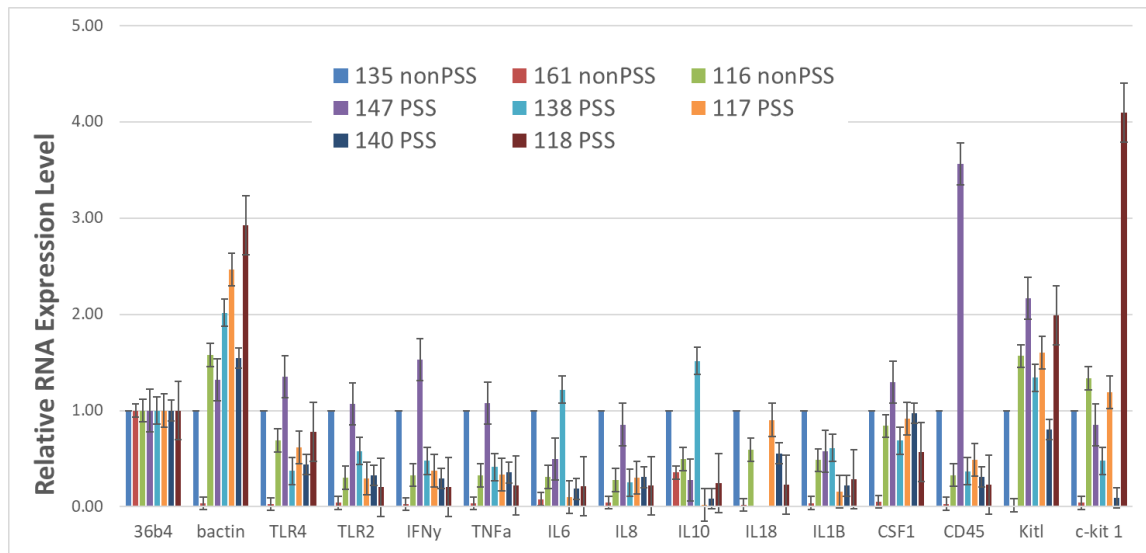


Figure 6.2-6 Relative RNA expression levels for a panel of markers in human derived mesenchymal cell culture lines from PSS and non-PSS patient salivary gland tissue. Error bars are representative of Standard Error of the Mean.

Mouse Derived Cell Culture Characterisation

Whilst selecting the most appropriate cell culture dish coating between poly-d-lysine and collagen, and the various culture media conditions, the cell phenotypes had to be confirmed, with RNA expression selected as one of the techniques to be used. Below, in Figure 6.2-7, the variable being explored was the dish coating method. The culture media had already been established as Amniomax (AM) for the growth of mesenchymal cells, and DMEM F12 with B27 Supplement (B27) for the growth of epithelial cells. Therefore, we cultured mouse derived cells, extracted as described previously in section 2.8 and 3.2.1, in each of these cell culture media, on dishes coated with either Poly-d-Lysine (PDL) or Collagen (Coll).

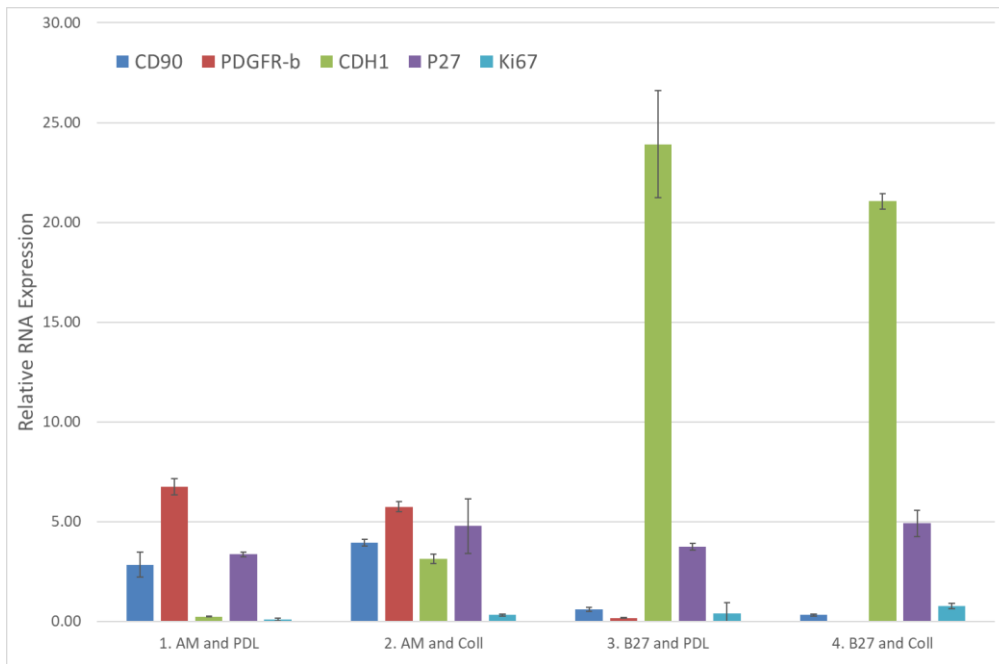


Figure 6.2-7 Relative RNA expression of cell markers whilst optimising cell culture environments for mouse salivary gland derived epithelial and mesenchymal cells. Error bars represent the standard error of the mean. Conditions 1. and 2. were both mesenchymal cells promoting conditions, Amniomax culture medium with either Poly-D-Lysine (PDL) or rat tail collagen (Coll) coating on the culture ware. Whilst 3. and 4. were epithelial cell promoting conditions in B27 culture media with PDL or Coll coating.

As demonstrated, the first condition (Amniomax and PDL) presented with higher CD90 and PDGFR-b than any of the epithelial growth conditions, however the cells also had much lower expression of E-cadherin (CDH1). Alternatively, the third and fourth conditions, comparing B27 culture media with PDL and Collagen, produced comparable results, with a higher expression of E-cadherin in B27 and PDL.

The inclusion of P27 and Ki67 was to investigate changes in the proliferative ability of the cells, with P27 being a cell cycle inhibitor and Ki67 expressed only during G1, S, G2 and the mitosis stages of the cell cycle, they could have been used to investigate if there were enriched populations of stem cells within certain conditions. The expression of these markers appeared consistent across all conditions and it was suggested that the heterogeneity of cells in culture would mask any stem cell identification in this way.

Spheroid Analysis

During the production of spheroid models for mouse, human, and the recombination assays using mouse and human derived cells together, RNA was extracted and processed, and analysed using the standard QPCR method. In Figure 6.2-8, experimental repeats of combined mouse epithelial and mesenchymal cell spheres were compared to epithelial only spheroid, acting as a control. As expected, E-cadherin is highest in the controls as these spheroids only contain epithelial cells. Vimentin is also highest in the combined sphere cultures, as these have the addition of mesenchymal cells, which are not present in the epithelial only condition, ergo inflating the relative level of expression accordingly. Most importantly, Aquaporin 5 is increased in the combined spheroids, as are alpha smooth muscle actin and PDGFRb, suggesting a more mature and fully differentiated phenotype.

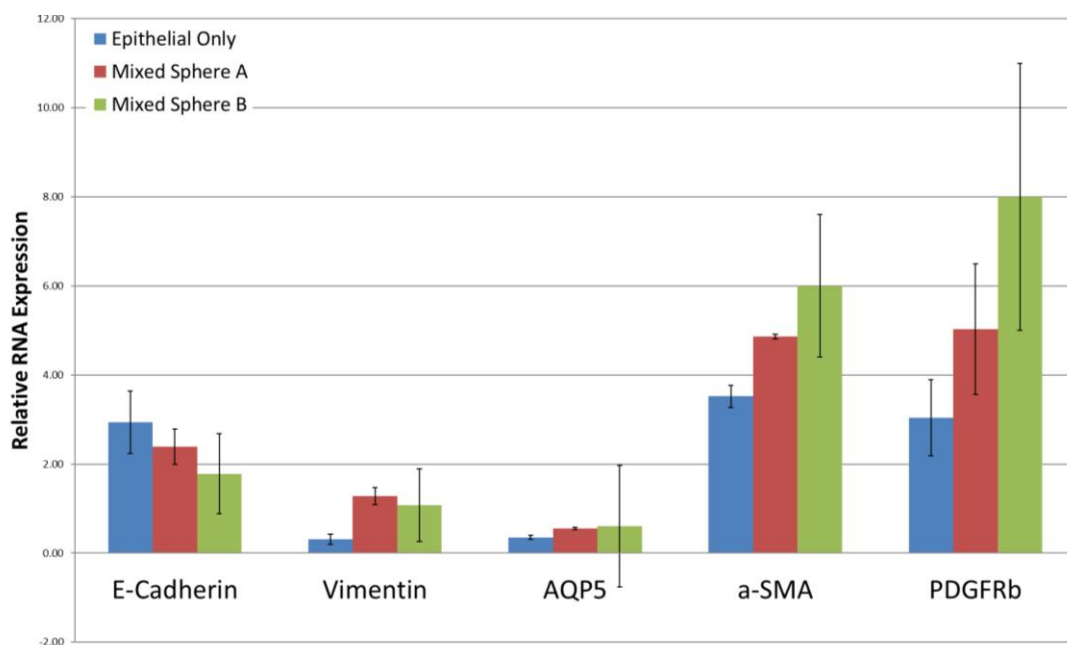


Figure 6.2-8 Relative RNA Expression of markers in spheroid structures generated from mouse epithelial and mouse mesenchymal spheroid structures. Spheres collected from epithelial only spheres and duplicated experimental repeats of mixed epithelial and mesenchymal spheres were lysed for RNA extraction and analysed using the standard QPCR LightCycler protocol described in section 2.13. Error bars represent the standard error of the mean.

In comparison, the analysis performed on human and mouse combination spheroids was less reliable due to the large standard deviation of error produced during the QPCR analysis; the error bars on the graph in Figure 6.2-9 demonstrate this, indicating why these results were not included in the main body of the thesis. These spheres were cultured for 14 days before extraction from the gel matrix for immunofluorescence and RNA extraction and analysis. The levels of AQP5, AMY1a and NSun2 were very low in all of the mouse-human combination spheres in comparison to the epithelial only control, although the standard error of the means frequently were very large.

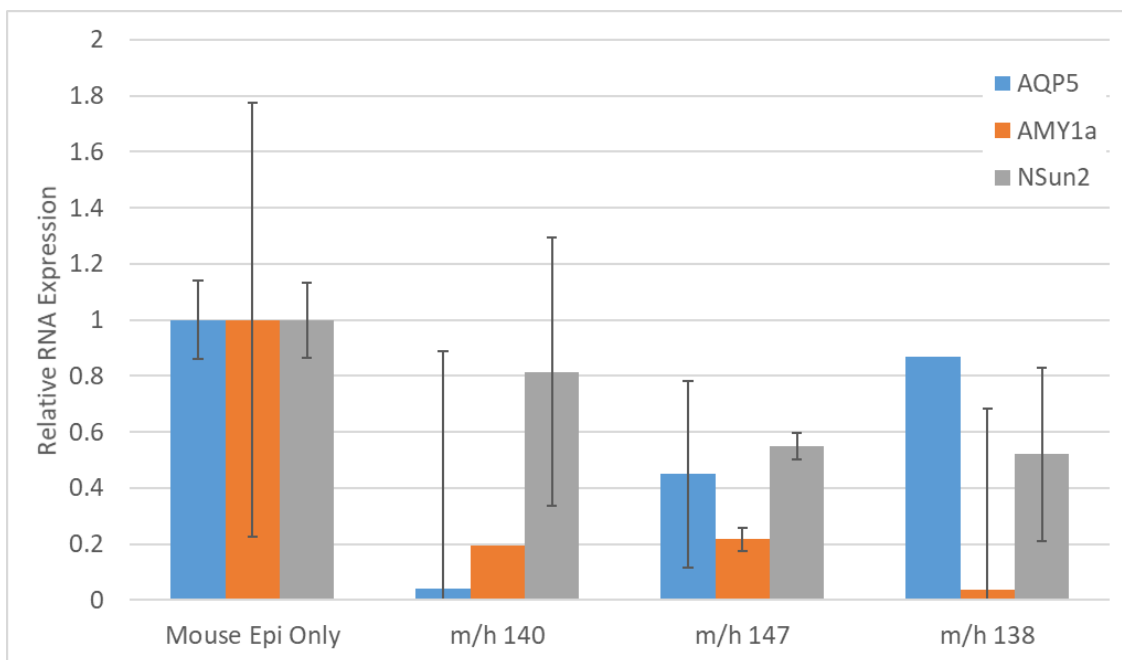


Figure 6.2-9 Relative RNA Expression of functional markers exhibited by mouse-human cell combination spheres in comparison to a control culture of mouse epithelial only spheres. Primers were designed specifically for the analysis of mouse RNA derived cDNA. Mouse-human spheres contained mouse epithelial combined with mesenchymal cells from patients DSO140, 147 and 138 individually. Error bars represent the standard error of the mean where shown.

6.2.4. Discussion of Primer Validation and QPCR Analysis

Optimisation of primers does not contribute directly to the results of this project, but was an important part of experimental design. Most primers used were also used by members of the research group, with functionality confirmed by Donald Singer and Jemma Walker also. When cDNA amplified with specific primers did not generate bands on the agarose gels, these primers were dropped out of the study, or redesigned and new primers ordered, with the cycle repeated to confirm functionality. In Figure 6.2-1 and 6.2-2, the absence of band indicates that the cDNA for the primer specific region of genetic material was not amplified sufficiently.

During LCM, the tissue could not be fixed, and had to be stained and then dried before the lasers could cut through the tissue and the membrane. This led to the tissue structural physiology deteriorating and the RNA degrading before it could be collected. Furthermore, the quantity of RNA eluted after isolation and purification was low, which meant that when the QPCR analysis was performed, the markers of interest didn't amplify sufficiently to be detected. However, it does provide us with a shortlist of markers that could be shown to be significantly affected by PSS, as described in section 3.1.2. Previously, the primers had been shown to function for all of the Gli and Glis family member genes, therefore demonstrating that the limiting factor in these experiments was RNA quality and quantity.

Whilst considering the analysis of markers from human cell culture extracted RNA, only a few markers demonstrated an adherence to a disease status associated pattern. These markers are known to be associated with immune regulation pathways and cell death, with Stat3 associated with apoptosis and P62 known to be associated with autophagy

(Martinet *et al.*, 2013; Morgan-Bathke *et al.*, 2015). Both of these markers were consistently reduced in the PSS positive cell populations compared to non-PSS derived mesenchymal cells. This suggests that, although salivary gland tissue is destroyed by the presence of the immune lesion, the cell death pathways are downregulated in an effort to preserve tissue and promote cell survival despite adverse tissue micro-environments, which would tie in with previous work that indicates the conflicting roles of cell death during Sjogren's Syndrome and the attempted tissue recovery (Herrera-Esparza *et al.*, 2008; Kramer, 2014). However, the majority of the samples had no consistency between disease matched samples, demonstrating the heterogeneity of the disease's influence on the tissue, and variability across patient derived samples, particularly in such a small cohort such as this one.

During the culture of mouse salivary gland derived cells, decisions were made on which conditions offered the optimal cell culture environment, although the expression of markers using QPCR analysis was not the only aspect taken into consideration. Whilst epithelial cells appeared to be more CDH1 positive when grown on PDL coated plates, in reality these cultures grew slowly and sparsely in comparison to the Coll coated conditions. As the results displayed in Figure 6.2-7 were only used to confirm cell culture phenotypes during the optimisation of cell culture techniques, they were not deemed as imperative to the story told during the bulk of the thesis, hence being displayed in the Appendix. The final selected culture conditions were described and characterised in section 3.2.3, using immunofluorescence to also confirm cell phenotype.

Ultimately, to characterise and identify our cells of interest, whilst taking into consideration the heterogeneity of many samples in both mouse and human culture

environments, the decision was taken to focus on major markers of interest such as Vimentin and E-Cadherin (CDH1), which could very easily determine the cell phenotype. Immunofluorescence was also relied on more heavily to indicate the location of markers of interest in a more functional aspect, rather than relying on RNA expression levels, which can be transient and have a variable correlation to functional expression of proteins in cells and tissue.

The analysis of RNA from the spheroid models resulted in large error bars and some unexpected results, with expression of differentiation markers at contrasting levels between the mouse only spheroids and the mouse-human recombination spheroids. The structures were small and gave a low quantity of RNA, suggesting that more experimental repeats were necessary to boost the RNA yield in experiments. This may have contributed to the error bars being so large.

Furthermore, when the mouse only spheres were characterised in section 3.2.3, we could demonstrate a very clear increase in the expression of AQP5 in the mouse mixed cell spheroids, in Figure 3.2-19C. However, in Figure 6.2-9 we showed that the spheres produced using human derived mesenchymal cells produced less AQP5 than the epithelial only controls, despite these mouse-human combined spheres presenting with larger structures with budding and branching phenotypes than the epithelial only controls. These contradicting results evidently have arisen from the novel technique used by combining mouse and human cells into one culture.

Although the physical presence of the mesenchymal cells was sufficient to promote an elevated growth phenotype, the signalling pathways were not sufficient to stimulate the increased expression of markers associated with heightened development of the

spheroid structures. Evidently, human growth factors released by the human mesenchymal cells did not elicit an appropriate response in mouse derived epithelial cells. Perhaps in future experiments, these growth factors could be supplemented into cell culture conditions in an attempt to also promote the cell differentiation pathways.

6.2.5. Conclusion

Although a lot of QPCR RNA analysis was performed, on different sections of the project, many of the investigations didn't highlight any markers of interest that could be taken further. Any markers that were highlighted were paired with immunofluorescent staining techniques to confirm the functional expression levels of the markers. Examples of these include Vimentin and E-cadherin, which were used as our main two markers for our populations of interest. However, the markers used in section 6.2 were hoped to demonstrate some significant change in signalling pathways between PSS and non-PSS cohorts, or suggesting an enriched developmental phenotype in the spheroid models developed.

What these results do demonstrate is how many other factors dictate the diversity of disease influence on the tissue, and that to perform a study of this level of detailed investigation would require a much larger cohort of patient derived samples. Although, for the purposes of analysing the functional developmental stages of the spheroid models, RNA extraction and analysis would be more reliable and flexible when compared to the limited immunofluorescent techniques that were adapted in sections 3.2 and 3.3 previously. If planning this project again, I believe that the most effective start would be to use RNA seq to generate a shortlist of genes that are significantly impacted between disease cohorts and using these to monitor and analyse the functional changes in spheroid models.